Investigation of the Performance of an Anaerobic Membrane Bioreactor in the Treatment of Mixed Municipal Sludge Under Ambient, Mesophilic and Thermophilic Operating Conditions

by

Vince Pileggi

A thesis
presented to the University of Waterloo
in fulfillment of the
thesis requirement for the degree of
Doctor of Philosophy
in
Civil and Environmental Engineering

Waterloo, Ontario, Canada, 2016

Author's Declaration

I hereby declare that I am the sole author of this thesis. This is a true copy of the thesis, including any required final revisions, as accepted by my examiners.

I understand that my thesis may be made electronically available to the public.

Abstract

Anaerobic membrane bioreactors (AnMBRs) may provide a sustainable treatment technology for the digestion of mixed municipal sludge based on their ability to achieve elevated volatile solids (VS) conversion and a net positive energy balance. However, AnMBRs may have throughput limitations particularly when operated at high solids inventories due to membrane fouling. This study characterized the anaerobic digestion bioprocess and the membrane performance under various operating conditions and identified the foulant mode using the classical 'Hermia-Field' blocking models while operating the system under low crossflow and low transmembrane pressures. Using the *in-vitro* yeast estrogen screen (YES) bioassay the sludge and permeate quality was assessed for its estrogenic potential. The permeate was analysed for a group of environmentally relevant trace organic compounds.

The study used a side-stream pilot scale AnMBR with two parallel negative tubular membranes and a flow through anaerobic digester (AD) as a control. Each reactor was fed in parallel from a common mixed sludge source. The tubular ultrafiltration membranes were polyvinylidene difluoride based with a nominal pore size of 20 nm, operated at a crossflow of 1–1.2 m/s and a transmembrane pressure of 34–54 kPa. Four operating conditions that included different SRT:HRT ratios under ambient (25 °C), mesophilic (35 °C) and thermophilic (55 °C) temperatures were investigated.

The main AnMBR advantage over the AD is the ability to decouple and independently control the system SRT and HRT resulting in increased throughput, at lower HRT, while maintaining a low food to microorganisms ratio by increasing the SRT. This operational strategy was used and under mesophilic conditions, the AnMBR showed a 54 and 64 % volatile solids conversion at SRT:HRT of 30:15 and 21:7 days, with loading rates of 2.1 $\pm$ 0.4 and 3.7 $\pm$ 0.9 kg COD/m$^3 \cdot d$, respectively. Under ambient and thermophilic operating conditions, the SRT/HRT ratio was adjusted considering the system kinetics and the AnMBR showed a 49 and 55 % volatile solids conversion at SRT/HRT of 40:8 and 22:7 days, with loading rates of 3.5 $\pm$ 0.4 and 3.4 $\pm$ 0.8 kg COD/m$^3 \cdot d$, respectively. Under all the operating conditions the AnMBR was operated at more than double the loading rate and showed an improvement of 13–30 % increase in volatile solids conversion, compared to the AD. A comparison of the energy balance between the AnMBR and AD showed a net positive energy balance for the AnMBR when operated at mesophilic and ambient temperatures but not during thermophilic operation. The AD proved sustainable under ambient operation only.

The membrane performance showed a median sustainable flux of 6–7 $\pm$ 2 LMH which was maintained through inter-permeation cycle rest and clean-in-place (CIP) strategy. The frequency of the CIP increased with an increase in SRT, TS and during ambient operation due to an increase in viscosity of the mixed liquor. The dominant fouling mode was found to be cake fouling under all operating conditions and primarily of a reversible type. The permeability decline was assessed and found to be affected primarily by TS, SRT/HRT ratio and extracellular polymeric substances (EPS) protein to polysaccharide ratio.

The estrogenicity of the feed sludge was found to persist in anaerobically treated mixed municipal sludges and the AnMBR permeate. This was corroborated by the permeate chemical analysis which found a significant contribution from a small number of estrogens.

Acknowledgements

Completing this thesis has been a humbling and a transformative experience. Fortunately I had many to help me along the way and I'm grateful and thank you all for your dedication to me and the work.

I'm particularly grateful and thank Dr. Wayne J. Parker, my thesis advisor, for his technical guidance and friendship. His vast technical knowledge, insight and dedication were inspirational and will serve as an ideal to aspire to.

I gratefully acknowledge and thank my PhD committee: Drs. Baoqiang Liao, Raymond L. Legge, William B. Anderson and Hyung-Sool Lee for giving their valuable time, expertise and having the interest to provide valuable feedback.

A truly heartfelt thank you to Dr. Peter Seto, of Environment Canada, for his care, technical insight, uncompromising support and friendship over the years. His support with the maintenance of the pilot plants at the Wastewater Technology Centre made everything run smoothly.

Thank you to all the technical support staff at Environment Canada, in Burlington, that kept things running smoothly over the years particularly Scott Dunlop, Steven Lee and Sam Dith. A thank you to Kyle Waldner, Susan Norman, Scott Douglas, Ankit Bhatt and Tushar Nayak for assistance in reactor operation and sampling. A thank you goes out to all the staff of the inorganic laboratory at WTC and particularly John Salvatore for providing analytical services.

A special thank you to all my research colleagues Daniela, Muyiwa, Qirong, Zebo and Kyle that made the long hours of research at WTC more fun.

A deserving thank you to Dr. Chris Metcalfe for providing the yeast stock for the YES bioassay, Dr. Xia Chen for helping me learn the subtleties of the YES bioassay analysis, Dr. Martha Dagnew for initial assistance with the pilot plant, Shirley Anne Smyth for helping me to maintain the EC lab protocols, Dr. Paul Yang of MOECC and Tung Vi Nguyen for chemical analysis of the permeate samples and Thomas Sullivan for administrative assistance.

A big thank you to all those involved with the open-source on-line LaTeX2e, CRAN and R-Studio community which provided me invaluable assistance making the typesetting and computational work possible and much more enjoyable.

A thank you goes also to all my MOECC colleagues and friends that either encouraged, inspired or supported me, in particular Jason, Julie, Paul, Shahram, Mano, Sonya, Albert, Dale, Steve, Minnie and Tim.

Thank You,

Vince Pileggi
University of Waterloo

Dedication

I dedicate this thesis to my wife Regina and daughter Justine for their enduring love that did the most by keeping me focused.

Table of Contents

List of Tables

List of Figures

Nomenclature

α	VFA to alkalinity ratio
α_c	Specific cake layer resistance (m/kg)
ΔE_{net}	Net energy balance (kJ/d)
ϵ	Cake layer porosity
η	Viscosity
η_{20}	Viscosity at 20 °C
η_T	Viscosity at temperature T
ρ	Density
θ	Hydraulic retention time (HRT, d)
θ_x	Solids retention time (SRT, d)
AD	Anaerobic digestion
AnMBR	Anaerobic membrane bioreactor
ANOVA	Analysis of vairance
A_o	Initial membrane area (m^2)
AcH	Acetic acid
ADM1	Anaerobic digestion model no. 1
AnMBR	Anaerobic membrane bioreactor
AR	Androgenic response
AS	Activated sludge
A_s	Membrane surface area (m^2)
ASE	Accelerated solvent extraction
A_x	Membrane cross sectional area (m^2)
BAP	Biomass associated products
bEPS	Bound EPS
BPA	Bisphenol A
BPC	Biopolymer clusters
BuH	Butyric acid
CBL	Concentration boundary layer
CODt	Total chemical oxygen demand (CODp + CODf)
CODc	Colloidal COD (CODf − CODs)
CODf	Filtered COD
CODp	Particulate COD
CODs	Soluble COD equal to the permeate CODt (UF, NPS of 20 nm)
CFV, v	Crossflow velocity (m/s)
CI	Confidence interval (95 %-ile)
COPAS	Complex organic particulate artificial sewage based on cat food
CSTR	Completely stirred tank reactor
cWW	Complex synthetic wastewater based on COPAS
D	Membrane module inside diameter (mm)
dm	Dry mass

Nomenclature (*continued*)

DSWR	Deliberate sludge wasting rate
dw	Dry weight
E1	Estrone
E2	17β-estradiol
E3	Estriol
ECCs	Emerging contaminants of concern
ECDF	Empirical cumulative distribution function
EDA	Exploratory data analysis
EDC	Endocrine disrupting compounds
EDX	Energy-dispersive X-ray spectroscopy
EE2	17α-ethinylestradiol
EEQ	E2 Equivalent Ratio
eEPS	Exactable extracellular polymeric substances
E_H	Energy to heat the sludge (kJ/d)
E_L	Energy heat loss from the reactor (kJ/d)
E_M	Energy recovered from methane (kJ/d)
E_P	Energy to pump the sludge (kJ/d)
EPS	Extracellular polymeric substances
EQ	Equilin
ER	Estrogenic response
ERE	Estrogen-responsive sequences
E_X	Energy to mix the sludge (kJ/d)
FI	Fouling index
FI_J	Fouling index at constant J
FI_P	Fouling index at constant TMP
FR	Membrane fouling rate
F/M	Food to microorganisms ratio (mg COD/mg VSS)
FS	Fixed solids
FSS	Fixed suspended solids
GAC	Granular activated carbon
GC	Gas chromatography
GC/MS	Gas Chromatography-Mass Spectrometry
hER	Human estrogen receptor
HRT	Hydraulic retention time
iAnMBR	Immersed anaerobic membrane bioreactor
iMBR	Immersed membrane bioreactor
J	Flux ($\mathrm{L}/m^2 \cdot h$, LMH)
J_s	Sustainable flux (LMH)
K	Permeability (LMH/kPa)
KEC	Kraft evaporator condensate
LCI	Lower 95 % confidence interval
LMH	Liters per meters squared per day [$\mathrm{L}/(\mathrm{m}^2 \cdot d)$]

Nomenclature (*continued*)

LTFR	Long term fouling rate (LMH/h)
LOD	Limit of detection
LOQ	Limit of quantification
MBR	Membrane bioreactor
MF	Microfiltration
MLSS	Mixed liquor suspended solids
MOA	Mode-of-action endpoints
MWCO	Molecular weight cut-off
MY_{CODr}	Methane yield based on COD reduction
NPS	Nominal pore size
OLR	organic loading rate
ON	organic nitrogen (mg/L)
PAC	Powdered activated carbon
PASBRs	Psychrophilic anaerobic sequencing batch reactors
PBDEs	Polybrominated diphenyl ethers
PCPs	Personal care products
PLC	Programmable logic controller
POME	Palm oil mill effluent
PPCPs	Pharmaceutical and personal care products
PPM	Parts per million (mg/L)
PrH	Propionic acid
PS	Primary sludge
PVDF	Polyvinylidene difluoride
pWW	Pressate wastewater from a pump mill
Q_b	Daily biogas production (m^3)
Q_f	Mass of sludge feed (kg/d)
Q_m	Normalized biogas production (NL CH_4/d)
R_i	Irreversible resistance of the fouled membrane (m^{-1})
R_m	Resistance of the virgin membrane (m^{-1})
R_o	Initial membrane resistance (1/m)
R_r	Reversible resistance of the fouled membrane (m^{-1})
R_t	Total resistance (m^{-1})
Re	Reynolds number
REP	Relative estrogenic potency as E2
sAnMBR	Sidestream anaerobic membrane bioreactor
sEPS	Soluble EPS
S_f	Feed sludge COD (g COD/L)
sMBR	Sidestream membrane bioreactor
SMP	Soluble microbial products
SMP_{VSf}	Specific methane production in terms of VS feed
SRT	Solids retention time
STP	Sewage treatment plant
STFR	Short term fouling rate (LMH/min)

Nomenclature (*continued*)

S_w	Water solubility (mg/L)
sWW	Synthetic wastewater
TADU	Thermophilic anaerobic digester with an ultrafilter
TAN	Total ammonia nitrogen
TAnMBR	Thermophilic anaerobic membrane bioreactor
TC	Triclocarban
TCS	Triclosan
TMP (ΔP)	Transmembrane pressure
TP	Total phosphorous (mg/L)
TrOC	Trace organic contaminants
TS	Total solids
TWAS	Thickened waste activated sludge
UAP	Utilization associated products
UCI	Upper 95 % confidence interval
UF	Ultrafiltration
USEPA	United state environmental protection agency
V	Reactor volume (m^3 or L)
VaH	Valeric acid
V_x	Cross flow velocity (m/s)
VFAs	Volatile fatty acids (mg/L)
VFM	Membrane Bioreactor-Vito Fouling Measurement
VS	Volatile solids (g/L)
VSLR	Volatile solids loading rate
VSr	Volatile solids reduction
VTG	Vitellogenin
WAS	Waste activated sludge
WW	Wastewater
WWTP	Wastewater treatment plant
wWW	Whitewater
X_f	Concentration of VS in feed sludge (g/L)
YES	Yeast estrogenic screen

Chapter 1

Introduction

1.1 Problem Statement

The mesophilic (35–40 °C) anaerobic treatment of mixed municipal sludges (combined PS, WAS or TWAS) is the most common form of digestion at large STP for the purpose of generating biosolids for soil amendment, biogas to supplement natural gas as a fuel and/or to reduce the sludge volume for more economical dewatering and subsequent handling. The relatively slow rates of hydrolysis and the slow growth of methanogens requires extended SRTs. A minimum of 15 days SRT is recommended for a single phase flow-through anaerobic digester and this necessitates the use of large AD with high capital expenditure and corresponding large operation and maintenance costs. Approaches to reduce costs associated with ADs and improve the economic feasibility of the system while trying to maintain a steady gas production and meet stabilization criteria include: (1) Operation at ambient (20–27 °C) or thermophilic (55–60 °C) conditions, (2) operating at higher SRT to HRT ratios and (3) adding membrane technologies to convert the AD to an AnMBR. The use of these strategies have potential benefits and associated challenges which are considered below:

Benefits

1. Membranes

1. Increased concentration of active biomass promoting the stabilization of the sludge and increased production of biogas [3];
2. ability to operate at higher solids feed rates reducing the reactor size and reducing operational and maintenance costs [2, 14];
3. concurrent thickening with treatment reducing sludge volumes for subsequent treatment and associated handling costs [15, 16];
4. possibility to recover nutrients (e.g., nitrogen, phosphorous, potassium and sodium) from the permeate [17]; and
5. increasing the concentration of intra- or extracellular enzymes promoting metabolism and cometabolism of recalcitrant substrates and TrOCs [18].

2. Ambient Temperature Operation

1. Reduced energy consumption since there is no need to apply external heat;
2. reduced sludge production with a stable process consistent with mesophilic operation; and
3. increased nutrient retention in the treated sludge with improved reuse value as a soil amendment.

3. Thermophilic Temperature Operation

1. Increased biochemical rates with corresponding increased biogas production;
2. increased bioconversion of recalcitrant including microcontaminants; and
3. increased rate of VS destruction and corresponding to reduced stabilized times and increases in loading rates or reduced reactor footprint.

4. Increased SRT:HRT Ratios

1. Increased active biomass concentration in the bioreactor leading to increased biochemical conversion rates;
2. increased loading rates reducing the reactor footprint; and
3. increased rate of VS destruction corresponding to reduced stabilized times and increased biochemical conversions of recalcitrant contaminants.

Challenges

1. Membranes

1. Membrane fouling due to high solids concentrations thereby reducing fluxes and potentially reducing the mass flow through of the system;
2. increased cleaning frequency and associated operational and maintenance costs;
3. pumping costs associated with maintaining transmembrane pressures;
4. potential for reduction of biomass activity associated with shear stresses on biofloc and disruption of symbiotic association of microbial consortia; and
5. issues associated with use and disposal of chemicals necessary to clean the membrane.

2. Ambient Temperature Operation

1. Reduced reaction rates requiring more time (i.e., higher SRT and HRT) to stabilize the sludge with corresponding lower methane production; and
2. increased viscosity resulting in increased membrane resistance and larger membrane reactors to maintain an equivalent sustainable membrane flux compared to higher operating temperatures.

3. Thermophilic Temperature Operation

1. Increased foaming potential leading to unstable process conditions;
2. increased energy demands to keep the reactor at steady high temperatures; and
3. loss of valuable nutrients (N, P) reducing the nutrient value of the treated sludge.

4. Increased SRT:HRT Ratios

1. Increased mixing requirements due to increased solids concentration; and

2. increased inert solids retention in reactor with corresponding loss in active biomass volume.

An emerging concern, associated with biosolids utilization, is the presence of trace organic contaminants (TrOCs) and particularly endocrine disrupting compounds (EDCs) in biosolids at environmentally relevant concentrations [4, 19]. EDCs have been reported to be present in runoff from biosolids amended sites and to impact non-target endpoints as identified through the use of in-vitro and in-vivo biological assays [5, 20, 21]. The presence, reduction and control of the release of EDCs in the natural environment, from biosolids, that may cause specific estrogenic response (ER) have become a source of particular concern among regulators, municipalities and the research community because of the serious potential long-term implications on wildlife sustainability [22, 23]. The EDCs that typically induce an ER are TrOCs classified as estrogenic mimicking compounds. The concentration of TrOCs are generally low and considered biological cosubstrates (not sufficient to support microbial growth alone) and assumed to undergo biochemical conversion cometabolically or fortuitously. The study of biologically mediated reductions of EDCs through the application of various sludge treatment processes and control strategies is an active area of research. Currently there exist knowledge gaps associated with fundamental process and operational issues related to the use of ambient, mesophilic and thermophilic AnMBR operation for the treatment of mixed municipal sludges and the associated concentration or partitioning of EDCs through the sludge treatment process.

1.2 Purpose Objectives and Scope

The purpose of this research was to:

1. Compare AnMBR with AD for the treatment of mixed municipal sludge under ambient, mesophilic and thermophilic operating conditions;

2. consider various AnMBR operating conditions for potential full scale application; and

3. assess the quality of the sludges and AnMBR permeate with respect to the concentrations of selected TrOCs and in-vitro estrogenic responses.

The objective and scope of the proposed research characterizes the performance of pilot scale sidestream cross flow tubular AnMBR operated at a low pressure and low V_x while treating mixed sludges. The research:

- Compared the performance of a sidestream AnMBR to a control AD under the following conditions: (1) mesophilic, ambient and thermophilic conditions; (2) different SRT to HRT ratios. Performance parameters will include volatile solids (VS) destruction, biogas production and chemical oxygen demand (COD) conversion.

- Investigated membrane performance under three temperature conditions (25, 35 and 55 °C) and different membrane cleaning strategies. The membrane performance will be assessed against the type of foulants and cleaning strategies.

- Evaluate the occurrence and concentration changes of selected TrOCs in combination with an assessment of estrogenic responses of sludge and permeate extracts.
- Investigate the equilibrium desorption from treated AD and AnMBR sludges and assess the EDC chemistry along with the estrogenic response of aqueous extracts.

The work was carried out using two pilot scale reactors located at the Wastewater Technology Centre (Science and Technology Branch of Environment Canada), in Burlington, Ontario. The TWAS came from the Burlington Skyway STP and the PS came from the Hamilton Woodward Avenue STP. The sludges were trucked weekly from each facility.

This research is unique with respect to the use of ambient AnMBR for the treatment of combined municipal sludges. The lessons learned from this research will assist municipalities operating full scale AD and considering upgrades to AnMBR with particular attention to enhanced economic feasibility of the treatment of mixed sludges and sludge quality with respect to EDCs and corresponding estrogenic responses of sludge and permeate extracts.

1.3 Thesis Structure

This thesis report is divided into six chapters, four appendices and references. Chapter 1 (current chapter) provides a brief introduction to the problem under investigation, the purpose, objectives and scope of the research. Chapter 2 provides a literature review including recent research related to the use of AD and AnMBR for the treatment of sludge and concentrated wastewaters. It also includes a review of recent work related to EDCs and ER of sludge extracts. Chapter 3 compares the AnMBR and AD conventional performance under ambient, mesophilic and thermophilic conditions. Biogas generation, COD conversions, VS destruction and energy balances are compared for both the AD and sAnMBR under four different operating conditions. Chapter 4 compares the sAnMBR membrane performance under similar conditions as described for Chapter 3. Flux, permeability and fouling indices with classical fouling modeling and regression analysis is used for the membrane performance assessment. Chapter 5 compares the YES bioassay ER between the different sludge and permeate extracts and compares the concentration of selected TrOCs found in the permeate under the four distinct operating conditions. Chapter 6 summarises the findings and provides recommendation to apply and extend the findings of this study.

Chapter 2

Literature Review

2.1 Municipal Sludge and Anaerobic Digestion

Municipal STP generate a large volume of primary sludge (PS) and waste activated sludge (WAS) as part of the solids-liquid separation and treatment processes. The management and treatment of the sludge consumes up to 50 % of the operating costs and its disposal or utilization is a major issue for STP operators, municipalities, regulators and the biosolids industry in Ontario and worldwide. Although different treatment options are available for sludges, AD continue to play an important role because of their ability to transform organic matter into biogas, effectively stabilize organics, reduce sludge volume and reduce vector attraction associated with residual putrescible matter [2, 24].

The stabilization of biodegradable organic matter in sludge is commonly quantified by volatile solids (VS) destruction and typically is in the range of 30–65 % in AD [25]. Typically 60% of the VS found in PS and 30–50 % of VS found in WAS, is converted to biogas [2, 3, 26]. The anaerobic digestion of municipal sludge involves complex biochemical processes that convert degradable organic compounds to methane (CH_4) and carbon dioxide (CO_2) in the absence of elemental oxygen. The conversion pathway (Figure 2.1) includes: (1) hydrolysis, (2) acidogenesis, (3) acetogenesis and (4) methanogenesis. These four main processes involve three different groups of microorganisms. The first group involves hydrolytic and acidogenic bacteria, which hydrolyze the complex substrates (carbohydrates, lipids, proteins) to dissolved monomers (sugars, fatty acids, amino acids) and further to CO_2 (g), H_2 (g), organic acids and alcohols. The second metabolic group of bacteria consists of hydrogen producing acetogens that convert monomers and fatty acids to acetate, H_2 (g) and CO_2 (g). The third group involves methanogens that utilize the H_2 (g), CO_2 and acetate to produce primarily CH_4 (g) and CO_2 (g). The overall conversion of the substrate to biogas is relatively slow and requires a long SRT. Typically the rate critical step is the solubilization of intracellular biopolymers and the conversion of solid degradable organics to the lower molecular weight compounds through hydrolysis [1, 3, 24, 27].

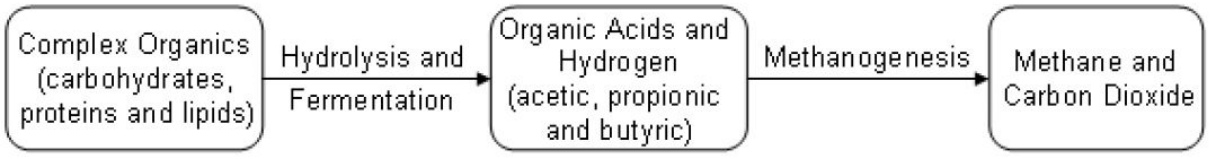

Figure 2.1: Simplified anaerobic digestion operation process [3].

For municipal wastewater sludges the typical OLR of anaerobic suspended growth CSTR operated at 35 °C range from 1 to 2 kg COD/(m^3/d) with a typical HRT of 15 to 20

days and the reactor MLVSS in the range of 4 to 8 g/L. External heating and mixing is commonly employed in the bioreactors to maintain ideal operating conditions [2, 26]. Methane production under these conditions is about 350 L of CH_4 per kg of biodegraded COD with a corresponding energy value of about 36 kJ/L of CH_4. As an example, a typical conventional activated sludge STP serving a population of 100,000 people generating 450 L of sewage per person equivalent results in about 2500 kg/d of sludge with a concentration of about 2% solids. This is equivalent to a total sludge volume of about 125 $m^3 \cdot d$. For a HRT of 15 days this would require a reactor of about 1900 m^3 (12m x 12m x 12m). The expected methane production from this sludge would be approximately 700 m^3/day or equivalent power generation of about 7 MW·h/d with a value of $ 763 per day or $ 278,500 per year based on a $ 0.109/(kW·h) (January 2014 mid-peak rate Ontario electricity value).

High rate anaerobic processes are common and these bioreactor configurations typically provide active biomass retention resulting in low HRT/SRT ratios and have increased active biomass in the bioreactor. The separation of biomass from the liquid stream may be accomplished by settling or other solid–liquid separation mechanisms (biofilm media and use of membranes). The SRT is typically controlled by the reactor sludge wastage rate and the HRT is maintained by adjusting the hydraulic input and output from the bioreactor subject to the concentration of the active biomass that can be attained in the bioreactor. The bioreactor VSS concentrations can vary from 5–30 g/L VSS, depending on the effectiveness of the biomass retention process.

Some of the limitations associated with AD include the need for large reactors and associated capital, operational and maintenance costs which may be partially offset by the value of the of the biogas produced if collected and used as a fuel. Areas of potential improvements to AD include:(1) increasing the OLR; (2) pretreatment to increase the biodegradable fraction; (3) increasing the active biomass concentration and reducing the F/M ratio and (4) operating the bioreactors at ambient temperatures reducing the energy input by eliminating the need to heat the digesters that are typically operated at mesophilic or thermophilic temperatures (35 or 55 °C). The next sections consider the key benefits and challenges with selected strategies to improve on conventional AD of mixed sludges.

2.2 Anaerobic Membrane Bioreactors (AnMBRs)

The addition of membranes to AD transforms the process reactor (typically CSTR) to an AnMBR. As compared to AD some of the reported benefits and challenges associated with AnBMR include [1, 28]: (1) enhanced biodegradation of slowly biodegradable substrates promoting the production of biogas; (2) increased solids feed rates reducing the reactor size and reducing operational and maintenance costs; (3) concurrent thickening reducing sludge volumes for subsequent treatment and handling costs reduction and (4) increased net energy production by operating at a higher solids inventory and increasing the biogas production rate. Some of the challenges include: (1) increased membrane fouling due to higher solids concentration reducing flux rate; (2) sludge pumping costs, membrane cleaning costs and associated operational and maintenance costs; (3) potential for reduction of biomass activity associated with increased shear stresses and (4) use and disposal of chemicals used to clean the membranes.

The membranes employed for wastewater and sludge treatment are typically in the ultrafiltration (UF) to microfiltration (MF) range. Figure 2.2 provides an overview of the pore size for various filtration processes. The pore size for ultrafiltration membranes is an order of magnitude finer than microfiltration membranes and is nominally defined as 0.01–0.05 μm. Ultrafiltration membranes can remove larger organic macromolecules and are typically defined by a molecular weight cut–off (MWCO). Typical MWCO levels for ultrafiltration membranes range from 10–500 kilo-daltons (kDa). The ultrafiltration membrane nominal pore size (NPS) is generally effective at providing a physical barrier to particulates and microorganisms down to viruses [8].

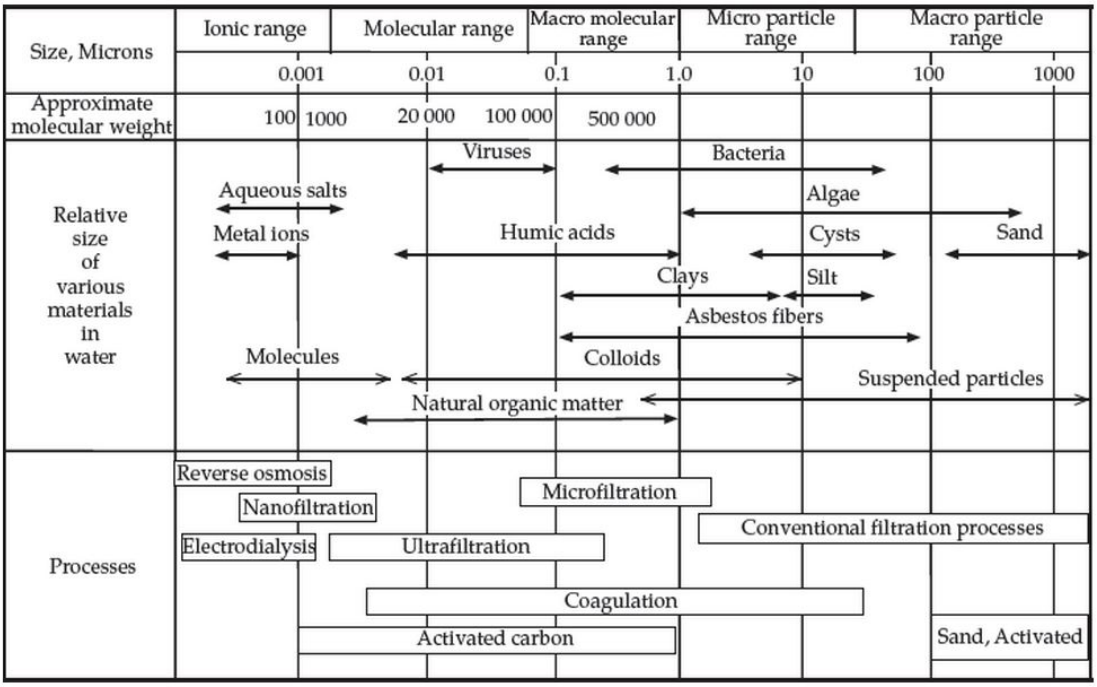

Figure 2.2: Membrane separation process overview based on the approximate MWCO range (adopted from [8]).

Two common membrane bioreactor (MBR) configurations include sidestream (sMBR) and immersed (iMBR) which generally use positive pressure or vacuum pressure pumping, respectively (Figure 2.3) [9]. The dominant commercial membrane configurations include flat sheet, hollow fibre and tubular membrane geometries. In the sMBR configuration permeate pumping creates shear abrasion on the membrane surface which may reduce the membrane reversible fouling. With the iMBR configuration gas sparging and agitation is commonly used to effect membrane scouring [8].

Typical membrane materials include polyvinylidene difluoride (PVDF), polyethylsulphone (PES), polyethylene (PE) and polypropylene (PP). These materials are generally hydrophobic in the bioreactor liquors they are filtering. Surface modifications such as chemical oxidation, organic chemical reaction, plasma treatment or grafting have been employed to make the polymer have particular proprietary characteristics [9, 29]. The choice of membrane materials and process configuration is constrained by membrane geometry and permeate flow direction and these are selected to: (1) maximize the membrane area per

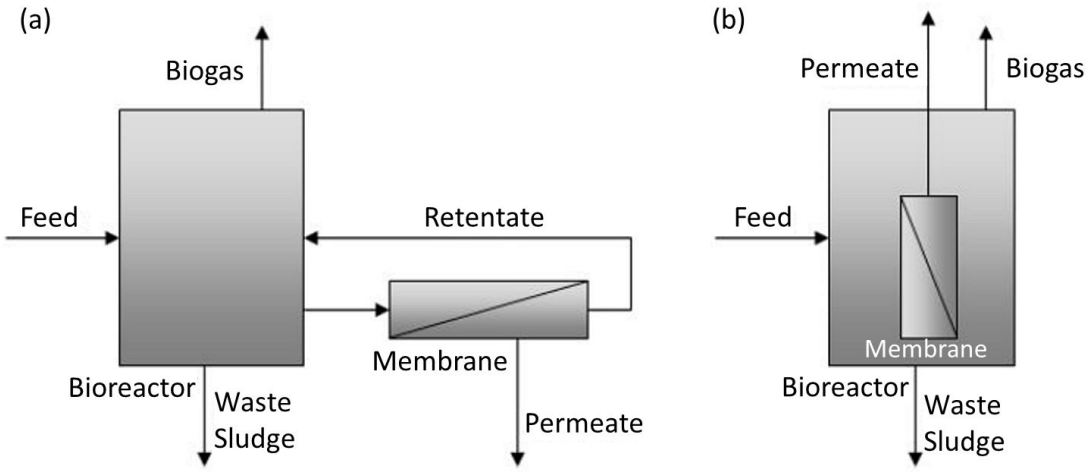

Figure 2.3: MBR process configuration (a) sidestream (sMBR) and (b) submerged or immersed MBR (iMBR) (adapted from [8, 9]).

bulk module volume, (2) ensure a high degree of turbulence to promote high flux on the feed side, (3) maximize flux per energy consumption, (4) allow ease of cleaning and (5) permit modularization [30].

2.3 Operating Conditions

Previous applications have evaluated the performance of AnMBRs treating concentrated wastewaters (Tables 2.1), municipal and industrial wastewaters (Table 2.2) and synthetic wastewaters (Table 2.3) at bench and pilot scale over a range of operating conditions with varying degrees of success. The key and most common operating conditions that have been found to influence the design and performance of AnMBRs included the wastewater feed characteristics (TSS, COD, soluble and insoluble fractions), hydrodynamic or reactor configuration (sAnMBR or iAnMBR, crossflow (CFV) or gas sparging), membrane characteristics (NPS or MWCO, membrane hydrophobicity, charge, roughness), temperature (psychrophilic, ambient, mesophilic, thermophilic), operating transmembrane pressure (ΔP), flux (J), organic loading rate (OLR), the bioreactor mixed liquor suspended solids (MLSS), the hydraulic retention time (HRT) and the solids retention time (SRT). An understanding of the complex interrelationships between these parameters is necessary to determine a viable design and operating strategy. The selection of optimum parameters is complicated by the heterogeneity of the matrix being treated and the membrane fouling interdependencies.

Many studies have attempted to simplify the study conditions to focus on specific fundamental aspects of a limited number of parameters. One common approach has been to use synthetic wastewater (sWW) at lab scale to reduce the matrix complexity or to better control matrix effects with focus on soluble constituents (Table 2.3). Other studies have used real wastewater streams with low suspended solids and tested the treatment process at lab or pilot scale (Table 2.2). Still fewer applications have used high solids authentic

Table 2.1: Summary of key operating conditions of previous applications treating municipal sludge, manures and high solids waste streams using AnMBRs

Feed Matrix[a]	R-S[b]	NPS[c] nm or $MWCO$	T[c] °C	ΔP[c] kPa	Flux[c] $\frac{L}{m^2 \cdot h}$	OLR[c] $\frac{kg\ COD}{m^3 \cdot d}$	MLSS[c] $\frac{g\ TSS}{L}$	HRT[c] d	SRT[c] d	Ref.
TWAS	S-P	40	35	30	11-30	1.2[e]	20-33	7-15	15-30	[31]
TWAS	S-B	40	35	30	32, 39	1.3[e]	8-14	15	30	[32]
mSL	S-B	35	35, 55	17-60	7-9	5-6	30, 50	7	30-50	[33]
WAS	uS-B	400	35	20	1-7	1-4[f]	10-100	8-3	40	[34]
mSL	S-P	100	35	510	145	0.1-0.5[e]	18	2-12	4-70	[35]
mSL	S-B	20	20, 35	-	2-12	0.1[e]	14	20	-	[36]
WAS	S-P	2 MDa	30-38	11	20-70	-	20-28	-	-	[37]
cWW	S-B	30	37	60-90	5-20	0.1	22	3	60	[38]
WW	S-B	10	37, 55	12, 25	7, 2	3, 12	9	3.2, 0.8	230	[39]
WW	S-B	200	30	-	5-10	6-8	20-55	1	-	[40]
sMA	S-B	10	37	20-70	5-10	1, 2[f]	27, 50	6	118, 211	[41]
sMA	S-B	-	30	37	30-70	5-10	20-40	6	30	[17]
dMA	S-P	200	55	-	40-80	1.9	50	23	30	[42]
pMA	pI-P	500	35	-	10-20	3-4	-	1-2	-	[43]

[a] Matrix being treated: TWAS, thickened waste activated sludge; mSL, mixed sludge consisting of primary sludge (PS) and waste activated sludge (WAS); WMS, combined municipal wastewater and digested mixed sludge; cWW, complex organic particulate artificial sewage (COPAS), based on granular cat food with high solids content; WW, municipal wastewater; sMA, homogenized swine manure; dMA, dairy manure consisting of a blend of cow manure and well water; mMA, piggetry manure [b] Reactor configuration and scale (R-S): I, immersed anaerobic membrane bioreactor; S, sidestream anaerobic membrane bioreactor (see Figure 2.3); uS, ultrasonic pretreatment followed by a sAnMBR; uI, upflow anaerobic iAnMBR; pI, a 63 μm prefilter immersed prior to the membrane. The reactor scale: B, bench-scale reactor; and P, pilot scale reactor.
[c] NPS, the membrane nominal pore size in nm in some cases given as MWCO; T, reactor operating temperature in °C; ΔP, mean transmembrane pressure in kPa; Flux, mean sustained flux in L/m^2·h or LMH; OLR, mean organic loading rate in kg COD/m$^3 \cdot d$; MLSS, mean mixed liquor suspended solids in g TSS/L; HRT, mean hydraulic retention time in days (d); SRT, mean solids retention time in days (d) based on controlled and deliberate sludge wasting from the CSTR.
[d] - means the value or condition was not reported and could not be calculated based on the supplementary information provided. [e] OLR in kg TS/m^3·d. [f] OLR in kg VS/m^3·d.

wastewaters or sludge matrices (Table 2.1) at lab or pilot scale to better assess some of the expected issues that would likely occur at full scale applications.

An investigation into the transferability of lab-scale microfiltration results to large-scale MBR processes was conducted by Buetehorn et al., 2012 [69]. The general findings suggested that rheology properties (viscosity, shear, mixed-media turbulence) associated with sludges with MLSS concentrations greater than 3.5 g TSS/L were not easily transferable from lab-scale and this was attributed to the highly complex multi-phase flow of MLSS, suspended

Table 2.2: Summary of key operating conditions of previous applications treating wastewaters using AnMBRs

Feed Matrix[a]	R-S[b]	NPS[c] nm or $MWCO$	T[c] °C	ΔP[c] kPa	Flux[c] $\frac{L}{m^2 \cdot h}$	OLR[c] $\frac{kg\ COD}{m^3 \cdot d}$	MLSS[c] $\frac{g\ TSS}{L}$	HRT[c] d	SRT[c] d	Ref.
WW	uI-P	10	22	< 130	< 50	2.6-3.0	0.1	0.25	180	[44]
WW	I-B	400	15-35	5-25	7	0.9-1.8	20	0.25	-[d]	[45]
WW	S-P	38	35, 20	18	4-7	0.6-1.1	15	0.6	-	[46]
WW	S-B	450	25-30	< 30	< 1	1	8-14	10	30, 60, 90	[47]
WW	I-P	80	20-25	-	6	0.3-0.5	8	0.8	100	[48]
WW	uI-B	220	-	< 15	30	-	0.3-0.6	-	-	[49]
pWW	I-B	300	37	< 30	7	0.24	11	2.5	350	[50]
wWW	I-B	300	37	< 30	5	0.21	9	3.8	220	[50]
wWW	uI-B	300	37, 42	5-40	6-13	2-24	5-10	1-2	350	[51]
wWW	I-B	70 kDa	30	-	12	1	6-9	0.4	-	[52]
WMS	I-P	40	10-25	60-150	6	40[e]	7-10	0.7	100	[53]
KEC	uI-B	300	37	5-40	6-13	2-24	5-10	1-2	-	[54]
KEC	I-B	300	55	< 30	2, 5	1-2	5-6	3, 7	200-260	[55]
LEC	I-B	400	20, 35	-	1-4	7-14	-	1-19	30, 300	[56]
POME	S-P	200 kDa	35	150	26-30	< 22	50-70	2.8-3.2	77-161	[57]

[a] WW, municipal wastewater; wWW, whitewater and pWW, pressate wastewater were both collected from the local thermochemical pulping mill; PPR, Thermo-mechanical pulping pressate collected from a local pulp and paper mill; KEC, kraft evaporator condensate from a pump mill digesters and evaporators with methanol as the main carbon sources at elevated concentration; LEC, high strength leachate generated from a solid waste transfer station; POME, filtered (1 mm) palm oil mill effluent. [b] Reactor configuration and scale (R-S): I, immersed anaerobic membrane bioreactor; S, sidestream anaerobic membrane bioreactor; uI, up-flow anaerobic sludge blanket (UASB) reactor. The reactor scale: B, bench-scale reactor; P, pilot scale reactor.
[c] NPS, the membrane nominal pore size in nm in some cases given as MWCO; T, reactor operating temperature in °C; ΔP, mean transmembrane pressure in kPa; Flux, mean sustained flux in L/m^2·h or LMH; OLR, mean organic loading rate in kg COD/m$^3 \cdot d$; MLSS, mean mixed liquor suspended solids in g TSS/L; HRT, mean hydraulic retention time in days (d); SRT, mean solids retention time in days (d) based on controlled and deliberate sludge wasting from the CSTR.
[d] - means the value or condition was not reported. [e] OLR in kg VS/m^3·d.

solids and gas bubbles interaction with the membrane fouling layers. Further, it was found that the extended time-scale of temperature and compositional variations in feed wastewaters of full-scale applications can influence biochemical kinetic rates, biodegradation pathways and hydrolysis rates, and these are not generally realized in lab-scale investigations. Because of these limitations it was considered essential that pilot-scale experiments treating real wastewater streams be conducted to complement the findings using model wastewater streams at lab-scale [69].

A synthesis of lab-scale and pilot-scale work results appears to the most economical approach

Table 2.3: Summary of key operating conditions of previous applications treating synthetic wastewaters using AnMBRs

Feed Matrix[a]	R-S[b]	NPS[c] nm or $MWCO$	T[c] °C	ΔP[c] kPa	Flux[c] $\frac{L}{m^2 \cdot h}$	OLR[c] $\frac{kg\ COD}{m^3 \cdot d}$	MLSS[c] $\frac{g\ TSS}{L}$	HRT[c] d	SRT[c] d	Ref.
sWW	I-B	400	35	5-25	7	0.7-1.5	31	0.2-0.35	-[d]	[58]
sWW	S-B	50	20	< 15	< 40	3	1.8[e]	0.33	3.5	[59]
sWW	I-B	450	30, 55	< 200	3-6	3-14	35, 13[e]	1-2	< 20	[60]
sWW	S-B	200	35	35	25-47	0.8-0.9[f]	3-22	1	30	[61]
sWW	I-B	400	35	< 20	2, 5, 9	5-20	0.25, 0.6	250		[62]
sWW	I-B	400	35	< 25	10, 20	10-20	0.25	150		[63]
sWW	I-B	400	35	< 25	10, 20	10-20	0.25	150		[63]
sWW	S-B	200	55	-	6.5	5-15	28	-	120	[64]
sWW	I-B	450	25-30	< 30	5-8	1.0-1.7	5-10	0.3-0.5	30-100	[65]
sWW	I-B	200	30	< 20	5-21	15	25-50	0.33	-	[66]
sWW	I-B	200	55	< 20	16-23	20	25-50	0.25	-	[66]
aWW	S-B	50-200	35	< 100	30-50	2[g]	0.13	-	-	[67]
cWW	S-B	100 kDa	30	-	8-10	5	0.5	1	50	[68]
cWW	S-B	30 kDa	30	-	3-5	5	0.5	1	50	[68]

[a] sWW, synthetic municipal based wastewaters; cWW, complex organic particulate synthetic cat food based wastewater; aWW, mainly acetic acid based synthetic wastewater. [b] Reactor configuration and scale (R-S): I, immersed anaerobic membrane bioreactor; S, sidestream anaerobic membrane bioreactor (see Figure 2.3). The reactor scale: B, bench-scale reactor; P, pilot scale reactor; F, full scale reactor. [c] NPS, the membrane nominal pore size in nm in some cases given as MWCO; T, reactor operating temperature in °C; ΔP, mean transmembrane pressure in kPa; Flux, mean sustained flux in L/m^2·h or LMH; OLR, mean organic loading rate in kg COD/m$^3 \cdot d$; MLSS, mean mixed liquor suspended solids in g TSS/L; HRT, mean hydraulic retention time in days (d); SRT, mean solids retention time in days (d) based on controlled and deliberate sludge wasting from the CSTR. [d] - means the value or condition was not reported.
[e] MLSS in g VSS/L. [f] OLR in kg COD/kg VSS·d. [g] OLR in kg TOC/kg VSS·d.

to better understand the fundamentals and determine optimum operating strategies that may be applicable to full-scale conditions. The main design and operating parameters, with a focus on sludge treatment applications, are critically reviewed in the subsequent sections.

2.3.1 Sludge Feed Matrix

The chemical and physical characteristics of the sludge feed matrix, along with its consistency over time plays a central role that influences the AnMBR treatment process. Feed characterization has typically been evaluated on the basis of parameters such as solids (total, suspended, dissolved), oxygen demand (COD, BOD), nutrients (N, P) species and alkalinity. Extended characterization under laboratory conditions has also included metals, particle size distribution (PSD), colloidal fractions ($< 1\mu m$) and viscosity measurements.

Municipal primary sludge (PS) is typically characterized in terms of TS (5–9 %), VS (60–80 % of TS), grease and fats (6–35 % of TS), alkalinity 0.5–1.5 g/L as $CaCO_3$), organic acids (0.2–2 g/L as HAc) and energy content (23–29 MJ/kg TSS). The protein content is generally around 20–30 % of the TS, with N 1.5–4 % of TS and P as P_2O_5, 0.8–2.8 % of TS [2]. An important issue when dealing with sludge treatment is the particulate fraction that needs to undergo disintegration and hydrolysis [1] prior to fermentation (Figure 2.1). The disintegration and hydrolysis steps are generally critical to ensure effective anaerobic digestion and many pretreatment steps (ultrasonic, ozonation, thermal, chemical) have been investigated to accelerate the disintegration and hydrolysis rates [70]. Despite sludge pre-treatment measures higher HRTs and SRTs, when compared to wastewaters (Table 2.1 compared to Table 2.2 and 2.3) are generally required for effective stabilization typically defined as > 50 % VS reduction of the feed sludge.

A detailed feed characterization in terms of particle size distribution and corresponding chemical characterization for a synthetic wastewater, municipal wastewater, cheese industry wastewater and swine manure was conducted by Sophonsiri et al., 2004 [71]. The particles sizes were divided into settleable ($> 100\ \mu m$), supra colloidal (1–100 μm), colloidal (0.08–1 μm) and soluble ($< 0.08\ \mu m$). The chemistry constituents associated with each particle size grouping included protein, polysaccharides, lipids and COD. A comparison of organic matter within each particle size range and type of wastewater showed that the amount of settleable matter was highest (35–55 %) with manure and generally not present with synthetic wastewater. Additionally the total non-soluble fraction, requiring hydrolysis prior to assimilation by microorganisms, was 59–96 % with manure, 69–73 % with raw or primary wastewater, about 50 % with secondary effluent and only about 1 % with synthetic wastewater [71].

The characterization of organic fractions (carbohydrate, COD and proteins) and total phosphorous (TP) with respect to particulate fractions for industrial primary effluent (PE) and swine manure (sMA) was also quantified [71]. The supra colloidal and settleable fractions combined for sMA ranged from 77–93 % compared to 46–53 % for PE for all the organic fractions and TP and this is indicative of the important role of disintegration and hydrolysis in the treatment of highly particulate waste streams. These results suggest that the supra colloidal and settleable fractions contribute a significant amount of the organic loading in a treatment system and highlights the important role of disintegration, hydrolysis and hydraulic retention time (HRT) to effectively access these carbon and nutrient sources biochemically. Generally at higher disintegration and hydrolysis rates one would expect a shift in particle size distribution (PSD) to smaller particle sizes and a higher sCOD fraction in the MLSS and permeate. This higher sCOD and shift in PSD was observed at lab-scale when using an ultrasonic pre-treatment step in a membrane bioreactor [71].

2.3.2 Reactor Configuration

The literature review revealed that most of the studies treating highly concentrated waste streams (Table 2.1) have used bench scale and side stream configurations (sAnMBR-B) [17, 32, 33, 36, 39–41, 47] with upflow sAnMBR also being used [34, 49]. The use of pilot scale sAnMBRs [31, 35, 37, 38, 42] has been less common and the immersed (iAnMBR)

configuration [43, 46, 53] least common. The preference of sAnMBR over iAnMBR, when dealing with sludge or manures, appears to be related to improved cake fouling control through crossflow shear as compared to that developed with gas sparging. The main advantages of using lab-scale reactors over pilot or full scale installations, include improved control and focus of operation, greater consistency of the feed stream and associated reduced costs. However, extending the findings of lab-scale results to full scale is generally challenging and needs to be qualified taking into consideration scalability issues. Operating at pilot scale is more costly but generally there are fewer issues with up-scaling the findings to full-scale applications. Typically at pilot scale the feed variability and process controls are closer to real conditions and the findings are better predictors of full-scale applications. However, the higher costs of pilot operations over bench-scale applications are often a deterrent. Currently there were no reported studies treating mixed sludge using full scale AnMBRs and there are few pilot-scale applications that reported treating municipal sludge (Table 2.1).

2.3.3 Membrane Selection

Both MF and UF membranes (Figure 2.2), with various NPS or MWCO (30–450 nm, 70 – 2000 kDa; mostly in the 200–400 nm range (Tables 2.1–2.3)) have been used and found to act as very efficient solid-liquid separators to allow for decoupling and independent control of the SRT and HRT. The key factor that influences the selection of the membrane is the NPS or MWCO because they have a direct bearing on the intrinsic membrane resistance (R_m). Theoretical R_m can be calculated using the Poiseuille flow model [72] (Eq. 2.1) and operationally using Darcy's Law (Eq. 2.2):

$$R_m = \frac{8\delta_m\theta}{\epsilon r^2} \tag{2.1}$$

$$J = \frac{Q}{A_m} = \frac{\Delta P}{\eta R_m} \tag{2.2}$$

where δ_m (m) the effective membrane thickness; θ, the pore tortuosity factor;ϵ is the porosity of the membrane; r (m), the effective pore radius; J ($m^3/m^2{\cdot}s$ or LMH), is the flux; Q (m^3/s), the filtration rate; A_m (m^2), the total membrane surface area; ΔP (Pa), the pressure drop across the membrane or the transmembrane pressure; η (Pa·s), the permeate dynamic viscosity and R_m (m^{-1}), the clean membrane resistance.

Typically because of the complexity of membrane structures the fundamental appropriate characteristics are difficult to determine and Eq. (2.2) is commonly used with a new membrane and clean water flux to determine the R_m based on a plot of changing ΔP versus flux curve with a known η.

The membrane physical–chemical properties and morphology (key functional groups, hydrophobicity, electrostatic charge, surface texture) also have a pronounced effect on R_m through particle-membrane interactions but are not easily quantifiable. It has been reported that when treating TWAS using a negatively charged tubular membrane the sustainable flux performance improved by 15–45 % (5–9 LMH) when compared to a neutral membrane [31].

2.3.4 Temperature Considerations

Temperature is known to influence a number of important factors related to the performance of AnMBRs. As the operating temperature is increased: (1) the maximum specific growth rates ($\hat{\mu}$) and substrate utilization rates, as predicted by the Arrhenius expression ($\mu_T = \mu_o \cdot \phi^{(T-T_o)}$), will increase up to an optimum and then will decrease; (2) the yields will decrease and the half saturation affinity constant will decrease due to increased lysis and maintenance energy requirements respectively; (3) a shift in reaction pathways due to microbial population changes (mesophiles to thermophiles) with corresponding changes in thermodynamic yields and (4) disintegration and hydrolysis rates increase due to the combined effect of an increase in kinetic rates of hydrolytic enzymes, bacterial growth and solubility [1, 3, 73].

Table 2.4 describes the typical temperature operating ranges and the corresponding ideal reaction rates expected from psychrophilic, ambient, mesophilic and thermophilic operation of anaerobic digesters treating municipal sludge [1] and identifies a minimum SRT to prevent washout. In terms of physical chemical processes, increased temperature, will also decrease the viscosity of sludge or wastewater and increase the solubility of lipids and long chain fatty acids [73].

Table 2.4: Temperature operating conditions and expected methanogens specific growth rates with corresponding minimum SRTs in anaerobic digestion [1–3]

Condition	$\hat{\mu}_{net}$ [a] (d^{-1})	SRT_{min} [b] (d)	Temperature (°C)	Notes
Psychrophilic	0.04 – 0.10	18 – 9	4 – 15	Lowest rates, stable process
Ambient	0.12 – 0.18	8 – 5	18 – 20	Low rates, stable process
Mesophilic	0.20 – 0.40	4 – 3	25 – 40	Higher rates, stable process
Thermophilic	0.5 – 0.8	2 – 1	45 – 62	Highest rates, less stable process

[a] Net specific growth rate range of methanogens ($\hat{\mu}_{net}$) at corresponding temperature ranges.
[b] The minimum solids retention time (SRT_{min}) ranges corresponding to washout conditions.

At lower operating temperatures (psychrophilic or ambient temperatures), lower kinetic rates, higher sludge density (Figures 2.4) and viscosity are expected and make these lower temperature regimes more challenging when compared to the more common mesophilic and thermophilic treatment applications (Tables 2.1–2.3). However operating at lower temperatures may improve the energy balance provided that the lower kinetic and viscosity issues can be addressed.

The equations for water density ρ_w as a function of temperature (T in K) and sludge density (ρ_{sl}) based on %TS are given in Eqs. 2.3 and 2.4 [2]. A contour plot shown in Figure 2.4 were derived by combining Eqs. 2.3 and 2.4 over a range of TS concentrations and temperatures that span psychrophilic to thermophilic operation:

$$\rho_w = 1000 \cdot \frac{1 - (T + 289)}{508929 \cdot (T + 68.1) \cdot (T - 4.0)^2} \tag{2.3}$$

$$\rho_{sl} = \frac{100 \cdot \rho_w \cdot \rho_s}{100 \cdot \rho_s + \%TS \cdot (\rho_s - \rho_w)} \tag{2.4}$$

Figure 2.4 shows a gradual increase of sludge density with increasing TS and decreasing temperature that is not immediately obvious from a cursory assessment of Eqs. 2.3 and 2.4 alone. From Figure 2.4 it can be seen that sludge densities don't appear significantly different within the typical operating TS and T range for anaerobic treatment of sludges.

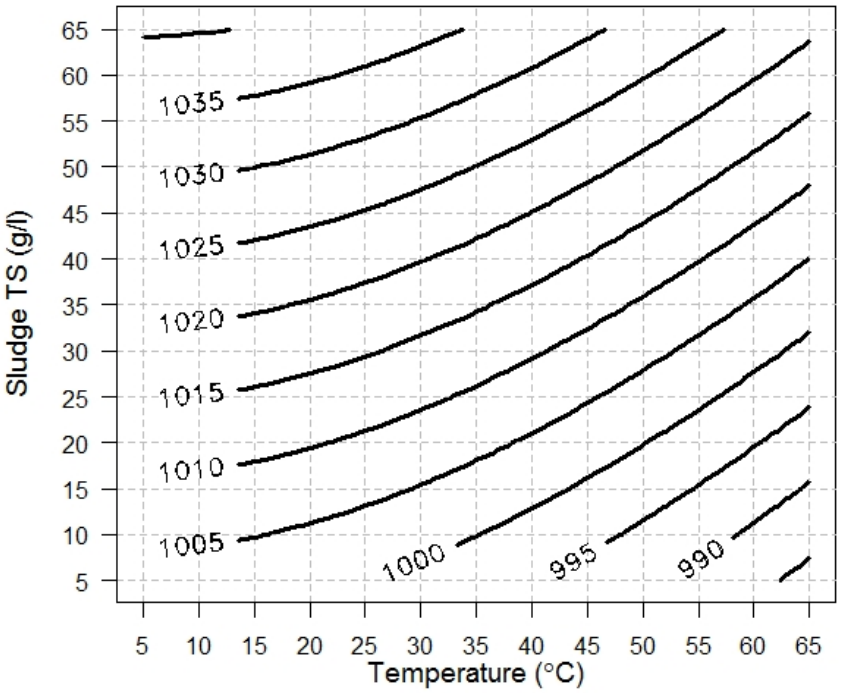

Figure 2.4: Sludge density (g/L) contour curves with respect to temperature and TS

A review of the IWA ADM1 model [1], which provides an established platform for anaerobic process modelling and simulation, identifies disintegration of composites, like municipal sludge, as the first important step and not considered to be biologically mediated but influenced by temperature through the temperature dependance of the disintegration rate coefficient. ADM1 models disintegration as a first order process based on the feed concentration of composite matrices (i.e., sludge) and the disintegration rate coefficient, a function of temperature (T), with HRT and SRT entering the formulation based on the reactor configuration.

Hydrolysis, as described by the ADM1 model, is also strongly affected by temperature due to the biokinetic parameters associated with the specific degraders that use exoenzymes to hydrolyse disintegrated products for energy and growth. For example carbohydrates are hydrolyzed to soluble monosaccharides and are readily consumed by monosaccharide acidogens.

When treating mixed sludge or highly particulate feeds, the appropriate design SRT/HRT ratio will be influenced by the operating T as well as the relative amount of each type of sludge. Generally a higher SRT/HRT and T result in a higher soluble fraction with improved stability and higher biogas generation, however this also demands higher operating costs (for heating the sludge) and an appropriate selection of SRT/HRT is warranted for sustainability. For a feed matrix that has a high percentage of soluble forms (most wastewaters (WW) and synthetic wastewaters (sWW) the disintegration and hydrolysis steps are less significant, when compared to highly particulate feed matrices. Because the soluble fraction in WW and sWW is generally higher the required bioreactor SRT/HRT is significantly lower (Table 2.2 and 2.3) when compared to high particulate feed streams (Table 2.1). Additionally AnMBR treating WW or sWW have a significantly less inert fraction to deal with which may otherwise occupy a significant fraction of the bioreactor and potentially burden the overall performance of the system.

A study of the treatment of mixed municipal sludge using a sAnMBR, operated at a constant flux mode (7 LMH) at mesophilic (35 °C) and thermophilic (55 °C) conditions was reported by Meabe et al. 2013 [33]. Better filtration was observed in the thermophilic conditions and this was partly attributed to lower sludge viscosity however a higher irreversible fouling was experienced and this required more extensive alkaline and acid chemical cleaning primarily attributed to inorganic fouling [33]. To ensure a viable operation the benefits of higher operational flux, due to lower viscosity at higher temperature, will need to be compared to the cost associated with more frequent chemical cleaning, downtime, wear on the membrane and higher heating energy costs.

The treatment of mixed municipal sludge (mSL) in a continuously operated bench-scale sAnMBR at 35 and 20 °C was reported by Takashima, 2012 [36]. The reactors were operated without wastage for 86 days causing the MLSS to increase from 12 to 35 g TSS/L and during this period the flux was found to decrease from 12 to 2 LMH. The VS reduction was 54 and 48 % at 35 and 20 °C, respectively and there was a corresponding 16 % reduction in biogas production. Based on the preliminary results it was recommended that sludge pretreatment may be necessary to improve the soluble fraction and reduce the MLSS accumulation during continuous long term operation of a sAnMBR [36]. This work suggests that low temperature treatment will experience a reduced biogas production but the reduction may not be significant when compared to mesophilic operation and operating at 20 °C. However preliminary disintegration or a hydrolysis enhancement step may be required to improve the system viability.

Two controlled lab-scale iAnMBR were used to compare the feasibility of treating kraft evaporate condensate (KEC) at mesophilic (37 °C) and thermophilic (55 °C) conditions over a 135 day period by Lin et al., 2009 [39]. A common feed KEC supplemented by methanol to raise the COD to 10 g COD/L was used and a similar bulk sludge MLSS was maintained in both reactors at 10 g TSS/L with minimal wasting resulting in a long SRT of 230 days. The filtration resistance in the thermophilic reactor was found to be about 5–10 fold higher than the mesophilic iAnMBR and it was found that the bulk sludge contained a higher concentration of soluble microbial products (SMP), biopolymer clusters (BPC) and larger proportion of smaller particles (< 15 ηm). Analysis of the cake layer found that the thermophilic iAnMBR contained a higher concentration of organic and inorganic

foulants, a larger proportion of smaller particles and a denser more compact structure. It was concluded that a smaller particle size distribution (PSD), increase in SMP, BPC, bound EPS as well as cake layer structure are major factors influencing membrane fouling [39]. The findings of this study when extended to sludge treatment will likely underestimate the impact of the inert particulate fraction on the cake structure and treatment performance but identifies relevant potential issues when operating at thermophilic conditions.

Performance comparisons at 35, 25 and 15 °C of sWW using a well controlled lab-scale integrated anaerobic fluidized bed iAnMBR was investigate by Gao et al., 2014 [58]. Under stable operating conditions the COD reductions were 74, 67 and 51% at 35 25 and 15 °C, respectively and these were influenced by the influent COD and temperature. VFAs were found to accumulate at the lower temperature and this was related to reduced methanogenic activity which was further observed in the methane generation reduction of 0.17, 0.15 and 0.1 L CH_4/L·d, at 35, 25 and 15 °C, respectively. Fouling was observed to be most severe during the 15 °C operation and GAC (7 g/L) was used as a fouling mitigating additive which proved to reduce fouling by protein adsorption. Others have compared PAC with GAC and found PAC to be more effective and this was attributed to the greater surface to volume ratio of PAC over GAC [62]. The EPS fouling layer analysis indicated that the protein fraction was the dominant factor causing membrane fouling at low temperatures (15 and 25 °C) [58, 74]. Because of the use of sWW the impacts of particulates, hydrolysis byproducts and their interactions with soluble fractions found in particulates of real wastewaters, were not investigated however the issues associated with EPS and effects of coagulant aids such as PAC or GAC are considered relevant to sludge treatment.

2.3.5 MLSS Considerations

The operating MLSS range of AnMBRs has generally been between 10 and 50 g TSS/L in high solids wastewater applications (Table 2.1), less than 10 g TSS/L for normal wastewater treatments (Table 2.2) and less than 5 g TSS/L for synthetic wastewaters (Table 2.3). Regardless of the wastewater matrix being treated a high mixed liquor suspended solids (MLSS) in a completely stirred tank reactor (CSTR) is desirable to maximize the active biomass concentration. By operating at high MLSS a low F/M is possible to minimize the time required for stabilization of the feed biodegradable constituents. However operating at high MLSS increases the viscosity and typically the fouling propensity in the membrane system.

The use of membrane reactors has the benefit of decoupling the SRT and HRT to allow a high reactor MLSS while maintaining a low HRT with a corresponding high throughput and maintaining a smaller reactor footprint. At extended SRTs the potential to improve recalcitrant contaminants and TrOCs reduction, including potential reduction of EDCs, was reported to a potential benefit [56].

A fundamental study, using anaerobic sludge and a sAnMBR-MF (NPS of 1 μm) bench scale apparatus with MLSS from 2–36 g TS/L and at ambient conditions (25 °C), was used to investigate the effect of MLSS and crossflow hydrodynamics (CFV range of 0.1–0.8 m/s) by Ho et al. 2009 [75]. The anaerobic sludge was found to follow non-Newtonian rheology characteristics that increased non-linearly with an increase in TS concentration.

The apparent dynamic viscosity (η) was reported to vary from 1.3–10 mPa·s over a TS concentration range of 5–30 g TS/L when the shear rate (γ) was 500 s^{-1}. A system of equations was presented for different shear-rates and TS and they showed that the η increased exponentially as the TS increased at both low and higher γ. These reported findings suggested that operating at high TS would require higher shear stresses (τ) to control cake build up but this would incur additional operating costs.

Operating in the turbulent domain ($R_e > 2100$) has been a common strategy to control membrane cake build up [9]. The crossflow velocity (CFV) when operating sAnMBR or gas sparging with iAnMBR, is commonly used to increase the shear rate (τ) to achieve turbulent hydrodynamic conditions. For sAnMBR the CFV is controlled by the pump flow setting of the recirculating sludge pump and directly affects the energy consumption of the system. Using a pump with a variable-speed drive to adjust to the minimum required CFV, depending on the TS reactor concentration to achieve turbulent conditions, would improve the sustainability of a system.

Municipal anaerobic digested sludge rheology was investigated by Baudez et al (2013) [76] and it was experimentally demonstrated that τ and η were dependent on T and TS according to the Herschel–Bulkley model coupled with a Bingham model as given by Eqs. 2.5 and 2.6. The γ and Newtonian Re are given by Eqs. 2.7 and 2.9 [75]:

$$\tau = \alpha(\phi - \phi_o)^m \tag{2.5}$$

$$\eta = \eta_o e^{\beta \cdot \phi} \tag{2.6}$$

$$\gamma = \frac{8v}{D} \tag{2.7}$$

$$Re = \frac{\rho v D}{\eta} \tag{2.8}$$

where τ, is the shear rate given in Pa; ϕ, the sludge percent TS (%); ϕ_o, the TS (%) below which there is no yield stress; m is a parameter related to the fractal dimension of sludge flocs (dimensionless); α, is a model parameter (Pa); η, the viscosity (mPa·s); η_o the dynamic viscosity of the sludge (mPa·s); β, is a model parameter (dimensionless); γ, shear strain (s^{-1}); v, crossflow velocity (m/s) and D, the membrane diameter (m) and Re, Reynolds number for Newtonian fluids. Anaerobic sludge at TS > 5 g/L acts as a non-Newtonian fluid and Eq. 2.5 needs to adapted according to the Re given in Ho et al (2009) [75]. Temperature corrections for the parameters in Eqs. 2.5–2.7 are required to account for temperature effects [76].

2.3.6 Transmembrane Pressure (ΔP) and Flux (J)

The operating transmembrane pressure (ΔP) and flux (J) are related through the permeability ($K = J/\Delta P$) based on Darcy's law and the operation of MBRs are typically defined as constant J or constant ΔP operations. The primary goal in MBR operation is to maximize the sustainable flux (J_s) while maintaining the ΔP at a minimum or to maximize the K in order to maximize the system viability.

The literature shows significant range in both the operating J and ΔP regardless of the feed matrix being treated (Table 2.1–2.3) and this is an indication of the complex inter-relationships between the key operating conditions and J–ΔP operating set points. The typical sustainable flux (J_s) when treating high solids waste streams has been between 5–20 LMH and ΔP was typically less $<$ 60 kPa except for short term high flux operations where the ΔP was as high as 500 kPa (Table 2.1). When treating wastewater streams the sustainable flux of 30–50 LMH was reported to be achievable at corresponding ΔP of $<$ 30 kPa but in some cases dealing with industrial wastewaters fluxes $<$ 10 LMH at ΔPs of $<$ 30 kPa have been reported. Synthetic wastewaters have typically consisted of completely soluble feed matrices and others that included a mixture of particulates (Table 2.3) and this was reflected in the high nominal flux range of 5–50 LMH and range of ΔP between 5–200 kPa.

The complex J and ΔP interrelationship have been explained by considering the hydrodynamic interactions of the system coupled with the wastewater constituent fractions (particulates, colloidal, soluble) and the membrane-particulate interactions that lead to the formation of fouling layers (gel or cake layers, or pore blocking) based on the concentration boundary layer (CBL) physical model [9, 15].

It was observed that the membrane surface resistance increases as the concentration of the rejected solute increases near the membrane surface (this is the effect of concentration polarization), the formation of a gel layer (precipitation sparingly soluble polymeric macromolecules and scaling) and the surface accumulation of retained particulates forming a cake layer. In sAnMBR configurations the CFV is typically used to induce turbulent conditions causing shear induced back diffusion diminishing the gel or cake layer buildup. Keeping the ΔP low is another common strategy to prevent cake layer compression or loss in the cake layer permeability [9].

A review by Wang and Wu, 2009 [15] of the recent literature, on type of fouling, reported that cake fouling is generally the dominant form and contributed up to 80 % of the overall fouling when treating wastewater. Further, the formation of the cake layer was attributed to operational flux (J) locally exceeding a critical flux (J_c) regime above which a certain particle size would deposit on the membrane. Specifically it was reported that if operation is started at a sub-critical flux ($J < J_c$) the cake layer is only gradually formed causing a gradual increase in the ΔP with cake layer formation only due to the local flux becoming supra-critical. Continued operation at this stage induces a compaction of the cake layer and forming a gel layer causing a decrease in the permeability. Typically the gel layers cause irreversible fouling while the cake layer forms mostly reversible fouling. When the operation starts at a supra-critical flux, a cake layer forms and the ΔP increases more rapidly causing immediate cake compression and loss of permeability. The cake layer was closely examined and found to consist of large quantities of sludge flocs and but mostly resulting in reversible fouling. The cake layer specific resistance has been qualitatively related to the structure and morphology as described by the cake surface roughness, thickness, particle size distribution, protein and polysaccharide composition and distribution associated with extracellular polymeric substances (EPS)[15].

Considered collectively the above review suggests that operating at a sub-critical flux and

minimum ΔP with optimized hydrodynamic conditions (crossflow velocity or gas sparging to induce turbulence at $Re > 2100$ and promote back transport) will maximize the sustainable flux (J_s) by keeping the cake layer thin and reducing cake compression. Alternatively, for low J_s a larger membrane area, would be required and as the cost of membranes becomes lower this may be an alternative strategy to extend the application of AnMBRs to more concentrated feed matrices.

2.3.7 Organic Loading Rate and Hydraulic Retention Time

The particulate fraction in the feed matrix and the associated HRT required to hydrolyze this particulate fraction has traditionally established the upper limit for the organic loading rate (OLR). When feed wastewaters had high particulate fractions (Table 2.1) the typical OLR has been $< 2\ kg\ COD/m^3{\cdot}d$ with a corresponding HRT range of $1-20$ days. The HRT variability was directly related to the feed particulate fraction. For wastewater treatment with a low particulate fraction (Table 2.2) $OLR < 3\ kg\ COD/m^3 \cdot d$ have been reported with a corresponding HRT range of < 4 days. The higher soluble fraction in the wastewater resulted in lower required HRT values for hydrolysis. For synthetic wastewater (sWW) treatment with mostly dissolved fractions (Table 2.3) the OLR was reported to be < 20 $kg\ COD/m^3 \cdot d$ with a corresponding HRT of < 1 day. Some sWW treatment applications were able to operated at a low HRT (< 0.25 d) and this was a result of operating at high ΔP (> 100 kPa) and treating a highly biodegradable soluble COD feed stream. The sWW studies had the most variability in OLR and HRT when compared to authentic wastewater and sludge streams. Some specific applications highlighting the OLR and HRT implications on the AnMBR operation are discussed further below.

Lin et al., 2013 [29] in their review, identified that the HRT range employed for high-solids content streams was $1.5-12$ days and this was primarily for the purpose of addressing the long hydrolysis time of particulates and simultaneously reducing the OLR when compared to the treatment of municipal and industrial wastewaters. The OLR when using AnMBR was observed to be quite variable from 1–10 kg COD/m_3·d but consistently maintaining a COD reduction above 90 % thereby demonstrating the capacity of AnMBRs to effectively handle large variations in organic loadings [29].

A review by Meng et al., 2009 [77] included HRT among other operating conditions (SRT, F/M and OLR) that alter the sludge characteristics and indirectly impact the fouling propensity of the system through microbial byproducts including bound (bEPS) and soluble EPS (sEPS) and inorganic foulants such as struvites, calcium carbonates, biological and inorganic precipitants. A higher HRT was recommended as a favourable operating condition to mitigate membrane fouling.

Fuchs et al., 2003 [40] investigated the treatment of wastewater from a chicken slaughterhouse and sauerkraut brine operation at an OLR of 6–8 kg COD/m^3·d using a controlled lab scale mesophilic sAnMBR with MLSS in the range of 38–55 g TSS/L and a CFV of 2–3 m/s as a reversible fouling control strategy. Prior to feeding the wastewater was screened (0.75 mm rotary sieve) effectively reducing the particulate fraction dimensions to less than 1 mm. The COD-removal efficiency was generally above 95 % with a corresponding methane generation rate of 0.12–0.32 and 0.20–0.34 NL $CH_4/g{\cdot}COD_r$, respectively. The reactor

stability was assessed by monitoring VFAs. When VFAs reached a critical value of 1700 mg/L the OLR was reduced from 6.3 to 4.2 kg COD/m^3·d to stabilize the system and prevent a pH drop. A maximum OLR of 8.6 kg COD/m^3·d was achieved for a short duration (10 days) at a MLSS of 55 g TSS/L with a maximum methane yield of 0.34 NL CH_4/g·COD_f. The slaughterhouse WW was treated at a loading rate of 4.3 kg COD/m^3·d at a HRT of 1.2 days and a stable VFA concentration of less than 500 mg/L. The reactor was overloaded at an OLR of 7.4 COD/m^3·d with the VFAs increasing to 3000 mg/L. This work demonstrated the feasibility of high organic loading rate of WW while maintaining a low F/M ratio by retaining the biomass and increasing the MLSS. The filtration flux was in the range of 5–10 LMH based on a CFV of 2–3 m/s. A high pumping rate was required to provide CFV velocity that controlled fouling but it was proposed that this may be offset by the energy value of the generated methane which was estimated at 5–20 $kW \cdot h/m^3$ when using slaughterhouse wastewater as the substrate [40]. The high OLR was indicative of a highly biodegradable WW and the effectiveness of the 0.75 mm rotary sieve at reducing the particulate-COD fraction. Such a high OLR could not be sustained when treating a high particulate WW due to the disintegration and hydrolysis requirements which suggests a minimum SRT and HRT of 10 days [2].

2.3.8 Solids Retention Time

Solids retention time (SRT) has been reported to be one of the most important operational parameters determining both treatment performance and affecting membrane fouling [77]. The interaction effect of SRT with T, OLR and HRT was discussed in the previous sections. However one main advantage of MBRs is the ability to decouple and independently control SRT and HRT. The membranes enable, effectively, complete retention of the active biomass and thus provide easier control of the bioreactor MLSS and F/M ratio.

When treating high solids waste streams the SRT have typically been in the range of 15–90 days with some higher SRT values corresponding to non-optimal lab-scale operations where sludge wasting was minimal or not applied over a short operational period (Table 2.1). When treating authentic wastewaters (WW) the SRT has been in a higher range from 30–300 days due to the higher particulate fraction generally requiring a larger SRT (to increase the MLSS) to minimize the hydrolysis time. When treating synthetic wastewaters (sWW) the SRT has generally not been controlled and significant variability in values in the range of 4–120 days have been reported. In a significant number of cases for authentic WW and sWW the SRT has not been reported because sludge wasting was not controlled. Not knowing the operating SRT makes the reproducibility, interpretation and extension of the findings, to full-scale applications, more challenging.

A review by Meng et al., 2009 [77] found the influence of SRT on fouling to be indirect and related to EPS (bound and soluble) and biopolymer clusters (BPC) that impacted sludge characteristics (hydrophobicity, flocculation ability, surface charge and sludge viscosity). As the SRT decreased from about 15 to 5 days at a MLSS of 5 g/L, the extracted EPS (eEPS) increased, which reduced the membrane permeability. Also when the SRT was increased from about 10 to 53 days, the eEPS decreased from about 52–30 mg/g VSS. Additionally increasing $SRTs$ (from 20 to 100 days) resulted in excessive membrane fouling and an SRT

range of $20-50$ days was considered optimum [77]. The above findings provide a basis for the selection of appropriate operating SRTs and HRT/SRT ranges.

Dagnew, et al., 2010, 2012 [31, 78], investigated the use of a sAnMBR to treat TWAS at HRT/SRT ratios of 16:30, 8:30 and 8:16 days with corresponding VSLR values of 0.8, 1.4 and 1.8 g VS/m^3·d. An overall decrease in solids (TS, VS, TSS) concentration with an increase in HRT and an increase in HRT/SRT ratio was observed. This was a result of the decreased organic loading and decreased thickening associated with decreasing HRT/SRT. The VS_r was found to decrease from 49 to 37 % as the OLR increased from 2 to 3 kg COD/m^3·d and the SRT decreased from 30 to 16 days. The reactor stability was monitored through tAlk and VFA measurements and a minimum α (VFA/tALK) factor of 0.003 indicated the reactor stability [31, 78]. If a system were operated with a higher $OLRs$ or lower $HRTs$ and high HRT/SRT ratio it should be monitored for reactor biochemical stability and VS_r to ensure stable treated sludge ($>$ 38% VS_r is typically required for treated sludge to be considered sufficiently stable for land utilization [2, 25]).

The additional challenge of operating at a high SRT is the need to decrease the wastage resulting in an increase in the reactor MLSS reducing the sustainable flux (J_s and requiring an increase in the membrane area (A_m). Thus reducing the SRT ratio by SRT or HRT control will likely incur additional costs due to the increase in membrane area or the implementation of membrane fouling mitigation strategies (increasing the level or frequency of membrane cleaning, increasing the CFV or gas sparging rate).

Reducing the HRT/SRT ratio by increasing the SRT will increase the MLSS and the viscosity in the bioreactor but will reduce the F/M ratio and may allow a greater OLR as demonstrated by Meabe et al. 2013 [33] at both mesophilic and thermophilic conditions. The sustainable OLRs of 6.4 and 4.6 kg COD/m^3·d were achieved at 55 and 30 °C, respectively, at a HRT/SRT ratio of 7/30. The reactor solids increased to 34–40 g VS/L and 90–120 g TS/L with a significant build up of inert solids in the system. An HRT/SRT of 7/50 was investigated for 74 days under thermophilic conditions but was not sustainable due to the significant buildup of solids (160 g TS/L) and a high viscosity of the MLSS causing difficulty in agitating the sludge with buildup of VFAs and COD in the permeate or soluble fraction [33]. This work identified the need to balance the HRT/SRT ratio with the OLR to ensure MLSS do not increase excessively in the system and impact permeability of the system and the biochemical process. The biochemical stability was effectively monitored by measuring the permeate or soluble COD and VFAs or α value in the system and ensuring these parameters stayed within established ranges indicative of stability [2].

2.4 Membrane Fouling and Mitigating Strategies

Fouling and the high cost of membranes are commonly considered the most significant barriers to the wider application of MBR technology [9, 79]. Fouling results from deposition of organic and inorganic solids, colloids and solutes onto or into the membrane pores by either adsorption, pore-clogging or pore-blocking. Operationally, fouling is generally considered as reversible (managed on-line through shear, back flushing, relaxation of permeation) or irreversible (requiring chemical cleaning typically off-line). Fouling has been attributed to

characteristics of the feed matrix, the biomass or the membrane and is influenced by the reactor operating conditions [9, 29, 77, 79, 80].

A recent extensive critical review on foulants and fouling indicators by Wang et al., 2013 [79] identified eEPS, soluble microbial products (SMP) and colloidal microbial products (CMP) as key fouling agents. Based on a review of extraction methods, EPS was divided into bound (bEPS) and soluble (sEPS) fractions. The bEPS was further divided into tightly (tbEPS) and loosely bound (lbEPS). The sEPS was identified as being equivalent to SMP. Colloids included colloidal microbial products (CMP) and are considered equivalent to biopolymer clusters (BPC) and different from SMP. Solutes included dissolved organic matter (DOM) and SMP. In terms of size distribution, solutes (DOM, SMP, EPS) are $< 0.5\ \mu m$, colloids (CMP, BPC) are between 0.5–10 μm and sludge particles (MLSS) are typically $> 5\ \mu m$. Interrelationships between the various foulants have been linked through cellular biochemical activity (synthesis, decay, hydrolysis, degradation) and physical processes (adsorption, transformation, solubilization) [79]. These observations were corroborated by Meng et al., 2009 [77] who identified SMP, bEPS and hydrodynamic conditions as the main factors influencing membrane fouling. Additionally a study by Gao et al., 2012 [74] on EPS, identified the EPS protein (PN) and polysaccharide (PS) distribution and concentration ratio (PN/PS), correlated to the biomass hydrophobicity, to be more significant in influencing fouling rates than the individual PN or PS alone.

The equality of sEPS to SMP, under conditions where hydrolysis was not significant, was previously suggested based on the proposed unified theory [81] which equated SMP to biomass associated products (BAP) and utilization associated products (UAP) closely linked to biomass decay and substrate utilization, respectively. However subsequent work using an anaerobic chemostat [82] investigating the production and consumption of SMP reported results that showed that SMP would be significantly overestimated if associated with substrate utilization. This controversy is still unresolved and has potentially significant implications in trying to predict the source and impacts of EPS and SMP on fouling propensity when treating concentrated wastewater streams.

From a detailed review of the literature (Table 2.1–2.3) and recent review papers [9, 29, 77, 79, 80] various fouling mitigation strategies have been identified including: (1) physical shearing of surface cake (CFV and gas sparging),(2) off-line use of chemical agents (water, bases, acids), (3) addition of reagents directly to the sludge (PAC, GAC, cationic polymers, EDTA), (4) permeation-relaxation operation and back flushing and (5) selection of charged membranes with particular materials, configuration, surface charge, hydrophobicity and nominal pore size (NPS) distribution. The main reported fouling mitigating strategies with the intended general effects are summarized in Table 2.5. Generally a sequence of steps including different procedures have been combined and reflected the complex nature of the fouling layers to be dealt with.

An example of a successful cleaning strategy that was reported for a sAnMBR with tubular membranes when treating TWAS, included: (1) a short hot water flush (50 °C), (2) scrubbing the membrane using sponge balls, (3) a caustic solution (NaOH(aq), pH=10) flush and (4) a citric acid and hydrochloric acid solution bath ($C_3H_4(CO_2H)_3OH + HCl$ (aq), pH=2) [86]. The primary mode of fouling was attributed to inorganic foulants since the

Table 2.5: Membrane fouling mitigating strategies and expected effects

Membrane Fouling Mitigating Strategies[a]	Expected Effects[b]
Hot water	A common first step with sAnMBR to remove loosely adhered solids [31]
Physical abrasion	Sponge balls, CFV and gas sparging ($Re \geq 2100$) were typically used to remove or reduce the sludge cake buildup, reduce the PSD and floc structure [31, 35, 44, 83, 84]
Alkaline solutions	Alkali solutions (pH=10) used to dissolve organic foulants [15]
Acid solutions	Acetic and hydrochloric acid (pH=2) and others acid solutions were used to dissociate salts within an organic matrix and help dissolve inorganic foulants [31]
Relaxation-permeation	To reduce the sludge cake compression and consolidation and reduce the sludge cake resistance to shear-induced back-diffusion [31]
PAC, GAC, polymers	Coagulant aids to promote aggregation of the colloidal fraction of particulates and increase the PSD [31, 37, 45]
Micro screens	Used to separate the membrane from direct contact with large particulates [43]
Low J and low ΔP	Reduced fouling propensity with operational flux (J) below the critical flux (J_c) at constant pressures operation or during low ΔP operation at constant J [31, 41, 49]
Membrane properties (NPS, MWCO)	MLSS-membrane interactions were found to vary based on membrane charge, hydrophobicity, NPS, MWCO and interrelated with hydrodynamic conditions [78, 85]

[a] PAC, powdered activated carbon; GAC, granular activated carbon; polymers, refers to cationic polymers; NPS, nominal pore size; MWCO, molecular weight cut-off.
[b] Generally a sequence of multiple fouling mitigating strategies were used with some methods particular to sAnMBR or iAnMBR.

caustic solution flush provided only minimal flux recovery. Dagnew et al. 2013 [32] also compared a sAnMBR and an iAnMBR (hollow fiber membrane) in the treatment of TWAS operating at a subcritical flux range in a constant pressure mode (about 30 kPa). Fouling was reported to be effectively controlled by crossflow abrasion (turbulent conditions were maintained by a crossflow velocity of 1 m/s) and permeation-relaxation (5:1 minutes cycles) for an operational period of 160 days. These approaches were considered typical of the sequential processes employed to mitigate membrane fouling and highlights some of the challenges related to fouling control.

As part of the fouling mitigation strategies concurrent measurement of fouling is typical with the application of a fouling index (FI) given by Eq. 2.9 for constant pressure (FI_P) operation or Eq. 2.10 when operating at constant flux mode (FI_J)

$$FI_P = \frac{\Delta J}{\Delta t} \tag{2.9}$$

$$FI_J = \frac{\Delta P}{\Delta t} \tag{2.10}$$

where Δt is the operational period or time of permeation. The fouling rate as measured by the FI has been found to transition from rapid to slow which was typically attributed to initial pore blocking followed by gradual cake dominated fouling [15, 16, 80].

2.5 Fouling Propensity using VFM

It is generally important to distinguish reversible from irreversible fouling since each requires different control strategies and potentially impact the operational visibility of an AnMBR. From an operational perspective reversible fouling is typically associated with cake fouling and controlled by on-line methods such a permeation rest or relaxation period or by increasing the operating shear using a higher crossflow velocity. Irreversible fouling is associated with the membrane pore constriction and controlled by off-line chemical cleaning. Residual membrane fouling is associated with foulants that where not adequately removed during a maintenance clean or rest period [9].

The Membrane Bioreactor–Vito Fouling Measurement (VFM) method has been used to distinguish and quantify reversible and irreversible fouling attributed to the system fouling propensity [87, 88]. The VFM method is useful both on-line or off-line under constant pressure crossflow operations and allows the measurement of both the cumulative reversible and irreversible fouling resistances at a given cumulative throughput. The method has been verified at lab-scale MBR from collected authentic wastewaters from a full-scale MBR plant [87] but not previously applied to sludge treatment using AnMBR. The VFM approach has the potential to be implemented in an on-line sensor for an advanced control system to determine the type of fouling and use of the appropriate cleaning strategy (i.e., timing and type of cleaning) to optimize the system viability [88].

The VFM method used the logged flowrate and pressure data to compute the permeability (K) and corresponding R at the beginning and end of each permeation cycle of a sequence of cycles. The K values are computed using Eq. 2.11 and normalized (at 20 °C) using the calculated dynamic viscosity ratios (η_T/η_{20}, Eq. 2.12) converted to resistances (R) using Eq. 2.13 and resolved into cumulative total resistance (R_t), reversible resistance (R_r) and irreversible resistance (R_i) based on the resistance in series model (Eq. 2.14) over a sequence of permeation cycles:

$$K = \frac{J}{\Delta P}\frac{\eta_T}{\eta_{20}} \tag{2.11}$$

$$\eta_T = \eta_{20} 1.024^{20-T} \tag{2.12}$$

$$R = \frac{1}{\eta_T K} \tag{2.13}$$

$$R_t = R_m + R_r + R_i \tag{2.14}$$

where η_{20} is the dynamic viscosity of pure water at 20 °C and η_T, is the temperature corrected permeate dynamic viscosity at temperature T (°C). Figure 2.5 provides an example of a typical VFM curves for both the reversible and irreversible fouling propensity at various normalized throughput.

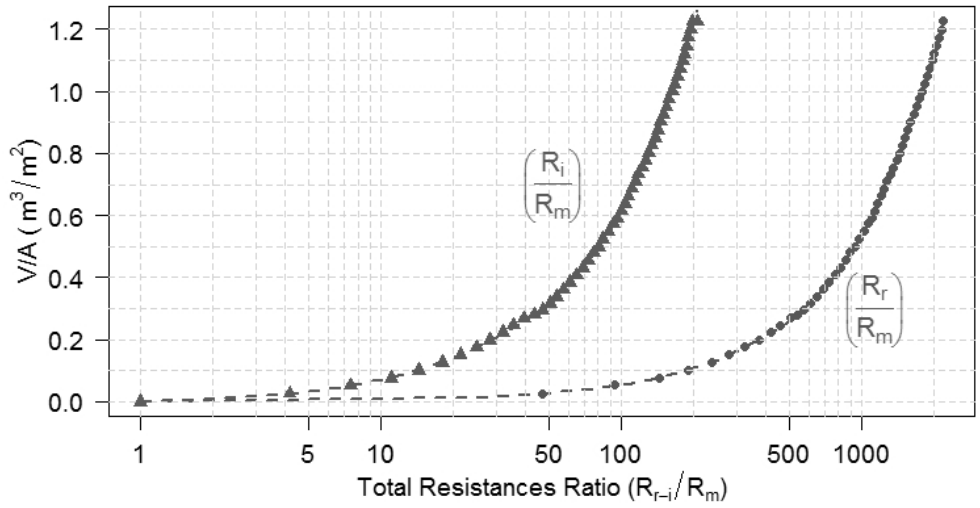

Figure 2.5: Example VFM diagram providing a measure of reversible (R_r/R_m) and irreversible (R_i/R_m) fouling propensity.

The total irreversible resistance ratio, R_i/R_m (x-axis of Figure 2.5), represents the cumulative irreversible accumulation of foulants necessary to be removed to recover the irreversible permeability based on a the corresponding cumulative throughput (V/A, y-axis). The total reversible resistance ratio, R_r/R_m (x-axis of Figure 2.5), represents the cumulative reversible foulants or the reversible permeability degradation accumulation, that was removed, during the rest or relaxation phase of the permeation cycles and corresponding to the cumulative throughput (V/A, y-axis). The VFM curve may be considered a standard system-matrix unique fingerprint due to the normalization of both the x- and y-axis [88]. The VFM method appears to be a potentially important method, based on direct measurements, that can distinguish and quantify reversible and irreversible fouling which may be used as part of a fouling control strategy.

2.6 Flux Modeling

A recent critical review of biokinetic and filtration modeling [89] has reported that models are starting to be used for hypothesis verification at full scale applications. However greater emphasis for the use of models for design, optimization and control, rather than continued

model development, was recommended along with improved data collection for model calibration and validation. In an effort to assess the factors that influence flux decline the now classical blocking models of Hermia [90] modified by Field et al, (1995) [91] by incorporating a crossflow parameter may be applied for in analysing a sAnMBR membrane performance. The fundamental characteristic equations that describes the main fouling modes were given by the system of differential equations given by Eq. 2.15 [91]:

$$\frac{-1}{A^2J^3}\frac{dJ}{dt} = k\left(\frac{1}{AJ}\right)^m \tag{2.15}$$

where k, the clogging constant, and m, the blocking mode. The functional forms of Eq. 2.15 with a crossflow parameter added for cases of m = 0, 1 and 2 apply directly to crossflow operations and given by Eqs. 2.16, 2.17 and 2.19. Equation 2.18 is the standard blocking model (m=3/2) and is not amenable to adaptation for crossflow operation [91]:

$$\frac{dJ}{dt} = -GJ^2(J - J_s) \qquad m = 0 \tag{2.16}$$

$$\frac{dJ}{dt} = -\sigma J^2 + K_i J \qquad m = 1 \tag{2.17}$$

$$\frac{dJ}{dt} = -K_s A^{\frac{1}{2}} J^{\frac{3}{2}} \qquad m = \frac{3}{2} \tag{2.18}$$

$$\frac{dJ}{dt} = -\left(\frac{\sigma J_o}{\epsilon_o}\right) J + K_b J_o \qquad m = 2 \tag{2.19}$$

The predictions of Eq. 2.16–2.19 may be used to investigate the dominant fouling mode by comparing the best model fit to measured flux data. Figure 2.6 provides example model predictions of the relative flux (J/J_o) decline versus filtration time based on a specific range of model parameter values within the expected practical range for sludge filtration.

The relative flux declining curves in Figure 2.6 show geometrical similarities but also significant differences associated with the specific parameter values within and between the different fouling mechanisms.

Equation 2.16 describes the flux (J) variation when cake filtration (m = 0) dominates with $G = \alpha k_c/J_o R_o$, where α, is the specific cake resistance (m/kg); k_c, the cake filtration constant (kg/m^3); J_o, the initial flux at $t = 0$ at the beginning of the filtration cycle ($m^3/m^2 \cdot s$); R_o, the initial membrane resistance at $t = 0$, at the beginning of the filtration cycle and J_s, is the critical flux or critical flux value if cake fouling is to be avoided.

Equation 2.17 describes the flux variation when intermediate blocking (m = 1) dominates with σ, the blocked area per unit volume of filtrate (m^{-1}); K_i, the back flux factor induced by crossflow (s^-1) and $J_i = \sigma K_i$, the critical flux or critical flux if intermediate blocking is to be avoided ($m^3/m^2 \cdot s$).

Equation 2.18 describes the change in flux when standard blocking (m = 3/2) dominates with the clogging constant $K_s = 2CQ_o^{\frac{1}{2}}/LA_o$ ($1/m^3$), representing the specific retention or

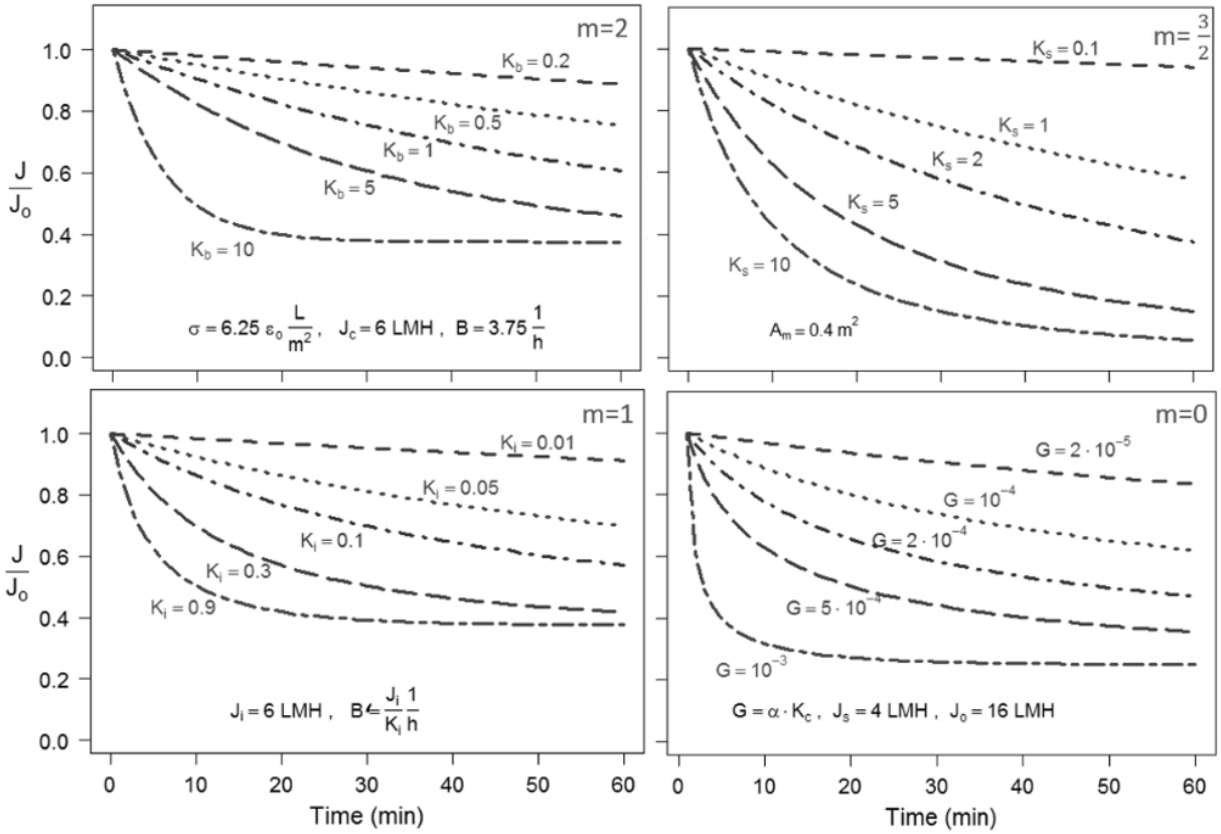

Figure 2.6: Example model predictions of the relative flux (J/J_o) declining curves versus time of filtration under a range of relevant parameter values based on solutions of Eqs. 2.16 – 2.19.

deposition of solid particles within the membrane pores per volume of filtrate [90]. This type of fouling is not impacted by crossflow induced shear forces and Eq. 2.18 is not able to predict a critical flux.

Equation 2.19 describes the change in flux when complete pore blocking (m = 2) dominates with ϵ_o, the membrane porosity; B, the back flux factor corresponding to the rate of particle removal from the top of the pore openings (s^{-1}) and $J_c = K_b \epsilon_o / \sigma$, the critical flux below which no flux decline occurs ($dJ/dt = 0$).

The role of flux in relation to fouling mechanisms was reviewed by Wang and Wu, 2009 [15] with a focus on gel and cake formation. A fundamental analysis on the causes of the gel layer and cake formation, based on hydrodynamic forces, was developed and related to three commonly observed distinct operational flux transitions when operating at a steady imposed ΔP. The three flux transitions were characterized as a rapid decline in flux, followed by a slow flux decline and then a further rapid flux decline. The transition points are point with the onset of non-linear changes in ΔP or J and shift from sub-critical to supra-critical flux operation. The flux decline and transitions were correlated to sludge cake characteristics, morphology and three dimensional structure that affect the overall cake resistance [15].

This flux modeling review highlights potential insights gained through modeling of flux decline through the adapted classical blocking models applied to sAnMBR operated under different operating conditions.

2.7 System Sustainability

Minimizing the energy or carbon footprint of wastewater and sludge treatment facilities along with resource recovery are global initiatives and recently highlighted in the report, "State of Science Report: Energy and Resource Recovery from Sludge", 2008 [92]. The report identifies sludge-to-biogas processes as the most suitable options for energy recovery and those technologies using the least amount of chemicals being the most preferred. The reports also identifies emerging technologies for energy recovery and includes an aerobic and anaerobic membrane system (AFC^{sm} Process) operated in the thermophilic temperature range (40–70 °C) for sludge treatment. The viability of TWAS treatment using AnMBR at mesophilic conditions, producing a net positive energy balance, was demonstrated at pilot scale [78] and opportunities to extend and demonstrate the energy balance for mixed sludges, other waste streams and operating under other conditions (ambient or psychrophilic temperature regimes) may further improve the energy balance.

An energy balance model for an AD was formulated by Lübken et al., 2007 [93] and included the major energy components including methane production (E_M) (thermal and electrical), pumping of the sludge (E_P), heating the sludge (E_H), stirring to maintain a CSTR (E_X) and heat losses (E_L) from the reactor and other miscellaneous heat losses (Eq. 2.20–2.25) [93]:

$$\Delta E = E_M - (E_P + E_H + E_X + E_L) \tag{2.20}$$

$$E_M = E_{Me} + E_{Mt} = Q_{CH_4} \cdot H_C \cdot (\eta_e + \eta_t) \tag{2.21}$$

$$E_P = q \cdot \rho \cdot g \cdot H \cdot t \cdot \frac{1}{\eta} \tag{2.22}$$

$$E_H = q_f \cdot \rho_s \cdot C_p \cdot (T_i - T_f) \tag{2.23}$$

$$E_X = S_x \cdot V_r \cdot t_m \tag{2.24}$$

$$E_L = A_r \cdot K \cdot t \cdot (T_i - T_o) \tag{2.25}$$

where ΔE is the net energy balance of the system; E_M is the potential energy recovery from methane generated divided into electrical (E_{Me}) and thermal (E_{Mt}) components; E_P is the pumping energy input; E_H is the energy to heat the sludge; E_X is the mixer energy input and E_L is the heat loss from the digester reactor tank all in (kWh/d). For AnMBR the AD model (above) may be readily adopted by including pumping associated with CFV (sAnMBR) or gas sparging (iAnMBR) to the E_P term to include the membrane component.

The calculation of E_H requires the energy needed to heat the sludge which depends on q_f the rate of sludge feed to the digesters (m^3/d), ρ_s the sludge density (kg/m^3), C_p the sludge specific heat capacity (assumed equal to that of water) and feed sludge temperatures (T_f).

The heat loss (E_L) is based on the reactor surface area (A_r), the heat transfer coefficient (K), the time of operation (t) under consideration and temperature difference between the reactor and surroundings (T_i–T_o) [93]. To compute the mixing energy (E_X) the average specific power of the stirrer (kw/m^3) of 0.0065 [2] may be applied to the bioreactor active volume (V_r) for the mixing duration (t_m).

The energy demands of wastewater treatment were considered for MBRs by Martin et al., 2011 [94] in an energy model which included the energy demands of operating the system and energy recovery from methane generation. The general model included the energy for fouling control measures (pumping to maintain a CFV or gas sparging), permeate pumping and energy recovery from methane. It was found that the energy requirements for heating the bioreactor to mesophilic conditions could only be compensated by methane generation with high strength wastewaters above 4–5 g COD/L and net energy recovery would only be achievable at low temperatures. The high membrane costs and typically lower sustainable fluxes under AnMBR have shown a high variability in energy demand (0.03–3.6 kWh/m^3) highlighted the need to investigate fouling control measures at pilot and full-scale applications [94].

Dagnew, 2010 [31] assessed the energy balance when treating TWAS under mesophilic conditions reported a net positive energy balance of 6 and 15 MWh/m^3 of feed sludge when operating pilot sAnMBR at HRT/SRT ratio of 15/30 and 7/30 with a corresponding VSLR of 0.8 and 1.6 kg VS/m^3· d, respectively. The feed sludge VS concentration in both operating conditions was 12 g VS/L or 1.2 % VS [31].

Opportunities to increase the positive energy balance include operating at ambient operating conditions (reduce energy heating inputs and heat losses) and adding PS to the feed to improve the biodegradable fraction and increasing the VS feed concentration to potentially increase the biogas generation potential. The methane yield, contributing to the viability of the system, was observed to be greater than 0.30 L CH_4/g COD_r with the biogas consisting of 60–70 % methane [29, 31].

2.8 EDCs in Sludge Treatment

The presence of endocrine disrupting compounds (EDCs) in sludge has been widely reported [4, 5] but there is limited information in the literature on the potential of EDCs to induce endocrine disruption effects on non-target organisms [95] and how sludge treatment processes [96–98] may alter the concentration or mobility of EDCs in the final treated sludge or biosolids. The concentration and mobility of EDCs in biosolids is an issue of primary concern in the reuse of biosolids to provide nutrients to agricultural lands that may result in the release of EDCs from solids to receiving ground water and surface water sources [99–101].

In an effort to better understand the fate of trace organic contaminants (TrOCs) and EDCs in sludge the United States Environmental Protection Agency (US EPA) published the results of a nation wide field survey in 2009 [4] that assessed the chemical quality of treated sludge for the presence and concentration of selected pharmaceutical, hormones and other TrOCs some of which are classified as EDCs. Another similar comprehensive review was

published by Clarke et al., 2011 [5] that investigated organic contaminants (OCs) present in biosolids destined for agricultural use. Table 2.6 lists the range of concentrations of various pharmaceuticals, hormones, bisphenol A and polybrominated diphenyl ethers (PBDEs) found in municipal sludge [4, 5]. From Table 2.6 a large concentration range is evident (low ng/g to low mg/g).

Table 2.6: Pharmaceuticals, hormones and suspected EDCs concentration ranges (ng/g) found in municipal sludge of various treatment levels [4, 5]

Pharmaceuticals	Min	Max	Median
Triclocarban	0.187	441	21.7
Ciprooxacin	0.075	41	5.4
Triclosan	0.334	133	3.9
Ooxacin	0.025	58	3.1
Tetracycline (TC)	0.038	5	0.6
4-ETC	0.041	4	0.6
Diphenhydramine	0.037	6	0.5
Doxycycline	0.034	5	0.4
Azithromycin	0.008	5	0.3
Miconazole	0.007	9	0.2
Cimetidine	0.004	8	0.2
Fluoxetine	0.01	3	0.1
Carbamazepine	0.009	6	0.1
Erythromycin-Total	0.002	0.2	0.02
Hormones	**Min**	**Max**	**Median**
Coprostanol	7.7	43700	827
Cholesterol	2.3	5390	295
Cholestanol	3.9	4590	187
Epicoprostanol	0.9	6030	108
Beta Stigmastanol	3.4	1330	63
Campesterol	2.8	524	47
Stigmasterol	0.5	569	42
17α-Ethinyloestradiol	0.004	0.02	0.005
17β-Estradiol	0.005	0.35	0.02
Oestriol	0.01	0.2	0.01
Oestrone	0.01	1	0.03
Others	**Min**	**Max**	**Median**
Bisphenol A	0.04	300	0.3
Polybrominated diphenyl ethers	0.01	4.7	1.4

The estrogens and xenoestrogens are well known EDCs and were typically found in the low ng/g range or at the limit of quantification. Despite the low concentration levels estrogens and estrogen mimicking compounds are within the range of potential adverse

environmental effects (low ng/L [95]) and are high on the priority list of the regulating community as evidenced in the inclusion of 17α-ethinylestradiol (αEE2) and 17β-estradiol (βE2) in the new list of 12 contaminants [22] which requires the EU under the Water Framework Directive [102] to develop strategic approaches towards mitigating the risk to the aquatic environment by improved treatment and management practices of wastewaters and residuals.

The mobility of selected TrOCs from biosolids amended sites has been reported on and found to be compound specific and influenced by the biosolids treatment and application method [99–101, 103, 104]. Generally it was found that rainfall will mobilize hormones from biosolids-amended agricultural fields resulting in concentrations in surface runoff from 2–220 ng/L. Many of the parent compounds were generally persistent over the study period and suggests that ambient soil conditions may not be sufficient for complete degradation or bioconversion. Various EDCs in municipal STP sludge extracts and aqueous leachates from biosolids amended sites were also found to contain transformation byproducts of E2 and EE2 with potential carryover into groundwater and surface water receivers [104].

To asses the impact of anaerobic and aerobic sludge treatment, Langdon et al., 2011 [96] conducted an Australia wide survey to investigate the presence and concentration of selected EDCs in biosolids. Biosolids samples were collected from 14 STPs and analyzed for eight compounds including: 4-t-octylphenol (4tOP), 4-nonylphenol (4NP), triclosan (TCS), bisphenol A (BPA), E1, βE2, estriol (E3) and αEE2. Only 4tOP, 4NP, TCS, and BPA were detected in all samples and E1 was detected in four of the 14 samples. In the four samples, the concentrations ranged from 0.05 to 3.08 mg/kg, 0.35 to 513 mg/kg, 0.01 to 11.2 mg/kg, 0.01 to 1.47 mg/kg and 45 to 370 ηg/kg, respectively. The sludge samples that were anaerobically treated generally had higher concentration of EDCs compared to aerobically treated sludge. A comparison to other survey work revealed that the 4NP, TCS and BPA concentrations in Australian biosolids were lower than global averages by 42, 12 and 62%, respectively. The European Union limit value for NP in biosolids is 50 mg/kg, which was exceeded in 29 % of the samples (4/14). The quality of the treated sludge and biosolids was not generally related to the treatment process conditions [96].

An extensive Canadian literature review, commissioned by the Canadian Council of the Ministers of the Environment (CCME) [98] tried to correlate chemistry to treatment processes. It was reported that in relation to hormones and sterols, αEE2, estrone (E1) and βE2) were among the most frequently reported and E1 was typically at the highest concentration (mean of 106 ng/g d.w.) with treatment type having an influence. Four sludge treatments were evaluated (composting, heat drying, mesophilic and thermophilic anaerobic digestion) and it was found that anaerobic digestion was the least effective at reducing hormones and sterols. The data on removals in various treatment methods was limited and the interpretation of data was made difficult by the reporting of different sludge types throughout the literature. The removal of αEE2, estrone (E1) and βE were highly variable but were as high as 70-90 % during mesophilic and thermophilic digestion under well controlled lab-scale studies [98]. The study identified gaps in knowledge of removal of estrogens and sterols with respect to sludge treatment and recommendations for policy direction included further work in better understanding sludge treatment, along with the fate of estrogens (conjugate and metabolites of estrogens or xenoestrogens) and sterols [98]. The findings

of the CCME study [98] were corroborated in a study by Lorenzen et al., 2014 [105] who investigated aerobically and anaerobically treated municipal sludge at 17 Ontario STPs (13 sites using mesophilic anaerobic digestion and 4 sites using aerobic digestion at ambient temperatures) to assess the estrogenic (17β-estradiol (βE2) as the positive reference) and androgenic (testosterone (T) as the positive reference) activity using two *in vitro* bioassay screens (recombinant yeast assay (YES) and human ovarian cell culture bioassay (HOC)). Further corroboration was provided in the work of Citulski (2012, [106]) in the use of YES to assess the ER of biosolids extracts from various Ontario STPs.

Treatment using an AnMBR for the removal of 38 TrOCs in a synthetic feed was investigated by Monsalvo et al., 2014 [107] with a focus on the role of the membrane fouling layers in removing TrOCs. The 38 TrOCs represented a range of relevant environmental contaminants and encompassed a range of physical chemical properties. A key reported finding was that 9 of 38 TrOCs received greater than 90% removal and the remaining 23 TrOCs showed less than 50 % and this was attributed primarily to biologically mediated biotransformation however sorption onto the fouling layers was considered an important process. The fouling layer that developed over the membrane was characterized into 4-separate operational layers, based on ease of removal, as: (1) external; (2) cake; (30 residual and (4) irreversible layers. The 4-fouling layers were analyzed for the 38 TrOCs and the percent removals were assigned to each layer. No definitive removal trends could be clearly established however the study clearly identified the importance of the fouling layer as a key removal barrier for TrOCs.

The use of bioassays, to compliment chemical analysis, both *in vitro* and *in vivo* has been used effectively to asses endocrine disruption associated with TrOCs found in treated sludge [105, 106]. The bioassay approach allows testing the complex mixture of chemicals that may be active under a similar mode of action. The yeast estrogen screen (YES) is a commonly reported bioassay developed by Routledge et al., 1996 [108] to assess whether chemicals are estrogenic through an *in vitro* estrogenic response (ER). In interpreting the ER bioassay results one needs to keep in mind that the ER only suggests a potential endocrine disruption *in vivo* which would need to be further verified though whole organism exposures. In addition it was recommended to investigate causality of *in vivo* effects by undertaking specific additional bioassays supported by analytical techniques [20, 109]. Through the use of bioassays the parent compounds, metabolites and conjugated forms typically present in complex environmental samples and for which analytical methods may not be readily available, are taken into account assuming a similar mode of activity to the test receptor [21].

The current knowledge base related to endocrine disruption associated with EDCs in sludge based on *in vitro* and *in vivo* studies and impacts of sludge treatment is growing yet still fragmented area of research. However, the current weight of evidence appears to support the concerns about impacts to the natural environment. Regulators have begun considering legislative measures to more fully characterize and control effluent discharges from sewage treatment plants (STP) (point sources) and industrial farm operations as related to the land application of treated sludges or biosolids (non-point sources). For example the EU 2000 Water Framework Directive (WFD) [110], lists 17α-ethinyl-oestradiol, oestrone, ibuprofen, anhydro-erythromycine, sulfamethoxazol, carbamazepine, sotalol and amidrotrizoic acid as priority substances of concern that need to be reduced to prescribed levels from point sources

or industrial farm operations discharging to heavily effluent impacted source waters. These source waters are not typically impacted from biosolids land application operations however concerns have been raised about a number of known EDCs including NPEOs, NP, Oestrone, 17α-estradiol originating from biosolids land utilization operations [4, 19, 111, 112].

An expert workshop (GWRC Workshop 2003, [113]) on EDCs analytical and biological tests provided three relevant recommendations: (1) not only estrogenic but also anti-estrogenic effects have to be considered because both effects may compensate each other in environmental samples; (2) when analysing waste water samples using bioassays, cytotoxic compounds have to be eliminated prior to analysis in order to get reasonable results and (3) sampling is at least as important as the analytical determination itself; this is especially true for solid samples and liquid samples containing solid material the results obtained will always depend on the extraction procedure used.

2.9 Summary of Literature Review

This literature review provided significant insight into the operating conditions that are likely to impact treated sludge quality, fouling mitigation strategies and the viability of sludge treatment by AnMBRs. This review also identified significant gaps in the area of sludge treatment with AnMBRs under ambient and thermophilic conditions. The reported research included a limited number of high strength wastewaters with most applications using well controlled lab-scale reactors. Little information has been generated at larger scales that might influence membrane performance when treating sludge under full scale operations.

The particulate fraction of the feed matrix was found to be the dominant distinguishing factor between sludge and WW. This is related closely to the need to incorporate disintegration and hydrolysis steps in the AnMBR design when treating concentrated wastewaters or sludge. Because of the strong temperature dependency of the disintegration and hydrolysis steps for sludge, the minimum design SRT based on reduced kinetics and increased viscosity at lower operating temperatures particularly below 35 °C is typically 15 days.

The preferred AnMBR configuration when treating sludge was the sAnMBR when compared to the iAnMBR. The key reason for this was the greater challenge of inducing turbulent conditions of high viscosity mixtures using sparging versus crossflow velocity (CFV) as a means to control cake fouling. To achieve turbulent conditions and effect scouring of the cake buildup on the membrane, CFV was preferred over gas sparging. For sAnMBR a workable CFV of about 1 m/s up to a MLSS concentration of 28 g/L would induce adequate turbulent conditions. Operating at higher MLSS would require higher CFV and may not be sustainable due to higher pumping costs.

Operating AnMBRs at constant pressure (ΔP) and constant flux (J) are both common when treating various wastewater streams. When treating sludge the typical sustainable flux was between 5–20 LMH with a ΔP typically < 60 kPa. A successful strategy to prolong the time between cleaning the membrane for a sAnMBR was to operate at sub-critical flux and incorporate a permeation-relaxation (P-R) strategy. At sub-critical flux solids concentration polarization towards the membrane is minimized and was found to

reduce overall fouling and maintain the membrane permeability for a longer duration versus operating at supra-critical flux. The P-R operational strategy allowed an opportunity to scour the membrane to remove sludge cake buildup during the relaxation period and reduce the cake compression that may otherwise promote gel formation and reduce the membrane permeability prematurely.

An organic loading rate (OLR) of 1–3 kg VS/$m^3 \cdot d$ was common for sludge treatment using AnMBR which typically achieved a VS reduction (VS_r) above 50 % with a corresponding methane yield of 0.56 Nm^3 CH_4/kg VS_r. The OLR is inversely related to the HRT which is a key parameter directly related to the viability of the process operation. A minimum HRT for a typical flowthrough single stage AD is 15 days [114] for treating sludge and this defines the minimum reactor volume. For AnMBR the HRT may be reduced by increasing the reactor MLSS through the increase of the SRT with the ability to reduce the reactor footprint and improve the system viability.

The AnMBR operating SRT has perhaps the most significant influence on the bioreactor performance affecting the VS_r, methane yield, the operating MLSS and viscosity. The SRT was found to be directly related to the MLSS causing an increase of the viscosity of the sludge matrix. The SRT was found to influence the membrane permeability indirectly though its effect on EPS generation within the bioreactor. An optimal SRT range of 20–50 days was found to be reasonable under mesophilic operating conditions. At lower SRT (5–15 days) and lower MLSS (5–10 g/L) the EPS concentration increased and reduced the membrane permeability. As the SRT was increased from 10 to 53 days the EPS decreased and membrane fouling was observed to decrease.

Membrane fouling is an unavoidable consequence of treating wastewater streams using AnMBRs and is attributed to characteristics of the feed matrix, the biomass, the membrane inherent characteristics (NPS, surface charge, surface structure) and is influenced by the reactor operating conditions in complex interrelated ways. The EPS, influenced predominantly by the SRT, was the key biological factor that directly influenced fouling. Inorganic foulants, related to the feed characteristics are dominated by the presence of cations (Fe^{3+}, Ca^{2+}, Mg^{2+}) forming chemical complexes. Effective fouling mitigation strategies have included: (1) operating at sub-critical flux; (2) judicious selection of SRT to control the MLSS and viscosity effects; (3) timely application of physical abrasion of the membrane to keep the thickness of the sludge cake to a minimum (online permeation-relaxation operation); (4) ΔP selection and control to minimize compression of the sludge cake that would reduce the permeability; (5) additives to reduce the colloidal fraction (PAC, GAC) and (6) off-line chemical cleaning using various alkaline solvents (for biological foulants) and acidic (citric acid, hydrochloric acid) to remove inorganic foulants. Due to the complex nature of fouling a multiple and sequential approach to fouling mitigation was generally applied. Fouling was quantified by using a fouling index (FI) formulated based on a constant pressure or constant flux operation.

The "Hermia-Field" flux-model formulations and VFM fouling propensity characterization provide general mechanism of analyzing dominant modes of fouling and the quantification of reversible (operationally removable on-line) and irreversible (needing a off-line chemical clean) modes of fouling. The identification of dominant flux-model parameters would

assist the choice of design, operating conditions that would potentially reduce maintenance cleaning and better utilize operational resources.

The system sustainability "black-box" model formulation identified the key heat loss factors (sludge heating, reactor heat loss, mixing, sludge pumping) with the ability to quantify the energy and heat potential generation from the methane production and to compare various operating conditions. An energy balance and sustainability comparison may be assessed using this model. It has already been reported that a net positive energy balance can be achieved, when treating TWAS [31] while operating at mesophilic conditions, but further enhancements may be achieved when operating at ambient temperatures and with mixed sludges that may have a higher volatile solids fraction.

There is growing concern among the industry of the quality of treated sludge and particularly the presence of TrOCs including EDCs, such as estrogens, found in treated sludge or biosolids that are used to supplement nutrient needs and for soil amendment in agriculture. The latest research has shown that AD is typically less effective at reducing selected TrOCs concentration in sludge compared to aerobic treatment but there is limited operational information in this area. The widespread practice of land application of biosolids to agricultural lands has peaked concerns related to the mobility of EDCs from soil with the potential for endocrine disruption at non-target endpoints. Screening level *in vitro* bioassays have been used to assess such an effect and provide a promising comprehensive approach to complement analytical chemical analysis that may be used to identify the likely chemicals of concern. With respect to sludge treatment by AnMBRs, there is a knowledge gap regarding the influence of different anaerobic treatment operating conditions on the fate of TrOCs.

Chapter 3

AnMBR and AD Digestion of Mixed Municipal Wastewater Treatment Sludges: Performance under Ambient, Mesophilic and Thermophilic Conditions

3.1 Introduction

Municipal STPs generate a large volume of primary sludge (PS) and waste activated sludge (WAS) as part of the solids-liquid separation and treatment processes of municipal wastewater. The management and treatment of the sludge consumes up to 50 % of the operating costs and its disposal or utilization is a major issue for sewage treatment plant (STP) operators, municipalities, regulators and the biosolids industry in Ontario and worldwide. Conventional anaerobic digestion (AD) is often employed for stabilization of these sludges however these digesters require extended hydraulic residence times (HRT) and hence are large and expensive processes. When compared to AD, anaerobic membrane bioreactors (AnMBRs) have the potential to: (1) increase the volatile solids loading rate (VSLRs), reduce the HRT and reactor footprint: (2) increase volatile solids reduction (VSr) and improve the rate of stabilization; (3) increase the rate of methane production and (4) reduce energy input through reduced heating load. However some of the challenges that need to be addressed when using AnMBR include: (1) the increase in the membrane fouling propensity as the MLSS increase; (2) pumping costs; (3) operational and maintenance costs associated with the membrane system and (4) potential reduction of biomass activity related to induced biofloc shear from the membrane operation. The present work compared the performance of a conventional anaerobic digester (AD) to an AnMBR over four selected operating strategies in terms of VSr, methane production and sustainability by considering the overall energy balance.

3.2 Materials and Methods

Over a 2-year period, two pilot scale (500 L) anaerobic reactors (AD and AnMBR, Figure 3.1, were set up at the Wastewater Technology Centre, of Environment Canada, in Burlington, Ontario) were fed with a common mixed sludge feed comprising an equal mass of TWAS from the Burlington Skyway STP and PS from the Hamilton Woodward Avenue STP. The reactors were operated under four different stable operating conditions that spanned a range

of solids residence times (15–40 days), hydraulic residence times (8–15 days) and operating temperatures (ambient (25 °C), mesophilic (35 °C) and thermophilic (55 °C). Table 3.1) summarizes the overall test plan. PS and TWAS were pumped from separate feed tanks to the digesters using a Moyno progressive cavity pump (Model C21B, Mississauga, Ontario) and the digested sludge was wasted from the bottom of the digesters by gravity. The reactors were mixed using an overhead 0.56 kW mechanical mixer to promote good contact between substrates and microorganism. The temperatures of the digesters were maintained by heating tape controlled by temperature controllers linked to temperature sensors in the digesters with no heating when the reactors were operated at ambient conditions in Phase 3 (P3). The program logic adopted to operate the pilot plants was based on a similar approach as described by Dagnew (2010, [31]) and involved the control of sludge feeding and wasting based on a mass basis. The feed and waste amounts were set based on the SRT and HRT set points (Table 3.1)). The mass of the AD and AnMBR pilot plants was monitored every minute by load cells located on the reactor supports. A batch operational period of 6 hours (feeding and wasting four times per day on average) was used throughout the system operation. Along with the mass, the biogas production and temperature of the reactors were logged every minute using a personal computer running Labview^{TM}.

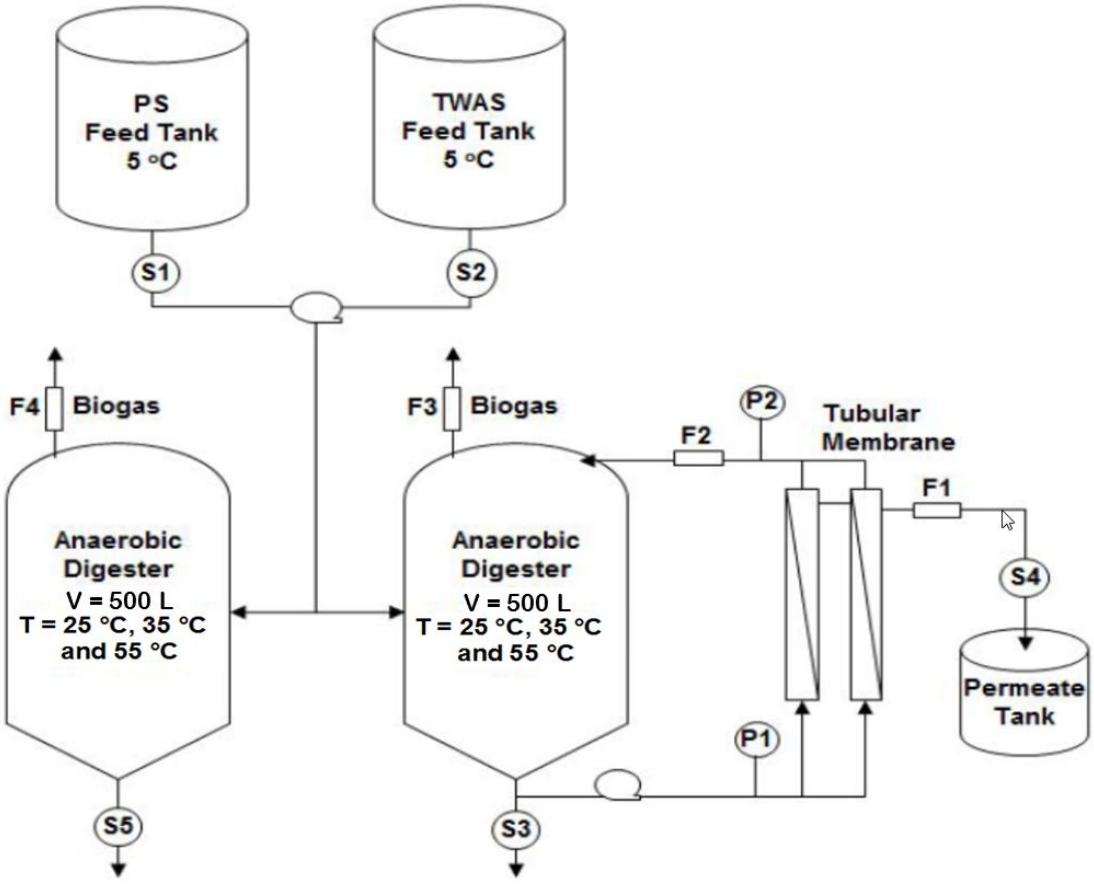

Figure 3.1: Schematic of the AD and AnMBR pilot scale bioreactors operated in parallel with sample ports (S1–S5), flow meters (F1–F4) and pressure sensors (P1–P2).

The membrane system consisted of two parallel tubular modules KOCH ABCOR® PVDF

Table 3.1: Design operating set points for AD and AnMBR Phase 1–4 (P1–P4)

Phase	Run	Operating Set Points		
		Reactor	SRT:HRT (d:d)	T (^{o}C)
P1	1	AD	1 (30:30)	35
	2	AnMBR	2 (30:15)	35
P2	3	AD	1 (15:15)	35
	4	AnMBR	3 (21:7)	35
P3	5	AD	1 (15:15)	25
	6	AnMBR	4 (30:7.5)	25
P4	7	AD	1 (15:15)	55
	8	AnMBR	3 (21:7)	55

negatively charged membrane modules with a 25 mm ID with a nominal pore size (NPS) of 20 nm or MWCO of 120 kDa and membrane area of 0.2 m^2 per module. The AnMBR was operated at constant low transmembrane pressure of 20–50 kPa using a permeation-rest mode to promote the on-line removal of reversible fouling associated with sludge cake build-up on the membrane. An off-line clean-in-place (CIP) water-flush, abrasion and chemical clean was used, as necessary, to recover lost flux due to irreversible fouling (additional details in §4.2.1). The permeation-rest duration was based on meeting the required permeation rate to match the HRT set points within each phase given in Table 3.1. The remaining time, within each 6-hour cycle, comprised the rest period (membrane module valves closed) during which time the membranes were scoured through the shearing action of the recirculating sludge to address reversible fouling (additional details in §4.2.2).

Samples were collected from the feed tanks sample ports and from the waste sludge streams for analysis of conventional sludge characteristics (TS, VS, COD, TKN) and analyzed by standard methods [115, 116]. Digester stability was investigated by measuring the concentration of VFAs (typically acetic and propionic acid), alkalinity, pH and α (ratio of VFAs to alkalinity). Data on the pilot operating conditions (mass, biogas, production membrane flux (J)) were recorded using sensors and were logged using a PLC linked to Labview^{TM}. Sources of variability in the data collection included sludge loss from pump components due to wear and noise on the load cells associated with the overhead mixers. To reduce vibration errors the mixers were programmed to turn off during the feed and waste period and this reduced the noise on the logged weight measurements. The pumps were carefully monitored for sludge leaks and pump parts serviced or replaced when the leaking was noticed.

The biogas generation rate was measured using a thermal mass flow meter (model FCI ST98L). The fractions of the biogas were determined using a gas chromatograph (GC/TCD Agilent 3000A micro GC) with a thermal detector. A molecular sieve was used to separate hydrogen, oxygen, nitrogen and methane. A second porous column was used to separate hydrogen sulfide and carbon dioxide. Argon and helium were used as carrier gases.

The COD (S) and TKN (N) are conserved through the anaerobic digestion process and mass balance calculations were conducted to assess data quality. Taking a control volume around the reactor, the mass flows entering and leaving were compared. The input sludge consisted of the combined TWAS and PS and the outputs consisted of the waste sludge from the reactor, permeate (for the AnMBR) and the methane (for COD balance only). The general equations used to calculate the COD (ΔS) and TKN (ΔN) mass balances for the AnMBR are given by Eqs. 3.1 and 3.2 with similar equations used for the AD:

$$\Delta N = Q_f N_f - (Q_w N_w + Q_p N_p) \tag{3.1}$$

$$\Delta S = Q_f S_f - \left(Q_w S_w + Q_p S_p + \frac{Q_m}{0.35}\right) \tag{3.2}$$

where Q is the mass flux (kg/d) of the feed (Q_f), waste (Q_w), permeate (Q_p) and methane (Q_m) with volume of methane in normal liters per day (NL/d); N and S, the corresponding concentration in g/L of TKN or COD in the various streams, respectively; the COD methane equivalent of 0.35 NL CH_4/g COD was used to convert methane volume to COD equivalent normalized to STP (0 °C and 1 atm) for comparison between the different phases operated at 25, 35 and 55 °C. The mass balance calculations were carried out based on 6-hour cycle measurements of the mass flux that were combined with the weekly measurements of TKN and COD for the full period through the stable operational phases P1–P4 for the AD and AnMBR pilot plants. The performance of the anaerobic digesters was compared by considering the median volatile solids loading rate, VSLR (kg VS/$m^3 \cdot d$), the organic loading rate, OLR (kg COD/$m^3 \cdot d$) and the normalized methane production (Q_m) in NL CH_4/d calculated according to Eqs. 3.3–3.5:

$$VSLR = X_f Q_f \tag{3.3}$$

$$OLR = \frac{S_f Q_f}{V} \tag{3.4}$$

$$Q_m = Q_b P_m \left(\frac{T + 273}{273}\right) \tag{3.5}$$

where X_f is the concentration of VS in the feed sludge (g/L); Q_f, the mass of sludge feed in kg/d; V, the reactor sludge volume (m^3); S_f, the feed sludge COD concentration (g COD/L); Q_m is the normalized biogas production (NL CH_4/d); Q_b, the daily biogas production (L/d); P_m is the fraction of methane in the biogas. For comparison between the P1–P4 and reactors (AD vs AnMBR) the specific methane production (SMP, Q_m/X_f or Q_m/S_f) and methane yields (MY, Q_m/X_r or Q_m/S_r), in terms of the mass fed or removed, respectively, were used.

A "black box" energy balance that accounted for the energy associated with sludge heating, pumping, mixing and heat losses and which could be potentially recovered from the produced methane was conducted to compare the sustainability of the AD and AnMBR processes

[93]. The model equations accounted for five energy inputs and outputs (Figure 3.2) with the net energy balance (ΔE_{net}) given by Eqs. 3.6–3.11:

$$\Delta E_{net} = E_M - (E_H + E_L + E_X + E_P) \tag{3.6}$$

$$E_M = E_{Me} + E_{Mt} = Q_m H_c \eta_{CHP} \tag{3.7}$$

$$E_H = Q_f \rho_s C_p (T_i - T_f) \tag{3.8}$$

$$E_L = AK(T_i - T_o) \tag{3.9}$$

$$E_X = S_x V t \tag{3.10}$$

$$E_P = Q \rho g H t \frac{1}{\eta} \tag{3.11}$$

where ΔE_{net} is the net energy balance of the system (kJ/d); E_M is the potential energy recovery from methane generated; E_H is the energy to heat the sludge, E_L is the heat loss from the digester reactor tank; E_X is the mixer energy input and E_P is the pumping energy input. The energy recovery of the system depended on the electrical E_{Me} and thermal E_{Mt} value of the methane. These in turn depended on the methane production (Q_m in Nm^3 CH_4/d), the caloric value of methane (H_c) and the use of the methane.

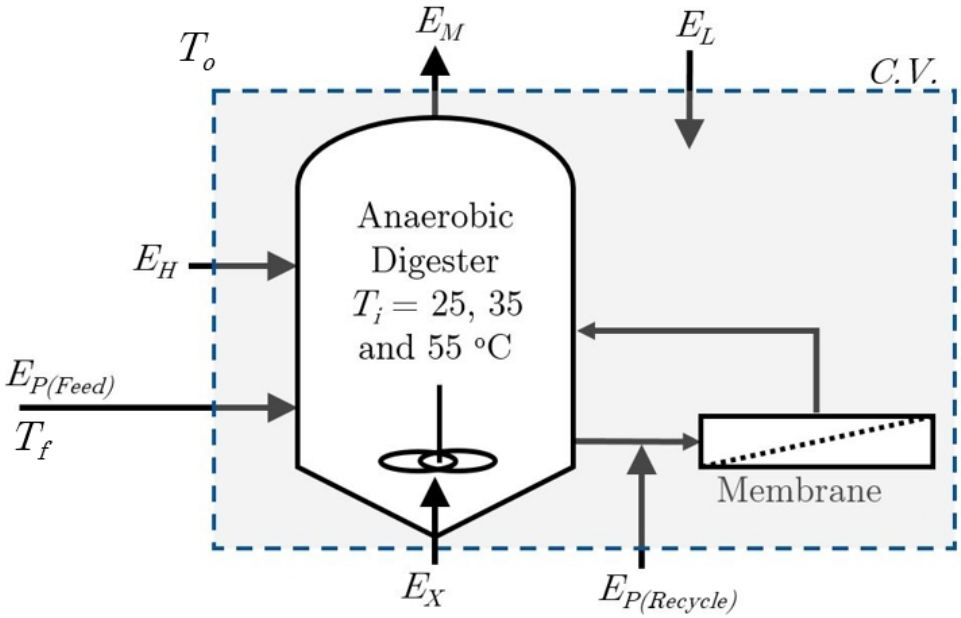

Figure 3.2: Black box energy balance model

E values represented the energy needed to heat the sludge and were calculated on the basis of the volume of sludge fed to the digesters (m^3/d), ρ_s the sludge density (taken as 1.0 kg/L), C_p the sludge specific heat capacity (assumed equal to that of water 4.18 kJ/kg·K) and feed sludge temperatures (T_f). The heat loss (E_L) was calculated from the reactor surface area (A, m^2), the heat transfer coefficient (K, kJ/$m^2 \cdot^\circ$ C) and temperature

difference between the reactor and surroundings (T_i–T_o). To compute the mixing energy (E_X) the average specific power of the stirrer (kJ/h·m^3) of 23.4 [2] was used with the reactor active volume (V) of 0.5 m^3. The net energy was also considered based on a sludge feed basis by dividing the energy components (Eqs. 3.6–3.11) by the daily amount of sludge fed to the reactors in MJ/m^3 sludge feed. The above energy model in terms of MJ/m^3 sludge feed was subsequently used to compare the energy balances and the sustainability of operation during the 4 Phases (Figure 3.5).

3.3 Statistical Assessments

The data generated in the testing was transcribed into MS Excel^{TM} files and imported into R [117] for exploratory data analyses (EDA) that included outlier detection, Normal and Log Normal goodness of fit distribution tests and basic descriptive statistics to evaluate the consistency of the data sets. The median and corresponding 95 % confidence intervals were calculated for each parameter (e.g., TS, COD and SRT) in each stream (PS, TWAS, AD, AnMBR and permeate) and each phase (P1–P4). For data sets which sere not symmetrically distributed, the median and median 95 % confidence interval (CI) represent more robust measures of central tendency and variability compared to the mean and standard deviation, and were used throughout. Comparisons between the operating conditions were conducted using the non-parametric Kruskal-Wallis (K-W) test at the 95 % confidence level [118].

3.4 Results and Discussion

This phase of the research sought to compare the performance of the AnMBR pilot with that of a conventional AD over a range of conventional and non-conventional temperatures. Table 3.2 summarizes the temperature data that was recorded during steady state operation in each phase of the testing. From Table 3.2, the temperature was controlled during the mesophilic operation (P1 and P2) with a median value of 35 °C with a 95 % median confidence interval (CI) of less than 0.4 degrees. The temperature during the ambient conditions (P3) was more variable (20–30 °C) and reflected the ambient air conditions with a median reactor temperature range of 24–26 °C and CI range of 0.4–0.8 degrees. During P4 the temperature was less variable than P3 but more variable than P1 or P2 with a median range of 54–55 °C with a CI range of 0.0–0.8 degrees. The median temperatures in P1, P2 and P4 reflect optimum temperature conditions for mesophilic and thermophilic operation [1]. Good temperature control was maintained throughout however greater temperature variability was observed during ambient operation (P3). The AnMBR compared to the AD showed a greater variability during thermophilic operation (55 °C, P4) and this was attributed to greater heat loss from the membrane system. It is believed that the temperature variability did not persist for sufficiently long times to influence the bioreactor performance.

The bioreactors were evaluated with respect to conventional sludge digestion responses to facilitate a comparison between configurations and to assess the impact of operating conditions (temperature, SRT, HRT) on performance. Table 3.2 shows that the observed operating conditions associated with stable operating periods in Phase 1–4 (P1–P4) were

consistent with the operating set points (Table 3.1). Phases 1 and 2 (P1 and P2) of this study assessed the impact of the SRT/HRT ratio on AnMBR performance at an optimum mesophilic temperature. In both phases the SRT was maintained at a relatively high value (25 and 35 days) to maximize solids conversion while the HRT was reduced by about 50 % (14.3–7.3 days). The SRT of the AD pilot was operated at values of 34 and 17 days in the two phases to establish the range of VSR that might be expected by conventional digestion at mesophilic temperatures.

Phases 3 and 4 (P3 and P4) were conducted at non-conventional temperatures to evaluate the performance of the bioreactor and membrane under conditions that would require less energy input for heating (ambient, 25 °C) or have reduced liquid viscosities (thermophilic, 55 °C). The operating SRT of the AnMBR in these phases was adjusted to accommodate expected changes in biodegradation kinetic rates at the different temperatures. The ratio of SRT/HRT was increased to 5 during P3 and maintained in the range of 3 during P4. The AD was operated at a constant SRT of 16 days (similar to Phase 2) to provide a baseline reference for the performance of conventional digestion.

Table 3.2: Key operating conditions and performance comparisons in Phase 1-4 (P1-P4)

Parameter	Reactor	Stable Operational Phases[a,b]			
		P1	P2	P3	P4
		Median(CI) n	Median(CI) n	Median(CI) n	Median(CI) n
T	AD	35.0 (0.0) 62	35.1 (0.0) 62	23.9 (0.4) 62	54.9 (0.0) 62
(°C)	AnMBR	35.0 (0.0) 62	35.1 (0.1) 62	25.7 (0.8) 62	54.5 (0.6) 62
HRT	AD	33.9 (0.2) 62	16.5 (0.2) 62	16.0 (0.1) 62	15.6 (0.1) 62
(d)	AnMBR	14.5 (0.1) 62	7.3 (0.1) 62	7.7 (0.1) 62	6.9 (0.2) 62
SRT	AD	33.9 (0.2) 62	16.5 (0.2) 62	16.0 (0.1) 62	15.6 (0.1) 62
(d)	AnMBR	34.7 (0.5) 62	24.6 (0.3) 62	39.4 (0.8) 62	22 (1) 62
SRT:HRT	AD	1.0 (0.01) 62	1.0 (0.01) 62	1.0 (0.01) 62	1.0 (0.01) 62
(d:d)	AnMBR	2.4 (0.02) 62	3.4 (0.02) 62	5.1 (0.1) 62	3.2 (0.1) 62
VSLR	AD	0.5 (0.1) 19	0.9 (0.3) 18	1.1 (0.2) 19	1.0 (0.1) 21
(kg VS/$m^3 \cdot d$)	AnMBR	1.3 (0.2) 19	2.5 (0.6) 18	2.3 (0.4) 19	2.4 (0.5) 21
OLR	AD	0.8 (0.1) 19	1.4 (0.4) 18	1.8 (0.3) 19	1.6 (0.2) 21
(kg COD/$m^3 \cdot d$)	AnMBR	2.1 (0.4) 19	3.7 (0.9) 18	3.5 (0.4) 19	3.4 (0.8) 21

[a] CI, refers to the 95% median confidence interval; n, the number of samples. [b] The stable operating period for P1–P4 was 88, 90, 95 and 87 days with a preliminary stabilization period of about 2–3-SRTs or 94, 96, 94 and 77 days, respectively.

3.4.1 Sludge Feed Characterization

Authentic sludges were obtained from operating wastewater treatment plants in this study. Hence, they were characterized for a selection of conventional sludge characteristics in order to characterize their variability with time and hence to effectively establish the loadings

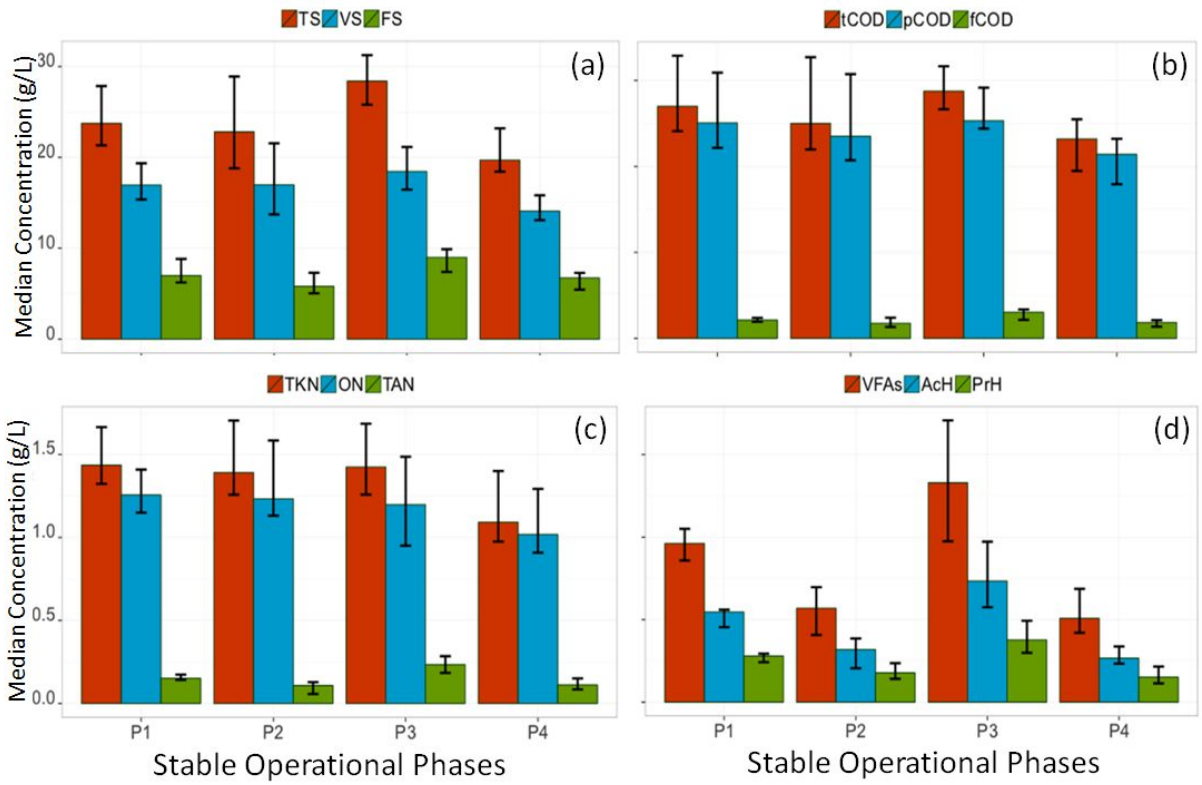

Figure 3.3: Feed (PS and TWAS combined) chemical characteristics in terms of solids (a), COD (b), nitrogen species (c) and VFAs (d) (the error bar represents the 95 % CI with n from 18–22).

onto the pilots. The values were also compared with typical values reported in the literature as a benchmark. The feed sludge was characterized for solids (TS, VS, FS); total COD (tCOD), 1.2 μm filtered (fCOD) and calculated particulate COD (pCOD = tCOD − fCOD); nitrogen species (TKN, TAN, ON) and VFAs (total VFAs as AcH, AcH, PrH). The mean values, along with the confidence intervals for these measurements are presented for each phase of the study in Figure 3.3.

From Figure 3.3(a), the feed solids varied from 2–3 % TS with the VS and FS representing 65–70 % and 35–30 % of the TS, respectively and consistent with typical municipal sludge [3, 114]. A paired comparison test between each phase for TS, VS and FS showed no statistical difference (p=0.05) between the feed for all paired phase comparisons except the following cases: (1) TS and FS concentrations in P3 were greater than those in P4 and (2) VS concentrations in P1 and P3 were greater than P4. During P4 for a significant period the feed TWAS from the Skyway STP and primary settler at the Woodward STP were both temporarily inoperative and the PS and TWAS TS concentration was lower than usual. These events caused a 30 % reduction in TS during P4 versus P3 in the common feed sludge to the AD and AnMBR pilot plants. Hence, as will be subsequently discussed, the digester results were normalized with respect to TS or VS for comparisons that were conducted between phases P1–P4.

From Figure 3.3(b), the pCOD represented between 90–93 % of the tCOD with 7–10 %

in the combined colloidal (cCOD) and soluble (sCOD) form. The high pCOD fraction is consistent with municipal sludge and intimates the importance of disintegration and hydrolysis in the conversion of composite organic material (as measured by the VS) to soluble substrates. A paired comparison test between the COD ratios (fCOD/tCOD and pCOD/tCOD) showed no statistical difference (p=0.05) between all phases except for fCOD where P3 > P2 by 30 % and pCOD where P2 > P3 by 3 %. Although statistically significant (p=0.05), the median difference between pCOD in P2 and P3 of 3 % was deemed to not be operationally significant. Similarly the 30 % fCOD difference was only 3 % of the total difference between the P2 and P3 fCOD and again did not appear to be operationally significant.

The nitrogen species (TKN, TAN, ON) in the feed sludge were considered to be indicative of the proteinaceous fraction of the sludge and showed that ON was significantly greater than the soluble (TAN) fraction. Under anaerobic or reducing conditions the TKN was considered to be equivalent to the TN since the nitrates levels would be negligible making TKN a useful measure to assess the system mass balance being conserved throughout the system. The median concentrations of TKN, TAN and ON in the feed sludge ranged from 1.1–1.4, 0.11–0.2 and 1.0–1.3 g/L, with CI ranges of 0.3–0.5, 0.03–0.1 and 0.03–0.5 g/L, respectively. A paired comparison test between phases for TKN, TAN and ON concentration showed no statistical difference (p=0.05) for TKN and ON in all cases. The feed TAN value in P3 was about 1.8 times greater than P2 and P4 and this was statistically significant. This was likely caused by a seasonal differences since P3 was conducted mostly in the summer season when pre-hydrolysis in the sewer and settlers was more feasible while P1, P2 and P4 were mostly conducted during the fall and winter seasons.

Volatile fatty acids (VFAs) comprise a readily biodegradable form for microorganisms and are generally quickly assimilated. In anaerobic digestion VFAs are typically dominated by acetic acid (AcH), and propionic acid (PrH) and to a lesser extent by butyric (BuH) and valeric (VaH) acid. The presence of these acids in the digester feed was investigated to determine the fraction of the organic loading that was contributed by readily biodegradable organics. From Figure 3.3(d), the total VFAs (AcH, PrH, BuH, iBuH, VaH and iVaH), AcH and PrH were measured and ranged from 0.5–1.3, 0.3–0.7, and 0.2–0.4 g/L, with the CI from 0.2–0.7, 0.1–0.4 and 0.1–0.2 g/L, respectively. The AcH/VFAs and PrH/VFAs ratios were between 50–60 % and 30–40 %, respectively with other VFAs (C4 and C5) representing less than 10 %. Over the duration of the study the VFAs contributed less that 10 percent of the feed COD and these results were consistent with the filtered COD results. Hence, readily biodegradable COD contributed only a small fraction of the total COD loading on the digesters. A comparison of the AcH/VFAs ratio showed no differences in all paired phases except in phase P4 which was greater than P1 by 17 %.

Overall, in terms of feed VFAs, phase P1 and P3 were equivalent but both different from P2 and P4. Similarly phase P2 and P4 were equivalent but both differed from P1 and P3. These differences in the feed VFAs between phases represent seasonal variability of the sludge generated at the STPs over the 2-year operational period but were deemed to have little impact on digester performance.

Overall, the feed sludge composition was found to be effectively constant across the 4 phases.

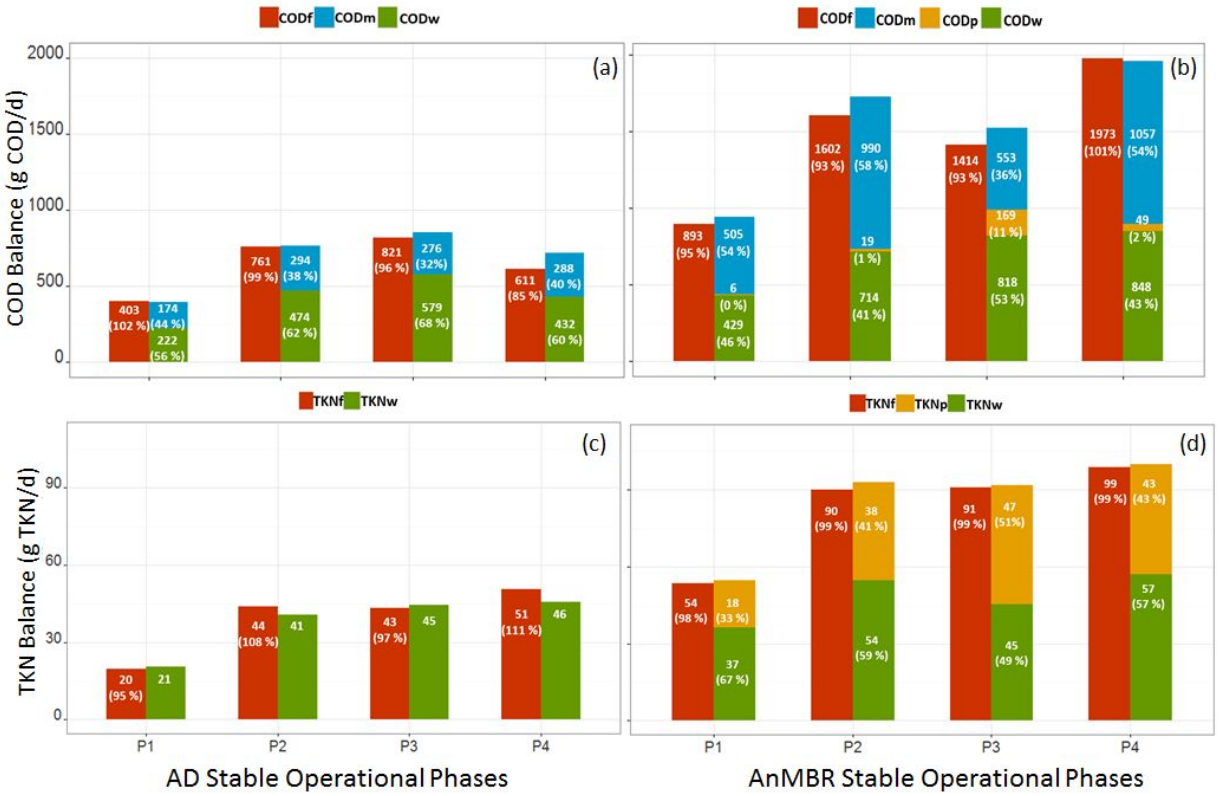

Figure 3.4: COD balance for AD (a), AnMBR (b) and TKN balance for AD (c) and AnMBR (d) with COD_f/TKN_f, COD_m, COD_p/TKN_p and COD_w/TKN_w refer to feed (f), methane (m), permeate (p) and waste (w) mass flows, respectively.

A limited number of feed properties differed statistically between phases (TS in P4 and VFAs in P2 and P4). Hence, for the purpose of comparison between phases (P1–P4) and reactors (AD, AnMBR) normalization (e.g., specific methane production (SMP), methane yields (MY)) was used to minimize the effect of the feed variability.

3.4.2 Mass Balances

COD and TKN are conserved through the anaerobic digestion process and hence mass balance closures were computed (Eqs. 3.1 and 3.2) to assess data quality. A summary of median values observed in each Phase that included the contribution of the streams entering and exiting the reactors is shown in Figure 3.4.

On the basis of the mass flows presented in Figure 4 it was determined that the COD mass balances closure varied from 85–102 % with a 95 % CI of 9–20 %. The TKN balance varied from 95–111 % with a 95 % CI of 7–24 %. The variation associated with the mass balances represented the combined experimental variability associated with the measured feed of the mixed sludge (kg/d), the waste sludge and permeate (kg/d), the associated chemistry with each sludge stream and permeate (g/L). The COD balance also included the biogas and percent methane measurements. The pilots were operated on the basis of the digester weight as measured with load cells that were somewhat subject to random vibrations. In

the data analysis the impact of these vibrations was reduced by averaging results. Overall, the observed variability in the COD and TKN mass balances were within the expected range for large pilot scale operations and were deemed to be of sufficient quality to make comparisons between operating conditions and reactor configurations.

3.4.3 Stability Considerations

In this study the pilots were operated at non-traditional temperature conditions that were anticipated to impact upon methanogenic activity. Hence, the results were assessed with respect to the stability of the digestion process. The stability of the anaerobic process is typically characterized by the ratio VFA/alkalinity (α) which is indicative of the balance between acid generation and alkalinity to maintain a neutral pH. Typical values of pH should range between 6.5–7.5 while the α value should be less than 0.2 with alkalinity below approximately 5000 mg/L as $CaCO_3$ and the percent CO_2 (g) typically between 25 to 45 % [3]. Table 3.3 summarises the values for these operating parameters and from this table it can be seen that stable operation was observed in all phases although the AnMBR in P3 (ambient operation at 25 °C) was operating at the upper limit of the recommended 0.20 α value. The lower temperature operation with the increased OLR to this reactor likely led to the increased α value.

Volatile solids reduction (VSr) is an important indicator of the conversion of organics to methane in anaerobic digestion and is also considered as a measure of the stability of the digested solids. Table 3.3 presents the values observed in this study and from this table it can be seen that values for the AnMBR varied from 49–64 % with the 95 % CI ranging between 4–8 %. The VSr for the AD varied from 39–48 % with 95 % CI of 7–11 %.

During the mesophilic operation (P1 and P2 at 35 °C) the VSLR was increased from 0.5 to 1.3 for the AD and from 0.9 to 2.5 kg $VS/m^3 \cdot d$ for the AnMBR by reducing the HRT from 34 to 17 days for the AD and from 15 to 7.5 days for the AnMBR. The VSr for the AD was reduced by 4 % (47 to 45 %) while the VSr in the AnMBR increased by 19 % (54 to 64 %) at an SRT:HRT of 25:7 days. During ambient operation (P3, 25 °C) and thermophilic operation (P4, 55 °C), the VSLRs were similar to P2 at 1.0 and 2.4k g $VS/m^3 \cdot d$ for the AD and AnMBR, respectively. During P3, the VSr values were lower at 39 and 49 %, in the AD and AnMBR, respectively when compared to P2. Despite the lower VSr, the AnMBR showed a 20 % increase in VSr at more than double the VSLR when compared to the AD during P3. The improved performance of the AnMBR was attributed to the increased SRT:HRT ratio of 40:8 days which accommodated the lower kinetics during ambient operation. During P4 the VSr values were 48 and 55 % for the AD and AnMBR, respectively, which represented a 15 % increase in VSr compared to the AD in P4. During P4 the AnMBR SRT:HRT was adjusted to 22:7 days, in anticipation of higher kinetic rates and maintained at 16 days for the AD. Overall the VSr in the AnMBR was on average 20 % higher compared to the AD and was consistent with typical VSr reductions of 40–60 % observed in full scale mesophilic high rate applications [2]. The AnMBR consistently showed improved VSr over the AD when operated at significantly higher VSLR and more challenging temperature regimes.

Table 3.3 shows that the AnMBR maintained VSr values of 49 and 55 % in phases P3 and

Table 3.3: Key operating conditions and performance comparisons in Phase 1-4 (P1-P4)

Parameter[a]	Reactor	Stable Operational Phases			
		P1 Median(CI) n	P2 Median(CI) n	P3 Median(CI) n	P4 Median(CI) n
AcH	AD	8 (2) 16	18 (3) 23	219 (96) 20	37 (13) 24
(mg/L)	AnMBR	11 (3) 16	16 (3) 23	800 (425) 20	48 (18) 24
PrH	AD	1 (0.1) 16	1 (0.1) 23	88 (40) 20	7 (3) 24
(mg/L)	AnMBR	1 (0.2) 16	1 (0.5) 23	575 (350) 20	14 (6) 24
tALK	AD	4.7 (0.3) 35	3.6 (0.5) 25	3.0 (0.2) 16	3.3 (0.3) 24
	AnMBR	6.0 (0.2) 35	5.1 (0.5) 25	6 (1) 16	3.6 (0.3) 24
α	AD	0.002 (0.001) 18	0.006 (0.003) 23	0.10 (0.05) 16	0.01 (0.01) 24
	AnMBR	0.002 (0.001) 18	0.003 (0.002) 23	0.20 (0.15) 16	0.02 (0.01) 24
pH	AD	7.1 (0.2) 16	7.0 (0.2) 16	6.7 (0.2) 16	7.1 (0.2) 16
	AnMBR	7.2 (0.1) 16	7.2 (0.1) 16	6.9 (0.3) 16	7.2 (0.1) 16
VSr	AD	47 (7) 35	45 (14) 15	39 (14) 16	48 (11) 21
(%)	AnMBR	54 (4) 35	64 (8) 15	49 (5) 16	55 (5) 21
SMP_{VSf}	AD	0.25 (0.03) 35	0.20 (0.04) 18	0.18 (0.02) 16	0.20 (0.01) 21
	AnMBR	0.27 (0.04) 35	0.28 (0.07) 18	0.19 (0.05) 16	0.34 (0.04) 21
MY_{CODr}	AD	0.36 (0.11) 18	0.35 (0.17) 15	0.31 (0.18) 16	0.22 (0.12) 19
	AnMBR	0.32 (0.07) 18	0.31 (0.08) 15	0.28 (0.04) 16	0.33 (0.06) 19

[a] tAlk, total alkalinity in g/L as $CaCO_3$; α, the ratio of VFAs/tAlk; SMP_{VSf}, specific methane production in terms of kg of VS fed (Nm^3 CH_4/kg VS_f); MY_{CODr}, methane yield in terms of COD reduction (COD_r) as Nm^3 CH_4/kg COD_r.

P4 and the corresponding methane yields were 0.19 and 0.34 Nm^3/kg VS_f, respectively. These values were obtained with HRTs of 8 and 7 days for the ambient and thermophilic conditions, respectively. By comparison, the median VSr values for the AD operating at an HRT of 16 days were 39 and 48 % for the corresponding conditions. These results demonstrate the sensitivity of the AD to temperature while the AnMBR configuration operated over the same temperature range and still maintained excellent volatile solids reduction typical of stabilized sludge or biosolids.

The treated sludge quality was assessed in terms of solids, COD fractions, TKN and TP as indicators of the final sludge quality for subsequent dewatering, further treatment or land utilization as biosolids for nutrient recovery [116]. A summary of the chemical characteristics of the treated sludge during stable operation is shown in Table 3.4. It can be seen that increasing the SRT in the AnMBR over the HRT, had the expected effect of increasing the solids (TS, VS and FS) of the sludge a ratio that was closely related to the SRT/HRT ratio. The median TS, VS and FS in the AnMBR were all consistently increased among P1–P4 within the range of 47–71 % compared to the AD, with the highest concentration increases found in P3 (ambient operation) and corresponding to the highest SRT/HRT ratio of 5.

The solids fractions ratios VS/TS and FS/TS were generally the same within a narrow

Table 3.4: Treated sludge (biosolids) in the AD and AnMBR during Phase 1-4 (P1-P4)

Parameter	Reactor	Stable Operational Phases			
		P1 Median(CI) n	P2 Median(CI) n	P3 Median(CI) n	P4 Median(CI) n
TS	AD	16 (2) 34	17 (2) 25	19 (2) 20	14 (2) 24
(g/L)	AnMBR	30 (3) 34	43 (3) 25	65 (11) 20	32 (2) 24
VS	AD	10 (1) 34	10 (2) 25	12 (3) 20	8 (3) 23
(g/L)	AnMBR	17 (1) 34	26 (2) 25	41 (7) 20	18 (1) 23
FS	AD	7 (1) 34	7 (1) 25	7 (2) 20	6 (2) 23
(g/L)	AnMBR	13 (2) 34	17 (2) 25	24 (6) 20	14 (2) 23
TKN	AD	1.5 (0.1) 17	1.5 (0.1) 14	1.3 (0.1) 13	1.3 (0.2) 21
(g/L)	AnMBR	2.1 (0.2) 17	2.8 (0.2) 22	3.3 (0.4) 14	1.8 (0.1) 21
TP	AD	0.44 (0.03) 16	0.42 (0.02) 14	0.48 (0.04) 13	0.39 (0.07) 21
(g/L)	AnMBR	0.9 (0.1) 17	1.2 (0.1) 22	1.6 (0.2) 14	0.9 (0.1) 21
TKN / TS	AD	9.4 (0.1) 17	8.2 (0.1) 14	6.8 (0.1) 13	9.3 (0.1) 21
(%)	AnMBR	7.0 (0.1) 17	6.5 (0.1) 22	5.1 (0.1) 14	5.6 (0.1) 21
TP / TS	AD	2.8 (0.1) 16	2.5 (0.1) 14	2.5 (0.1) 13	2.8 (0.1) 21
(%)	AnMBR	3.0 (0.1) 17	2.8 (0.1) 22	2.5 (0.1) 14	2.8 (0.1) 21

range of 55–62 % and 38–45 %, respectively, for both the AD and AnMBR throughout P1–P4. During P3 the TS and FS reached the highest concentration of 65 and 41 g/L, respectively and this coincided with the lowest VSr (49 %) attributed mostly to the ambient operating temperature of 25 °C.

The nutrient content of the digested sludges is important when land application is considered as a reuse alternative [119]. From Table 3.4, the values of TKN/TS ratio ranged between 7–9 % and 6–7 % in the AD and AnMBR, respectively. This represented a 24 % higher TKN/TS ratio in the AD versus the AnMBR treated sludge. The TKN balance for the AnMBR (Figure 3.4) demonstrated that the permeate TKN (TKN_p) contributed 41–51 % of the total TKN leaving the system in the soluble NH_4 form. Hence, the permeate is a valuable source of soluble N for recovery or reuse. The TP/TS ratio was 2.5–3.0 % in phases P1–P4 for both the AD and AnMBR with less than 20 % between all the values and not considered operationally significant. Overall the nutrient contents of the digested sludges fell within the ranges typically found in wastewater biosolids [120].

3.4.4 Energy Balance

The energy balance on alternative sludge digester configurations is an important element in determining whether improvements in sustainability are achieved. For comparison between the reactors (AD vs AnMBR) and between the four phases (P1–P4) Figure 3.5 shows the summary energy balance in MJ/m^3 of feed sludge calculated using Eqs. 3.6–3.11. Figure 3.5 shows, for each phase, the energy consumed (E_L, E_H, E_X and E_P) as compared to the energy value of the methane generated (E_M) bar, for the AD and AnMBR in separate

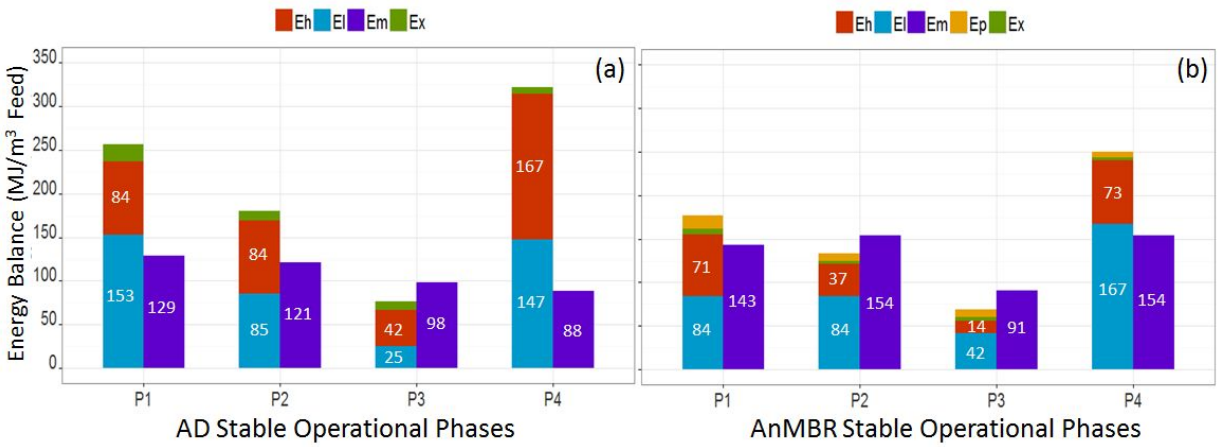

Figure 3.5: Energy balance for the AD (a) and AnMBR (b).

diagrams. A comparison of the energy terms showed that sludge heating (E_H) and heat losses (E_L) combined to represent over 90 % of the energy consumption with reactor mixing (E_X) and sludge pumping (E_P) combining to consume less than 10 % of the overall energy for both configurations. The net energy balance (ΔE_{net}) was better for all phases in the AnMBR as compared to the AD, when comparing the same phase. A positive energy balance was achieved in the AD and AnMBR during ambient operation (P3 at 25 °C) and for the AnMBR during the mesophilic operation (P2) at the VSLR of 2.5 kg VS/$m^3 \cdot d$. When comparing the AD and AnMBR mesophilic operation (P2 at 35 °C), the higher VSLR (2.5 versus 0.9 kg VS/$m^3 \cdot d$), that reduced the effective reactor volume by more than 50 %, was the key difference that made the AnMBR have a positive energy balance. The results of the energy balance provided valuable insight when comparing modes of operation. However, it is expected that the relative contribution of each of the components will differ at full scale when the ratio of surface area to volume are smaller and the mixing requirements may differ from that of the pilot.

3.5 Conclusions

This phase of the study compared the performance of an AnMBR digester with that of a conventional digester over a range of temperatures at pilot scale. Phases 1 and 2 of this study assessed the impact of the SRT/HRT ratio on AnMBR performance at an optimum mesophilic temperature. In both phases the SRT was maintained at a relatively high value (25 and 35 days) to maximize solids destruction while the HRT was reduced from 14 to 7 days. The SRT of the AD pilot was operated at values of 34 days in P1 and 16 days in P2 to establish the range of VSR that might be expected by conventional digestion at mesophilic temperatures. The AnMBR consistently had greater VSr and increased methane yields (0.19–0.34 Nm^3/kg VS_f when compared to the AD. Further, the TS concentrations in the waste stream from the AnMBr were considerably greater by 2.0–3.4 times than those of the AD as a result of the extended SRTs. The VSr in the AnMBR was maintained at high values (49–64 %) even when the HRT was reduced to 7.3 days in Phase 2 (Table 3.2). Viewed collectively, the data indicate that the AnMBR could achieve high levels of solids

destruction and concentration when operated at what are considered short HRTs for sludge digestion.

The AnMBR demonstrated higher volatile solids reduction (VSr) between 49–64 % when compared to 39–48 % in the AD. During the mesophilic operation (P1 and P2 at 35 °C) the VSLR was increased from 0.5–0.9 to 1.3–2.5 kg VS/$m^3 \cdot d$ for the AD and AnMBR, respectively, by reducing the HRT from 34 to 17 days for the AD and 15 to 7.3 days for the AnMBR. The VSr for the AD vas reduced by 4 % (47 to 45 %) while the VSr in the AnMBR increased by 19 % (54 to 64 %) at an SRT: HRT of 25:7.3 days from P1 to P2. During ambient operation (P3, 25 °C) and thermophilic operation (P4, 55 °C), the VSLRs were similar to P2 at 1.1 and 2.4 kg VS/$m^3 \cdot d$ for the AD and AnMBR, respectively. During P3, the VSr was lower at 39 and 49 %, in the AD and AnMBR, respectively. Despite the lower VSr compared to P2, the AnMBR showed a 20% increase in VSr at more than double the VSLR compared to the AD during P3. The main reason for the improved performance of the AnMBR was the increased SRT:HRT ratio of 40:8 days adjusted for the lower kinetics during ambient operation. During P4 the VSr was 48 and 55 % for the AD and AnMBR, respectively, which represented a 15 % increase in VSr. During P4 the AnMBR SRT:HRT was adjusted to 22:7 days, for the expected improved kinetic rates and maintained at 16 days for the AD. Overall the AnMBR showed improved VSr over the AD when operated at significantly higher VSLR and more challenging temperature regimes.

The nutrient content of the digested sludges is important when land application is considered as a reuse alternative [119]. From Table 3.4, the values of TKN/TS ratio ranged between 7–9 % and 6–7 % in the AD and AnMBR, respectively. This represented a 24 % higher TKN/TS ratio in the AD versus the AnMBR treated sludge. This was due to the permeate TKN (TKNp) that represented 41–51 % of the total TKN leaving the system in the soluble NH4 form. Hence, the permeate may be a valuable source of soluble N for recovery or reuse. The TP/TS ratio was 3 % in all phases (P1–P4) for both the AD and AnMBR except P2 for the AD in which it was 2 % (a 33 % higher TP/TS ratio in the AnMBR compared to the AD). Overall the nutrient contents of the digested sludges fell within the ranges typically reported [120].

An energy balance showed that an improved net energy production may be realized using AnMBR over AD which was directly related to the higher methane yield (38 % on average) and higher VSLR by a factor of 2.1–2.8 compared to the AD made possible by the decoupling of the HRT and SRT. When considering energy consumption for sludge heating, pumping, mixing, methane generation and heat losses per m^3 of sludge fed, a positive net energy production was realized for the AD and AnMBR in P3 operated at ambient conditions (25 °C) and the AnMBR in P2 operated at mesophilic (35 °C) conditions (Figure 3.5). The results from this study therefore suggest that a net energy production system is feasible when treating mixed sludge using an AD and AnMBR operated at both ambient mesophilic conditions. The results of this study will be of particular interest to designers, owners and operators of municipal wastewater treatment plants that are seeking solutions to increase the capacity of existing digesters.

Chapter 4

AnMBR Membrane Performance

4.1 Introduction

The sustainable operation of AnMBRs rely on the membrane system's ability to maintain a sufficiently high flux over a range of operational conditions. Strategies to achieve a sustainable flux when treating concentrated wastewaters include dealing with various forms of membrane fouling. Fouling and the high cost of membranes are commonly considered the most significant barriers to the wider application of MBR technologies. Fouling results from deposition of organic and inorganic solids, colloids and solutes onto or into the membrane pores by either adsorption, pore-clogging or pore-blocking. Operationally, fouling is generally considered as reversible (managed on-line through shear, back flushing, relaxation) or irreversible (requiring chemical cleaning typically offline). Fouling has been attributed to characteristics of the feed matrix, the biomass or the membrane and is influenced by the reactor operating conditions [9, 29, 77, 79, 80].

Recently, extractable extracellular polymeric substances (eEPS) have been considered a major cause of membrane fouling in membrane bioreactors (MBRs) with several reactor operating conditions and feed matrix properties being identified as primary factors influencing eEPS concentration and distribution between protein and polysaccharide fractions [121]. The key factors included the sludge age (θ_x), hydraulic and organic loading rate (HLR, OLR), MLSS concentration, feed matrix particulate and soluble constituents, transient or unsteady operating conditions and mechanical strain or stress on the biomass. All the above factors, to some degree, have been associated with changes in fouling propensity of a system and numerous attempts have been made to correlate the system operating conditions or fundamental properties of the matrix, such as eEPS with the fouling propensity [9, 29, 39, 44, 52, 77, 79, 80, 121, 122].

To better understand fouling propensity extensive efforts have been made to model membrane fouling and recently EPS has been included as a model state variable in an effort to improve operational predictions associated with both fundamental parameters and operational controls that can then be applied to full scale applications [90, 91, 123–126]. Empirical models have been employed to fit responses to operating parameters without any direct connection to the underlying physical mechanisms involved. They are generally of limited usefulness except for conditions similar to which they were developed. The mechanistic models that have been developed, can be more insightful that empirical models about underlying causes, but are often over parameterized and more difficult to apply in practical applications unless they were simplified to single mechanisms [90, 91]. Statistical models have been used to integrate a large number of unknown mechanisms through regression of observable parameters and can establish correlations to operating conditions for improved operational strategies [124]. Collectively all the modeling efforts to predict

fouling to date simplify the complexities associated with real applications and are limited in their predictions. However mechanistic models like the 'Hermia-Field' models (§ 2.6), that are not over parameterized, provide useful insights that can assist practitioners in developing operational strategies.

An analysis method that does not rely on modeling and relies on direct filtration measurements is the Membrane Bioreactor–Vito Fouling Measurement (VFM) method (§ 2.5). The VFM method was introduced by Huyskens et al. (2008) [88] based on previous work by Brauns et al. (2002) [87]. This method is useful at distinguishing between reversible and irreversible membrane fouling and to characterize system fouling propensity. It may be used as an on-line or off-line method applicable to constant pressure crossflow operations which allows the measurement of the fouling propensity of the matrix as a function of cumulative throughput of a system [44]. In conjunction with the VFM method direct measurement of the change in flux over time ($\Delta J/\Delta t$) have been used to characterize the fouling rate during short term and long term filtration to better understand the general effectiveness of the fouling control strategy [122].

This chapter includes a summary of operating conditions, a characterization of membrane performance over these operating conditions and then examines relationships between permeability through regression with the use of VFM diagrams to differentiate reversible from irreversible fouling. Subsequently, the 'Hermia-Field' mechanistic models were employed to estimate the dominant fouling mode and compute the flux decline under the different operating conditions.

4.2 Materials and Methods

The membrane system of the AnMBR was operated at a transmembrane pressure (ΔP) of 20–55 kPa (Eq. 4.1) that was associated with crossflow velocities (v) of 1.0–1.2 m/s (Eq. 4.2). These were controlled roughly by manual adjustment of a variable speed drive that controlled the recirculating sludge pump (20–26 L/min) to achieve turbulent conditions as defined by a Reynolds number above 2100 [75]. The permeate flowrate (Q_p), the time of permeation (t_p), feed pressure (P_f) and concentrate pressure (P_c) were monitored on-line and logged on a PC using Labview^{TM} every minute. The ΔP, crossflow velocity (v), flux (J) and permeability (K) were calculated using Eqs. 4.1–4.4:

$$\Delta P = \frac{P_f + P_c}{2} - P_p \tag{4.1}$$

$$v = \frac{Q_r}{A_x} \tag{4.2}$$

$$J = \frac{Q_p}{A_s} \tag{4.3}$$

$$K = \frac{J}{\Delta P} \tag{4.4}$$

where Q_r, is the recycle flowrate of the sludge to the membrane module; A_x, the tubular module cross sectional area and A_s, the membrane surface area. The J, ΔP and K were

computed and assessed in P1–P4 where each phase had distinct operating conditions with respect to θ_x:θ ratios, temperature (25, 35 and 55 °C) and VSLRs that resulted in different MLSS values in the bioreactors (see Table 3.1, Chapter 3). When comparing between phases the J was corrected to 20 °C or J_{20} using Eq. 4.9. The process was monitored through the analysis of the sludge for solids, COD and eEPS fractions on a weekly basis and the permeate was monitored for solids and COD fractions (Table 4.1).

Table 4.1: Parameters monitored during stable operating conditions[a]

AnMBR Parameters	Sampling Frequency
Flowrate (Q, in mL/min)	Logged every minute, Labview^{TM}
Pressure (P_f, P_c, in psi)	Logged every minute, Labview^{TM}
Time (t, min), Temperature (T, °C)	Logged every minute, Labview^{TM}
Weight of reactors (kg)	Logged every minute, Labview^{TM}
Solids fractions (TS, VS, FS, TDS)	Weekly
COD fractions (tCOD, fCOD, sCOD)	Weekly
eEPS Biopolymers (CH, PR)	Weekly

[a] TS, total solids; VS, volatile solids; FS, fixed or inert solids residue from combustion at 550 °C; TDS, total dissolved solids; tCOD, total chemical oxygen demand; fCOD, filtered at 1.5 μm; sCOD, soluble COD passing 0.4 μm filter.

4.2.1 Permeation-Rest Operation Cycle

The sAnMBR was operated using a permeation-rest cycle at constant pressure and this method allowed the membrane to be scoured by crossflow induced shear to remove the reversible fouling during the rest period of the filtration phases. This was achieved by using a 6-hour batch feed, react, permeation and waste cycle. The permeation and waste masses were set based on the θ_x and θ set points (Table 3.1) and were controlled through monitoring of load cells that measured the mass of the reactor. Computer controlled valves were controlled using PLCs linked to Labview^{TM} for wastage and feeding of the sludge to the reactors. The reactor mass, membrane pressures and permeate flow rate were logged every minute by Labview^{TM}. The permeation cycle duration was set to match the permeation rate and corresponding θ with the rest period consisting of the remaining period within each 6-hour cycle. Figure 4.1 gives an example flux (LMH) versus time (min) diagram showing three example permeation-rest cycles. The HRT ($V/(Q_w + Q_p)$) set points (Table 3.1) were achieved by measuring the permeate mass during each 6-hour cycle to meet 25 % of the daily permeate rate (Q_p). The Q_p value was synchronized with the Q_w, wasted directly from the bioreactor to meet the SRT (V/Q_w) set points.

Initially a more complicated mode of operation which included within-cycle relaxation was used since it was reported to be effective at improving the short term flux recovery when treating municipal waste activated sludge (WAS) [31]. However, valve failures and lack of timely replacement valves made this mode of operation unfeasible. Figure 4.1 shows three typical filtration cycles identifying the flux declining curve during permeation (P) and the rest period (R) with a complete cycle lasting about 6-hours. Figure 4.1 also shows

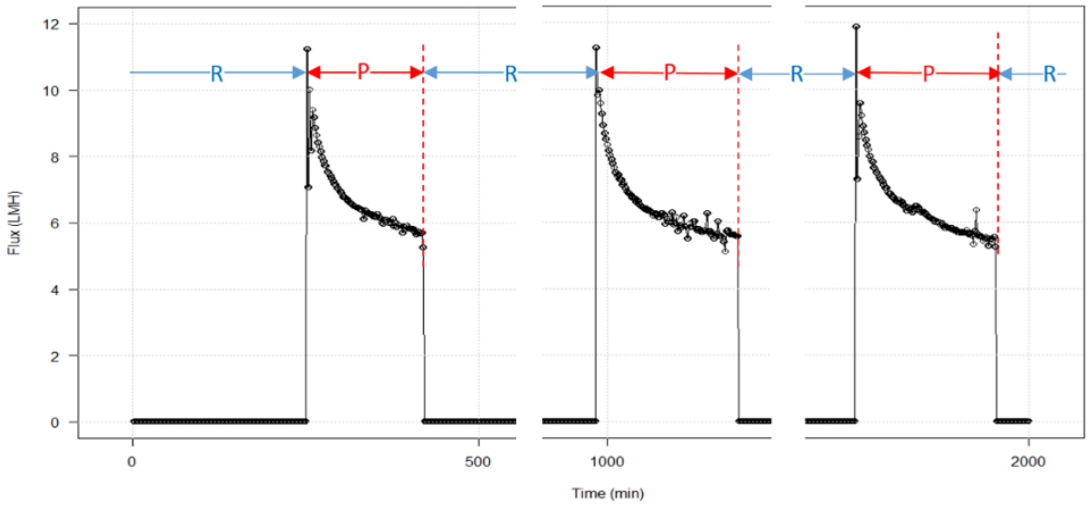

Figure 4.1: Example of three typical logged filtration cycles with permeation (P, about 1–2 hours each) and inter-cycle rest period (R, about 5-4 hours) within a typical 6 hour cycle.

an example of how the flux decline during filtration was mostly recovered at the beginning of the next cycle. This mode of operation was applied throughout P1–P4.

4.2.2 Membrane Cleaning

Membrane cleaning-in-place (CIP) was used to remove irreversible fouling that accumulated over time which reduced the permeability and the the membrane operating flux below the operating set point. For tubular membrane systems treating sludge a multi-step sequential approach including a water flush, an abrasive clean followed by an alkali or acid clean has been reported to be successful at recovering membrane permeability [31, 41]. The water flush was designed to remove residual surface solids; the abrasive clean removed any scaling attached to the membrane; the alkali flush primarily addressed organic foulants and the acid clean was intended for the removal of inorganic precipitates.

The ultrafiltration sAnMBR membrane system that was used in the current study consisted of two parallel tubular modules that incorporated KOCH® ABCOR^{TM} polyvinylidene fluoride (PVDF) negatively charged membranes and were operated in parallel. Each membrane had a 25 mm ID and 3.1 m length with a nominal pore size (NPS) of 20 nm and a corresponding molecular weight cut-off (MWCO) of 120 kDa and a membrane surface area of 0.2 m^2 per module with other specifications provided in Table 4.2. This membrane selected was reported to be effective in a similar application when treating TWAS [31] and was selected based on the similarity of the mixed sludge feed composition.

The membrane clean included four CIP sequential steps: (1) hot water-flush conducted at 55–60 °C, pH 7.2–7.8; (2) abrasion clean using manufacturer recommended 25 mm diameter sponge balls, 3 per cleaning operation that were flushed through the module using water; (3) base/alkali clean was conducted using NaOH (aq) added to water to pH 10 at 55–60 °C and (4) acid clean was conducted using citric acid $C_6H_8O_7$ (aq) and HCl added to achieve

a pH 2 at 55–60 °C. This CIP was consistent with a previous TWAS treatment application [31] and was expected to be effective when treating mixed sludge.

In the case of the base and acid clean, a 2-hour soaking period was part of the cleaning process. A water flux test followed each cleaning step to determine the flux recovery relative to the virgin membrane water flux. The cleaning apparatus included a 150 L tank equipped with a heater and a dedicated cleaning pump rated at 53 L/min that was configured to flush the membrane modules. The water tank was used for hot water flushes at 60 °C and for acid bath preparation using citric and hydrochloric acid to bring the water to a pH range of 2–3 and temperature from 50–60 °C, within the PVDF-HFC module specifications (Table 4.2).

Table 4.2: KOCH ABCOR^{TM} ultrafiltration (UF) membrane specifications[a]

Parameters	Specifications	Parameters	Specifications
Membrane code	10-HFP-276-PVI	Cross sectional Area	5.1 cm^2
Membrane chemistry	PVDF-HFP (-)	Surface Area	0.2 m^2
NPS / MWCO	20 nm / 120 kDa	Maximum inlet pressure	630 kPa (90 psi)
Diameter x Length	2.54 cm x 305 cm	pH Range	pH = 2–10
Maximum back pressure	35 kPa (5 psi)	Temperature, maximum	60 °C

[a] PVDF-HFP (-), polyvinylidene fluoride (-($C_2H_2F_2$)n-) hexafluoropropanol ($C_3H_2F_6O$) with a negative (-) surface charge; NPS, nominal pore size; MWCO, molecular weight cut-off.

4.2.3 Hydrodynamic Conditions

The membrane reactor configuration influences the hydrodynamic conditions which represent physical operating constraints which are important for a better understanding of the membrane performance. Baudez et al (2013) [76] previously invested the municipal anaerobic digested sludge rheology and experimentally demonstrated that τ and η were dependent on T and TS according to the Herschel–Bulkley model coupled with a Bingham model as given by Eqs. 4.5 and 4.6. The γ and Re are given by Eqs. 4.7 and 4.8 [75]:

$$\tau = \alpha(\phi - \phi_o)^m \tag{4.5}$$

$$\eta = \eta_o e^{\beta \cdot \phi} \tag{4.6}$$

$$\gamma = \frac{8v}{D} \tag{4.7}$$

$$Re = \frac{\rho v D}{\eta} \tag{4.8}$$

where τ, is the shear rate given in Pa; ϕ, the sludge percent TS (%); ϕ_o, the TS (%) below which there is no yield stress; m is a parameter related to the fractal dimension of sludge flocs (dimensionless); α, is a model parameter (Pa); η, the viscosity (mPa·s); η_o the dynamic viscosity of the sludge (mPa·s); β, is a model parameter (dimensionless); γ,

shear strain (s^{-1}); v, crossflow velocity (m/s) and D, the membrane diameter (m) and Re, Reynolds number for Newtonian fluids. Anaerobic sludge at TS > 5 g/L acts as a non-Newtonian fluid and Eq. 4.8 needs to adapted according to the Re given in Ho et al (2009) [75]. Temperature corrections for the parameters in Eqs. 4.5–4.7 are required to account for temperature effects [76] and these were used to estimate the rheological sludge properties in P–P4 of this study.

4.2.4 Flux, TMP and Permeability

The effect of flux (J) and transmembrane pressure (ΔP) are combined through the permeability ($K = J/\Delta P$) which plays a key role in the viability and sustainability of AnMBRs treating sludge or concentrated wastewater streams [9]. The median daily J, ΔP and K were computed from data that was collected on a minute basis which was aggregated and averaged to daily median values. The corresponding normalized K_{20} values were calculated based on temperature-corrected values of the water viscosity [88] for the different operating conditions based on Eqs. 4.9 to 4.12 [9]:

$$J_{20} = \frac{J_T}{1.025^{T-20}} \tag{4.9}$$

$$\eta_{20} = \frac{\eta_T}{1.024^{20-T}} \tag{4.10}$$

$$K_{20} = \frac{J_{20}}{\Delta P} \tag{4.11}$$

where J_{20}, η_{20} and K_{20} are the 20 °C normalized parameter values. Using K_{20} provided a more direct comparison between P1–P4 and the ability to combine the different data sets from each operating conditions for subsequent regression analysis.

4.2.5 Sludge eEPS Measurements

The AnMBR treated sludge was characterized with respect to free (C_f) and bound (C_b) extractable extracellular polymeric substances (eEPS) and subsequently in terms of protein (C_{pr}) and polysaccharide (C_{ch}) concentrations. The sludge samples were initially centrifuged at 14000 g for 17 minutes at 4 °C and the supernatant (containing free eEPS, C_f) was decanted and separated from the solid sludge pellet (containing the bound eEPS, C_b). The supernatant was filtered through 1.5 μm Whatman^{TM} glass microfiber binder free filters to remove interfering particulates. The C_b was extracted from the sludge pellet through re-suspension and washing using a 0.85 % NaCl solution followed by extraction using a 2 % ethylenediamine tetra-acetic acid (EDTA) solution with a 3 hour contact time at 4 °C followed by separation using centrifugation. The aqueous phase containing the released C_b was filtered through 1.5 μm filters prior to colorimetric analysis. Colorimetric analysis for eEPS-proteins was conducted using the Piercer BCA Assay [127] using bovine serum albumin (BSA) as a reference while the eEPS-polysaccharides were characterized using the Phenol-Sulfuric Acid Assay [128], using glucose as a reference, to differentiate the eEPS polysaccharides (C_{ch}) and protein fractions (C_{pr}). The BSA and glucose solutions in the

concentration range from 0 to 120 mg/L were used to generate protein and polysaccharide calibration standard reference curves. The protein and carbohydrate samples were measured at wavelengths of 750 and 490 nm respectively. The total free eEPS (C_f) concentration (mg eEPS/L) was calculated as the sum of the protein $C_{f,pr}$ and polysaccharide $C_{f,ch}$ fractions. Similarly the total bound eEPS (C_b) concentration (mg/L) was calculated as the sum of the $C_{b,pr}$ and $C_{b,ch}$ fractions. The AnMBR treated sludge eEPS was subsequently compared between P1–P4.

4.2.6 Short and Long Term Fouling Rates

The effectiveness of the clean-in-place (CIP) cleaning process and the on-line rest period, for membrane scouring action, were assessed by measuring the short (STFR) and long term (LTFR) fouling rates. Figure 4.2 provides a schematic representation of the method used which included using linear regression to compute the slope of a flux decline over the permeation cycle to quantify the "cycle fouling" or STFR and the "residual fouling" or LTFR.

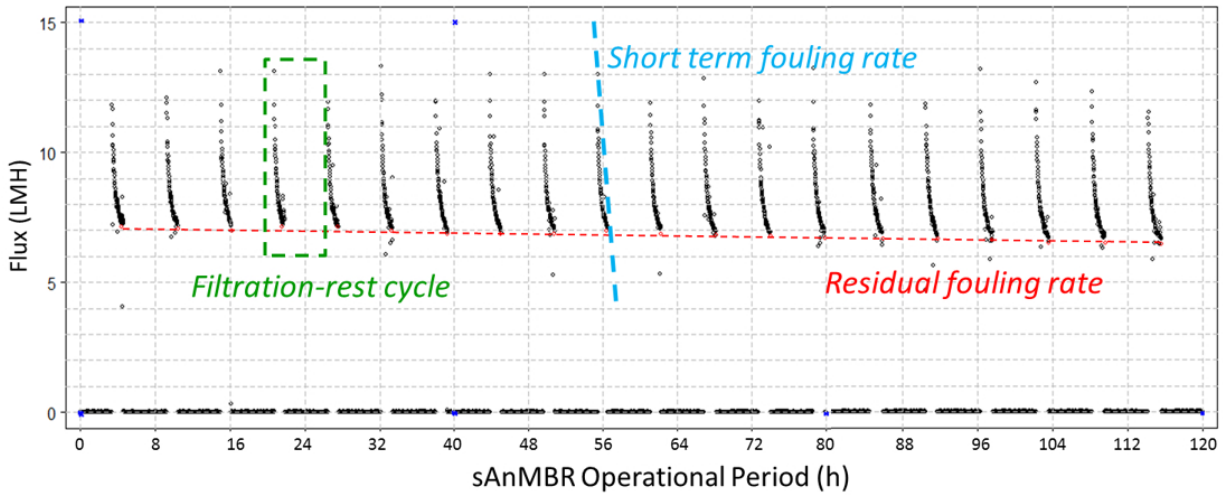

Figure 4.2: Flux versus time curve showing a typical filtration sequence with the filtration-rest cycle identified (single cycle in green); the individual cycle "short term fouling rate" (blue) and the longer term "residual fouling rate" (red).

The STFR has been attributed to concentration polarization and initial pore constriction while the LTFR has been associated with irreversible fouling accumulating over many filtration cycles [9]. These fouling rate measurements reflect the effectiveness of the between cycle rest period and the CIP fouling control strategies. The determination of the fouling rates was based on filtration rates that were calculated on one minute intervals and then converted to flux values which were averaged using linear regression [117, 129]. The estimated STFR and LTFR fouling rates were subsequently compared between P1–P4 and assessed against operating conditions.

4.2.7 Fouling Propensity using VFM

It was deemed important to distinguish between the contributions of reversible and irreversible fouling to the total membrane fouling to gain greater insight into the type of fouling that occurred. From an operational perspective reversible fouling is typically associated with cake fouling and controlled by on-line methods such as use of a relaxation period or by increasing the operating shear using a higher crossflow velocity. Irreversible fouling is associated with membrane pore constriction and controlled by chemical cleaning. Residual membrane fouling, that contributes to the membrane long-term fouling, is associated with foulants that are not removed during a maintenance clean or rest period [9]. The VFM method [87, 88] is a useful on-line or off-line method that is applicable to constant pressure crossflow operations and allows estimation of cumulative reversible and irreversible fouling resistances as a function of the cumulative throughput of the system. The VFM method has been verified for a lab-scale MBR [87] but it has however not been applied to systems that are treating sludges in AnMBR. The VFM approach has the potential to be implemented with on-line sensors in advanced control systems that manipulate cleaning strategies (i.e., timing and type of cleaning) to provide overall system optimization [88].

The VFM method was used to generate VFM-curves which are figures of the cumulative normalized throughput ($\Sigma V/A$) versus the cumulative normalized reversible resistance ($\Sigma R_r/R_m$) or the cumulative normalized irreversible resistance ($\Sigma R_i/R_m$) over a sequence of permeation cycles occurring between membrane cleans [88]. The VFM method computes the permeability (K) over a sequence of permeation cycles from the measured filtration rate (Q), membrane area (A), transmembrane pressure (ΔP) and the permeate dynamic viscosity (η). The temperature-normalized (at 20 °C) K values and corresponding resistances (R) were computed using Eq. 4.12–4.16:

$$K = \frac{J}{\Delta P}\frac{\eta_T}{\eta_{20}} \tag{4.12}$$

$$\eta_T = \eta_2 0 \cdot 1.024^{20-T} \tag{4.13}$$

$$R = \frac{1}{\eta_T K} \tag{4.14}$$

$$R_t = R_m + R_r + R_i \tag{4.15}$$

where η_T, is the permeate viscosity at the AnMBR operating temperature (T, °C); η_{20}, the water viscosity at 20 °C; R_m, is the measured virgin membrane water resistance measured value of $3.6 \cdot 10^{11}$ (m^{-1}); R_r, is the reversible fouling resistance and R_i is the irreversible membrane resistance both measured in m^{-1}.

The irreversible resistance (R_i) was calculated as the difference between R_m and the resistance associated with the K value at the beginning of a cycle. The total cycle resistance (R_t) was calculated based on the K value associated with the end of the cycle. The reversible resistance (R_r) was calculated by difference using the resistances-in-series model given by Eq. 4.14. This process was repeated for each cycle within a sequence of permeation cycles between cleaning events. The normalized cumulative throughput and cumulative

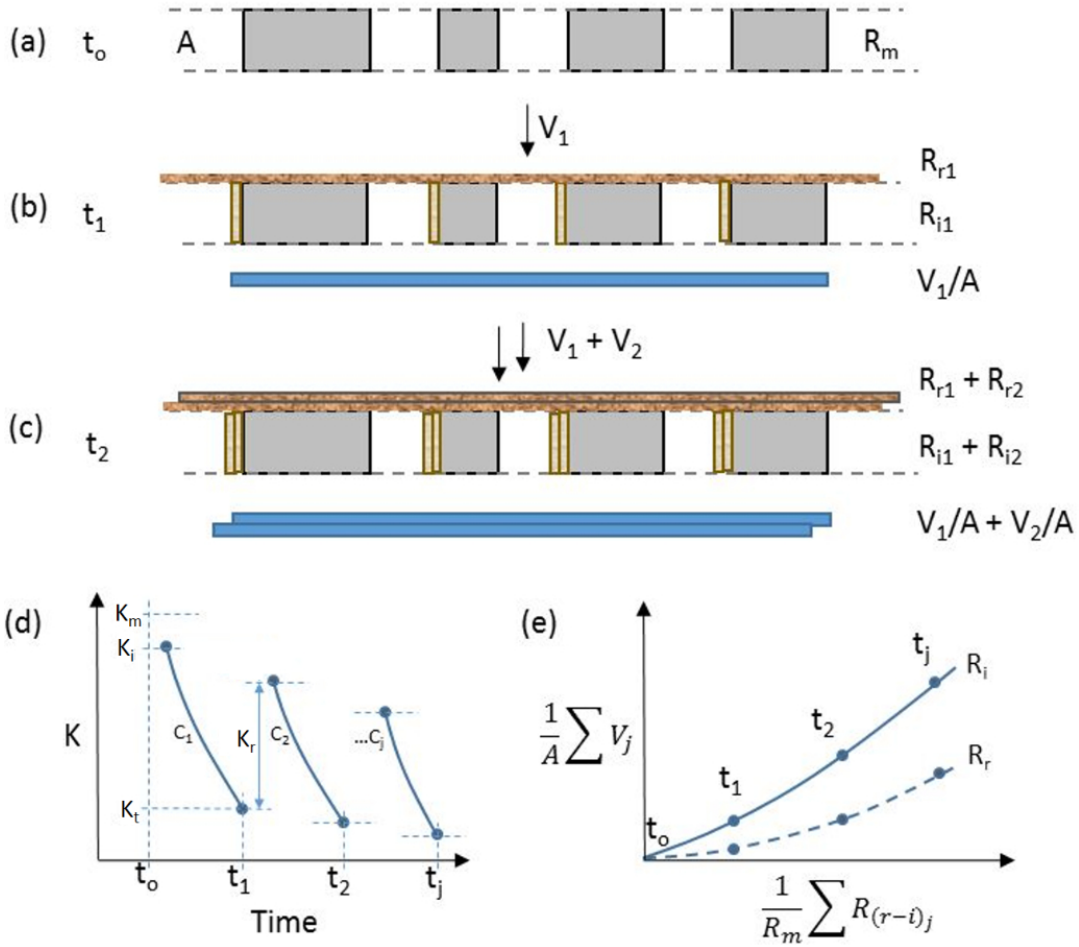

Figure 4.3: A simplified schematic of the conceptual fouling model assumed by the VFM approach with the cross-section of a clean membrane (a); surface fouling and pore fouling after the first cycle of permeation (b); accumulated fouling after two permeation cycles (c); the K curves used to derive the resistances (d) and the generated VFM curves (e) comparing the cumulative throughput ($\Sigma V/A$) versus the cumulative reversible ($\Sigma R_r/R_m$) and irreversible ($\Sigma R_i/R_m$) normalized resistance ratios.

resistances were then plotted to create a VFM curve as shown in a simplified schematic in Figure 4.3.

Figure 4.3 provides a simplified idealized schematic of the derivation of the VFM fouling propensity curve that shows the process that leads to surface or cake fouling or reversible resistance (R_r) and pore constriction characterized by the irreversible resistance (R_i) as shown in Figure 4.3 (a)–(c). The cumulative volume of permeate (ΣV) is normalized by the membrane area (A) and is the volume accumulated (or throughput) over a series of permeation cycles shown in Figure 4.3 (c). The normalized permeability curves (Figure 4.3 (d)) were generated for each cycle and then used to compute the corresponding resistances used in the VFM curves shown in Figure 4.3 (e). A horizontal curve on the VFM graph implies serious fouling with very little throughput and indicative of a matrix and system with a high fouling propensity. By contrast, a vertical curve implies a high throughput

with little fouling and indicative of matrix and system that has a low fouling propensity.

Typical VFM curves representative of the complete operation for phase P1–P4 were generated and to better compare phases individual curves were combined and averaged. The findings in each phase were further assessed based on operating conditions.

4.2.8 Membrane Filtration Modeling

The filtration process was also modeled using the classical blocking models of Hermia [90] modified by Field et al, (1995) [91] by incorporating a crossflow parameter to the fundamental characteristic equations (Eq. 4.16):

$$\frac{-1}{A^2J^3}\frac{dJ}{dt} = k\left(\frac{1}{AJ}\right)^m \tag{4.16}$$

where k is the clogging constant and m the blocking mode. The functional forms of Eq. 4.16 with a crossflow parameter added for cases of m = 0, 1 and 2 apply directly to crossflow operations and are given by Eqs. 4.17, 4.18 and 4.20. Equation 4.19 is the standard blocking model (m=3/2), considering only pore blocking and was not amenable to adaptation for crossflow operation [91].

Equation 4.17 describes the flux (J) variation when cake filtration (m = 0) dominates with $G = \alpha k_c/J_oR_o$, where α, is the specific cake resistance (m/kg); k_c, the cake filtration constant (kg/m^3); J_o, the initial flux at $t = 0$ at the beginning of the filtration cycle ($m^3/m^2 \cdot s$); R_o, the initial membrane resistance at $t = 0$, at the beginning of the filtration cycle and J_s, is the limiting flux or steady state flux if cake fouling is to be avoided.

$$\frac{dJ}{dt} = -GJ^2(J - J_s) \qquad m = 0 \tag{4.17}$$

Equation 4.18 describes the flux (J) variation when intermediate blocking (m = 1) dominates with σ, the blocked area per unit volume of filtrate (m^{-1}); K_i, the back transport flux factor induced by crossflow (s^{-1}) and $J_i = K_i/\sigma$, the limiting flux or flux if intermediate blocking is to be avoided ($m^3/m^2 \cdot s$).

$$\frac{dJ}{dt} = -\sigma J^2 + K_iJ \qquad m = 1 \tag{4.18}$$

Equation 4.19 describes the change in flux when standard blocking (m = 3/2) dominates with the clogging constant $K_s = 2CQ_o^{\frac{1}{2}}/LA_o$ ($1/m^3$), representing the specific retention or deposition of solid particles within the membrane pores per volume of filtrate [90]. This type of fouling is not impacted by crossflow induced shear forces and Eq. 4.12 is not able to predict a limiting flux. The model was still considered for comparative analysis.

$$\frac{dJ}{dt} = -K_sA^{\frac{1}{2}}J^{\frac{3}{2}} \qquad m = \frac{3}{2} \tag{4.19}$$

Equation 4.20 describes the change in flux when complete pore blocking (m = 2) dominates and with ϵ_o, the membrane porosity; B, the back flux factor corresponding to the rate of particle removal from the top of the pore openings (s^{-1}) and $J_c = K_b\epsilon_o/\sigma$, the limiting flux below which no flux decline occurs ($dJ/dt = 0$).

$$\frac{dJ}{dt} = -\left(\frac{\sigma J_o}{\epsilon_o}\right) J + K_b J_o \qquad m = 2 \tag{4.20}$$

Solutions to the modified classical blocking models (Eq. 4.17–4.20) were used to investigate the dominant fouling mode by comparing the best model fit to the measured flux data. The explicit functional forms in terms of J were provided [91] and solved directly for $m = 1$, 3/2 and 2. In the case Eq. 4.17 where only an implicit solution was possible [91]), the differential equation was solved numerically [130]. R-scripts were written and executed [117, 129, 131] to automate estimation of the model parameters using non-linear least squares regression [132]. A typical best fit curve analysis is shown in Figure 4.4 and the best model fit was selected based on the minimum residual sum of squared errors (RSE). This method was used to model the observed filtrate data logged every minute using LabView^{TM} throughout P1–P4.

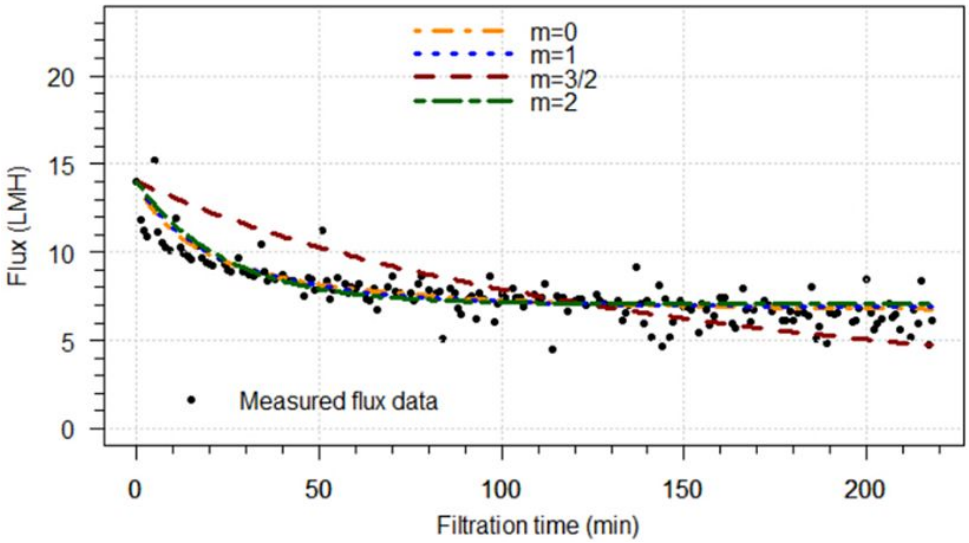

Figure 4.4: An example model curve fit analysis used to determine the best model.

4.3 Statistical Assessments

The data text files logged by Labview^{TM} were transferred directly into MS Excel^{TM} files and then imported into R [117, 129] for exploratory data analyses (EDA) [133] that included checking for gross errors, outlier detection, Normal and Log Normal goodness of fit distribution tests and the calculation of descriptive statistics used to evaluate the consistency of the data sets. The median and corresponding 95 % confidence intervals were calculated for each parameter (e.g., TS, COD and θ_x) in each phase (P1–P4). For data sets that were not symmetrically distributed, the median and median 95 % confidence interval (CI) were

deemed to provide more robust measures of central tendency and variability, respectively, compared to the mean and standard deviation and these were used throughout.

Group and paired comparisons, between the operating conditions of parameter variables, were conducted using the non-parametric Kruskal-Wallis (K-W) test at the 95 % confidence level followed by paired comparisons using the Tukey-type all-pairs comparisons and Fisher multivariate approximation method with adjusted p-values and confidence intervals [118, 134].

Regression analysis was conducted using multivariate adaptive regression splines [10, 135] using the *earth*-R package and model predictions were plotted using the *plotmo*-R package [136]. This modeling approach uses a non-parametric multivariate adaptive regression spline technique using hinge functions while considering non-linearities and interactions between predictor variables. The modeling routines [10] include a predictive modeling algorithm that iteratively pruned the model base functions towards arriving at an improved predictive model. The resulting model chosen was based on the minimum cross validation regression statistics which had the optimum number of predictors corresponding to the largest predictive power based on parsimonious principles. While other modeling approaches were tested (not reported on) the approach used proved the most useful to arrive at a balance between goodness-of-fit and model complexity while not over fitting results.

4.4 Results and Discussion

This phase of the research sought to compare the performance of the AnMBR membrane system under the different operating conditions that included solids retention time (θ_x), hydraulic retention time (θ), temperatures and VSLR. Table 3.2 provides the key operating conditions that defined P1–P4 and were expected to control, at an operational level, the membrane performance.

During P1 and P2, the impact of the θ_x/θ ratio on AnMBR performance at mesophilic temperature was assessed. In both phases θ_x was maintained at a relatively high value (25 and 35 days) to maximize solids conversion while θ was reduced by about 50 % in P2 relative to P1 (14.3 to 7.3 days). During P3 and P4, the impact of temperature on the AnMBR performance under conditions that would require less energy input for heating (ambient, 25 °C) or have reduced liquid viscosities (η) (thermophilic, 55 °C) were investigated. The operating θ_x of the AnMBR in these phases was adjusted to accommodate expected changes in biodegradation rates at the different temperatures. The ratio of θ_x/θ was increased to 5 during P3 and maintained in the range of 3 during P4.

Viewed collectively, the different operating conditions (θ_x, θ, VSLR and temperature) established a range of mixed liquor properties (MLSS concentrations, MLSS composition, viscosity) that were expected to impact on the membrane performance. Hence, the datasets that were generated allowed for an assessment of the impact of the parameters on membrane performance and cleaning requirements. To assist with the interpretation of the results regression analysis, the VFM approach and classical filtration modeling were employed.

4.4.1 AnMBR Operating Conditions

The parameters that were measured included solids (TS, TVS, TSS, TDS) and COD (CODt, CODp, CODf, CODc) concentrations, extractable extracellular polymeric substances (eEPS) as concentrations, J, ΔP and crossflow velocity (v). To better understand the hydrodynamic conditions, the sludge density (ρ_s), sludge dynamic viscosity (η), shear rate (γ), stress rate (τ) and Reynolds number (Re) were then calculated for the operating conditions. These parameters have been reported to be interrelated and impact membrane fouling [9, 137] and thus served as a basis for a comparison between phases P1–P4.

Solids and COD Concentrations

The role of solids and COD concentrations, with the key operating conditions in P1–P4, were considered for their impact on fouling in a general way based on reported findings from the literature review in Chapter 2. The median concentrations for solids and COD concentrations during the stable operating period for each phase were compared and are shown in Figure 4.5. From Figure 4.5 (a) the median operating MLSS (or TSS) concentrations were 25, 39, 52 and 25 g/L during P1–P4, respectively. These values were greater than 15 g/L which has been reported to be a threshold concentration above which cake or reversible fouling is exacerbated [9]. Hence, the MLSS concentrations would suggest that reversible fouling would be highest in P3, least in P1 and P4 while P2 fouling propensity would lie between.

The dissolved and colloidal fractions are known to impact directly on pore blocking or constriction causing irreversible fouling [9] and were characterized by the total dissolved solids (TDS) and the colloidal COD (CODc) concentrations. The TDS include the colloidal fraction ($< 0.4\mu$m). The median concentrations of TDS were 3.5, 3.5, 7 and 5 g/L for P1–P4, respectively while the median concentrations for CODc were 1.8, 2.4, 10 and 0.8 g/L for P1–P4, respectively. Considering the TDS and CODc concentrations (Figure 4.5 (a)) collectively the results indicate that irreversible fouling would be expected to be highest in P3 and least in P1 or P4 with P2 values in between.

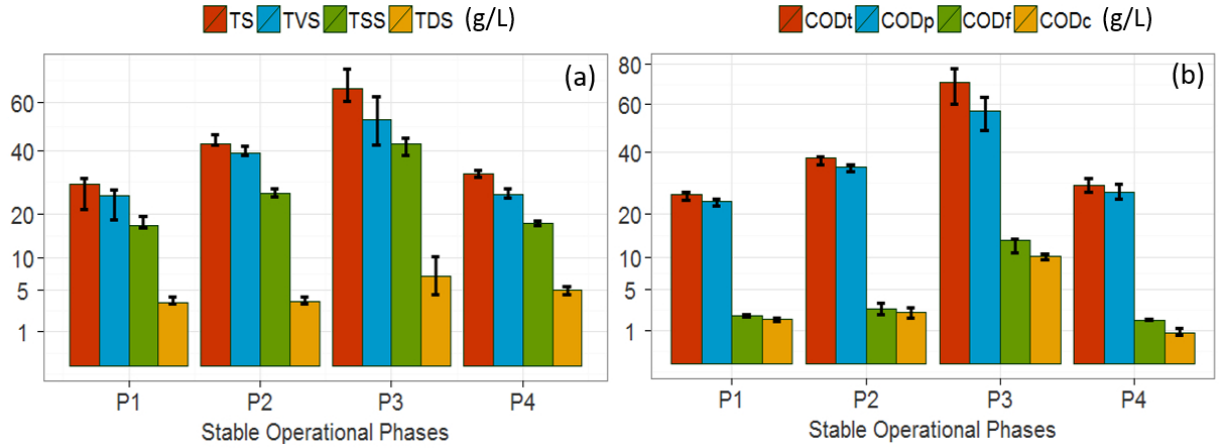

Figure 4.5: Solids (a) and COD concentrations (b) under stable operating conditions in P1–P4.

A comparison between P1 and P2 (Figure 4.5 (b)) showed that at mesophilic conditions, the MLSS increased by 60% and the CODc correspondingly increased by 30% and in both cases would be expected to increase the AnMBR fouling propensity of P2 compared to P1.

A comparison between P3 and P4 showed the combined impact of doubling the θ_x (22–39 d) and operating under ambient and thermophilic temperatures respectively. The operational change from P4 to P3 resulted in a 110% increase in MLSS (Figure 4.5 (a)) and a 13 fold increase in CODc (Figure 4.5 (b)). Due to the changes in MLSS and CODc both the reversible and irreversible fouling would be expected to increase substantially in P3 as compared to P4.

A comparison between P2 and P3 showed the combined impact of increasing the θ_x (25–39 d) and reducing the T from mesophilic to ambient operation, while keeping the throughput or θ constant at 7–8 days. The operational change from P2 to P3 resulted in a 33% increase in MLSS (Figure 4.5 (a)) and a 4 fold increase in CODc (Figure 4.5 (b)). Due to the MLSS increase and CODc increase, both, the reversible and irreversible fouling would be expected to increase during P3 compared to P2 but the difference would be less than between P3 and P4.

Based on the above considerations it is expected that membrane operation in P3 would be impacted most severely by fouling, P1 the least and P2 with P4 would be somewhere in between. Aside from the important role of the MLSS concentration, the role of temperature and θ_x, particularly in the extremes cases of P3 and P4, were considered significant indirect predictors of fouling propensity.

Hydrodynamic Conditions

The hydrodynamic conditions of a membrane process represent physical operating constraints and are fundamental to a thorough understanding of the membrane performance. In the current study the sludge shear strain (γ), the dynamic viscosity (η), shear rate (τ) and the Reynolds number (Re) were investigated. These parameter values were calculated based on the operating crossflow velocity (v), reactor temperatures (T) and MLSS using Eqs. 4.5–4.8 temperature adjusted and Re adapted to account for non-Newtonian rheological properties [75].

Based on the v, sludge density (ρ) and other membrane module configuration properties, the median Re values were 3300, 4200, 1650 and 2200 in P1–P4, respectively. Except for P3, the Re values indicated that operation was in the turbulent regime while P3 operation was in the laminar-turbulent transition zone. Increasing the recirculating sludge pump to increase v beyond 1.1 m/s was investigated during P3 but proved to be problematic due to excessive pump wear and system leaks associated primarily with abrasion from the high fixed solids (FS). It was anticipated that fouling may have been slightly exacerbated in P3 compared to the other phases due to the lower Re.

The η and τ are interrelated through the γ and are controlling factors which affect fouling. The sludge η, is a measure of the sludge resistance to flow, a strong function of MLSS and weaker function of T, however direct correlations to fouling are complicated by the non-Newtonian pseudoplastic nature of the sludge [9]. The induced τ is associated with the

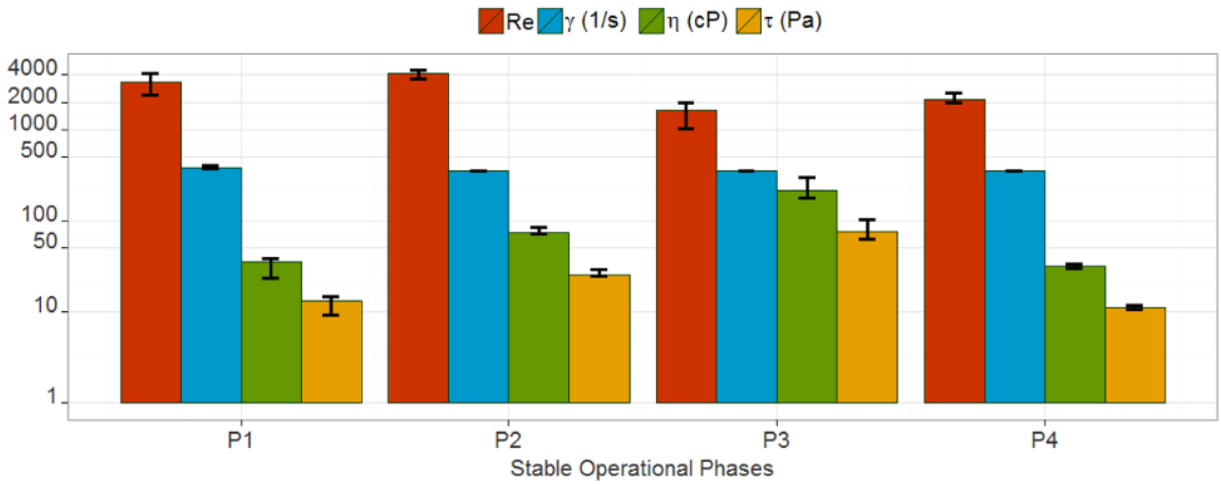

Figure 4.6: Median sludge Reynolds number (Re), shear strain (γ), the sludge dynamic viscosity (η) and shear rate (τ) during stable operating conditions in P1–P4.

sludge pumping rate and as τ increases the sludge floc size is reduced and further promotes the release of bound EPS (bEPS) in the form of free EPS (fEPS) in the bulk MLSS solution and both phenomena have been reported to exacerbate fouling [9].

A statistical paired comparison of η and τ showed a ranking of P3 > P2 > P1 ≈ P4 (p = 0.05) which suggests P3 to be the most, P1 and P4 the least, and P2 somewhere between with respect to increased fouling propensity. Both the highest operating MLSS and lowest T in P3 increased the η and τ which tended to exacerbate fouling. In the case of P4 and P2, the MLSS were similar but the temperature was 20 °C higher in P4 causing the η to be lower.

Considered collectively, the hydrodynamic conditions suggest P3 would be the most severely impacted through increased η, τ and lower Re. Similarly P1 and P4 would likely experience the least amount of fouling with P2 somewhere between based on paired statistical comparisons.

Flux, TMP and Permeability

The effect of flux (J) and transmembrane pressure (ΔP) are combined through the permeability ($K = J/\Delta P$) which plays a key role in the viability and sustainability of AnMBRs treating sludge or concentrated wastewater streams [9]. The median daily J, ΔP and K were computed from data that was collected on a minute basis which was aggregated and averaged to daily median values and shown in Figure 4.7 (a). The corresponding normalized K_{20} values are given in Figure 4.7, (b) which were calculated based on temperature-corrected values of the water viscosity [88] for the different operating conditions based on Eqs. 4.18 to 4.20 [9]:

From Figure 4.7 (a) it can be seen that the median J values were 7.1, 6.1, 6.0 and 6.7 LMH at the corresponding ΔP of 20, 28, 50 and 16 kPa and K values of 0.32, 0.22, 0.12 and 0.40, LMH/kPa for P1–P4, respectively. The lowest K occurred in P3 when compared to the other phases. However P3 had the highest operating ΔP which increased the flux

to the same level as P2. Phases P1 and P4 with the higher K values had the higher flux values. These observations suggest that the K parameter is the the most appropriate for comparing the membrane performance.

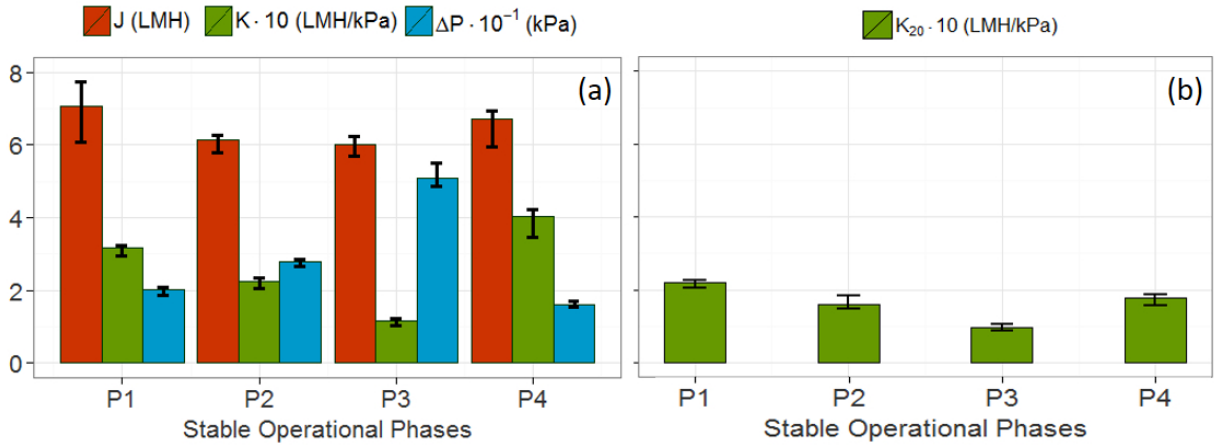

Figure 4.7: The median J, K, and ΔP (a) and K_{20} (b) during P1–P4 under stable operating conditions. The error bars represent the 95 % confidence interval.

To investigate the effect of other factors on K other than temperature the temperature-normalised K at 20 °C (K_{20}) was compared in Figure 4.7 (b). From Figure 4.7 (b) the K_{20} value showed a significant adjustment in P4, compared to K, however the general trends of K and K_{20} were consistent throughout P1–P4. The K_{20} values were 0.10, 0.16, 0.20 and 0.23 LMH/kPa, for P3, P2, P4, P1, respectively and based on paired comparisons ($p = 0.05$) showed a ranking with P3 < P2 < P1 ≈ P4. Despite the lowest K_{20} in P3, the J value was equivalent to P1 suggesting that the higher operating ΔP was sufficient to achieve the operational flux set point for P3. These observations suggest that K_{20} is preferred over K when comparing operational conditions with significant temperature differences. In the case of P3, operating at a higher ΔP proved significant at ensuring that the J set point was achieved.

Collectively the high MLSS during P3 proved to be the dominant factor, with temperature, at reducing the K as seen by a comparison of the K_{20} values. The flux during P3 was also the lowest but comparable to P2 and this was achieved by operating at a higher ΔP in P3 compared to P2 and the other phases.

eEPS Fractions

Extracted extracellular polymeric substances (eEPS) have been reported to be a key agent of fouling with a distinction generally made between the free (C_f) and bound (C_b) eEPS as well as the protein (C_{pr}) to polysaccharides (C_{ch}) ratio (C_{pr}/C_{ch}) [9, 52, 77]. The focus on C_{pr} and C_{ch} associated with bound and free eEPS has been due to their large molecular weights (generally retained by MF and UF membranes) along with their extensive hydrophobic and hydrophilic functional groups, that can cause strong interactions with the membrane and other particles causing fouling [29, 39]. Hence in this study the focus was on the bulk sludge eEPS concentration in the free and bound form and in the characterization

of the C_{pr} and C_{ch} concentrations. The eEPS concentrations during the stable operating periods were compared and are shown in Figure 4.8.

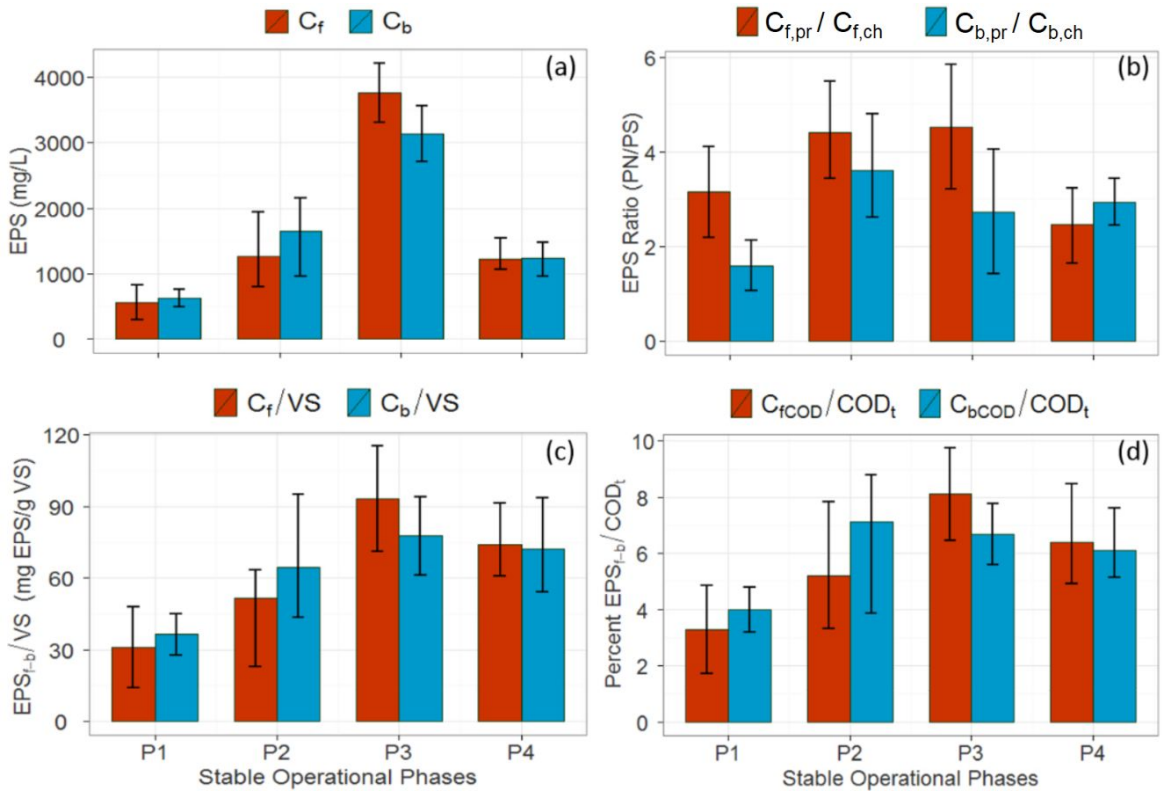

Figure 4.8: The median concentrations of free versus bound eEPS (a); C_{pr}/C_{ch} ratio (b); relative to AnMBR VS in mg eEPS/g VS (c) and percent relative AnMBR total COD (CODt) (d) during P1–P4 stable operating conditions. The error bars represent the 95 % confidence interval.

From Figure 4.8 (a) the median concentration C_f ranged from 550–3800 mg/L and the C_b values from 600–3100 mg/L. A paired comparison of the free eEPS values between phases showed that the P2 and P4 values were not statistically different (p=0.05) but all other paired comparisons were statistically different (p=0.05). Similarly a paired comparison between the bound eEPS showed similar results at the 95 % confidence level (p=0.05). The eEPS levels measured suggest a ranking of P3 > P2 > P4 ≈ P1, with respect to an increasing fouling propensity for both reversible and irreversible fouling types [9, 52, 77].

The concentrations of eEPS observed in this study were about 2–10 fold higher than those reported in various wastewater streams [48, 50, 52] and this was attributed to the higher VS content of the mixed sludge. According to the generally accepted conceptual models of EPS generation [81, 82, 126] active cells generate bound EPS (C_b) and through hydrolysis, cell lysis or shearing the C_b is liberated into the bulk mixed liquor becoming free EPS (C_f). Greater active biomass concentrations lead to higher eEPS, when other conditions are similar. Additionally, in this case, the use of 50 % TWAS, in the feed, likely contributed EPS to the reactor above that which would be generated by bioreactor activity alone. A recent study [138] reported that the added waste activated sludge (up to 15 %) to primary

sludge in an AnMBR, increased the fouling measured as specific resistance to filtration and supernatant filterability. This additional fouling was attributed to excess aerobic sludge hydrolysis resulting in increased biopolymers and EPS in the bulk mixed liquor.

The free and bound eEPS ratios ($C_{f,pr}/C_{f,ch}$ and $C_{b,pr}/C_{b,ch}$) have been previously attributed to exacerbated fouling conditions and in some cases considered more important than separate protein and polysaccharide eEPS concentrations alone [55, 139]. From Figure 4.8 (b) the median $C_{f,pr}/C_{f,ch}$ ratios varied between 3.2–4.5 and the corresponding values for $C_{b,pr}/C_{b,ch}$ ranged between 1.6–3.6. These ratios were consistent with previously reported ratios in the range of 2–5 when TWAS was treated alone [31] suggesting that the addition of primary sludge (PS) had a small effect on the C_{pr}/C_{ch} ratio. When compared to other wastewaters [55, 139] the C_{pr}/C_{ch} for mixed sludge (TWAS + PS), in this study, was within the reported lower range of 2–10.

Further from Figure 4.8 (b) a paired comparison of the free eEPS ratio indicated no difference between P1–P2 and P3–P4 (p=0.05) and a difference in all other paired comparisons (p=0.05). For the bound eEPS ratio ($C_{b,pr}/C_{b,ch}$), a paired comparison indicated no difference between P2–P3, P2–P4 and P3–P4 (p=0.05) and a difference in all other paired comparisons to P1 (p=0.05). The free eEPS ratio comparisons results, with consideration of the median values, suggest a ranking of irreversible fouling propensity to be P3 $\approx$ P4 $>$ P2 $\approx$ P1. The results of the bound eEPS ratios and median values suggest a reversible fouling propensity ranking of P3 $\approx$ P4 $>$ P2$\approx$ P1 [55, 139].

The VS specific eEPS provides another normalized measure for comparison between phases and is a commonly used metric that indicates VS independent factors, such as reactor temperature and hydrodynamic conditions, that may have also contributed to eEPS differences between phases. From Figure 4.8 (c) the free eEPS to VS ratio (C_f/VS) in the AnMBR varied from 31–93 mg/g VS and from 37–77 in the bound eEPS (C_b/VS) for P1–P4. The range in this normalized eEPS value was consistent with other reported values in the range of 5–75 mg/g VSS but exceeded the maximum marginally in P3. The increase in P3 is primarily attributed to the lower operating temperature difference compared to the cited studies [9].

A paired phase comparison between the C_f/VS showed no difference between P1–P2 and P4–P3 (p=0.05) however a statistically significant difference for the other paired comparisons resulting in a ranking of P3 $\approx$ P4 $>$ P2 $\approx$ P1 which is also indicative of irreversible fouling propensity priority ranking. A paired comparison of the C_b/VS values between phases showed no difference between P2–P3, P2–P4 and P4–P3 (p=0.05) however a statistically significant difference for the other paired comparisons with P1 was observed. These comparisons indicate a ranking of P3 $\approx$ P4 $\approx$ P2 $>$ P1 which would be reflective of the reversible fouling propensity priority ranking. When considered collectively these results suggest that P3, P4 and P2 would experience exacerbated fouling propensity compared to P1.

The eEPS is generally a part of the CODt and to determine how this may vary during the phases the eEPS/CODt ratio was calculated and compared. Figure 4.8 (d) provides the eEPS/CODt as a percent based on the eEPS estimated conversion rate of 1.5 mg COD/mg eEPS [3]. On this basis the percent free eEPS of the treated sludge COD values ranged

from 3–8 % and for the bound eEPS from 4–7 %. These values were within the same order of magnitude of previously reported values of 1.6 % in an activated floc [140] and an anaerobic chemostat treating wastewater resulting in a 3 % eEPS/COD ratio [82]. The free and bound eEPS/CODt ratios were highest in P3 and lowest in P1 with P2 and P4 in between and these findings correspond well the trends associated with the eEPS/VS ratio in 4.8 (c). These findings suggests that both VS or COD_t normalized eEPS measures show an equivalent trend between phases.

When considered collectively the above eEPS analysis and comparisons suggested a priority ranking of P3 > P4 ≈ P2 > P1 with respect to overall fouling propensity. The eEPS/VS and percent eEPS/CODt provide equivalent normalised metrics and may be useful for comparisons of the expected quantity of eEPS when monitoring the VS or CODt concentrations in a system. The eEPS distinctions with respect to free, bound and protein/polysaccharides ratios were found to provide useful qualitative trends into the likelihood of both the reversible and irreversible fouling propensity.

Single Parameter Regression

A single parameter non-parametric regression analysis on K_{20} with respect to other system parameters was conducted to better understand the single parameter linear relationships that may exist between the membrane fouling propensity and operating conditions [137, 141, 142]. Through regression empirical relationships are statistically inferred that may provide useful simplified models to direct further fundamental research or provide practical guidance within well defined constraints. The results of the regression analysis [10, 136] were summarised in Table 4.3 and in Figure 4.9. Table 4.3 provides the range, data set size (n) and coefficient of determination (R^2) values for each parameter with respect to K_{20} and Figure 4.9 shows the key graphical results.

Table 4.3: Summary of linear regressions on K_{20} with respect to individual operating parameters in the combined data set in Phase 1–4[a]

Parameter	Range	n	R^2	Parameter	Range	n	R^2
C_f	290–8100	50	0.3	C_b	390–4300	32	0.32
$C_{f,ch}$	90–1360	50	0.2	$C_{b,ch}$	110–1050	36	0.43
$C_{f,pr}$	200–6900	50	0.29	$C_{b,pr}$	220–3350	36	0.25
$C_{f,pr}/C_{f,ch}$	1–9	50	0.0	$C_{b,pr}/C_{b,ch}$	2–6	32	0.0
C_f/VS	10–330	50	0.0	C_b/VS	20–115	32	0.0
$C_{f,ch}$/VS	3–74	50	0.0	$C_{b,ch}$/VS	5-28	36	0.0
$C_{f,pr}$/VS	7–280	50	0.0	$C_{b,pr}$/VS	12–95	36	0.0
T (°C)	22–57	85	0.24	τ (Pa)	2–17	85	0.21
Re	600–6200	85	0.23	θ_x/θ	2–6	85	0.43
θ_x (d)	20–32	36	0.71	θ_x (d)	47–57	20	0.29
TS (g/L)	25–33	35	0.49	TS (g/L)	40–91	42	0.73

[a] Dimensions of C_f, C_b, $C_{f,ch}$, $C_{b,ch}$, $C_{f,pr}$ and $C_{b,pr}$ are in mg eEPS/L mixed liquor; dimensions of C_f/VS, C_b/VS, $C_{f,ch}$/VS, $C_{b,ch}$/VS, $C_{f,pr}$/VS and $C_{b,pr}$/VS are in mg eEPS/g VS.

From Figure 4.9 (a)–(d) the K_{20} showed a decline with an increase in the bulk concentration of total free (C_f) and bound (C_b) eEPS as well as the free and bound polysaccharide fractions

($C_{f,ch}$, $C_{b,ch}$). The individual R^2 values for the eEPS fractions varied between 0.2–0.43 (Table 4.3) and this suggests that less than 43 % of the observed variability in the K_{20} can be explained by these linear models. Among the eEPS fractions, the bound polysaccharide fraction ($C_{b,ch}$) showed the largest R^2 (0.43) to K_{20} and the free polysaccharides ($C_{f,ch}$) the smallest (0.20) with the other fractions in between. This is consistent with other reported observations [52, 55] that showed various eEPS fractions having a variable impact on fouling propensity.

From Figure 4.9 (e) the mean K_{20} showed no change with respect to changes in C_f/VS giving an R^2 of 0.0 (Table 4.3) and this was reflected in other VS normalized eEPS parameters (C_f/VS, C_b/VS, polysaccharides and protein fractions) and included the protein to polysaccharide ratios ($C_{f,pr}/C_{f,ch}$, $C_{b,pr}/C_{b,ch}$). These observations suggest no linear effects of these normalized parameters but this does not exclude potential non-linear or interaction effects which other studies [52, 55] when treating less concentrated wastewaters have reported.

From Figure 4.9 (f) the K_{20} relative to T showed four separate clusters corresponding to the the P1–P4 set temperature operating conditions. The two 35 °C show different K_{20} and this is not captured by this univariate linear regression model suggesting other important factors are missing. From T consideration alone, one would predict that at a lower T a lower K_{20} is expected with no difference above 35 and up to 55 °C. Other studies have shown the effect of T on fouling to be indirect [9] suggesting a multivariate analysis to include other parameters would be needed to fully elucidate the impact of temperature.

From Figure 4.9 (g) the K_{20} showed a dramatic decline from TS of 22–33 g/L followed by a gradual decline from TS 40–91 g/L. The derived functional relationships given by Eqs. 4.21 and 4.22 identify a threshold between TS of 33–40 where the K_{20} rate of decline goes from 0.024 to 0.0025 LMH/kPa. The two equations combined give a coefficient of predictability (GR^2) of 0.66 suggesting that TS alone predict 66 % of the variability in the mean K_{20} over the complete range of operating conditions in P1–P4. A similar TS threshold between 24–34 g/L was previously described as an upper limit with a sharp viscosity increase occurring above these TS values and which led to severe fouling [143] however the link to the rate of change in permeability was not quantified.

$$K_{20} = 0.17 + 0.024 \cdot (33 - TS) \qquad \text{TS} = 22\text{–}33 \text{ g/L} \tag{4.21}$$

$$K_{20} = 0.17 - 0.0025 \cdot (TS - 40) \qquad \text{TS} = 40\text{–}91 \text{ g/L} \tag{4.22}$$

From Figure 4.9 (h) the K_{20} tends to decrease as the shear stress (τ) increases however the R^2 value of 0.21 (Table 4.3) indicates a low explanation of the variability of K_{20} based on τ alone. A previous study treating sludge up to 35 g/L [75] showed how the τ increased exponentially with TS and this would suggest an indirect or non-linear correlation to K_{20}.

Similar to T, Figure 4.9 (i) identifies four clusters around the operating set points of the θ_x/θ in P1–P4. The K_{20} generally declines as θ_x/θ increased with an R^2 value 0.43 suggesting a weak linear correlation. The θ_x was also analyzed and divided into two separate regions and from Table 4.3 a good correlation (0.71) between 20–33 days and a weak linear correlation

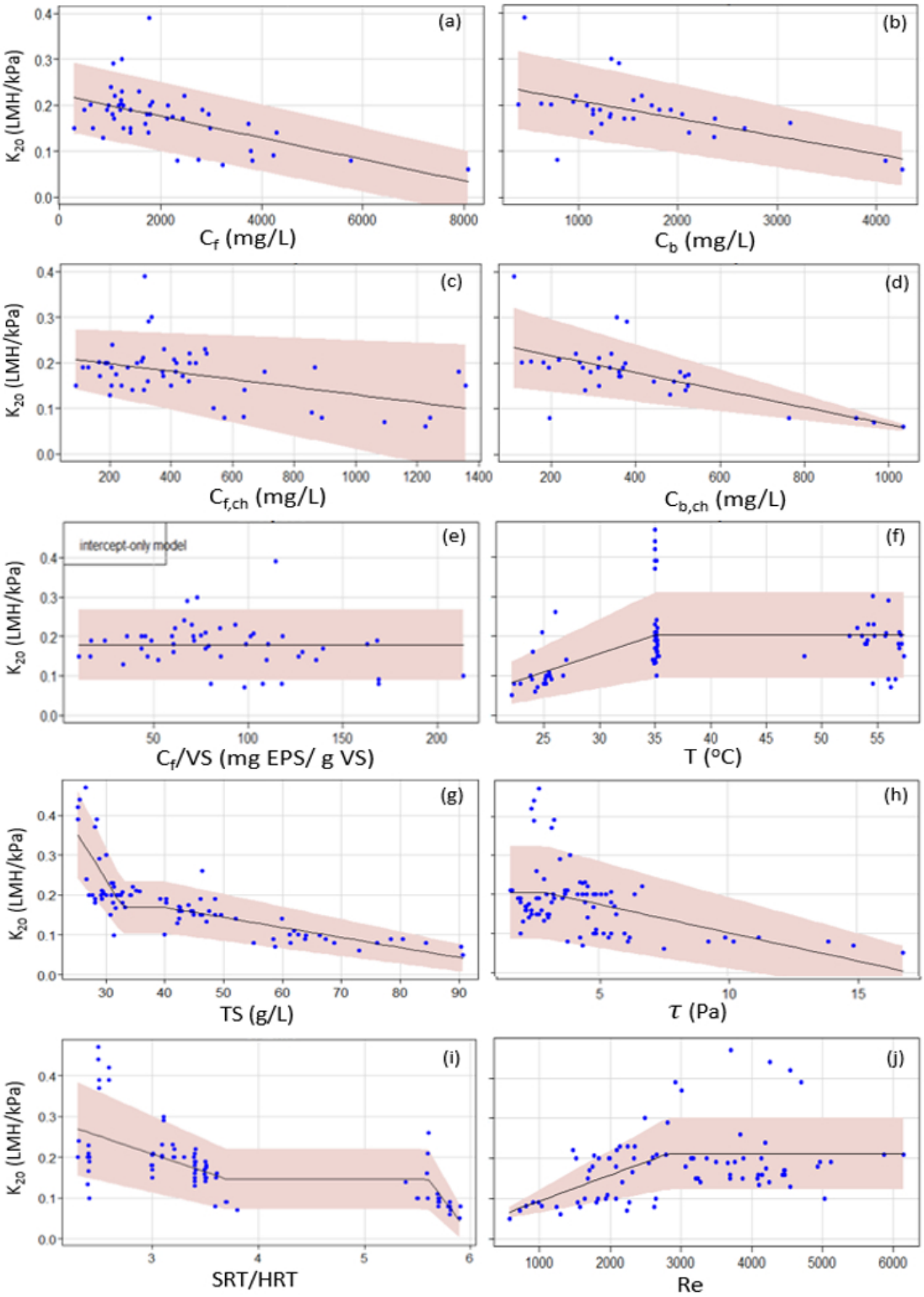

Figure 4.9: Figures showing non-parametric single parameter model results of K_{20} versus C_f (a), C_b (b), $C_{f,ch}$ (c), $C_{b,ch}$ (d), C_f/VS (e), T (°C) (f), TS (g), τ (h), θ_x/θ (i) and Re (j) with 90 %-ile confidence band (shaded).

(0.29) between 45–57 days. The θ_x but not θ_x/θ has been previously found [9, 80] to be a primary operational parameter affecting fouling propensity indirectly. A multivariate regression with a link to eEPS or other primary fouling agents is suggested and has been previously recommended [9].

From Figure 4.9 (j) the effect of increasing Re resulted in an increase in K_{20} up to a value of 2800 followed by a stable K_{20} above this threshold. A previous study reported that a value of Re above 2100, for TS up to 35 g/L [75], did not provide any additional improvement in permeability. This study suggests that a higher Re up to a 2800 value may improve the permeability but beyond this point no additional benefit would observed. Considered that Re is exponentially related to TS the observed Re difference is not significant.

Considered collectively the univariate regression analysis modeling found the TS to be the most appropriate predicator of K_{20} during ambient, mesophilic and thermophilic operation. A threshold was observed between TS of 33–40 g/L that showed a 10 fold decrease in the rate of permeability decline above 40 g/L compared to when TS were less than 33 g/L. These findings suggest that at a lower TS the cake fouling is not adequately developed to exclude colloids and solutes from getting into the membrane pores and fouling is occurring at a rapid rate due to pore constriction. At higher TS concentration the dynamic cake filtering action is well developed and acts efficiently to exclude colloidal and solutes that could have entered the membrane pores [9]. Other individual parameter effects on K_{20} were found to be linearly less important than the TS however interaction or non-linear effects require a multivariate regression analysis to be more thoroughly explored.

Multivariate Regression

To determine the combined effect of eEPS constituents, TS and operating conditions the combined parameter data set were analysed using multivariate regression. The results showed that the TS, θ_x/θ and $C_{b,pr}/C_{b,ch}$ provided the best predictive model (Eqs. 4.23 and 4.24) with a GR^2 and R^2 of 0.75 and 0.89, respectively. The corresponding relative importance factors for TS, θ_x/θ and $C_{b,pr}/C_{b,ch}$ were $1.0 : 0.45 : 0.16$, respectively. The other parameters did not increase the predictability of the model (i.e., GR^2 was not increased) and were excluded from the model. These results suggested that the TS is about 2-fold more important at predicting the mean permeability than θ_x/θ and about 6 fold more important than the bound protein to polysaccharide ratio. Similarly the θ_x/θ ratio is 3.3-fold more important than the $C_{b,pr}/C_{b,ch}$ ratio at explaining the K_{20} variability.

$$K_{20} = 0.20 + (33 - TS)\left(0.17 - 0.032\frac{\theta_x}{\theta} - 0.018\frac{C_{b,pr}}{C_{b,ch}}\right) \tag{4.23}$$

$$K_{20} = 0.20 - 0.003 \cdot (TS - 33) \tag{4.24}$$

Equation 4.23 is valid for TS in the range of 25–33 g/L, θ_x/θ in the range of 2.4–3.5 and $C_{b,pr}/C_{b,ch}$ in the range of 2.0–3.9. Similarly Eq. 4.24 is valid for TS in the range of 33–76 g/L with a corresponding θ_x/θ in the range of 3.0–5.8 and $C_{b,pr}/C_{b,ch}$ in the range of 1.5–6.1 throughout P1–P4 operating conditions. Equation 4.23 predicts a rapid decline of K_{20} within a TS range of 25–33 g/L interaction effects reduce K_{20} further as the ratios

$C_{b,pr}/C_{b,ch}$ and SRT/HRT increase. Beyond the TS threshold of 33 g/L, Eq. 4.24 predicts a gradual decline of K_{20} with no interaction effect from SRT/HRT or $C_{b,pr}/C_{b,ch}$.

Equation 4.23 and 4.24 predict a K_{20} decrease rate of about 0.025 LMH/kPa per g TS at the TS range of 25–33 g/L and at a rate of 0.003 LMH/kPa per g TS at the TS range of 33–76 g/L. The K_{20} is predicted to decrease at about an 8-fold rate faster at the lower TS range compared to the higher TS range. At the lower TS range the θ_x/θ and $C_{b,pr}/C_{b,ch}$ played a more significant role in affecting the K_{20} compared to the higher TS range where no significant interaction effects were observed. This phenomena had been previously reported in other studies using concentrated wastewater streams and explained by the role of the cake fouling acting as a dynamic pre-filter [9].

The multivariate regression analysis results suggest that TS, θ_x/θ and C_{pr}/C_{ch} are the most appropriate predictors of the K_{20} under P1–P4 explaining about 89% of the observed variability in the mean permeability with a 75% estimated model predictability. Further at the TS range of 25–33 g/L there is significant interaction between the TS with the SRT/HRT and C_{pr}/C_{ch} which affected the K_{20}. However at the higher TS range of 33–76 g/L, no significant interaction effects were observed.

4.4.2 Membrane Cleaning

The clean-in-place (CIP) sequential cleaning cycle was used and found to be effective at maintaining the operational set points determined by the operating HRT and SRT (Table 3.1). The four CIP steps included a hot water flush, abrasive clean, base and acid clean in sequence. No cleaning-off-place (COP) was practiced for the full operating period which included a 3-month stabilization period during each phase to minimize down-time. The frequency of the CIP was greatest in P3 (every 3–7 days) and least in P1 (14–21 days) and about every 7-days for P2 and P4.

The effectiveness of the flux recovery, during the stable operation, was measured by the percent flux recovery (FR) index [144] given by Eq. 4.25:

$$FR = \frac{J_c}{J_o} \cdot 100 \tag{4.25}$$

where J_c is the water cleaned membrane flux at a given ΔP and J_o is the water flux through the virgin membrane measured at an average of 300 LMH at 30 kPa. The results of the flux recovery comparisons during P1–P4 are shown in Figure 4.10.

From Figure 4.10 (a), the total flux recovery was typically about 38 % or 115 LMH in P1 and 12 % or 36 LMH in P2–P4 at 30 kPa. However despite this degree of water flux recovery during the cleaning, once the membrane was put back in operation the flux adjusted rapidly to a reduced initial flux in the range of 12–25 LMH. A recent review on fouling and cleaning UF membranes by Shi et al (2014) [145], found that typically less than 20 % of the clean water flux is recovered in wastewater applications and a further reduction is immediately experienced once the membrane in placed back in operation which is consistent with the observations in this study.

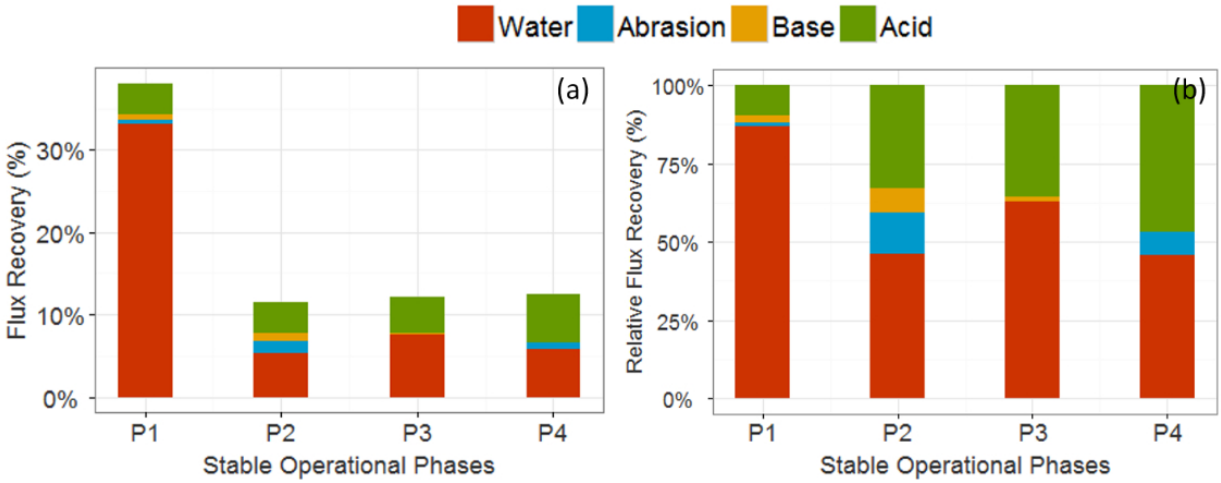

Figure 4.10: Comparison of percent flux recovery (a) and relative flux recovery (b) in P1–P4

From Figure 4.10 (b), the flux recovery was primarily due to the water flush which provided between 45–80 % of the relative flux recovery, followed by the acid clean which provided between 10–45 % of the overall flux recovery. The base and abrasion clean typically resulted in less than 10 % relative flux recovery throughout P1–P4. Base cleaning was typically less effective than abrasion except in P3 where abrasion was generally insignificant at improving the flux recovery compared to the water, base or acid clean.

The effectiveness of the water flush, compared to the other cleaning modes (Figure 4.10 (b)), suggests that surface cake fouling was the primary mode of fouling in P1–P4. This was consistent with other studies treating concentrated wastewater or TWAS under anaerobic conditions [9, 31, 145, 146] which identified cake fouling a the most important contributor to filtration resistance.

The citric acid used in the acid clean is known to be effective at dissolving predominantly inorganic precipitates and acting as a chelating agent to destabilize cationic bridging commonly known to stabilize EPS aggregates [9, 145, 147]. During P2–P4 30–50 % of the relative fouling was recovered with the acid clean as compared to P1 where only 10 % of the relative fouling was recovered using the acid clean. A decrease in MLSS during P1 may have explained the reduced fouling associated with inorganic or cationic-EPS aggregates as compared to P2–P4. Another study treating concentrated wastewaters anaerobically using an AnMBR [146] found inorganic fouling to be associated with the cake layer as well as the membrane. The results suggest that the acid clean works to destabilize the cake fouling layer and any residual irreversible fouling. This would explain the relatively good flux recovery during the acid clean.

The abrasive clean, using the manufacturer recommended 25 mm diameter sponge balls, was visibly effective at removing scaling residuals which formed between cleaning events. However there was a small contribution (< 10 %) to the measured flux recovery as shown in Figure 4.10. Abrasion is effective at dislodging particulates adsorbed on the membrane surface however it may simultaneously dislodge fine particulates that could enter the pores

resulting in pore constriction or blocking which would partly explain the low flux recovery consistent with findings reported in other studies [9, 31, 145].

The use of a base or alkali (NaOH (aq)) is known to be effective at dissolving predominantly organic foulants [9, 145] however it was found that the base clean provided minimal flux recovery (< 10 %) during P1–P4. A study investigating various chemical cleaners on UF membranes fouled by activated sludge found the NaOH (aq) at 10.5 pH solution was less than 23 % effective at restoring the clean water flux and it was suggested that the hydrolysis of polysaccharides and proteins was insufficient to solubilize these foulants [147]. Increasing the contact time by extending the soaking period (> 2 hours) may have improved the base clean effect.

Overall the results of the cleaning strategy suggest that the operational set points during P1–P4, based on variable HRT and SRT, may be maintained by a cleaning strategy using variable frequency CIP alone and using a 4-step sequential cleaning strategy. The frequency of the CIP was greatest in P3 (every 3–7 days) and least in P1 (14–21 days) and about every 7-days for P2 and P4. However the CIP approach employed left a significant flux potential (68–88 % of the clean water flux) under-utilized throughout the study. An improved cleaning strategy by adding membrane relaxation [31] and a clean-out of-place (COP) step to increase the acid or base soaking time [9, 145, 148], may increase the overall clean water flux recovery and reduce the frequency of the CIP.

4.4.3 Short Term and Residual Fouling Rate

The influence of operating conditions on the short term fouling rate (STFR) during the first 10 minutes of the permeation cycles and the residual fouling rate (RFR), over a sequence of permeation cycles), between cleaning events, was investigated to better understand how the rate of fouling changed with operating conditions. The STFR is a measure of the rapid flux decline rate within the first 10 minutes of operation and has been previously classified as reversible fouling, associated with cake filtration. In contrast the LTFR (residual fouling) has been attributed to irreversible fouling and reported to be about 10–100 fold lower than the STFR during constant flux operation [80]. Figure 4.11 shows the median STFR and RFR measured during P1–P4.

From Figure 4.11 (a), the STFR was found to be significantly greater than the LTFR throughout P1–P4 with P3 $\approx$ P4 $<$ P2 $<$ P1 and the LTFR had a similar but reverse trend with P3 $\approx$ P4 $>$ P2 $>$ P1. From Figure 4.11 (b) the ratio of the STFR/LTFR was generally greater than 10 with P1 $>$ P2 $>$ P3 $\approx$ P4. Further the observed ratio of STFR/LTFR in this study, operating at our constant pressure, varied from 30–120 in P2–P4 and was about 900 in P1, which is on the high range but still within the same order of magnitude compared to other reported values [80].

The results of this fouling rate comparisons suggest that the STFR operates over a shorter time-scale with a significant higher flux decline during the initial permeation period compared to the LTFR and this was consistent under all the different phases. The reason for the relative magnitudes and ranking of the STFR between phases is not immediately apparent but it is anticipated that the subsequent flux decline modeling may provide some insights into the casues of these observations. Generally efforts to better understand the

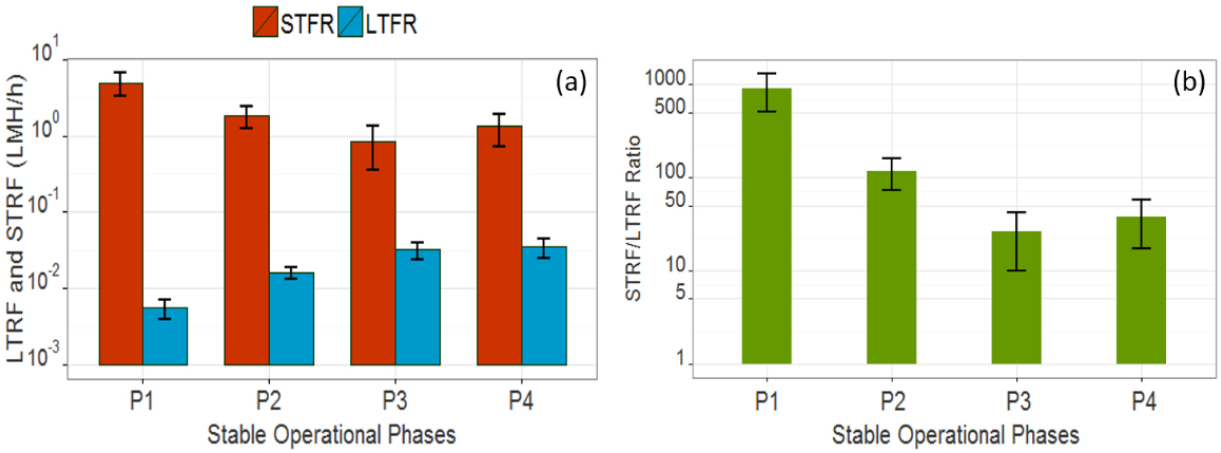

Figure 4.11: Median STFR and LTFR (LMH/h) in each phase (a) and ratio of the STFR/LTFR (b).

underlying causes and to reduce the STFR would prove more cost-effective at improving the overall membrane system viability compared to similar efforts at controlling the LTFR.

4.4.4 Fouling Propensity Using VFM

Following the VFM approach [88] individual fouling propensity curves were generated for permeation cycles during stable operation in P1–P4 and these are shown in Appendix B Figures B.11–B.13. Each VFM curve represents the cumulative throughput ($\Sigma V/A$) versus the membrane normalized cumulative reversible ($\Sigma R_r/R_m$) or irreversible ($\Sigma R_i/R_m$) resistance over a series of permeation cycles between cleaning events. The individual curves in each phase were combined to generate median curves for each phase for comparison between reversible and irreversible fouling propensity as shown in Figure 4.12.

From Figure 4.12 a significant increase in both the irreversible and reversible fouling propensities occurred with a throughput of less than 0.2 m^3/m^2. At a throughput greater than 0.2 m^3/m^2 the irreversible fouling decreased but increased for the reversible fouling (note the x-axis is a log scale) in all the phases. This suggests that at a low throughput different permeability control strategies to target the higher reversible fouling would be more effective at recovering flux than other strategies targeting irreversible fouling.

From Figure 4.12 (a) the irreversible fouling propensity showed similar trends in P1–P4 with a rapid fouling for throughputs of less than 0.2 m^3/m^2 followed by a more gradual fouling rate above this level of throughput. Considering 0.5 m^3/m^2, for comparison purposes, the cumulative irreversible fouling ($\Sigma R_i/R_m$), primarily attributed to pore constriction and blocking [16], were 500, 300, 220 and 80, with P1 > P3 > P4 > P2, respectively. Each phase showed clearly distinct levels of irreversible fouling but similar overall trends. The relative differences in irreversible fouling suggests that chemical cleaning would be a more effective strategy in recovering lost permeability in P1 and least in P2 with P3 and P4 somewhere between.

From Figure 4.12 (b), the corresponding reversible fouling propensity ($\Sigma R_r/R_m$) primarily attributed to cake fouling, biofilm growth and further pore blocking [16], was significant

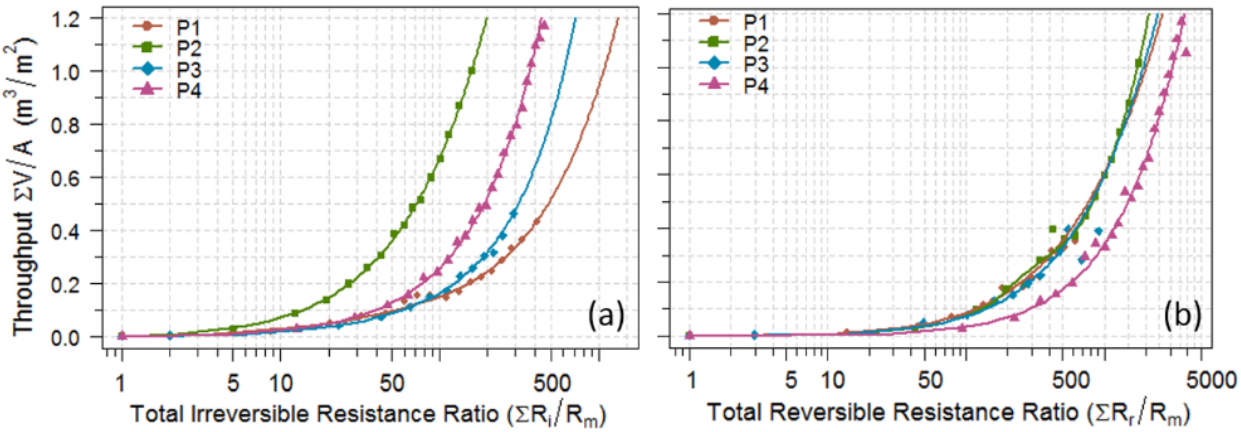

Figure 4.12: Comparison of the fouling propensity as measured by VFM diagrams for the median irreversible (a) and reversible (b) resistances during P1–P4.

during the first 0.1 m^3/m^2 throughput reaching a $\Sigma R_r/R_m$ value of 100 in P1–P3 and 300 in P4. At a throughput of 0.5 m^3/m^2, for comparison purposes, the $\Sigma R_r/R_m$ values were 1500 for P4 and 600 for P1–P3. These differences are consistent over the complete throughput range and suggest that a rest or relaxation period to recover permeability associated with reversible fouling would be most effective in P4 and less but equally effective in P1–P3.

These findings were consistent with the relative values of the reversible and irreversible fouling observed with the treatment of TWAS using a sAnMBR which showed the reversible fouling propensity to be 5 to 10 times greater than the irreversible fouling propensity [31]. Another study that investigated the filtration of activated sludge resistance from a PVDF membrane showed that the combined pore and membrane resistance (irreversible) accounted for 10% and the cake fouling (reversible) for 90% of the total filtration resistance [142] is also consistent with the findings in this study.

Considering the VFM analysis results collectively, differences in reversible and irreversible fouling propensities between P1–P4, were clearly quantified and discernable. This clear distinction suggests that the VFM approach may be a valuable tool to quantify the type of fouling, relative to throughput, which can then be used as a trigger in a smart fouling controller. The controller may then be programmed to activate different operational or membrane cleaning strategies in a timely fashion consistent with the type of fouling and thus improve the system viability. Similar operational controllers but based on flux, TMP and shear control (CFV or sparging rates) have been proposed [149] particularly for the economical control of cake formation when operating at high solids concentrations. However to further substantiate the accuracy of the VFM method results, an independent measure of fouling type should be investigated for comparison.

4.4.5 Membrane Flux Modeling

To better understand the underlying dominant fouling mechanism in P1–P4, the crossflow adjusted classical blocking models (Eqs. 4.9–4.13) were used to fit the measured flux decline data. A representative number (100–200) of permeation cycles within each phase P1–P4

were modeled using the cake filtration (m = 0), intermittent blocking (m = 1), complete blocking (m = 2) and standard blocking (m = 3/2) models [90, 91]. The permeation cycles modeled covered between 25 to 50 days of operation during each phase equivalent to approximately 1–2 SRTs during stable operation. This extensive data set was analyzed to better understand the variability associated with treating a complex concentrated sludge matrix and to find the expected range of suitable model parameters for practical use. Examples of best fit model curves, relevant parameter values and corresponding sum of residual standard errors (RSEs) are provided Appendix B.

Dominant Fouling Mode Analysis

Application of the 'Hermia-Field' mechanistic models facilitated an investigation of the dominant fouling mode. An examination of the model fits in each phase (given in Appendix B, Table B.4 and Figure B.5–B.8) showed that the best-model fit (n=124–224) was demonstrated by the cake filtration model (m = 0) which had the lowest median RSE (0.3–0.4) while the standard blocking model (m = 3/2), had the largest RSE (1.2–2.3) with the poorest model fit.

The poor fit of the standard blocking model (m=3/2) was attributed to the model structure that only accounts for particle deposits within the membrane pores and does not address membrane surface fouling and is not affected by shear induced crossflow. These limitations of the standard blocking model likely accounted for the failure of the model to adequately describe the observed flux decline in all phases (Figure 4.13).

To compare the models best data fit between each phase, a statistical paired comparison at the 95 % confidence level of the RSE was conducted. The paired comparison (Table B.2) showed that during P1 the cake filtration model (m = 0) provided the best model fit; during P2 and P4 the three models (m = 0, 1 and 2) were equivalent (p = 0.05) and no dominant single mode of fouling could be identified. During P3 the cake filtration model (m = 0) and intermediate blocking (m = 1) were equivalent (p = 0.05) and provided a better model fit than the complete blocking model (m = 2). Based on this comparison the cake filtration model (m = 0) proved to be the most appropriate model to predict the flux decline for the full filtration period when considering all the phases combined.

Despite the generally good model fit of the three "Hermia-Field" models (m= 0, 1 and 2) to the measured flux decline data, areas of less than optimum fit were observed and these areas were considered further. The curves presented in Figure 4.13, were representative of all the fitted curves and showed that the model curves (m = 0, 1 and 2) consistently underestimated the rapid flux decline ($t_p \leq 10$ min). This underestimation suggests that the early fouling mode is not adequately modeled by any one of the fouling modes alone. Further, after about a t_p of 100 minutes, all the models tended to over predict the flux level and this was likely related to the incompressible particles assumption made in all the four models [90, 91].

It has been shown that when sludge cake compressibility was accounted for in changing pressure (ΔP) operation, improved model fitting was observed [150]. Cake compressibility has been attributed to deformation of sludge flocs and rearrangement of particles within the cake and both these phenomena have been shown to be time dependent [151].

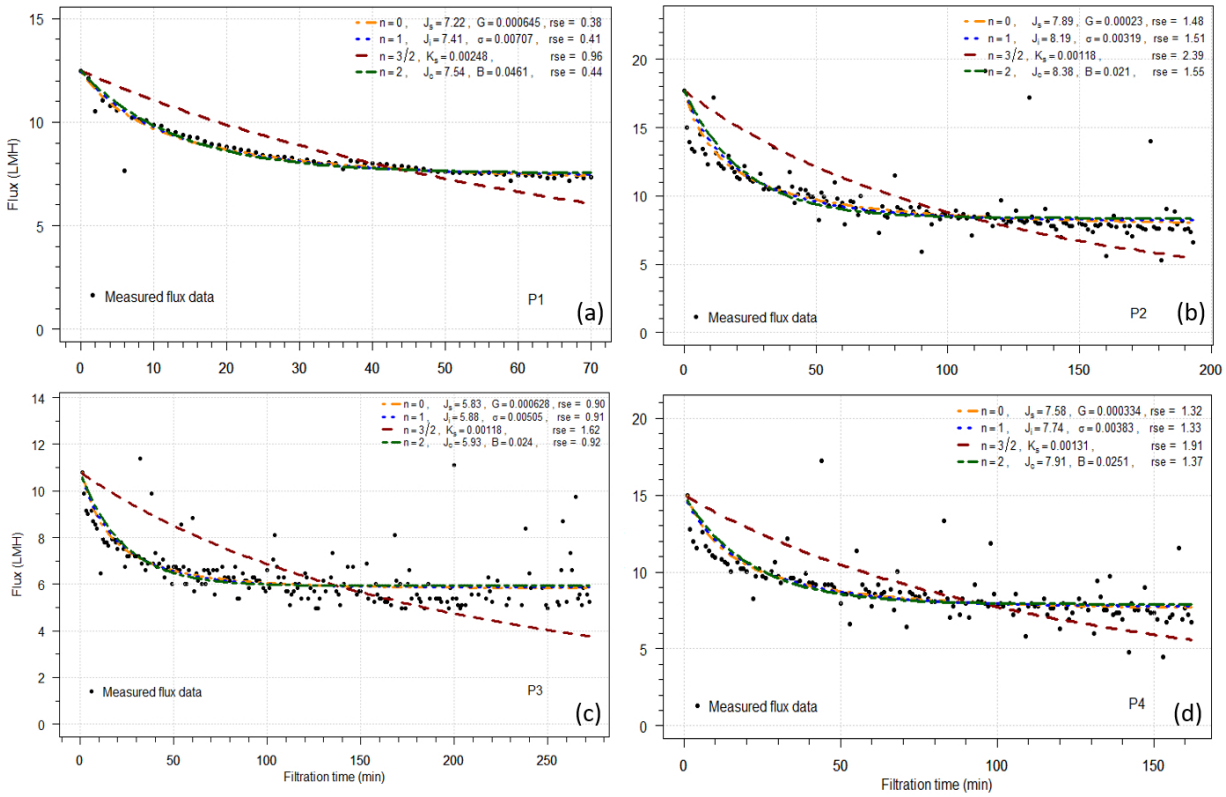

Figure 4.13: Representative model fit analysis for P1 (a), P2 (b), P3 (c) and P4 (d) showing the model parameters and RSE.

Two possible improvements to the present modeling approach would be to formulate a model that combines 2 or 3 modes of fouling concurrently and to include cake compression in the model formulations, however these are non-trivial extensions for constant pressure cross flow operation. Recently 2-mode [152] and 3-mode [123] models have been developed for dead end filtration and shown to provide improved flux decay predictions for simple protein mixtures. However these 2 or 3-mode dead-end filtration models tend to be highly parameterized requiring more extensive and intensive monitoring than provided in practical applications. Their predictive abilities have also not been investigated in complex matrices such as concentrated wastewaters which are known to contain a complex array of foulant types.

Another approach that has been used is to segment and separate parts of the flux decay curve and model each part by the most appropriate model separately [153]. This latter approach has been reported to improve flux decay predictions but was also limited to one dominant fouling mode, at any period, and has been shown to need appropriate data filtering. The data filtering became limiting when the frequency of on-line data acquisition increased, which was associated with heightened noise in the measurements. Measurement noise in the current study during on-line minute-data acquisition also proved to be an interference factor when trying to decipher the dominant fouling modes in P2–P4 but not in P1.

The results presented in this section demonstrated the application of the 'Hermia-Field'

models applied to a sludge matrix and concluded that cake filtration (m=0) was the dominant fouling mode. However the modeling generally underestimated the flux decline in the first 10-minutes and underestimated the flux decline after 100-minutes of permeation. It is suggested that these limitations may be overcome by extending the model to incorporate multiple modes of fouling concurrently and by incorporating a sludge compression parameter. The model is still considered useful as on-line model based controller to help identify the dominant fouling mode and assist with a fouling mitigation strategy.

Key Model Parameter Predictions

As previously described the cake filtration model (m=0) proved to be the most appropriate model to predict the flux decline for the full filtration period during P1–P4. As such the calibrated model parameters including J_s, G, J_o, R_o, $\alpha \cdot k_c$ and $\alpha \cdot S$ were calculated (Table 4.4) for comparison.

Table 4.4: Cake filtration model (m=0) median parameter values in P1–P4

Parameter[a]	Stable Operational Phases			
	P1 Median(CI) n	P2 Median(CI) n	P3 Median(CI) n	P4 Median(CI) n
J_s (LMH)	6.0 (0.3) 114	6.7 (0.1) 224	5.5 (0.1) 120	6.5 (0.2) 185
$G \cdot 10^{-4}$ $(s \cdot m^{-2})$	7.6 (0.4) 114	6 (1) 224	5.6 (0.6) 120	4.5 (0.7) 185
J_o (LMH)	13.0 (0.3) 114	13.0 (0.4) 224	10.8 (0.5) 120	17.3 (0.8) 185
$R_o \cdot 10^{-12}$ (m^{-1})	6.3 (0.1) 114	5.3 (0.2) 224	13.6 (0.1) 120	5.9 (0.6) 185
$\alpha \cdot k_c \cdot 10^{-15}$ (m^{-2})	3.9 (0.3) 114	2.6 (0.6) 224	5.1 (0.8) 120	2.9 (0.5) 185
$\alpha \cdot S \cdot 10^{-9}$ $(m^{-1} \cdot s^{-1})$	6.6 (0.5) 114	4.5 (1.1) 224	7.7 (1.3) 120	5.3 (1.1) 185

The J_o and J_s values are the initial and limiting or steady state flux within the filtration cycle, respectively and reflect the hydrodynamic conditions of the reactor. Particularly J_o reflects the effectiveness of the flux recovery during the rest period between filtration cycles. The J_s reflects the balance between the convective transport to the membrane balanced by the shear induced back transport. The R_o value is the hydraulic resistance associated with the fouled membrane at the beginning of a cycle. The G value is a composite model parameter given by $\alpha k_c/(J_o R_o)$ and may be interpreted as the accumulated resistance for a given throughput rate. The α value is the specific cake resistance and k_c is the cake filtration constant and the product of the two parameters is related to the resistance of the cake fouling per volume of filtrate. The S parameter is the rate of cake erosion per unit area and the product $\alpha \cdot S$ may be interpreted as the cake resistance reduction rate based on cake erosion associated with crossflow induced shear [91].

From Table 4.4 the R_o, $\alpha \cdot k_c$ and $\alpha \cdot S$ values were highest in P3 and suggests a significantly higher membrane fouling resistance, higher cake fouling per volume of filtrate but also a higher cake erosional resistance reduction rate, respectively, compared to P1, P2 and P4. The model predictions correspond well with both the MLSS, free and bound eEPS and highest τ value of ambient operation in P3. All these factors have been previously reported [55, 80, 121] to exacerbate fouling and confirm our observations of P3. The high erosional

resistance reduction rate in P3, however, assisted in the the recovery of J_o but the median J_o was still less when compared to P1, P2 and P4.

To compare the cake filtration predictions of the flux decline, the measured median G, J_s and J_o values for P1–P4 (n=120-224) in Table 4.4 were used to model the flux decay curves predicted by the cake filtration model (m = 0) (Eq. 4.9) were solved numerically along with the relative rate of flux decline ($D = -J^{-1} \cdot dJ/dt$) and the change in D ($D^2 = -J^{-2} \cdot (d^2J)/(dt^2)$) shown in Figure 4.14 (a) to (d), respectively.

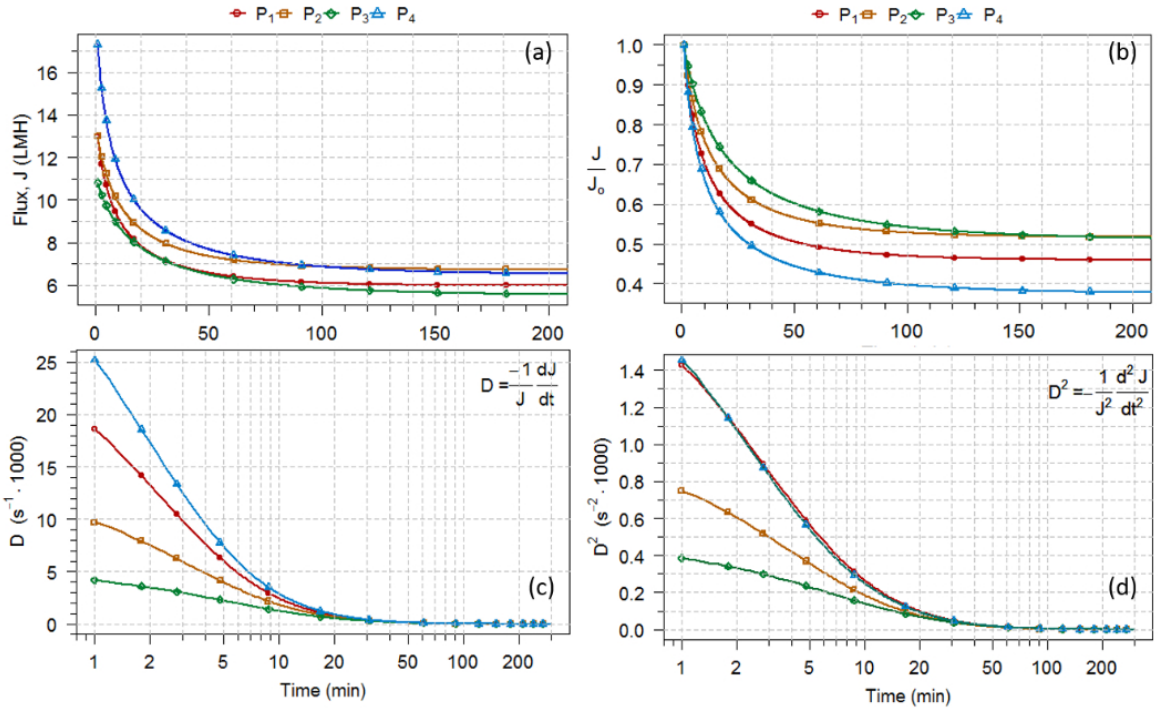

Figure 4.14: Modeled (m = 0) median flux decline (a), normalized flux (J/J_o) declining curves (b), rate of flux decay (D) (c) and change in the rate of flux decay (D^2) (d) for P1 – P4 stable operating conditions.

From Figure 4.14 (a) we see a rapid flux decline was predicted for the first 10 minutes followed by a more gradual flux decline up to the 60 minute filtration time leading to limiting or steady state flux (J_s) within an additional 40 minutes of filtration and the flux decline can be divided into a three stage process. The three stages of flux decline have been previously reported on [151] and characterized in terms of hydrodynamic conditions where the convective transport of particles decreases with filtrate flux and steady-state or limiting flux is reached when the convective transport is balanced by the shear induced back transport. In each phase the median J_s values were different with P3 < P1 < P4 < $P2$ however in all cases it J_s was reached at about 100 minutes of permeation. This suggests that operationally maintaining a constant filtration run beyond 40–50 minutes without a rest period will not improve the throughput.

The normalized flux decline curves (J/J_o), shown in Figure 4.14 (b), were investigated for each phase to better understand the overall flux decline in each phase. From Figure 4.14 (b)

the overall flux decline, when reaching J_s, was 45, 40, 34 and 28 % for P4, P1, P2 and P3, respectively. These total flux losses were found to be inversely related to the J_o. The higher the J_o value the greater initial percent flux decline observed and lower the J_s. However in the comparison of P1 and P2, which had the same J_o, the different G values affected the flux decline and the J_s. Comparing P1 and P2, the $G_1 > G_2$ by 21 % and made the flux decline in P1 15 % greater than P2. This difference in the total flux decline between P1 and P2, is consistent with the interpretation of G which represents the accumulated resistance for a given throughput rate, which would result in a greater flux decline based on Darcy's law. These results suggest that both J_o and factors associated with G should be considered in selecting an initial flux operating range since it has a direct effect on the initial flux decline along with the time and value to reach the limiting flux.

It was previously reported [154] that the rate of flux decline (D) can predict the presence of intermolecular aggregation and this was part of the motivation for investigated this as shown in Figure 4.14 (c). From Figure 4.14 (c) the rates of flux decline (D) were compared between P1–P4 and evaluated for any peaks. The D values have been previously reported [154] to pass through a distinct maximum where protein aggregation or strong intermolecular linkages occur and to be absent otherwise. In the current study no distinct maximum under any of the phases was observed suggesting no strong intermolecular linkages occurred when treating mixed municipal sludge under P1–P4. The initial D values were 25, 18, 10 and $4 \cdot 10^3$ (s^{-1}) with a ranking of P4 > P1 > P2 > P3 showing the flux decline rate to correspond to the J_o model median values. The D values were consistently lower for P3 up to a filtration period of 20 minutes. A convergence of the D values for all the phases P1–P4 was observed beyond 20 minutes and reaching a value of zero above 50 minute filtration period. These observations suggest that flux decline rate and underlying fouled membrane conditions, after a filtration time of 20 minutes, are equivalent in terms of the flux decline rate. Based on a D value of 0 above 50 minutes filtration time under all the phases anticipating the onset of the limiting flux and suggests an appropriate time to use the CIP to recover the lost flux.

The rate of change in D (D^2) was also considered in an effort to quantify the rate of flux decline under the different phases as shown in Figure 4.14 (d). From Figure 4.14 (d), the initial D^2 values were 1.4, 1.4, 0.75 and $0.4 \cdot 10^3$ (s^{-2}) with a ranking of P4 $\approx$ P1 > P2 > P3, respectively. The D^2 values were consistently lower for P2 and P3 with P3 being about 50% of P2 and 30 % of P1 or P4 up to a filtration period of 30 minutes. A convergence of the D^2 values for all the phases P1–P4 was observed beyond 30 minutes and reaching a value of zero above 60 minute filtration period. Similar to D, D^2 may be used as a supporting indicator to anticipate the onset of the J_s by providing an independent measure of how fast the rate of fouling changes.

The results of the flux modeling, when considered collectively, suggest that the cake filtration model (m=0), when modeling the complete filtration cycle, provided a better prediction of flux decline in the sAnMBR mixed sludge treatment operation during P1–P4 compared to intermediate blocking (m=1), standard blocking (m=3/2) and complete pore blocking (m=2). The J_o and G parameters were found to be good predictors of the limiting flux (J_s) based on the cake filtration model (m=0). The D and D^2 rates can anticipate the onset of J_s by 20–30 minutes earlier than J values alone and can be used as trigger variables in model-

based fouling control strategies. The "Hermia-Field" modeling approach was observed to underestimate the flux decline at the beginning ($<$ 10 minutes) and latter parts of the permeation cycle ($>$ 100 minutes). Potential improvements to the model are suggested by incorporating multiple fouling modes to operate concurrently and incorporating a a sludge compression factor. However these model improvements, for crossflow applications, require some conceptual challenges and are not considered trivial extensions.

4.5 Summary and Conclusions

This phase of the study, on the membrane performance, demonstrated that fouling mitigating strategies that included a rest period between permeation cycles and a 4-step CIP strategy, applied at different frequencies from 3–21 days, were adequate to maintain the sAnMBR operational under ambient, mesophilic and thermophilic operation when treating mixed municipal sludge. Ambient operating conditions which also had the highest MLSS operating conditions and highest SRT/HRT ratio proved to be the most challenging in terms of fouling control effort.

A review of the operating solids, COD concentrations, eEPS fractions and AnMBR hydrodynamic conditions which included Re, η and τ proved useful as predictive qualitative indicators of potential fouling. Temperature correction (at 20 °C) of the permeability, based on viscosity temperature adjustment, proved to be a useful way to combine the data sets from each phase for subsequent regression analysis.

In an effort to quantify the effect of various parameters on the membrane permeability, regression analysis was effective and showed that TS, θ_x/θ and the bound EPS ratio ($C_{b,pr}/C_{b,ch}$) were the main predictors of the K_{20} throughout P1–P4 operating conditions explaining up to 89 % of the observed variability in the mean permeability with a 75 % estimated model predictability. At the TS range of 25–33 g/L there was significant interaction between TS with SRT/HRT and C_{pr}/C_{ch} affecting the K_{20} while at TS range of 33–76 g/L, no significant interaction effect was observed. These findings suggest a TS threshold in the range of 30–33 g/L that can impact the viability of AnMBRs when treating sludge or concentrated wastewaters. The interaction effect of SRT/HRT and $C_{b,pr}/C_{b,ch}$, on permeability at a TS range of 25–33 g/L highlight the need to consider biofouling and operating SRT/HRT in the AnMBR system design.

To distinguish between reversible and irreversible fouling, the VFM approach showed the ability to clearly quantify differences in reversible and irreversible fouling propensities between P1–P4. The VFM approach is considered a valuable tool for integration with an on-line operational control scheme that can trigger a targeted fouling mitigation strategy. Due to the limited literature data available to corroborate the findings of the VFM method, it is recommended that an independent measure of fouling type should be further verified.

The 'Hermia-Field' flux modeling results identified cake filtration (m=0) as the dominant fouling mode which provided a good prediction of flux decline during P1–P4. Both, the initial flux (J_o) and G model parameter were found to be important predictors of the limiting flux (J_s). The D and D^2 rates were found to anticipate the onset of J_s by 20–30 minutes compared to the J measurements alone. The D, D^2 and VFM approach, in combination, may be used to provide a model-based on-line targeted fouling control strategy.

The methods and knowledge gained in this phase of the study are considered transferable and may be applied to the treatment of concentrated municipal wastewater streams similar to mixed municipal sludge using AnMBR at full scale applications.

Chapter 5

Comparison of Estrogenicity in Sludge and Permeate with Trace Organic Contaminants in Permeate[1]

5.1 Introduction

The mobilization of micro-contaminants (MCs) into the natural environment from run-off after land application of municipal biosolids, is a concern for municipalities [112], regulators worldwide [4, 5, 98, 102, 155] and the research community [99–101, 156, 157]. Field studies targeting estrogens (a class of endocrine disrupting chemicals (EDCs)) have detected these chemicals in both the run-off and subsurface tile drainage from fields that have received biosolids [99–101, 156, 157] and at low concentration levels in vegetables grown on biosolids amended soil sites [158, 159]. Estrogenic activity is a particular concern associated with runoff from lands where biosolids are applied due to the potentially severe biological responses associated with even low levels of exposure to this class of substances [19, 160]. For instance, the presence of 17α-ethynylestradiol (EE2) at a concentration of 5−6 ng/L was shown to destabilize population balances and cause a decline in fish population during a 7-year whole-lake study [95]. There is however, relatively little information on the presence of estrogen mimicking chemicals and their conjugates in biosolids. Further, there has been little study of the impact of anaerobic sludge digestion operating conditions on this fate of xenoestrogens.

This part of the study focused on comparing the net estrogenicity of municipal sludge extracts including treated mixed sludges that were generated by a conventional anaerobic digester (AD) and an anaerobic membrane bioreactor (AnMBR) at pilot scale. The digesters were operated over a range of hydraulic and solids residence times and temperatures given in Table 3.1.

The reason for this assessment was to determine if different treatment operating conditions affected the release of TrOCs mimicking estrogens that could induce an estrogenic response on non-target organisms from the runoff of land applied biosolids. The sludge, permeate and aqueous extracts were compared against the 17β-estradiol (E2) standard known to elicit an estrogenic response (ER) as measured using the yeast estrogen screen (YES) bioassay. Equilibrium desorption resulting in aqueous extracts from the biosolids were examined and were intended to emulate mobilization of EDCs in the runoff from biosolids application sites.

[1] An abridged version of this chapter was submitted as a conference paper and presented at the Water Environment Federation Technology Exposition and Conference (WEFTEC), Sep 27-Oct 1, 2014, New Orleans, USA.

The permeate, a digestion sidestream, was also chemically analyzed for a selected group of model TrOCs having a large range of physical-chemical characteristics and considered environmentally relevant model compounds.

5.2 Materials and Methods

Over a 2-year period, two pilot scale (500 L active volume) anaerobic reactors (AD and AnMBR, Figure 3.1), receiving a common feed of primary sludge (PS) and thickened waste activated sludge (TWAS) were operated under four different steady state operating conditions (Table 3.1). From Table 3.1 it can be seen that the digester operation spanned a range of conventional and unconventional conditions with respect to HRT (approx. 6-43 days), SRT (15-43 days) and temperature (ambient (25 °C), mesophilic (35 °C) and thermophilic (55 °C)). Conventional chemical parameters and operating conditions (e.g., TS, VS, solids and organic loading) were measured or logged using Labview^{TM}. Digested sludge samples (450 mL of 15-50 g/L mixed liquor) were frozen and subsequently freeze dried (7–21 days lyophilisation process) prior to extraction for TrOCs analysis, YES response analysis and desorption study described below.

5.2.1 Extractions and Chemistry Analysis

Sludge samples which included the feed sludge TWAS and PS along with the treated AD and AnMBR were sampled and analysed during P1–P4 for comparative estrogenicity response (ER) using the YES bioassay tests. A total of 140 mixed liquor samples and 40 permeate samples during P1–P4 were sampled and subsequently analyzed using the YES bioassay. A 40 permeate samples included 9 replicates from P2–P4 were also subsequently analyzed for TrOCs and compared.

Feed Sludge and Mixed Liquor

The feed sludge (PS and TWAS) and mixed liquor (AD and AnMBR treated mixed liquor) samples (450 mL) were frozen at -20 °C immediately following the collection period. The frozen feed sludge and mixed liquor samples were subsequently lyophilized resulting in about 5–15 g of dried solids. The dried solids were sieved using a 1 mm screen and pulverized using a ceramic mortar and pestle. Subsamples of 1 g of homogenized dried solids were then transferred to ashed amber glass 25 mL vials and stored at -20 °C for later extraction. The stored samples were then extracted according to US EPA Method 1698 (2007) [161] without spiking of surrogates. The spiking adjustment was the only modification to Method 1698 and this was consistent with the modification made by Citulski (2012) [106] when working with sludge for YES bioassay testing. Briefly, the sludge extraction process involved using solvent extraction of the sample, solid-phase extraction (SPE) using HyperSep C18 cartridges with 500 mg bed weight/6 mL volume (Fisher Scientific, Oakville, ON), followed by cleanup step with a layered alumina/Florisil column and the removal of sulfur using copper.

AnMBR Permeate

The collected 4 litre permeate samples were sub-sampled into 1 L aliquots and sequentially filtered by 1.5 and 0.4 μm glass microfiber filters (Whatman, Toronto, Ontario, Canada) before being neutralized to pH 7 by 10% aqueous solutions of H_2SO_4 and NaOH and then stored at 4 °C. One set of 40 samples were extracted using US EPA Method 1698 [161] for YES Bioassay analysis and the other set of 40 samples were shipped to the MOE Laboratory Services Branch for chemical analysis according to the Ministry of the Environment, Laboratory Services Branch (MOE LaSB) LC-MS/MS method E3454 [6].

The permeate samples were analyzed for 14 TrOCs given in Appendix D §D.1 Table D.1 with associated classification, isotope and method method detection limit (MDL). Figure D.1 shows the sequence of steps in the TrOCs analysis. The TrOCs spanned a wide range of physical chemical properties given in §D.2 Table D.2 and Figure D.3 with chemical structures shown in Figure D.2. Identification and quantification of target analytes relied on specific product ion mass (mass accuracy of ± 5 ppm), LC retention time with quantification based on fourteen internal standards and method surrogates (isotopes) given in Table D.1 at the quantification method detection limit (MDL). Values below the MDL were reported as < MDL and referred to as censored data.

5.2.2 YES Bioassay Analysis

The yeast estrogenic screen (YES) bioassay was used to evaluate the estrogenic response (ER) of the feed sludge solids, mixed liquor solids, permeate and aqueous extracts throughout P1–P4. The YES analysis procedure was conducted as described by Routledge and Sumpter (1996) [108]) and as modified by Citulski (2012) [106]) using a yeast strain stock provided by C. D. Metcalfe which was originally provided by J. Sumpter. Briefly, the in-vitro YES bioassay uses a recombinant yeast strain that includes the human estrogen receptor that when activated releases a reporter gene which signals transcription leading to a colorimetric response that can be quantified through an absorbance measurement. The degree of color response, in successive dilutions, of the 96-well microtiter plates, provides a relative measure of estrogenicity as compared to the 17β-estradiol (E2) a known estrogen.

Prior to executing the YES bioassay, stock solutions of the E2 standard and yeast fortified assay media solutions were prepared with all work conducted in a laminar flow hood. New yeast solutions, used in the bioassay medium, were grown from frozen stock solutions the same day during which the YES bioassay was conducted. The standard E2 solution was periodically renewed from a stock E2 standard originally prepared from 55.6 mg of 98 % pure 17β-estradiol (CAS 50-28-2, Sigma-Aldrich, St. Louis, MI, USA) and stored at -20 °C. Aliquots of E2 standard (positive control), ethanol (negative control) and sample extracts were serially diluted by two in each of the 12 columns of the 96-well microtiter plates using an 8 and 12 multichannel pipettes and allowed to evaporate to dryness. Each 300 μL well in the microtiter plates was then filled with 200 μL aliquot of the yeast bioassay medium. The microtiter plates were sealed using autoclave tape and incubated at 32 °C for 72 hours in an incubator set to rotate at 120 RPM. Each microtiter plate included sample extracts in triplicates (n=3), negative controls (ethanol) and positive controls (E2) for reference absorbance measurements (Sunrise Basic TECAN Microplate Absorbance Reader, Virginia, USA) to determine the relative absorbance, related to the ER, according to Eq. 5.1:

$$A^c_{540} = A^s_{540} - (A^s_{620} - \bar{A}^b_{620}) \tag{5.1}$$

where A^c_{540}, A^s_{540} refer to the corrected and sample absorbance reading tuned to the red color absorbance of 540 nm wavelength, respectively. The A^s_{620} and $\bar{A}^b_{620}$ refer to the turbidity associated with the yeast cells of the sample replicates and average of the negative blank at 620 nm wavelength, respectively.

The corrected absorbance measurements (A^c_{540}) were used to generate dose-response curves and determine the EC_{50} for E2 standards and corresponding dilution factor for environmental samples. The calculations and graphical plots were conducted in R [117] by fitting a four-parameter log-logistic model [162] given by Eq 5.2:

$$L(x) = c + \frac{d - c}{1 + exp(b \cdot log(x) - log(e))} \tag{5.2}$$

where e is referred to the EC_{50} or the dose or dilution (x) producing a 50 % response located half-way between the lower limit c and upper limit d of the dose-response curve $L(x)$; b, the exponential fitting parameter.

The estrogenicity values for environmental samples were correlated to the E2 estrogenic response (within each microtiter plate) and a calculated "equivalent" E2 estrogenicity (EEQ) value was reported according to Eq. 5.3 [105, 106]:

$$EEQ\ \left(\frac{ng}{g}\right) = \left(\frac{EC_{50,E2}\ (\frac{ng}{ml})}{EC_{50,SE}}\right) \cdot \left(\frac{V_{AM}\ (\mu L)}{V_{SE}\ (\mu L)}\right) \cdot \left(\frac{V_{STE}\ (mL)}{M_S\ (g)}\right) \tag{5.3}$$

where EEQ, is the equivalent sample extract E2 concentration (ng/g); $EC_{50,E2}$, is the reference standard concentration (ng/mL) value that elicits 50 % of the maximal response when calculated using YES bioassay in the 96-well microtiter plates; $EC_{50,SE}$, is the sample extract dilution-fraction that corresponds to the 50 % of the maximal response; V_{AM} (μL) volume of yeast enriched assay media added to each well of the 96-well microtiter plate; V_{SE} (μL), volume of sample extract added to the well; V_{STE}, volume (mL) of the stock extract reduced from the original sample volume and M_S, original sample mass (g). In the case of aqueous extracts V_S (L) would replace M_S (g) and the EEQ would be in ng/L. Standard sample volumes were used throughout with V_{AM}, V_{SE}, V_{STE}, M_S and V_S values of 200 μL, 80 μL, 2 mL, 1 g and 250 mL, respectively. Each of the 96-wells in the microtiter plates held 300 μL. An example showing the derivation of the EC_{50} and calculation of the EEQ is provided in Appendix C § C.1. Figure C.9 (c) shows the steps in the YES process.

5.2.3 Desorption Investigation

A mixed liquor dried solids equilibrium desorption test was conducted to investigate the release of estrogenic mimicking chemicals from P1–P4 treated AD and AnMBR biosolids into the aqueous phase. This was tested to determine if treatment differences in P1–P4 influenced the combined effect of equilibrium desorption and estrogenic potency of the

aqueous extracts of the treated dried solids from the treated mixed liquor. The test involved: (1) lyophilization of 400 mL of mixed liquor samples which reduced to dried sludge samples (5–15 g dry weight); (2) sieving (1 mm screen) and pulverization (mortar and pestle); (3) subsamples of the homogenized biosolids of 1 g were added to 250 mL of deionized water (4 g/L) for equilibrium desorption experiments at 25 °C and 150 rpm for 24 hours on a shaker table to simulate desorption from land applied biosolids; and (4) the aqueous fractions were extracted using using US EPA Method 1698 [161] and the eluent was collected and stored at -20 °C for subsequent YES bioassay analysis [106, 108]. Figure C.9 (a) and (b) shows the steps in the desorption test.

5.3 Statistical Analysis

The calculations of the EC_{50} values were conducted in R [117] by fitting a four-parameter log-logistic model (Eq. 5.2) using the *drc*-R package [162] which implemented non-linear regression analysis. Comparisons within the various streams were conducted using non-parametric asymptotic method considered appropriate for small sample size ($n < 10$) analysis [134]. For the TrOCs analysis censored data analysis was necessary to determine point statistics, distributions and regression plots. The analysis and curve fitting was conducted as recommended by Helsel (2012) [12] when dealing with censored data. The censored data distribution was determined to test the log-normal data fit and the Peto-Peto modification of the Gehan-Wilcoxon test, which is considered the most appropriate test for left-censored log-distributed data [12, 13], was used for group and paired comparisons. Implementation of statistical methods according to Helsel (2012) [12] were available in the *NADA*-R package [13] and this package was used for the analysis throughout.

5.4 Results and Discussion

The anaerobic digestion pilot plants were operated over a range of conventional and non-conventional operating conditions where HRT/SRT, VSLR and temperature were evaluated over 4 phases (Table 3.1). The various operating conditions resulted in varying volatile solids reductions (VS_r) rates which were expected to affect the estrogenic potential of the sludge and permeate from the AnMBR, as measured by the *in vitro* YES bioassay correlated to the concentration of trace organic contaminants (TrOCs). This initial assessment formed the basis for comparisons among the AD and AnMBR performance.

5.4.1 VS Reductions

It was expected that the volatile solids reduction (VS_r) being directly related to biological activity would impact the YES responses and TrOCs associated with the solids and dissolved phase or the permeate of the AnMBR. The percent VS reductions (VSr %) were calculated and shown in Figure 5.1. Compared to the AD, the AnMBR provided an increase in the VS_r of 13, 30, 20 and 13 % in P1–P4, respectively. The highest difference was during Phase 2 when the reactors were operated under mesophilic temperature conditions (35 °C) with the corresponding highest VSLR and OLR of 2.5 kg $VS/m^3 \cdot d$ and 3.7 kg $COD/m^3 \cdot d$, for the AD and AnMBR, respectively (Table 3.2). The results suggest that differences should

be expected in terms of TrOCs concentrations and YES responses between the AD and AnMBR treated sludge and within each reactor between the highest and lowest VS_r rates of P2 and P3, respectively. Similarly no differences would be expected between P1 and P4 of the AD and AnMBR based on VR_r differences alone.

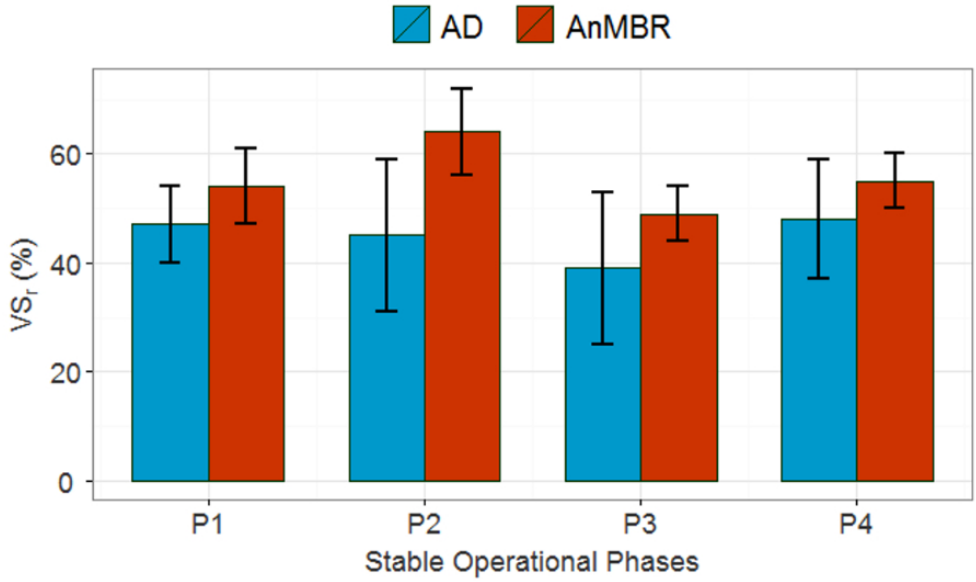

Figure 5.1: Volatile solids reductions (VS_r %) during P1–P4 in AD and AnMBR.

5.4.2 Feed, Mixed Liquor and Permeate YES Results

The feed sludge (PS, TWAS) and mixed liquor (AD, AnMBR) EEQ (EEQ_m) along with the permeate EEQ (EEQ_v) median values by phase P1–P4 were calculated using Eq. 5.3 and given in Table 5.1. These median results represent the average values from each phase and matrix given in Appendix C, Tables C.1–C.5 and example microtiter plates of the YES bioassay results shown in Figures C.4–C.8. The corresponding E2 standard EC_{50} measured values had a median and 95 % confidence interval of 35 ± 5 ng/L (n=92) during the sludge analysis and 24 ± 4 ng/L (n=31) during the permeate analysis and this is consistent with previous reported values in the range of 20–50 ng/L [106, 163, 164].

From Table 5.1 the feed sludge and treated mixed liquor estrogenic responses (ER) observed corresponded to median EEQ_m values in the range of 1–30 ng/g. The EEQ_m values associated with the feed sludge and treated mixed liquor in this study are consistent with reported values in the range of 5–30 ng/g EEQ_m which included PS, TWAS and mesophilic anaerobically digested sludge [106, 164]. Figure 5.2 provides the full range of measured EEQ_m values in terms of individual box plots (Figure 5.2 (a)), as ECDFs of the combined AD, Feed and AnMBR (Figure 5.2 (b), n = 30–32) and all the sludge samples combined (Figure 5.2 (c), n = 92). Figure 5.2 (c) suggests 80 % of all feed sludge and treated mixed liquor samples to be < 10 ng/g EEQ_m which represent P1–P3 for both the AD and AnMBR. Phase P4 AD and AnMBR treated sludge samples appear to dominate values above 10 ng/g EEQ_m. This observation is discussed subsequently.

Table 5.1: EEQ during P1–P4 stable operation[a]

Matrix	EEQ Values (ng/g) or (ng/L)[b]			
	P1 Median (CI) n	P2 Median (CI) n	P3 Median (CI) n	P4 Median (CI) n
TWAS	10 (8) 6	7 (3) 4	8 (14) 3	6 (2) 4
PS	6 (6) 6	6 (9) 4	7 (6) 3	8 (9) 4
PS + TWAS	9 (6) 12	7 (8) 8	7 (14) 6	7 (9) 8
AD	2 (4) 7	3 (4) 8	3 (11) 7	9 (33) 7
AnMBR	1 (2) 7	3 (3) 8	3 (6) 7	30 (23) 7
Permeate[c]	–	0.3 (0.7) 6	0.3 (0.7) 10	0.5 (0.4) 15

[a] Median, 50 %-ile; CI, the 95% confidence interval; n, the number of samples.
[b] For feed sludge (TWAS, PS) and treated mixed liquor (AD and AnMBR) EEQ is in ng/g and for permeate in ng/L. The PS+TWAS represents the feed sludge EEQ_m common to both the AD and AnMBR pilot reactors. [c] Permeate extracts in P1 used a preliminary extraction procedure that was not consistent with P2–P4 and not reported on.

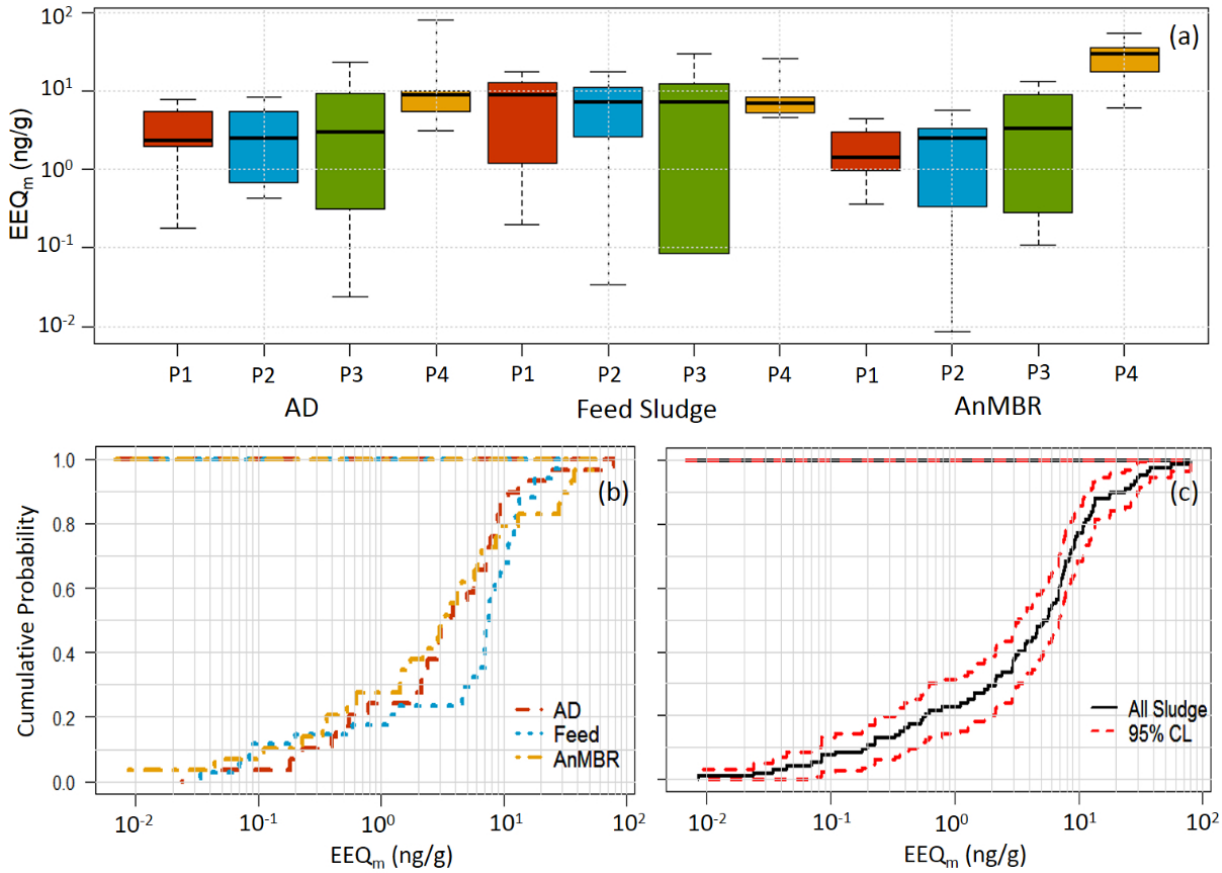

Figure 5.2: EEQ_m (ng/g) box plots of treated mixed liquor (AD and AnMBR) and feed sludge (a); ECDF of combined feed (n=34), AD (n=29) and AnMBR (n=29)(b) and ECDF of all sludge EEQ_m samples (n=92) with 95 % CI (c).

From Table 5.1 the permeate estrogenic responses (ER) corresponded to median EEQ_v values in the range of 0.3–0.5 ng/L. The permeate EEQ_v values in this study were consistent with reported values of aerobic MBR permeate samples from the Ontario, Oxford STP with an average of 0.2 ng/L (n = 3) [106]. The full range of EEQ_v measured values is shown in Figure 5.3 in terms of individual box plots (Figure 5.3 (a)), as a log-normal distribution fit (Figure 5.3 (b)), as individual ECDF curves (Figure 5.3 (c)) and all the permeate EEQ_v values combined (Figure 5.3 (d), n = 31). Overall the permeate showed a low estrogenic potential based on Figure 5.3 all of the permeate EEQ_v were less than 3 ng/L suggesting no direct estrogenic environmental impacts since a a minimum 6 ng/L E2 concentration has been previously reported to be required to elicit and estrogenic impairment resulting in the population decline of wild fathead minnows [95]. However other in-vivo controlled studies have shown decreased reproductive success at fish exposed to < 1–5 ng/L of EE2 (equivalent to 1.2–6 ng/L of E2) [165]. From Figure 5.3 (b) the 80 %-ile EQQ_v value 1.2 ng/L (n = 31) suggesting that more than 20 % of the AnMBR permeate sidestream may induce an estrogenic effect. Figure 5.3 (b)–(d) suggest a strong log-normal distribution of the results and consistent range of EEQ_v values indicating consistent and predictable permeate estrogenic response based on P2–P4 operating conditions.

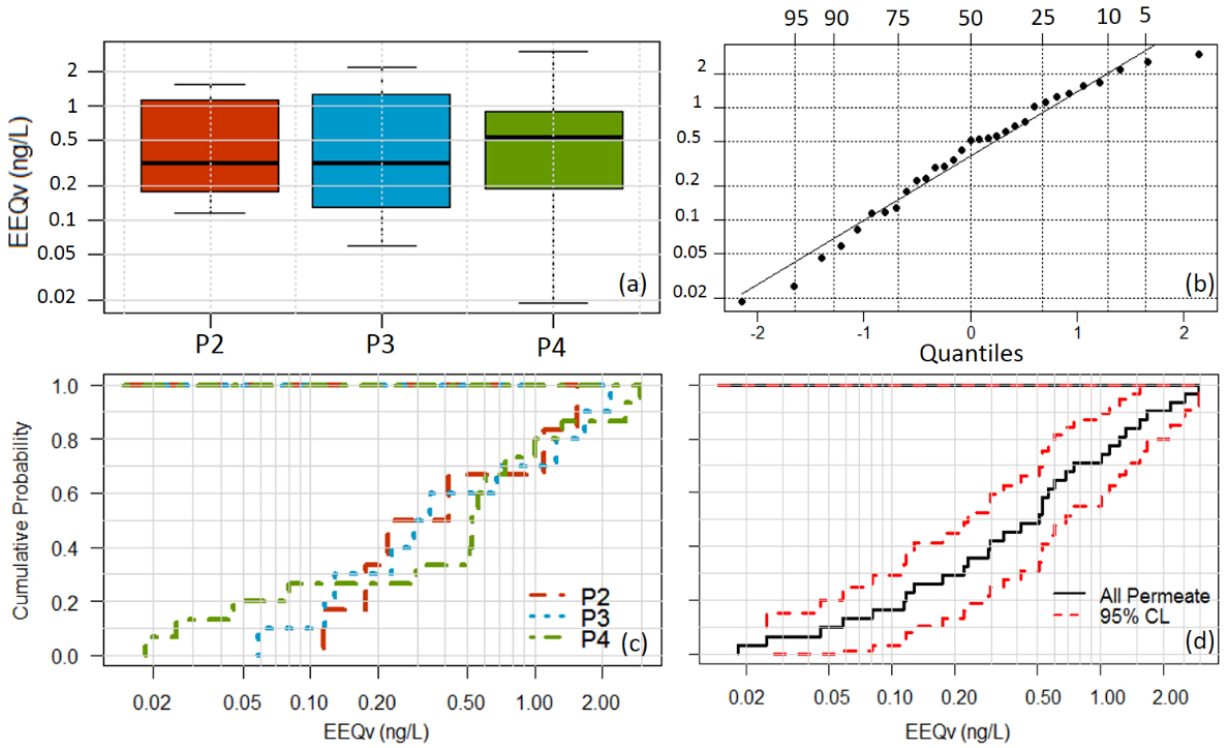

Figure 5.3: EEQ_v (ng/L) box plots of AnMBR permeate P2–P4 (a); log-normal probability distribution fit (b) of all samples (n=31); individual ECDFs (c) and combined ECDF of all permeated EEQ_v combined (n=31) with 95 % CI (d).

To determine if the differences observed under P4 treatment conditions were statistically significant from other phases a comparative analysis was conducted. Initially the feed sludge EEQ_m consistency was considered and then compared to the EEQ_m values of the

final treated sludge in each phase.

From Table 5.1 the feed sludge EEQ_m, through P1–P4, showed a median range of 6–10 ng/g EEQ_m. A paired comparison analysis between the EEq_m of TWAS and PS by phase and with all phases combined, showed no statistical difference ($p = 0.05$) and this is strongly suggested from the overlap in the whiskers of the box plots in Figure 5.2 (a). Based on this comparative analysis the EEQ_m values for PS and TWAS were combined to form the feed EEQ_m values for comparison between the treated mixed liquor from the AD and AnMBR in each phase.

A paired comparison within each phase of the feed EEQ_m to the treated AD and AnMBR mixed liquor samples in P1–P4 showed no statistical differences ($p = 0.05$) within each phase except for the AnMBR in P4. In P4 the AnMBR treated mixed liquor had a significantly larger EEQ_m with a greater estrogenic potential compared to the feed ($p = 0.05$). This suggested that the anaerobic treatment conditions in the AD and AnMBR in P1–P3 and AD for P4, under ambient, mesophilic and thermophilic operating conditions, did not change estrogenic potential of the feed sludge ($p = 0.05$). Except for AnMBR-P4, these findings are generally contrary to previously reported results that indicate that AD of municipal sludge tend's to increase the estrogenic potential of the treated mixed liquor [106].

Further comparison between different treatments found the EEQ_m in AnMBR-P4 to be statistically higher than the EEq_m mixed liquor values from AnMBR-P1, AnMBR-P2, AD-P1 and AD-P3 ($p = 0.05$). As can be seen from Figure 5.2 (a), the median EEQ_m for AnMBR-P4 was always higher with median percent difference between AnMBR-P1, AnMBR-P2, AD-P1 and AD-P3 of 83, 50, 17 and 67 %, respectively. These findings suggest a higher estrogenic potential in the treated mixed liquor from the thermophilic operated AnMBR system compared to the ambient and mesophilic operating conditions. Other differences in P1–P3 operating conditions such as T, SRT/HRT, VSLR and VS_r did not appear to impart a significant effect on the changes in estrogenic potential of the treated sludge based on similar EEQ_m values in P1–P3.

Considering the ECDF curves in Figure 5.2 (b) ($n = 29$–32) between the 20–80 %-ile, the feed had a greater EEQ_m compared to AD and AnMBR treated mixed liquor in all phases. In the range below the 20 %-ile no difference was observed and above the 80 %-ile the AnMBR-P4 performance was reflected having the highest EEQ_m values. From Figure 5.2 (b) the AD and AnMBR treated mixed liquor EEQ_m 70 %-ile value was 7 ng/g. This EEQ_m value suggests that more than 30 % of the treated mixed liquor may exert a noticeable estrogenic impact under environmental conditions based on the work of Kidd et al (2007) [95] that showed that under chronic exposure of EE2 at $<$ 5–6 ng/L (equivalent to 6–7.2 ng/L of E2) caused male fathead minnow feminization (under natural conditions) leading to a severe decline on fish population in a Northern Ontario lake. Considering Figure 5.2 (b) feed EEQ_m distribution, the 40 %-ile value is 7 ng/L suggesting that 60 % of untreated sludge, if directly applied to land, would potentially incur an estrogenic affect on non-target receptors. Figure 5.2 (c) ($n = 92$) provides the distribution of the complete sludge EEQ_m values which shows a narrow 95 % confidence level and provides the expected range of both the treated mixed liquor and feed sludge EEQ_m as an overall measure of sludge estrogenic potential.

When considered collectively, the observed EEQ values of feed sludge, treated mixed liquor and permeate extracts tested using the YES bioassay, suggest that both raw and treated mixed liquor along with the AnMBR permeate side stream under all the phases, have a potential for inducing an estrogenic effect between 20–30 % of the time when compared to the effect of EE2 on fathead minnows. The AnMBR treated mixed liquor extract from P4 under thermophilic operating conditions showed significant elevated EQQ_m values, compared to ambient and mesophilic anaerobic treatment, and suggests that thermophilic (55 °C) operating conditions may increase the available estrogen-mimicking compounds in the mixed liquor matrix. The permeate median EEQ_v value was 40 % greater in P4 compared to P2 and P3, although not a statistically significant difference at the 95 % confidence level, still suggests a potential temperature effect similar to the AnMBR sludge treatment under P4. Contrary to other reported findings the AD and AnMBR treated mixed liquor estrogenic potential was found to be less by about 30 % than the feed sludge during the 20–80 %-ile range (n = 29–32) when considered collectively.

5.4.3 YES Desorption Results

To further assess the potential desorption of estrogen mimicking compounds following the land application of anaerobically treated biosolids the equilibrium desorption aqueous extracts from AD and AnMBR treated mixed liquor dried solids were tested using the YES bioassay. The AD and AnMBR aqueous extracts EEQ_v median values by phase P1–P4 are given in Table 5.2 which represent the average results from each phase and matrix given in Appendix C §C.4, Tables C.6–C.7 and example microtiter plates of the YES bioassay results shown in Figures C.10–C.11. The corresponding E2 standard EC_{50} measurements values had a median and 95 % confidence interval of 24 ± 1 ng/L (n = 40) which was consistent with previous reported values in the range of 20–50 ng/L [106, 163, 164].

From Table 5.2 the aqueous extracts estrogenic responses (ER) observed corresponded to median EEQ_v values in the range of 2–11 ng/L. The EEQ_v values associated with the aqueous phase are consistent with final effluent from STPs with a reported high range of 1–75 ng/L EEQ_v [106, 164]. Figure 5.4 provides the full range of measured EEQ_m values in terms of individual box plots (Figure 5.4 (a) and (b)), as ECDFs of the combined AD and AnMBR aqueous extracts (Figure 5.4 (c), n = 20) and all the sludge samples combined (Figure 5.4 (d), n = 40). From Figure 5.4 (d) the 10 %-ile value was 1.4 ng/L (n = 40) and this suggests that potentially 90 % of the aqueous extracts from AD or AnMBR, P1–P4, treated sludge can potentially induce an estrogenic effect on non-target receptors (e.g., fathead minnows [165]). From Figure 5.4 (d) the 85 %-ile value was 6 ng/L (n = 40) and this suggests that potentially 15 % of the aqueous extracts from AD or AnMBR, P1–P4, treated sludge can potentially induce a more significant estrogenic effect by affecting the sustainability of wild fish population (e.g., fathead minnows [95]). The above potential impacts assume limited dilution of the runoff from biosolids amended sites and limited bioconversion in the soil-biosolids matrix under environmental conditions into less estrogenic compounds than present in the original biosolids runoff.

To determine if the median EEQ_v observed values were statistically different under various treatment conditions, P1–P4 were compared within and between treatments. A paired

Table 5.2: EEQ of aqueous extracts from desorption of AD and AnMBR treated sludge

Matrix	EEQ_v Values (ng/L)			
	P1 Median (CI) n	P2 Median (CI) n	P3 Median (CI) n	P4 Median (CI) n
AD	3 (3) 5	3 (1) 5	4 (2) 5	2.1 (0.5) 5
AnMBR	2 (2) 5	2 (1) 5	4 (2) 5	11 (6) 5

[a] Median, 50 %-ile; CI, the 95% confidence interval; n, the number of samples.

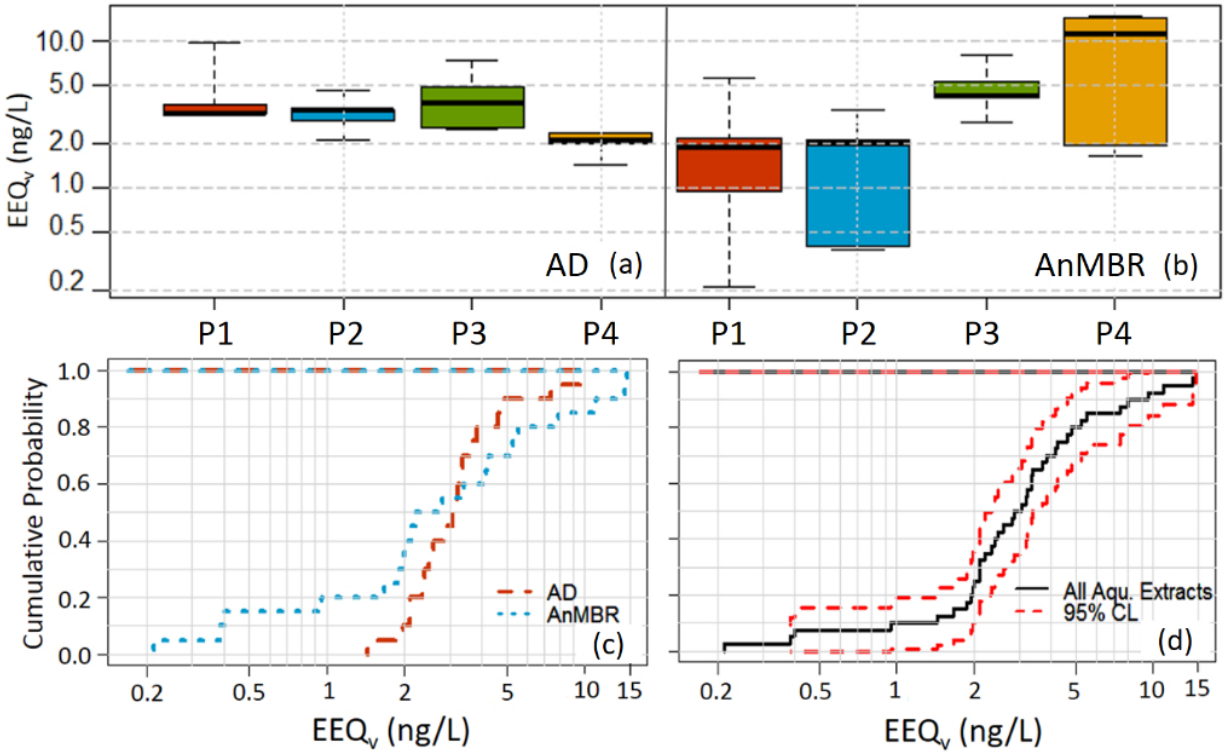

Figure 5.4: EEQ_v (ng/L) box plots of AD (a) and AnMBR (b) desorbed aqueous extracts P1–P4; ECDFs of AD and AnMBR samples combined (n=20) (c) and combined ECDF of all aqueous extracts EEQ_v combined (n=40) with 95 % CI (d).

comparison within treatments in the AD P1–P4 showed no statistical difference ($p = 0.05$) and in the case of AnMBR P1–P4 only P3 showed a statistically higher EEQ_v value than P2 ($p = 0.05$). A between treatment comparison showed AnMBR-P3 to have a statistically higher EEQ_v value than AD-P4 ($p = 0.05$). These observations suggest that AnMBR-P3 operating at ambient temperatures and higher VSLR with lower volatile solids reductions (VS_r) may have retained more of the estrogen mimicking compounds in the mixed liquor compared to AnMBR-P2 operating at mesophilic operating conditions. Similarly AD-P4 operating a lower VSLR and higher temperature would have likely had increased bioconversion rates compared to AnMBR-P3 and reduced the concentration of estrogen mimicking compounds in the mixed liquor.

From Figure 5.4 (c), considering the AD (n=20) and AnMBR (n=20) processes collectively,

the AnMBR showed a higher estrogen potential above the 60 %-ile EEQ_v levels compared to the AD processes suggesting that AnMBR treated mixed liquor will have a higher potential estrogenic impact compared to the AD treated mixed liquor. This suggests that AD P1–P4 operation is more effective at reducing estrogenic potential, from aqueous biosolids runoff, than ambient or thermophilic AnMBR operation. Conversely at the lower EEQ_v levels below the 60 %-ile EEQ_v values the AD would have a higher potential estrogenic impact from aqueous runoff. This suggests that mesophilic AnMBR operation is more effective at reducing EEQ_v values compared to the AD digesters during P1–P4. Figure 5.4 (d) provides the full expected range of EEQ_v equivalents with a fairly narrow 95 % confidence band (n = 40) and this suggests that the expected estrogenic potential from anaerobic digested municipal mixed sludge is fairly well predictable.

Considered collectively, these results suggest that estrogenicity, as measured by the in-vitro YES bioassay, persists in anaerobically treated digestion of mixed municipal sludges and carries over into aqueous extracts of saturated mixed liquor samples. Although not statistically significant at the 95 % confidence level, the treatment at higher VSLR and SRT during ambient and thermophilic temperatures using AnMBR, compared to AD P1–P4 operation, exacerbated the estrogenic potential of the aqueous mixed liquor extracts. Conversely AnMBR operation at mesophilic P1–P2 operating conditions, reduced the estrogenic potential of aqueous extracts, compared to AD P1–P4 operation.

5.4.4 TrOCs in the Permeate

In an effort to correlate YES bioassay estrogenic responses observed in the permeate and associated with the AnMBR aqueous phase of the mixed liquor, the permeate was analysed for a suite of 14 environmentally relevant trace organic contaminants (TrOCs). The list of the TrOCs, which included a number of environmentally pervasive estrogens, is provided in Table D.1 which includes the classification, the analytical isotope and method detection limit (MDL). The environmentally relevant physical-chemical properties are provided in Table D.2 and Figure D.3 with the chemical structure in Figure D.2. The complete box plots, ECDF curves and log-normal distribution analysis for the TrOCs analyzed is provided in Figures D.4 to D.8 of Appendix D.

Table 5.3 provides the summary point statistics of the 14 TrOCs found from the analysis of 40 (9 replicate) permeate samples from the AnMBR during P1–P4 with an example distribution analysis for Estrone provided in Figure 5.5.

From Table 5.3, the chemical analysis of TrOCs was found to report significant number of non-detects (< MDL) and this necessitated the use of censored data analysis [12] to eliminate bias in the statistics. Traditionally reported values < MDL were replaced with 0, 1/2 MDL or MDL values but this has been found to bias the results [12] and not recommended. Implementation of robust regression on order statistics (ROS) in the R-package NADA [13] has allowed for the analysis of censored data without the need for substitution of reported data below the MDL. Table 5.3 gives the the median or mean (M), 95% confidence interval (CI), number of samples analyzed (n) and percent number of detected values (d). From Table 5.2 the percent of detected TrOCs varied from 9–100% and this varied between P1–P4 and by TrOCs with no particular overarching trend. However

Table 5.3: Concentration (μg/L) of TrOCs in the permeate extract during P1–P4

TrOCs	Stable Operational Phases[a]			
	P1 M (CI) n (d)	P2 M (CI) n (d)	P3 M (CI) n (d)	P4 M (CI) n (d)
Acetaminophen	0.5[b] (0.2) 9 (23)	0.8 (0.2) 7 (100)	4 (3) 11 (100)	14 (3) 14 (79)
Bisphenol A	2.5[b] (5) 9 (44)	4.2 (5) 7 (100)	4.7 (25) 11 (82)	16 (20) 14 (100)
Carbamazepine	0.3 (0.5) 9 (56)	1.8 (0.6) 7 (100)	1.6 (0.5) 11 (100)	8 (3) 14 (100)
Ciprofloxacin	0.2 (0.8) 9 (66)	3.2 (0.4) 7 (100)	3.2 (0.3) 11 (81)	20 (30) 14 (50)
Clofibric acid	0.06[b] (0.03) 9 (22)	9[b] (20) 7 (43)	0.9 (103) 11 (64)	60[b] (160) 14 (43)
Diclofenac	0.3 (0.2) 9 (89)	1.3 (0.3) 7 (100)	1.0 (0.4) 11 (100)	6.4 (4) 14 (79)
Equilin	nc (nc) 9 (0)	nc (nc) 7 (0)	2.2[b] (10) 11 (45)	0.4[b] (5) 14 (36)
Estriol	nc (nc) 9 (0)	0.26[b] (0.06) 7 (43)	4.4 (6) 11 (45)	0.7 (4) 14 (64)
Estrone	nc (nc) 9 (0)	0.4[b] (0.1) 7 (43)	0.4[b] (0.4) 11 (45)	0.3 (0.2) 14 (64)
Ibuprofen	0.1 (5) 9 (56)	5.3 (37) 7 (86)	1.8 (3) 11 (73)	0.1 (16) 14 (64)
Indomethacin	nc (nc) 9 (0)	0.1 (nc) 7 (14)	0.1 (nc) 11 (9)	1.3 (1) 14 (36)
Progesterone	13[b] (nc) 9 (12)	0.6 (0.3) 7 (86)	0.3 (0.7) 11 (82)	7[b] (7) 14 (43)
Sulfamethazine	0.03[b] (nc) 9 (11)	0.03 (0.01) 7 (71)	0.06 (0.01) 11 (91)	0.03 (0.01) 14 (64)
Sulfamethoxazole	0.2[b] (0.1) 9 (44)	0.2 (1) 7 (57)	0.3[b] (0.3) 11 (27)	0.8 (2) 14 (64)

[a] M, median concentration in μg/L; CI, the 95% confidence interval; n, the number of samples; d, percent detected or greater than the MDL; nc, non-computable due to $\geq$ 80% percent of sample results being < MDL. [b] Mean value was computed since the median was not computable since number of detected samples, d was < 50%.

the largest number of non-detect values were in P1 and least in P4 and this suggests both a solids concentration and temperature effect. The TrOCs concentration distribution was generally in the low ng/L to μg/L range and this was 1–2 orders of magnitude higher than similar compounds found in typical municipal wastewater streams [166, 167]. The higher concentration levels in permeate are not surprising due to the expected contribution due desorption from the high concentration of the MLSS in the AnMBR. However the average estrogen concentrations of equilin, estriol and estrone were consistently below the MDL of 100 ng/L in P1; equilin was below the MDL in P2 but in P3 and P4 all three estrogens were detected in 40–60 % of the samples at elevated concentrations in the 0.3–2.2 μg/L range. Based on the highest median concentration of equilin and estriol, which are potent estrogens, the estrogenic potential of the permeate suggests a ranking with P3 > P4 > P2 > P1.

To assess the effect of AnMBR treatment on the concentration of the TrOCs in the permeate a paired statistical comparison of the distribution at the 95 % confidence level was conducted and summarized in Table 5.4. This analysis assumed a similar feed concentration of TrOCs but this could only be inferred based on the similar median feed sludge YES bioassay results (Table 5.1 and Figure 5.2) for estrogen mimicking compounds such as bisphenol A, equilin, estrone and estriol. From Table 5.4 there was no paired difference between P1–P4 for estrone, ciprofloxacin, estriol, ibuprofen, progesterone, sulfamethazine, clofibric acid, equlin and indomethacin with p-values ranging from 0.06–0.92. The other five TrOCs showed significant differences (p = 0.05) with P4 and P3 showing the highest concentrations of

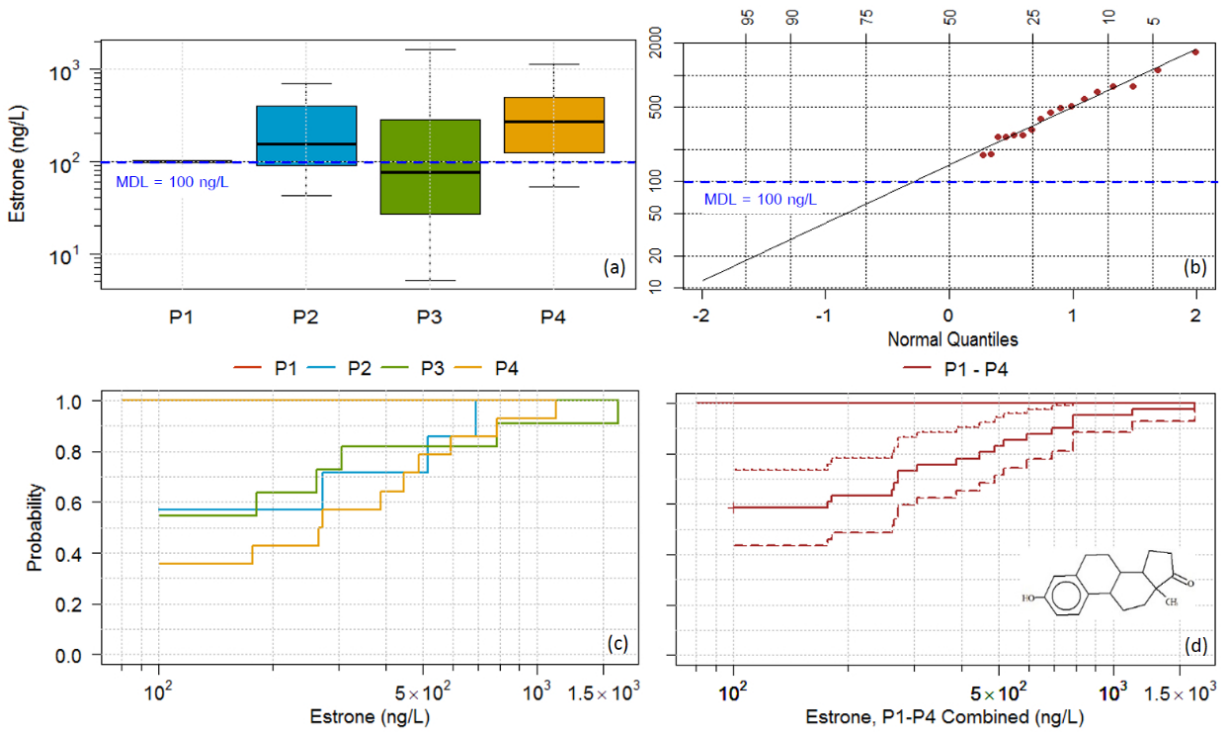

Figure 5.5: Comparison and analysis of Estrone concentration in permeate in P1–P4 with data shown as box plots (a), combined log-normal regression distribution fit (b), individual cumulative probability plot (c) and combined cumulative probability plot (n = 41, with 41 % > MDL of 100 ng/L) (d)

carbamazepine, sulfamethoxazole, bisphenol A, acetaminophen and diclofenac, compared to P1 and P1. Phase P1 generally showed the lowest concentrations with P2 in between. The median and relative median concentration levels are also shown graphed in Figure 5.6 which show that P4 generally had the highest median TrOCs concentration levels compared to the P1–P3.

Based on the physical chemical properties in Table D.2, carbamazepine, sulfamethoxazole, bisphenol A, acetaminophen and diclofenac show a negative or very low anaerobic biodegradation potential, a relatively high solubility range of 2–14000 mg/L at 25 °C and low % adsorption in the range of 2–9 %, with the exception of diclofenac (56 %), all suggesting a preponderance to find these compounds in the permeate or soluble fraction of the mixed liquor. Phase P3 with the lowest VS_r (Figure 5.1 and lowest operating temperature (lowest kinetic rates) would tend to have the lowest biotransformation potential of these TrOCs compared to P1, P2 and P4. In contrast, in P4, operating at thermophilic temperatures would increase the kinetic rates and promote the solubilization of TrOCs associated with the solids, compared to P1–P3. Considered collectively the TrOCs concentration levels in the permeate suggest complicated underlying mechanisms that likely include desorption, solubilization and biotransformation factors related to the physical-chemical properties of the TrOCs. A recent study considering 22 TrOCs using MBR and other technologies, corroborated the findings of this study, by concluding generally unpredictable removal of

biologically persistent and hydrophilic TrOC using MBR treatment [168]

Table 5.4: Comparison results (p-values) based on the Peto-Peto[a] test of the empirical distribution data set during P1–P4[b]

TrOCs	Resulting P-value Between Paired Comparisons					
	P1 ∼ P2	P1 ∼ P3	P1 ∼ P4	P2 ∼ P3	P2 ∼ P4	P3 ∼ P4
Carbamazepine	0.001	0.003	0.001	0.144	0.001	0.001
Sulfamethoxazole	0.041	0.001	0.022	0.036	0.695	0.001
Bisphenol A	0.014	0.057	0.001	0.964	0.046	0.029
Acetaminophen	0.003	0.001	0.002	0.003	0.005	0.226
Diclofenac	0.001	0.001	0.019	0.047	0.086	0.126
	Summary Comparisons Between Phases					
Carbamazepine	P4 > P3 ≈ P2 > P1					
Sulfamethoxazole	P4 > P3, P3 > P1 > P2, P2 ≈ P4					
Bisphenol A	P4 > P2 ≈ P3, P4 > P1, P2 > P1, P3≈ P1					
Acetaminophen	P4 ≈ P3 > P2 > P1					
Diclofenac	P4 ≈ P3 > P1, P4 ≈ P2, P2 > P3 > P1					

[b] The Peto-Peto comparison test assumes a log-normal data distribution and this was confirmed and shown in Figure D.8 which shows good to very good agreement to the log-normal distribution of the TrOCs. [b] The group comparisons for Estrone, Ciprofloxacin, Estriol, Ibuprofen, Progesterone, Sulfamethazine, Clofibric Acid, Equlin and Indomethacin had the following p-values, 0.237, 0.926, 0.101. 0.236, 0.122, 0.060, 0.173. 0.746 and 0.279, respectively, indicating no statistical difference at the 95% confidence level.

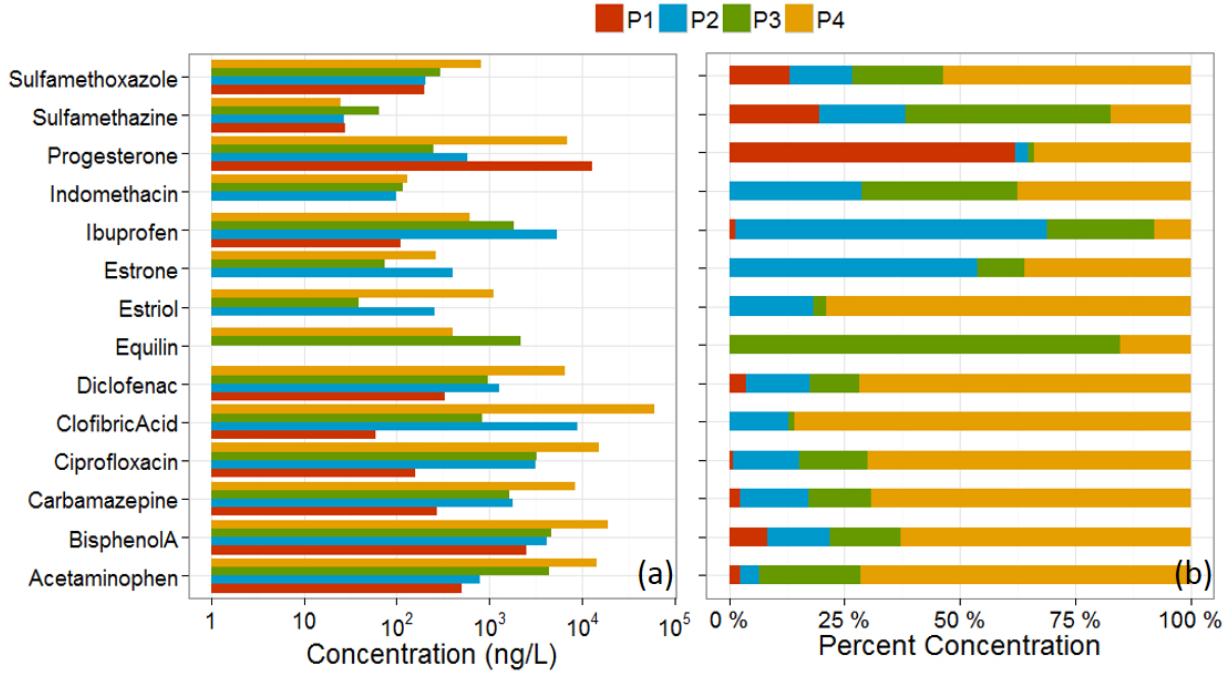

Figure 5.6: Permeate TrOCs median concentration levels (a) and relative percent median concentrations (b) by phase P1–P4.

To compare the YES bioassay results of the permeate with the estrogenic potential based on the chemistry, the estrogenic chemicals measured 90 %-ile concentration levels where converted to E2 equivalents (EEQ_v) based on E2 relative estrogenic potency (REP) factors while assuming a common mode of action [169]. The 90 %-ile concentration values were used to provide a conservative estimate of the estrogenic potential based on permeate chemistry. The results of this analysis are shown in Table 5.5.

Table 5.5: YES measured potencies of selected estrogenic TrOCs and 90 %-ile permeate REP

TrOcs	CAS RN	YES Relative Potency		Reference
		E2	EC_{50} (μg/L)[a]	
17α-ethylynestradiol (EE2)	57-63-6	1.2	0.020	[169, 170]
17β-Estradiol (E2)	50-28-2	1.0	0.024	[169, 170]
Estrone (E1)	53-16-7	0.38	0.063	[170]
Equilin (EQ)	474-86-2	0.12	0.200	[171]
Estriol (E3)	50-27-1	0.0024	10	[170]
Bisphenol A (BPA)	80-05-7	0.00011	218	[169]

TrOCs	90 %-ile Relative Estrogenic Potency (REP)[b] (ng/L as E2)			
	P1	P2	P3	P4
Estrone (E1)	0.14	0.79	1.1	1.0
Equilin (EQ)	0.02	0.02	2.1	0.081
Estriol (E3)	0.002	0.003	0.19	0.10
Bisphenol A (BPA)	0.001	0.002	0.002	0.006
Total REP (ng/L as E2)	0.16	0.82	3.4	1.2

[a] YES relative potency compared to E2 standard median of 24 ng/L (n = 31) measured in the permeate YES bioassay analysis in this study (§5.4.2). For example EC_{50} of E1 was calculated as 63 ng/L and this would be required to exert an equivalent E2 EC_{50}) as measured by the YES bioassay. [b] The REP for each estrogen was calculated based on the product of the 90%-ile concentration value in the permeate with the E2 YES Relative Potency value given above (e.g., estrone has a 0.38 E2 REP).

From Table 5.5 the chemistry EEQ of the permeate P2–P4 at the 90 %-ile level varies from 0.82–3.4 ng/L E2 with estrone and equilin contributing over 90 % of the total estrogenic potential of the permeate in all phases. Compared to the 90 %-ile YES bioassay permeate results of 1.5–2.5 ng/L E2 (Figure 5.3 (c)) the chemistry EEQ analysis suggests that estrone and equilin may have contributed significantly to the observed YES bioassay results with estriol and bisphenol A making a minimal contribution. These findings may also be relevant to the observed YES bioassay results of the aqueous extracts (Table 5.2 and Figure 5.4) since the dried mixed liquor solids included the dissolved aqueous phase that would have readily contributed the dissolved TrOCs to the aqueous phase.

5.5 Summary and Conclusions

The results of this phase of the study showed that estrogenicity, as measured by the *in-vitro* YES bioassay, persists in anaerobically treated digestion of mixed municipal sludges,

the AnMBR permeate and carries over into aqueous extracts of saturated treated mixed liquor solids samples. In reviewing these findings one should consider that: (1) field saturation conditions for a period of 24-hours were emulated with marginal biological activity under anoxic conditions; (2) to extrapolate to field conditions, one would need to include surface or subsurface transport phenomena to the contact organisms and (3) consider environmental mitigation factors that may dilute the estrogenicity observed. The physicochemical characteristics and particularly the water solubility and sorption-desorption characteristics should be investigated particularly to biosolids-soil matrices with different organic-C content. However, the *in-vitro* YES bioassay proved to be a useful metric to evaluate the quality of treated anaerobic sludge to assess its estrogenic potential but should be further corroborated by *in-vivo* studies. To apply YES to many different sludge types, the sensitivity and robustness of the YES bioassay should be investigated to build a database for the expected E2-equivalent range in environmental sludge matrices.

The chemistry analysis of the AnMBR permeate sidestream suggests that TrOCs are present in low ng/L to low μg/L range and tend to accumulate in high solids and high SRT anaerobic sludge treatment systems. The permeate showed elevated TrOCs levels compared to typical raw municipal wastewater and would contribute significantly to the TrOCs loading when returned to the head works of a STP (as currently practiced). The permeate chemistry E2 equivalent potency analysis suggested that estrone and equilin were major contributors to the YES bioassay measured estrogenic responses while estriol and bisphenol A made a minimal contribution to the permeate estrogenic response. To more fully determine the source chemicals causing the estrogenic response the chemical analysis of parent and conjugates species should be investigated.

The finding of this phase of the study will inform policy makers and operating agencies on the potential TrOCs loading from anaerobic digestion side streams, the estrogenic effect from microcontaminants that can desorb into the aqueous runoff from land applied biosolids and potentially impact non-target organisms in the natural environment.

Chapter 6

Conclusions and Recommendations

This research provided a thorough understanding of the treatment of mixed municipal sludge using an AnMBR compared to a conventional high rate flow through AD under ambient, mesophilic and thermophilic operating conditions. The main objectives of this study included: (1) a comparison of the performance of a sidestream AnMBR to a control AD under different SRT to HRT ratios and VSLRs; (2) an investigation into the membrane performance; (3) an evaluation of the occurrence and concentration levels of selected TrOCs in combination with an assessment of estrogenic responses using the YES bioassay and (4) an investigation into the estrogenic responses of aqueous extracts from treated AD and AnMBR sludges, emulating biosolids runoff. Based on the results of this study the following general conclusions can be made:

6.1 General Conclusions

1. **The AnMBR provided a reduced footprint and improved sustainability over the AD reactor**. The AnMBR has the advantage over the flowthrough AD in that it can decouple and control the SRT independently of the HRT. By increasing the SRT:HRT ratio, in the AnMBR, the MLSS was increased, maintaining a high F/M ratio, allowing a doubling of the throughput while maintaining a high VS reduction during ambient, mesophilic and thermophilic operating conditions. The AnBMR showed a net positive energy balance during ambient and mesophilic operating conditions but not during thermophilic operation. The AD control digester showed a net positive energy balance during ambient operation. The AnMBR, under ambient, mesophilic and thermophilic operating conditions, could achieve high levels of solids destruction and concentration when operated at what are considered short HRTs for sludge digestion.

2. **The CIP fouling control strategies allowed operation at high solids loading rates**. A clean-in-place (CIP) and rest-permeation fouling control strategy proved effective at maintaining the flux throughput set points under high MLSS operating conditions at low MLSS viscosities and significant throughput. However, operation at ambient and high solids operating conditions necessitated a more frequent cleaning cycle to maintain the set flux point for sustainable operating conditions.

3. **The AnMBR fouling mode was dominated by cake fouling and by reversible fouling**. The application of the 'Hermia-Field' classical blocking models, to characterize the flux decline, proved useful at identifying the dominant mode of fouling as cake fouling. The VFM-method, provided a direct way to distinguish reversible from irreversible fouling, based on direct permeability measurements and regression

analysis of the normalized permeability demonstrated an important TS, SRT/HRT and bound EPS protein to polysaccharide ratio dependency. The TS proved to be the single most significant parameter influencing permeability throughout all the operating conditions.

4. **Estrogenicity, as measured by the *in-vitro* YES bioassay, persists in anaerobically treated sludge and permeate**. Under all the different AD and AnMBR operating conditions the feed sludge estrogenicity was found to persist in the treated mixed sludge and permeate. Based on *in-vitro* YES bioassay testing, the treated sludge, permeate and aqueous extracts from biosolids were found to have the potential to elicit an estrogenic response. The YES bioassay proved to be a useful measure and provided a new metric that can be readily applied as a screening tool to assess estrogenicity in biosolids and permeate. It is advisable however to consider field conditions, such as dilution factors, that may reduce the *in-vitro* results observed in this study.

5. **The presence of TrOCs in the AnMBR permeate included estrogens that contributed to the estrogenic potential of the sludge and aqueous streams**. The permeate TrOCs concentration levels, which included estrogens, were found to be significant to potentially induce an estrogenic effect as measured by the YES bioassay screening tool. Based on the presence of estrogens in the permeate, the calculated relative chemical estrogenic potency identified specific estrogens that appeared to contribute significantly to the overall YES bioassay estrogenic signal.

6.2 Specific Conclusions

The specific conclusions from this study are summarized below:

Conventional Performance

The impact of the SRT/HRT ratio on AnMBR performance at an optimum mesophilic temperatures showed that the AnMBR consistently had greater VS_r and increased methane yields (0.19–0.34 Nm^3/kg VS_f when compared to the AD. Further, the TS concentrations in the waste stream from the AnMBr were considerably greater by 2–3.4 times than those of the AD as a result of the extended SRTs. The VS_r in the AnMBR was maintained at high values (49–64 %) even when the HRT was reduced to 7.3 days under mesophilic temperatures. Despite the lower VS_r under ambient conditions, compared to mesophilic conditions, the AnMBR showed a 20 % increase in VS_r at more than double the VSLR compared to the AD. The main reason for the improved performance of the AnMBR was the increased SRT:HRT ratio of 40:8 days adjusted for the lower kinetics during ambient operation. During thermophilic operation the VS_r was 48 and 55 % for the AD and AnMBR, respectively, which represented a 15 % increase in VS_r. During thermophilic operation, the AnMBR SRT:HRT was adjusted to 22:7 days, for the expected improved kinetic rates and maintained at 16 days for the AD.

The AD and AnMBR treated sludge sludge quality was considered in term of N and P content. The TKN/TS content of the digested sludges ranged between 7–9 % and 6–7 % in

the AD and AnMBR, respectively. This represented a 24 % higher TKN/TS ratio in the AD versus the AnMBR treated sludge. However the permeate TKN represented 41–51 % of the total TKN leaving the system in the soluble NH_4 form. Hence, the permeate may be a valuable source of soluble N for recovery or reuse. The TP/TS ratio was 3 % in all four phases for both the AD and AnMBR except mesophilic conditions for the AD in which case it was 2 % (a 33 % higher TP/TS ratio in the AnMBR compared to the AD).

An energy balance comparison between the AD and AnMBR showed that an improved net energy production may be realized using AnMBR over AD which was directly related to the higher methane yield (38 % on average) and higher VSLR by a factor of 2.1–2.8 compared to the AD made possible by the decoupling of the HRT and SRT. When considering energy consumption for sludge heating, pumping, mixing, methane generation and heat losses per m^3 of sludge fed, a positive net energy production was realized for the AD and AnMBR during ambient operating conditions (25 °C) and for the AnMBR when operated at mesophilic (35 °C) conditions.

Membrane Performance

This phase of the study, on the membrane performance, demonstrated that fouling mitigating strategies that included a rest period between permeation cycles and a 4-step CIP strategy, applied at different frequencies from 3–21 days, were adequate to maintain the AnMBR flux throughput set point under ambient, mesophilic and thermophilic operation when treating mixed municipal sludge. Ambient operating conditions which also had the highest MLSS operating conditions and highest SRT/HRT ratio proved to be the most challenging in terms of fouling control effort.

It was determined through regression analysis that the TS, θ_x/θ and the bound EPS ratio ($C_{b,pr}/C_{b,ch}$) were the main predictors of the K_{20} throughout P1–P4 operating conditions explaining up to 89 % of the observed variability in the mean permeability with a 75 % estimated model predictability. A TS threshold was also observed at the TS range of 25–33 g/L with significant interaction between TS and with the SRT/HRT (2.4–3.5) and C_{pr}/C_{ch} (2.0–3.9) affecting the K_{20} (0.4–0.2 LMH/kPa). However at TS range of 33–76 g/L, no significant interaction effect was observed. These findings suggest a TS threshold in the range of 30–33 g/L that can impact the viability of AnMBRs when treating sludge or concentrated wastewaters.

To distinguish between reversible and irreversible fouling, the VFM approach, based on direct permeability measurements, showed the ability to clearly quantify differences in reversible and irreversible fouling propensities. As a complementary approach the use of modeling by the classical 'Hermia-Field' blocking modeling provided a means to identify that cake fouling (m=0) as the dominant fouling mode which provided a good prediction of flux decline during all four operating conditions.

YES Bioassay and TrOCs

The results of this phase of the study showed that estrogenicity, as measured by the *in-vitro* YES bioassay, persists in anaerobically treated digestion of mixed municipal sludges, the AnMBR permeate sidestream and carries over into aqueous extracts of saturated treated

mixed liquor solids samples. These findings should be considered in the context of potential dilution factors under field conditions.

The TrOCs chemistry analysis of the AnMBR permeate sidestream determined that TrOCs are present in low ng/L to low μg/L range depending on the TrOC. The measured TrOCs were found to accumulate in high solids and high SRT anaerobic sludge treatment systems. The permeate showed elevated TrOCs levels compared to typical raw municipal wastewater and would contribute significantly to the TrOCs loading when returned to the head works of a STP. The permeate chemistry E2 relative estrogenic potency analysis suggested that estrone and equilin were major contributors to the estrogenic responses measured while estriol and bisphenol A made a minimal contribution to the overall estrogenic responses.

6.3 Recommendations for Future Work

The following recommendations are suggested for future work to extend and apply the findings of this study towards improved sustainable sludge treatment practices.

This study showed, at pilot scale, that AnMBR can achieve a net positive energy balance when treating mixed municipal sludge operated at ambient and mesophilic conditions. Testing these findings though a full-scale demonstration would extend the findings and improve our understanding about scaling affects. A parallel full-scale demonstration of a sAnMBR and an iAnMBR would also address some of the unknown issues regarding the fouling mitigating strategies of side-stream versus immersed reactors and related costs associated with sludge pumping versus fouling mitigation strategies when treating concentrated wastewater streams.

The use of CIP and rest period to mitigate fouling effects, in this study, left a significant percentage of the 'flux potential' under-utilized. Investigating COP, relaxation, additives and other reactor configurations may improve the sustainable flux and improve the system throughput under the same AnMBR footprint thus reducing the capital and operating costs.

The application of the VFM and 'Hermia-Field' classical blocking modeling provided a means to quantify the type and mode of fouling through both direct measurement and modeling, respectively. Both these approached are complimentary and may be numerically integrated. Data from logged performance (as measured in this study) would provide the input data that can be used to feed an on-line 'smart-controller' used to identify the type and mode of fouling conditions. Based on this new model-based identification of fouling, it is anticipated that a timely application of the appropriate fouling control strategy can than be implemented. A simulation study of a controller logic implementation may be devised and simulated using Labview^{TM} or the R-coding framework to prove the concept before refinement and application to a bench scale and pilot scale demonstration.

The 'Hermia-Field' blocking model proved generally accurate but tended to underestimate the initial and latter degree of flux decline primarily due to a single mode of fouling and the assumption of incompressible cake fouling. A natural extension and expected improvement to the model predictability would be to incorporate a 2 or 3-mode of fouling simultaneously, consider adding an EPS parameter to address biofouling and incorporate

cake compressibility into the model framework. This has been partly accomplished for dead-end filtration however the models tend to be highly parameterized and less practicable. The new model extension for crossflow operation may use the existing models as starting points for the development but should work towards a less parameterized framework.

The *in-vitro* YES bioassay was found to be an effective screening tool to assess the estrogenic potential of biosolids and permeate or aqueous extracts. To become a more robust indicator and new metric that may be more widely applied, the YES bioassay should be corroborated by *in-vivo* studies. Further investigations of the YES bioassay to differently treated sludge types with a thorough assessment of the the sensitivity and robustness of the YES metric should also be investigated to build a database for the expected E2-equivalent range of values in environmental sludge matrices.

The investigation of TrOCs in this study should be extended to include a larger array of potential estrogens and anti-estrogens that could act as antagonists. Further with the chemical characterization of the parent compounds, the conjugated forms along with potential byproducts that may form under reducing conditions should be included which may require a non-targeted analytical approach. In this study many of the TrOCs analytical results were below MDLs which made predictions of effects more challenging and further work in the area of improved analytical techniques to reduce the MDLs, particularly of estrogenic compounds, is environmentally important.

References

[1] Batstone, D. J., Keller, J., Angelidaki, I., Kalyuzhnyi, S. V., Pavlostathis, S. G., Rozzi, A., Sanders, W. T. M., Siegrist, H., Vavilin, V. A. *Anaerobic Digestion Model No. 1 (ADM1), Scientific and Technical Report No. 13.* IWA Task Group for Mathematical Modelling of Anaerobic Digestion Processes, IWA Publishing, London, UK, 2002.

[2] Metcalf and Eddy. *Wastewater Engineering Treatment and Reuse.* McGraw-Hill, New York, NY, USA, 2003.

[3] Rittman, B. E. and McCarty, P. L. *Environmental Biotechnology:Principles and Applications.* McGraw-Hill, New York, NY, USA, 2001.

[4] U.S. Environmental Protection Agency Office of Water. Targeted national sewage sludge survey tnsss overview report. US EPA TNSSSS Overview Report, January 2009. Retrieved August 28, 2013 from the World Wide Web.

[5] Clarke, B. O., Smith, S. R. Review of emerging organic contaminants in biosolids and assessment of international research priorities for the agricultural use of biosolids. *Environment International*, 36:226–247, 2011.

[6] Laboratory Services Branch. *The Determination Of Emerging Organic Pollutants In Environmental Matrices By LC-MS-MS Analysis: Method E3454.* Ministry of the Environment and Climate Change, Toronto, ON, 2012.

[7] US EPA. *Estimation Programs Interface Suite™ for Microsoft® Windows, v 4.11.* United States Environmental Protection Agency, Washington, DC, USA, 2015. Retrieved October 24, 2015 from, US EPA EPI Suite.

[8] Water Environment Federation. *Membrane Bioreactors: WEF Manual of Practice No. 36.* McGraw-Hilll Education, New York, 2012.

[9] Judd, S., Judd, C., editors. *The MBR Book Principles and Applications of Membrane Bioreactors for Water and Wastewater Treatment.* McGraw-Hilll Education, New York, second edition, 2011.

[10] Milborrow, S., Trevor, H., Tibshirani, R. *Earth: Multivariate Adaptive Regression Splines*, 2015. Uses Alan Miller's Fortran utilities with Thomas Lumley's leaps wrapper. Earth.

[11] Konietschke, F., Placzek, M., Schaarschmidt, F., Hothorn, L. A. nparcomp: An R software package for nonparametric multiple comparisons and simultaneous confidence intervals. *Journal of Statistical Software*, 64(9):1–17, 2015. nparcomp.

[12] Helsel, D. R. *Statistics for Censored Environmental Data Using Minitab® and R, Second edition.* John Wiley and Sons, Inc., Hoboken, NJ, USA, 2012.

[13] Lee, L. *NADA: Nondetects And Data Analysis for environmental data*, 2013. URL http://CRAN.R-project.org/package=NADA. R package version 1.5-6.

[14] Le-Clech, P. Membrane bioreactors and their uses in wastewater treatments. *Applied Microbiology and Biotechnology*, 88(6):1253–1260, 2010.

[15] Wang, Z., Wu, Z. A Review of Membrane Fouling in MBRs: Characteristics and Role of Sludge Cake Formed on Membrane Surfaces. *Separation Science and Technology*, 44:3571–3596, 2009.

[16] Le-Clech, P., Chen, V., Fane, T. A. G. Review - Fouling in membrane bioreactors used in wastewater treatment. *Journal of Membrane Science*, 284(1–2):17–53, 2006.

[17] Padmasiria, S. I., Zhanga, J., Fitch, M., Norddahl, B., Morgenroth, E., Raskine, L. Methanogenic population dynamics and performance of an anaerobic membrane bioreactor (AnMBR) treating swine manure under high shear conditions. *Water Research*, 41(1):134–144, 2007.

[18] Santos, A., Ma, W., Judd, S. J. Membrane bioreactors: Two decades of research and implementation. *Desalination*, 273:148–154, 2011.

[19] Kanda, R. Endocrine Disrupters In Sewage Sludge: A Comparison Of Analytical Methods. Technical Report 04/TX/04/8, Water Environment Research Foundation and Global Water Research Coalition, 2004.

[20] Gray, J. L., Quanrud, D. M., Teske, S. S., Esposito, K., Marine, J., Ela, W. P., Stinson, B., Kolpin, D. W., Phillips, P. J. Fate of estrogenic compounds during municipal sludge stabilization and dewatering, biosolids, final report. Technical report, Water Environment Research Foundation and IWA Publishing, 2010.

[21] Besse, J. P., Garric, J. Progestagens for human use, exposure and hazard assessment for the aquatic environment. *Environmental Pollution*, 157:3485–3494, 2009.

[22] European Commission. European commission study on the scientific evaluation of 12 substances in the context of endocrine disrupter priority list of actions. Technical report, EUC, November 2002.

[23] Xia, K., Bhandari, A., Das, K., Pillar, G. Occurrence and Fate of Pharmaceuticals and Personal Care Products (PPCPs) in Biosolids. *Journal of Environmental Quality*, 34:94–91, 2005.

[24] Appels, L., Baeyens, J., Degrève, J. and Dewil, R. Principles and potential of the anaerobic digestion of waste-activated sludge. *Progress in Energy and Combustion Science*, 34:755–781, 2008.

[25] Switzenbaum, M. S., Pincince, A. B., Donovan, J., Epstein, E., Farrell, J. B. Developing protocosls for measuring biosolids stability. Technical report, Water Environment Research Foundation, 2002.

[26] Grady, C. P. L., Jr., Daigger, G. T., Lim, H. C. *Biological Wastewater Treatment, Second Edition, Revised and Expanded*. Marcell Dekker, Inc., New York, NY, USA, 1999.

[27] Pilli, S., Bhunia, P., Yan, S., LeBlanc, R. J., Tyagi, R. D., Surampalli, R. Y. Ultrasonic pretreatment of sludge: A review. *Ultrasonics Sonochemistry*, 18:1–18, 2011.

[28] Jeison, D., van Lier, J. B. Thermophilic treatment of acidified and partially acidified wastewater using an anaerobic submerged MBR: Factors affecting long-term operational flux. *Water Research*, 41:3868–3879, 2007.

[29] Lin, H., Peng, W., Zhang, M., Chen, J., Hong, H., Zhang, Y. A review on anaerobic membrane bioreactors: Applications, membrane fouling and future perspectives. *Desalination*, 314:169–188, 2013.

[30] Henze, M., van Loosdrecht, M. C. M., Ekama, G. A., Brdjanovic, D. *Biological Wastewater Treatment Principles, Modelling and Design*. IWA Publishing, London, UK, 2008.

[31] Dagnew, M. *Characterization of Anaerobic Membrane Digesters for Stabilization of Waste Activated Sludge*. Doctor of philosophy, University of Waterloo, 2010. Retrieved September 8, 2013 from the WWW PhD Thesis Report.

[32] Dagnew, M. and Pickel, J. and Parker, W. and Seto, P. Anaerobic membrane bioreactors for waste activated sludge digestion: Tubular versus hollow fiber membrane configurations. *Environmental Progress and Sustainable Energy*, 32(3):598–604, 2013.

[33] Meabe, E., Déléris, S., Soroa, S., Sancho, L. Performance of anaerobic membrane bioreactor for sewage sludge treatment: Mesophilic and thermophilic processes. *Journal of Membrane Science*, 446:26–33, 2013.

[34] Xu, M., Wena, X., Yu, Z., Li, Y., Huang, X. A hybrid anaerobic membrane bioreactor coupled with online ultrasonic equipment for digestion of waste activated sludge. *Bioresource Technology*, 102:5617–5625, 2011.

[35] Pierkiel, A., Lanting, J. Membrane-coupled anaerobic digestion of municipal sewage sludge. *Water Science and Technology, IWA Publishing*, 52(1–2):253–258, 2005.

[36] Takashima, M. Performance of anaerobic membrane bioreactor for sewage sludge at ambient and mesophilic temperature. *Prcedia Engineering*, 44:1095–1097, 2012.

[37] Sato, T., Ishii, Y. Effects of activated sludge properties on water flux of ultrafiltration membrane used for human excrement treatment. *Water Science and Technology*, 23: 1601–1608, 1991.

[38] Prieto, A. L., Futselaar, H., Lens, P. N. L., Bair, R., Yeh, D. H. Development and startup of a gas-lift anaerobic membrane bioreactor (gl-anmbr) for conversion of sewage to energy, water and nutrients. *Journal of Membrane Science*, 441:158–167, 2013.

[39] Lin, H. J., Xie, K., Mahendran, B., Bagley, D. M., Leungand, K. T., Liss, S. N., Liao, B. Q. Sludge properties and their effects on membrane fouling in submerged anaerobic membrane bioreactors (sanmbrs). *Water Research*, 43(15):3827Ű–3837, 2009.

[40] Fuchs, W., Binder, H., Mavrias, G., Braun, R. Anaerobic treatment of wastewater with high organic content using a stirred tank reactor coupled with a membrane filtration unit. *Water Research*, 37(4):902–908, 2003.

[41] Zhang, J., Padmasiri, S. I., Fitch, M., Norddahl, B., Raskin, L., Morgenroth, E. Influence of cleaning frequency and membrane history on fouling in an anaerobic membrane bioreactor. *Desalination*, 207:153–166, 2007.

[42] Zitomer, D. H., Bachman, T. C., Vogel, D. S. Thermophilic anaerobic digester with ultrafilter for solids stabilization. *Water Science and Technology, IWA Publishing*, 52(1–2):525–530, 2005.

[43] Lee, S. M., Jung, J., Chung, Y. Novel method for enhancing permeate flux of submerged membrane system in two-phase anaerobic reactor. *Water Research*, 35(2): 471–477, 2001.

[44] Herrera-Robledo, M., Cid-León, D. M., Morgan-Sagastume, J. M., Noyola, A. Biofouling in an anaerobic membrane bioreactor treating municipal sewage. *Separation and Purification Technology*, 81:49–55, 2011.

[45] Gao, D. W., Hu, Q., Yao, C., Ren, N. Q. Treatment of domestic wastewater by an integrated anaerobic fluidized-bed membrane bioreactor under moderate to low temperature conditions. *Bioresource Technology*, 159:193–198, 2014.

[46] Martinez-Sosa, D., Helmreich, B., Netter, T., Paris, S., Bischof, F., Horn, H. Anaerobic submerged membrane bioreactor (ansmbr) for municipal wastewater treatment under mesophilic and psychrophilic temperature conditions. *Bioresource Technology*, 102(22):10377–10385, 2011.

[47] Huang, Z., Ong, S. L., Ng, H. Y. Performance of submerged anaerobic membrane bioreactor at different srts for domestic wastewater treatment. *Journal of Biotechnology*, 164(1):82–90, 2013.

[48] Martin-Garcia, I., Monsalvo, V., Pidou, M., Le-Clech, P., Judda, S. J., McAdam, E. J., Jefferson, B. Impact of membrane configuration on fouling in anaerobic membrane bioreactors. *Journal of Membrane Science*, 382:41–49, 2011.

[49] Cho, B. D., Fane, A. G. Fouling transients in nominally sub-critical flux operation of a membrane bioreactor. *Journal of Membrane Science*, 2:27–28, 2002.

[50] Gao, W. J., Han, M. N., Qu, X., Xu, C., Liao, B. Q. Characteristics of wastewater and mixed liquor and their role in membrane fouling. *Bioresource Technology*, 128: 207–214, 2013.

[51] Gao, W. J., Leung, K. T., Qin, W. S., Liao, B. Q. Effects of temperature and temperature shock on the performance and microbial community structure of a submerged anaerobic membrane bioreactor. *Bioresource Technology*, 102(19):8733–8740, 2011.

[52] Lin, H., Liao, B. Q., Chen, J., Gao, W., Wang, L., Wang, F., Lu, x. New insights into membrane fouling in a submerged anaerobic membrane bioreactor based on characterization of cake sludge and bulk sludge. *Bioresource Technology*, 102:2373–2379, 2011.

[53] Martin-Garcia, I., Mokosch, M., Soares, A., Pidou, M., Jefferson, B. Impact on reactor configuration on the performance of anaerobic mbrs: Treatment of settled sewage in temperate climates. *Water Research*, 47:4853–4860, 2013.

[54] Xie, S., Lina, H. J., Mahendran, B., Bagley, D. M., Leung, K. T., Liss, S. N., Liao, B. Q. Performance and fouling characteristics of a submerged anaerobic membrane bioreactor for kraft evaporator condensate treatment. *Environmental Technology*, 31 (5):511–521, 2010.

[55] Liao, B. Q., Xie, K., Lin, H. J., Bertoldo, B. Treatment of kraft evaporator condensate using a thermophilic submerged anaerobic membrane bioreactor. *Water Science and Technology, IWA Publishing*, 61(9):2177–2183, 2010.

[56] Trzcinski, A. P., Stuckey, D. C. Treatment of municipal solid waste leachate using a submerged anaerobic membrane bioreactor at mesophilic and psychrophilic temperatures: Analysis of recalcitrants in the permeate using gc-ms. *Water Research*, 44(3): 671–680, 2010.

[57] Fakhru'l-Razi, A., Noor, M. J. M. M. Treatment of palm oil mill effuent (POME) with the membrane anaerobic system (MAS). *Water Science and Technology*, 39 (10–11):159–163, 1999.

[58] Gao, D. W., Hu, Q., Yao, C., Ren, N. Q., Wu, W. M. Integrated anaerobic fluidized-bed membrane bioreactor for domestic wastewater treatment. *Chemical Engineering Journal*, 240:362–368, 2014.

[59] Ognier, S., Wisniewski, C., Grasmick, A. Membrane bioreactor fouling in subcritical filtration conditions: a local critical flux concept. *Journal of Membrane Science*, 229: 171–177, 2004.

[60] Jeison, D., van Betuw, W., van Lier, J. B. Feasibility of anaerobic membrane bioreactors for the treatment of wastewaters with particulate oranic matter. *Separation Science and Technology*, 43:3417–3431, 2008.

[61] Beaubien, D. J., Bâty, M., Jeannot, F., Francoeur, E., Manem, J. Design and operation of anaerobic membrane bioreactors: Development of a filtration testing strategy. *Journal of Membrane Science*, 109(2):173–184, 1996.

[62] Akram, A., Stuckey, D. C. Flux and performance improvement in a submerged anaerobic membrane bioreactor (sambr) using powdered activated carbon (pac). *Process Biochemistry*, 43:93–102, 2008.

[63] Aquino, S. F., Yu, A. Y., Akram, A., Stuckey, D. C. Characterization of dissolved compounds in submerged anaerobic membrane bioreactors (sambrs). *Journal of Chemical Technology and Biotechnology*, 81(12):1894–1904, 2006.

[64] Jeison, D., Plugge, C. M., Pereira, A., van Lier, J. B. Effects of the acidogenic biomass on the performance of an anaerobic membrane bioreactor for wastewater treatment. *Bioresource Technology*, 100(6):1951–1956, 2009.

[65] Huang, Z., Ong, S. L., Ng, H. Y. Submerged anaerobic membrane bioreactor for low-strength wastewater treatment: Effect of hrt and srt on treatment performance and membrane fouling. *Water Research*, 45(2):705–713, 2011.

[66] Jeison, D., van Lier, J. B. Cake layer formation in anaerobic submerged membrane bioreactors (ansmbr) for wastewater treatment. *Journal of Membrane Science*, 284 (1–2):227–236, 2006.

[67] Elmaleh, S., Abdelmoumni, L. Experimental test to evaluate performance of an anaerobic reactor provided with an external membrane unit. *Water Science and Technology*, 38(8):385–392, 1998.

[68] Gao, D. W., Zhang, T., Tang, C. Y. Y., Wu, W. M., Wong, C. H., Lee, Y. H., Yeh, D. H., Criddle, C. S. Membrane fouling in an anaerobic membrane bioreactor: Differences in relative abundance of bacterial species in the membrane foulant layer and in suspension. *Journal of Membrane Science*, 364(1–2):331–338, 2010.

[69] Buetehorn, S., Brannock, M., Le-Clech, P., Leslie, G., Volmering, K., D. Vossenkaul, Wintgens, T., Wessling, M., Melin, T. Limitations for transferring lab-scale microfiltration results to large-scale membrane bioreactor (MBR) processes. *Separation and Purification Technology*, 95:202–215, 2012.

[70] Carrère, H., Dumas, C., Battimelli, A., Batstone, D. J., Delgenès, J. P., Steyer, J. P., Ferrer, I. Review pretreatment methods to improve sludge anaerobic degradability: A review. *Journal of Hazardous Materials*, 183:1–15, 2010.

[71] Sophonsiri, C., Morgenroth, E. Chemical composition associated with different particle size fractions in municipal, industrial, and agricultural wastewaters. *Chemosphere*, 55(5):691–703, 2004.

[72] Bai, R., Leoq, H. F. Microfiltration of activated sludge wastewater - effect of system operation parameters. *Separation and Purification Technology*, 29:189–198, 2002.

[73] Sanders, W. T. M. *Anaerobic Hydrolysis During Digestion of Complex Substrates*. PhD thesis, Wageningen University, Wageningen, The Netherlands, 2001. Retrieved September 9, 2014 from the WWB: PhD Thesis Report.

[74] Gao, W. J., Qu, X., Leung, K. T., Liao, B. Q. Influence of temperature and temperature shock on sludge properties, cake layer structure and membrane fouling in a submerged naerobic membrane bioreactor. *Journal of Membrane Science*, 421-422:131–144, 2012.

[75] Ho, J., Sung, S. Effects of solid concentrations and cross-flow hydrodynamics on microfiltration of anaerobic sludge. *Journal of Membrane Science*, 345(1–2):142–147, 2009.

[76] Baudez, J. C., Slatter, P., Eshtiaghi, N. The impact of temperature on the rheological behaviour of anaerobic digested sludge. *Chemical Engineering Journal*, 215–216:182–187, 2013.

[77] Meng, F., Chae, S. R., Drews, A., Kraume, M., Shin, H. S., Yang, F. Review - Recent advances in membrane bioreactors (MBRs): Membrane fouling and membrane material. *Water Research*, 43:1489–1512, 2009.

[78] Dagnew, M., Parker, W., Seto, P. Anaerobic membrane bioreactors for treating waste activated sludge: Short term membrane fouling characterization and control tests. *Journal of Membrane Science*, 421–422:103–110, 2012.

[79] Wang, Z., Mei, X., Ma, J., Grasmick, A., Wu, Z. Potential foulants and fouling indicators in MBRs: A Critical Review. *Separation Science and Technology*, 48: 22–50, 2013.

[80] Drews, A. Review - Membrane fouling in membrane bioreactors - Characterization contradictions, cause and cures. *Journal of Membrane Science*, 363:1–28, 2010.

[81] Laspidou, C. S., Rittmann, B. E. A unified theory for extracellular polymeric substances, soluble microbial products, and active and inert biomass. *Water Research*, 36:2711–2720, 2002.

[82] Aquino, S. F., Stukey, D. C. Integrated model of the production of soluble microbial products (SMP) and extracellular polymeric substances (EPS) in anaerobic chemostats during transient conditions. *Biochemical Engineering Journal*, 38:138–146, 2008.

[83] Ho, J., Sung, S. Anaerobic membrane bioreactor treatment of synthetic municipal wastewater at ambient emperature. *Water Environment Research*, 81(9):922–928, 2009.

[84] Stricot, M., Filali, A., Lesage, N., Sprandio, M., Cabassud, C. Side-stream membrane bioreactors: Influence of stress generated by hydrodynamics on floc structure, supernatant quality and fouling propensity. *Water Research*, 44(7):2113–2124, 2010.

[85] Madaeni, S. S., Fane, A. G., Wiley, D. E. Factors influencing critical flux in membrane filtration of activated sludge. *Journal of Chemical Technology and Biotechnology*, 74: 539–543, 1999.

[86] Dagnew, M., Parker, W., Seto, P. A pilot study of anaerobic membrane digesters for concurrent thickening and digestion of waste activated sludge (WAS). *Water Science and Technology, IWA Publishing*, 61(6):1451–1458, 2010.

[87] Brauns, E., Van Hoff, E., Molenberghs, B., Dotremont, C. , Doyen, W., Leysen, R. A new method of measuring and presenting the membrane fouling potential. *Desalination*, 150:31–43, 2002.

[88] Huyskens, C., Brauns, E., Van Hoof, E., De Wever, H. A new method for the evaluation of the reversible and irreversible fouling propensity of MBR mixed liquor. *Journal of Membrane Science*, 323:185–192, 2008.

[89] Naessens, W., Maere, T., Nopens, I. Critical review of membrane bioreactor models - Part 1: Biokinetic and filtration models. *Bioresource Technology*, 122:95–106, 2012.

[90] Hermia, J. Constant pressure blocking filtration laws. application to power-law non-newtonian fluids. *Transactions of the Institute of Chemical Engineering*, 60: 183–187, 1982.

[91] Field, R. W., Wu, D., Howell, J. A., Gupta, B. B. Critical flux concept for micrfiltration fouling. *Journal of Membrane Science*, 100:259–272, 1995.

[92] Kalogo, Y., Monteith, H. State Of Science Report: Energy And Resource Recovery From Sludge. Technical report, Hydromantis Inc., Canada; Global Water Research Coalition, UK WIR, WERF, STOWA, 2008.

[93] Lübken, M., Wichern, M., Schlattmann, M., Gronauer, A., Horn, H. Modelling the energy balance of an anaerobic digester fed with cattle manure and renewable energy crops. *Water Research*, 41:4085–4096, 2007.

[94] Martin, I., Pidou, M., Soares, A., Judd, S., and Jefferson, B. Modelling the energy demands of aerobic and anaerobic membrane bioreactors for wastewater treatment: Review Article. *Environmental Technology*, 32(9):921–932, 2011.

[95] Kidd, K. A., Blanchfield, P. J., Mills, K. H., Palace, V. P., Evans, R. E., Lazorchak, J. M., Flick, R. M. Collapse of a fish population after exposure to a synthetic estrogen. *Proceedings of the National Academy of Sciences of the USA*, 104(21):8897–Ű8901, 2007.

[96] Langdon, K. A., Warne, M. S. J., Smernik, R. J., Shareef, A., Kookana, R. S. Selected personal care products and endocrine disruptors in biosolids - an australia-wide survey. *Science of the Total Environment*, 409(6):1075–1081, 2011.

[97] Citulski, J. A. and Farahbakhsh, K. Fate of Endocrine-Active Compounds during Municipal Biosolids Treatment: A Review. *Environmental Science and Technology*, 44:8367–8376, 2010.

[98] Canadian Council Of Ministers Of The Environment. *Emerging Substances Of Concern In Biosolids: Concentrations And Effects Of Treatment Processes, Final Report – Literature Review, CCME Project No. 447-2009*. CCME, 2009. Accessed from the WWW on August 16, 2014.

[99] Yang, Y. Y., Gray, J. L., Furlong, E. T., Davis, J. G., ReVello, R. C., and Borch, T. Steroid hormone runoff from agricultural test plots applied with municipal biosolids. *Environmental Science and Technology*, 46:2746–2754, 2012.

[100] Edwards, M., Topp, E., Metcalfe, C. D., Li, H., Gottschall, N., Bolton, P., Curnoe, W., Payne, M., Beck, A., S., K., Lapen, D. R. Pharmaceutical and personal care products in tile drainage following surface spreading and injection of dewatered municipal biosolids to an agricultural field. *Journal of Biotechnology*, 407(14):4220–4230, 2009.

[101] Topp, E., Monteiro, S. C., Beck, A., Coelho, B. B., Boxall, A. B. A., Duenk, P. W., Kleywegt, S., Lapen, D. R., Payne, M., Sabourin, L., Li, H., Metcalfe, C. D. Runoff of pharmaceuticals and personal care products following application of biosolids to an agricultural field. *Science of the Total Environment*, 396:52–59, 2008.

[102] European Commission. *Directive 2008/98/EC of the European Parliament and of the Council of 19 November 2008 on waste and repealing certain Directives (Text with EEA relevance)*. Official Journal Of The European Union, November 2008. Accessed from the WWW on August 16, 2014.

[103] Chari, B. P., Halden, R. U. Predicting the concentration range of unmonitored chemicals in wastewater-dominated streams and in run-off from biosolids-amended soils. *Science of the Total Environment*, 440:314–320, 2012.

[104] Stumpe, B., Marschner, B. Dissolved organic carbon from sewage sludge and manure can affect estrogen sorption and mineralization in soils. *Environmental Pollution*, 158:148–154, 2010.

[105] Lorenzen, A., Hendel, J. G., Conn, K. L., Bittman, S., Kwabiah, A. B., Lazarovitz, G., Massé, D., McAllister, T. A., Topp, E. Survey of hormone activities in municipal biosolids and animal manures. *Environmental Toxicology*, 19(3):216–225, 2004.

[106] Citulski, J. A. *The Fate of Net Estrogenicity and Anti-Estrogenicity During Conventional and Advanced Biosolids Treatment Processes*. Engineering PhD, University of Guelph, Guelph, ON, January 2012. Thesis Report.

[107] Monsalvo, V. M., McDonald, J. A., Khan, S. J., Le-Clech, P. Removal of trace organics by anaerobic membrane bioreactors. *Water Research*, 49:103–112, 2014.

[108] Routledge, E. J., Sumpter, J. P. Estrogenic activity of surfactants and some of their degradation products assessed using a recombinant yeast screen. *Environmental Toxicology and Chemistry*, 15(3):241–248, 1996.

[109] Williams, M., Woods, M., Kumar, A., Ying, G. G., Shareef, A., M., K., and Kookana, R. Endocrine disrupting chemicals in the australian riverine environment: A pilot study on estrogenic compounds. Technical report, CSIRO and Land and Water Australia, November 2007. Retrieved from the WWW on January 21, 2014.

[110] de Jong, P., Kramer, J. F., Slotema, W. F., Third, K. A. Exploratory Study for Wastewater Treatment Techniques and The European Water Framework Directive Technical Report 34. Technical report, STOWA, 2005.

[111] Miao, X. S., Yang, J. J., Metcalf, C. D. Carbamazepine and its metabolites in wastewater and in biosolids in a municipal wastewater treatment plant. *Environmental Science and Technology*, 39(19):7469–7475, 2005.

[112] Hydromantis, Inc., Webber Environmental, University of Waterloo Civil and Environmental Engineering. Assessing the fate and significance of microconstituents and pathogens in sewage biosolids update of the 2001 weao report on fate and significance, final report. WEAO Report on Fate and Significance, 2009. Retrieved August 28, 2013 from the World Wide Web.

[113] Global Water Research Coalition. GWRC Workshop on Methodologies for Chemical and Biological Analysis of EDC in Water Systems Karlsruhe (Germany), March 31 –April 2, 2003. Technical report, DVGWŰTechnologiezentrum Wasser (TZW), London, UK, September 2003. Retrieved September 2, 2013 from GWRC Workshop.

[114] MOE-SDB. MOE Design Guidelines for Sewage Works, 2008. MOE Design Guidelines, 2008. Retrieved from the WWW on August 14, 2014.

[115] APHA, AWWA and WEF. *Standard methods for examination of water and wastewater*. WEF, Washington, DC, 21 edition, 1998.

[116] Environment Canada Wastewater Technology Centre Analytical Laboratory. *INV 5011 QuAAtro Applications Methods Q-022-04, Q-024-04, Q-026-04, Dionex Method 5.17*. Burlington, Ontario, Canada, 2010–2013.

[117] R Core Team. R: A Language and Environment for Statistical Computing. R, 2014.

[118] Zar, J. H. *Biostatistical Analysis, Fourth edition*. Prentice Hall, Inc., Upper Saddle River, NJ, USA, 1999.

[119] Ontario Ministry of the Environment (MOE). Nutrient management act, 2002, ontario regulation 267/03. MOE NMA, January 2014. Retrieved from the WWW on January 19, 2014.

[120] McFarland, M. J. *Biosolids Engineering*. McGraw-Hill, New York, NY, USA., 2000.

[121] Drews, A., Vocks, M., Iversen, V., Lejean, B., Kraume, M. Influence of unsteady bioreactor operation on EPS formation and filtration resistance. *Desalination*, 192: 1–9, 2006.

[122] Drews, A., Lee, C.-H., Kraume, M. Membrane fouling Ű a review of the role of EPS. *Desalination*, 200:186 – 188, 2006.

[123] Duclos-Orsello, C., Li, Weiyi, Ho, C.-C. A three mechanism model to describe fouling of microfiltration membranes. *Journal of Membrane Science*, 280:856 – 866, 2006.

[124] Philippe, N., Racault, Y., Stricker, A. E., Spérandio, P. A., Vanrollenghem, P. A. Modelling the long-term evolution of permeability in a full-scale municipal MBR: A multivariate statistical modelling approach. *Procedia Engineering*, 44:574–580, 2012.

[125] Kim, M., Sankararao, B., Lee, S. and Yoo, C.-Y. Prediction and Identification of Membrane Fouling Mechanism in a Membrane Bioreactor Using a Combined Mechanistic Model. *Industrial and Engineering Chemistry Research*, 52:17198–17205, 2013.

[126] Zuthi, M. F. R., Ngo, H. H., Guo, W. S., Zhang, J., Liang, S. A review towards finding a simplified approach for modelling the kinetics of the soluble microbial products (smp) in an integrated mathematical model of membrane bioreactor (mbr). *International Biodeterioration and Biodegradation*, 85:466–473, 2013.

[127] Smith, P. K., Krohn, R. I., Hermanson, G. T., Mallia, A. K., Gartner, F. H., Provenzano, M. D., Fujimoto, E. K., Goeke, N. M., Olson, B. J., Klenk, D. C. Measurement of protein using bicinchoninic acid. *Analytical Biochemistry*, 1:76–85, 1985.

[128] Dubois, M., Gilles, K. A., Hamilton, J. K., Rebers, P. A., Smith, F. Colorimetric method for determination of sugars and related substances. *Analytical Chemistry*, 28:350–356, 1956.

[129] RStudio, Inc., Boston MA, USA. Rstudio. RStudio, 2014. Retrieved September 25, 2013 from the World Wide Web.

[130] Soetaert, K. and Herman, P.M.J. *A Practical Guide to Ecological Modelling. Using R as a Simulation Platform*. Springer, 2009. 372 pp.

[131] Maechler, M. sfsmisc: Utilities from Seminar fuer Statistik ETH Zurich. sfsmisc, 2015. R package version 1.0-27.

[132] Elzhov, T. V., Mullen, K. M., Spiess, A.-N. and Bolker, B. minpack.lm: R interface to the Levenberg-Marquardt nonlinear least-squares algorithm found in MINPACK, plus support for bounds. MINPACK, 2013. R package version 1.1-8.

[133] Tukey, J. W. *Exploratory Data Analysis: Past, Present and Future*, volume Technical Report No. 302. Princeton University, Priceton, NJ, 1993.

[134] Konietschke, F., Placzek, M., Schaarschmidt, F. and Hothorn, L. A. nparcomp: An R Software Package for Nonparametric Multiple Comparisons and Simultaneous Confidence Intervals. nparcomp, 2015.

[135] Friedman, J. H. *Multivariate Adaptive Regression Splines*, 1990. MARS.

[136] Milborrow, S. *plotmo: Plot a Model's Response and Residuals*, 2015. R package version 3.1.4.

[137] Meng, F., Shi, B., Yang, F., Zhang, H. New insights into membrane fouling in submerged membrane bioreactor based on rheology and hydrodynamics concepts. *Journal of Membrane Science*, 302:87–94, 2007.

[138] Buntner, D., Spanjers, H., van Lier, J. B. The influence of hydrolysis induced biopolymers from recycled aerobic sludge on specific methanogenic activity and sludge filterability in an anaerobic membrane bioreactor. *Water Wesearch*, 51:284–292, 2014.

[139] Liao, B. Q., Allen, D. G., Droppo, I. G., Leppard, G. G. and Liss, S. N. Surface Properties Of Sludge and Their Role In Bioflocculation and Settleability. *Water Research*, 35(2):339–350, 2001.

[140] Sheng, G.-P., Yu, H.-Q., Li, X.-Y. Stability of Sludge Flocs Under Shear Conditions: Roles of Extracellular Polymeric Substances (EPS). *Biotechnology and Bioengineering*, 93(6):1095–1102, 2006.

[141] Cho, J., Song, K.-G., Ahn, K.-H. The activated sludge and microbial substances influences on membrane fouling in submerged membrane bioreactor: unstirred batch cell test. *Desalination*, 183:425–429, 2005.

[142] Fang, H. H. P., Shi, X. Pore fouling of microfiltration membranes by activated sludge. *Journal of Membrane Science*, 264:161–166, 2005.

[143] Schwarz, A. O., Rittmann, B. E., Crawford, G. V., Klein, A. M., and Daigger, G. T. Critical Review on the Effects of Mixed Liquor Suspended Solids on Membrane Bioreactor Operation. *Separation Science and Technology*, 41:1489–1511, 2006.

[144] Astudillo, C., Parra, J., González, S., Cancino, B. A new parameter for membrane cleaning evaluation. *Separation and Purification Technology*, 73(2):286–293, 2010.

[145] Shi, X., Tal, G., Hankins, N. P., Gitis, V. Fouling and cleaning of ultrafiltration membranes: A review. *Journal of Water Process Engineering*, 1:121–138, 2014.

[146] Dereli, R. K., Heffernan, B., Grelot, A., van der Zee, F. P., van Lier, J. B. Influence of high lipid containing wastewater on filtration performance and fouling in AnMBRs operated at different solids retention times. *Separation and Purification Technology*, 139:43– 2, 2015.

[147] Nguyen, S. T., Roddick, F. A. Chemical cleaning of ultrafiltration membrane fouled an activated sludge effluent. *Desalination and Water Treatment*, 34:94–99, 2011.

[148] Ramos, C., Zecchino, F., Ezquerra, D., Diez, V. Chemical cleaning of membranes from ananaerobic membrane bioreactortreatingfoodindustrywastewater. *Journal of Membrane Science*, 458:179–188, 2014.

[149] Jeison, D., van Lier, J. B. On-line cake-layer management by trans-membrane pressure steady state assessment in anaerobic membrane bioreactors for wastewater treatment. *Biochemical Engineering Journal*, 29:204–209, 2006.

[150] Bugge, T. V., Jørgensen, J. K., Christensen, M. L., Keiding, K. Modeling cake buildup under tmp-step filtration in a membrane bioreactor: Cake compressibility is significant. *Water Research*, 46:4330–4338, 2012.

[151] Christensen, M. L., Nielsen, T. B., Andersen, M. B. O., Keiding, K. Effect of water-swollen organic materials on crossflow filtration performance. *Journal of Membrane Science*, 333:94–99, 2009.

[152] Ho, C.-C. and Zydney, A. L. A combined pore blockage and cake filtration model for protein fouling during microfiltration. *Journal of Colloid and Interface Science*, 232:389 – 399, 2000.

[153] Drews, A., Arellano-Garcia, H., Schöneberger, J., Schaller, J., Wozny, G., Kraume, M. Model-based recognition of fouling mechanisms in membrane bioreactors. *Desalination*, 236:224–233, 2009.

[154] Palacio, L., Ho, C.-C., Zydney, A. L. Application of a Pore-Blockage - Cake-Filtration Model to Protein Fouling During Microfiltraiton. *Biotechnology and Bioengineering*, 79(3):260 – 270, 2002.

[155] Canadian Council Of Ministers Of The Environment. *Emerging Substances Of Concern In Biosolids: Concentrations And Effects Of Treatment Process Final Report – Field Sampling Program Ccme Project No. 447-2009*. CCME, 2010. Accessed from the WWW on August 16, 2014.

[156] Gottschall, N., Topp, E., Metcalfe, C., Edwards, M., Payne, M., Kleywegt, S., Russell, P., Lapen, O. R. Pharmaceutical and personal care products in groundwater, subsurface drainage, soil, and wheat grain, following a high single application of municipal biosolids to a field. *Chemosphere*, 87:194Ű203, 2012.

[157] Sabourin, L., Duenk, P., Bonte-Gelok, S., Payne, M., Lapen, D. R., Topp, E. Uptake of pharmaceuticals, hormones and parabens into vegetables grown in soil fertilized with municipal biosolids. *Science of the Total Environment*, 431:233–236, 2012.

[158] Sabourin, L., Beck, A., Duenk, P., Kleywegt, S., Lapen, D. R., Li, H., Metcalfe, C. D., Payne, M. Runoff of pharmaceuticals and personal care products following application of dewatered municipal biosolids to an agricultural field. *Science of the Total Environment*, 407:4596–4604, 2009.

[159] Wu, C., Spongberg, A. L., Witter, J. D., Sridhar, B. B. M. Transfer of wastewater associated pharmaceuticals and personal care products to crop plants from biosolids treated soil. *Ecotoxicology and Environmental Safety*, 85:104–109, 2012.

[160] Grund, S., Higley, E., Schönenberger, R., Suter, M. J. F., Giesy, J. P., Braunbeck, T., Hecker, M., Hollert, H. The endocrine disrupting potential of sediments from the upper danube river (germany) as revealed by in vitro bioassays and chemical analysis. *Environmental Science and Pollution Research*, 18:446–460, 2011.

[161] U.S. Environmental Protection Agency Office of Water Office of Science and Technology Engineering and Analysis Division (4303T). *Method 1698: Steroids and Hormones in Water, Soil, Sediment, and Biosolids by HRGC/HRMS*. US EPA, 1200 Pennsylvania Avenue, NW Washington, DC 20460, EPA-821-R-08-003 edition, December 2007.

[162] Ritz, C., Streibig, J. C. Bioassay analysis using r. *Journal of Statistical Software*, 12, 2005. URL http://www.bioassay.dk.

[163] Metcalfe, C. D., Metcalfe, T. L., Kiparissis, Y., Koenig, B. G., Khan, C., Hughes, R. J., Croley, T. R., March, R. E., and Potter, T. Estrogenic Potency Of Chemicals Detected In Sewage Treatment Plant Effluents As Determined By In Vivo Assays With Japanese Medaka (Oryzias Latipes). *Environmental Toxicology and Chemistry*, 20(2):297–308, 2001.

[164] Holbrook, R. D., Novak, J. T., Grizzard, T. J., and Love, N. G. Estrogen Receptor Agonist Fate During Wastewater and Biosolids Treatment Processes: A Mass Balance Analysis. *Environmental Science and Technology*, 36(21):4533–4539, 2002.

[165] Lange, R., Hutchinson, T. H., Croudace, C. P., Siegmund, F., Schweinfurth, H., Hampe, P., Panter, G. H., and Sumpter, J. P. Effects Of The Synthetic Estrogen 17A-Ethinylestradiol On The Life-Cycle Of The Fathead Minnow (Pimephales Promelas). *Environmental Toxicology and Chemistry*, 20(6):1216–1227, 2001.

[166] Pileggi, V., Feisthauer, N., Chen, X., Parker, W. J., Parrott, J., Van Der Kraak, G., Tabe, T., Kleywegt, S., Schroeder, J., Yang, Y. and Seto, P. Impact of Wastewater Treatment Process Configuration on Effluent Chemistry and Biological Responses. *WEFTEC*, pages 1763–1779, 2011. Published in Conference proceedings.

[167] Pileggi, V., Ogunlaja, M., Chen, X., Parker, W. J., Yang, P., Kleywegt, S., Feisthauer, N., Tabe, S., Schroeder, J., Fletcher, T. and Seto, P. Comparison Of Effluent Conventional and Microcontaminant Chemistry In Three Pilot Wastewater Treatment Processes During Winter And Summer Simulated Conditions. *WEFTEC*, 2013. Published on line in Conference proceedings.

[168] Nguyen, P. N., Hai, F. I., Kang, J., Price, W. E., Nghiem, L. D. Removal of emerging trace organic contaminants by MBR-based hybrid treatment processes. *International Biodeterioration and Biodegradation*, 85:474–482, 2013.

[169] Rutishauser, B. V., Pesonen, M., Escher, B. I., Ackermann, G. E., Aerni, H.-R., Suter, M., J.-F., and Eggen, R. I. L. Comparative Analysis Of Estrogenic Activity In Sewage Treatment Plant Effluents Involving Three In Vitro Assays And Chemical Analysis Of Steroids. *Environmental Toxicology and Chemistry*, 23(4):857–864, 2004.

[170] Aerni, H.-R., Kobler, B., Rutishauser, B. V., Wettstein, F. E., Fischer, R., Giger, W., Hungerbühler, A., Marazuela, M. D., Peter, A., Schönenberger, R., Vögeli, A. C., Suter, M. J.-F., Eggen, R. I. L. Combined biological and chemical assessment of estrogenic activities in wastewater treatment plant effluents. *Analytical and Bioanalytical Chemistry*, 378:688–696, 2004.

[171] Whidbey, C. M., Daumit, K. E., Nguyen, T.-H., Ashworth, D. D., Davis, J. C. C., Latch, D. E. Photochemical induced changes of in vitro estrogenic activity of steroid hormones. *Water Research*, 46:5287–5296, 2012.

[172] Pereira C., de B. Pereira, C. A. and Polpo, A. Medor: Order of medians based on confidence statements. *arXiv.org*, 2012. URL http://arxiv.org/abs/1212.5405.

[173] Meylan, W., Boethling, R. S., Aronson, D., Howard, P., Tunkel. Chemical structure-based predictive model for methanogenic anaerobic biodegradation potential. *Environmental Toxicology and Chemistry*, 26(9):1785–1792, 2007.

[174] Clark, B., Henry, J. G. and Mackay, D. Fugacity Analysis and Model of Organic Chemical Fate in a Sewage Treatment Plant. *Environmental Science and Technology*, 29(6):1488–1494, 1995.

Appendix A

Operating Parameters and Conventional Chemistry

A.1 AnMBR and AD Pilot Plants

Figure A.1 shows a photograph of the pilot plants and SCADA control system.

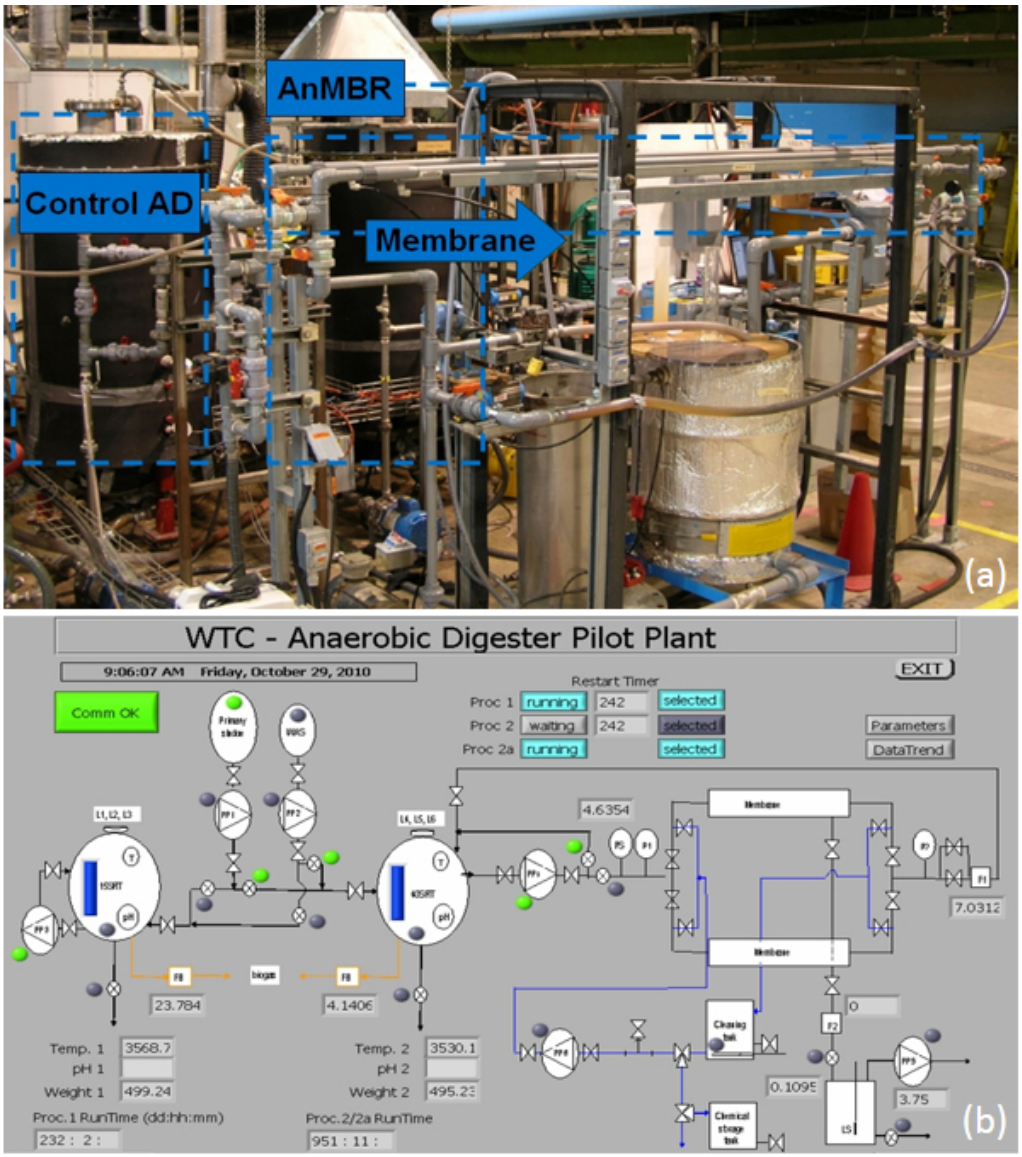

Figure A.1: Photograph of the pilot plants (a) and SCADA display system (b).

A.2 Temperature During P1–P4

The temperature control over the operating periods in each phase for the AD and AnMBR is shown in Figure A.2. During the transient phase (following P1) the dissolved air floatation (DAF) system at the Burlington Skyway STP was inoperative, for a significant period and the TWAS was not thickened. Since the TWAS was significantly different compared to the other periods, this transient phase had to be excluded from the main phases (P1–P4).

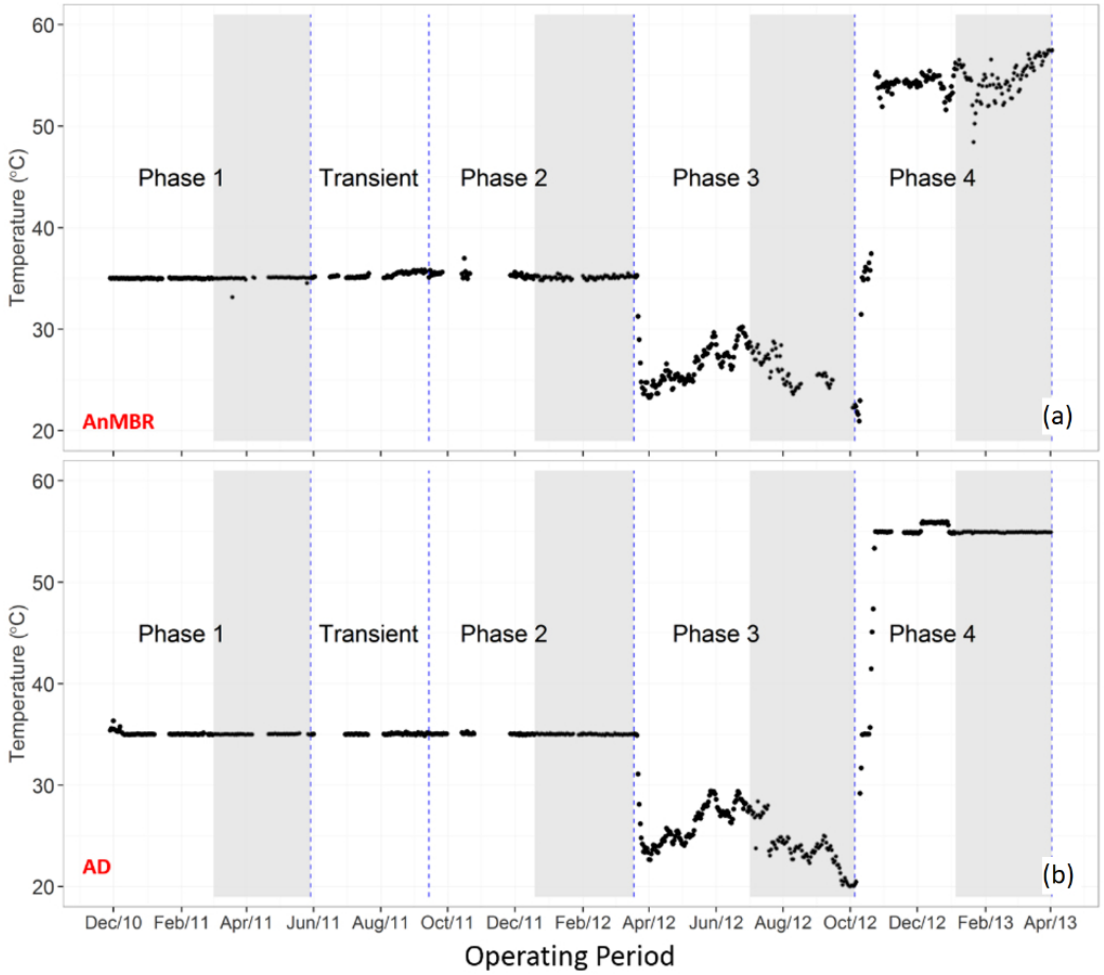

Figure A.2: Daily temperature (°C) of the AnMBR (b) and the AD (b) during the four Phases including a transient, stabilizing and stable operating periods (shaded). Note: During the transient phase TWAS was not thickened for a significant period and excluded from the main phases.

A.3 AnMBR and AD Operating Parameters

The key operating parameters, besides the temperature, included the SRT and HRT set points shown in Figure A.3 and A.4.

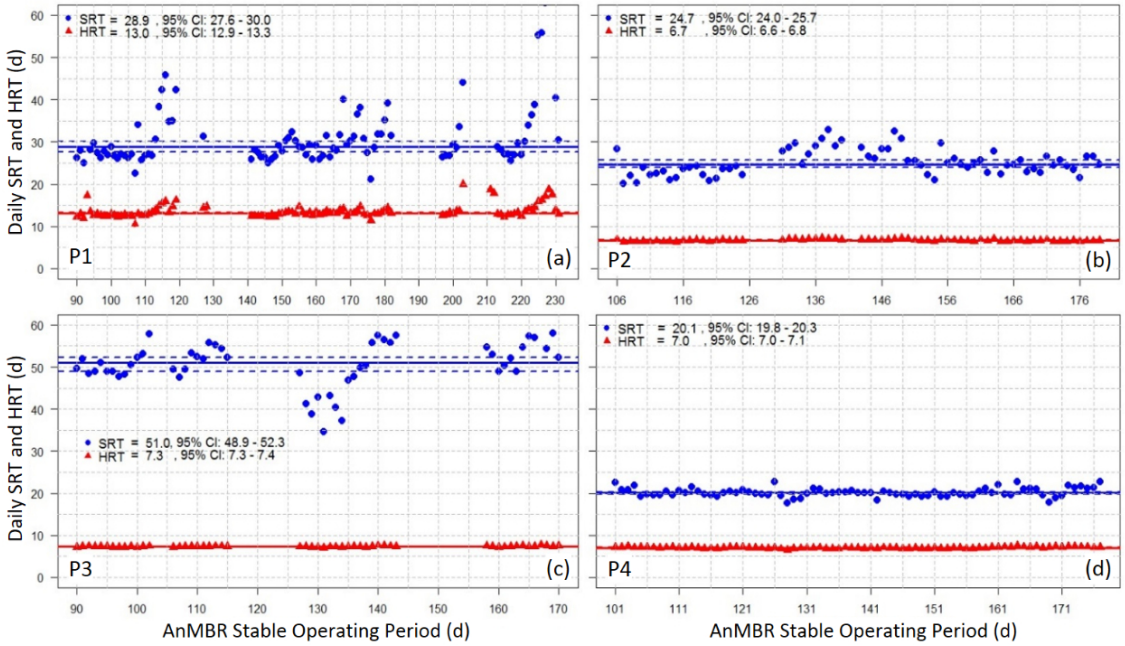

Figure A.3: The AnMBR operation daily SRT and HRT with median and 95% confidence interval in Phase 1–4 in (a)–(d), respectively.

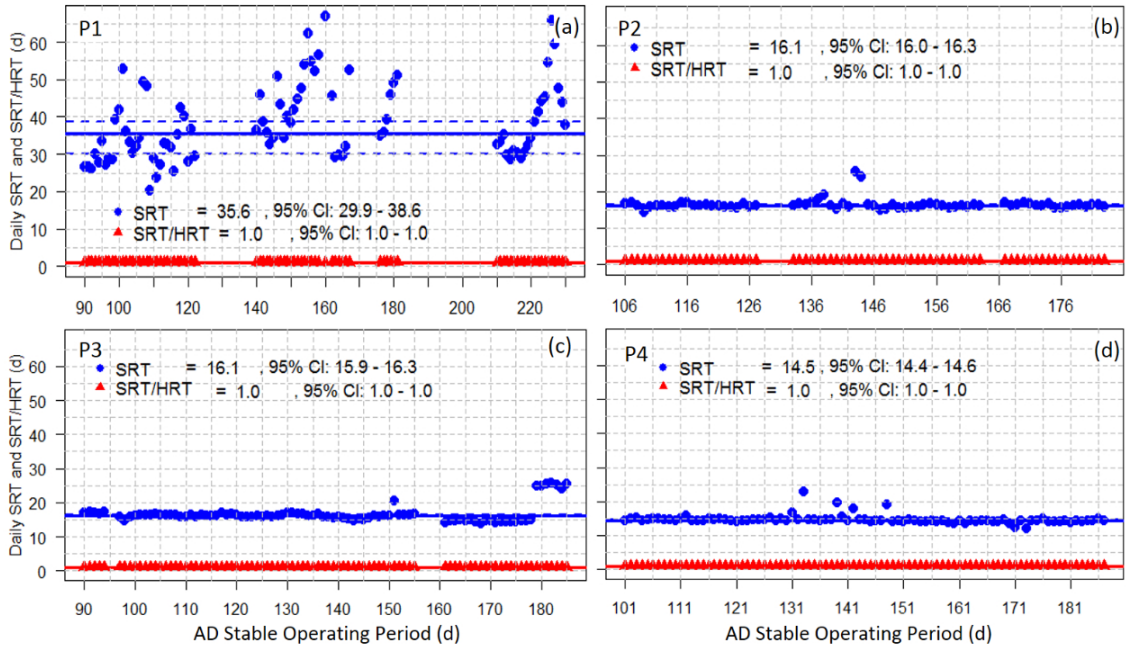

Figure A.4: The AD operation daily SRT and HRT with median and 95% confidence interval in Phase 1–4 in (a)–(d), respectively.

A.4 Chemistry

The analytical chemistry methods and method detection limits for the complete chemistry parameters (17) analyzed by the Environment Canada Wastewater Technology Centre Analytical Laboratory (EC WTC AL) are given in Table A.1.

Table A.1: Chemical parameters, reported MDLs and analytical methods from the Environment Canada Wastewater Technology Centre Analytical Laboratory (EC WTC AL)

Parameters		Units	MDL[a]	Method[b]
Acetic Acid	(HAc)	μg/mL	0.279	DM 5.17
Propionic Acid	(HPr)	μg/mL	0.6	DM 5.17
Isobutyric Acid	(HIBu)	μg/mL	0.6	DM 5.17
Butyric Acid	(HBu)	μg/mL	0.3	DM 5.17
Isovaleric Acid	(HIVa)	μg/mL	0.9	DM 5.17
Valeric Acid	(HVa)	μg/mL	1	DM 5.17
Total Alkalinity	(ALK)	mg/L $CaCO_3$	0.3	2320B
Phosphate as P by CFA	(PO4-P)	mg/L as P	0.02	Q-025-04
Total Phosphorus by CFA	(TP)	mg/L as P	0.06	Q-026-04
Ammonia as N by CFA	(TAN)	mg/L as N	0.02	Q-022-04
TKN by CFA	(TKN)	mg/L as N	0.04	Q-024-04
COD	(COD)	mg/L	5	5520D
Total Dissolved Solids	(TDS)	mg/L	16	2540C
Total Suspended Solids	(TSS)	mg/L	5	2540D
Total Solids	(TS)	mg/L	16	2540B
Volatile Suspended Solids	(VSS)	mg/L	6	2540E
Volatile Solids	(VS)	mg/L	9	2540E

[a] Reported method detection limits by the EC WTC Analytical Laboratory. [b] DM 5.17 refers to Dionex Method; Q-methods refer to QuAAtro Application Methods and others refer to Standard Methods 21st Edition [115].

The chemistry results and descriptive statistics including the mean, median, coefficient of variation (CV), lower (LCI) and upper (UCI) 95 %-ile confidence limits, normal p-value (nPV) along with the log-normal p-value (lnPV) are tabulated for P1 in Tables A.2–A.5. Time series sequence plots of selected conventional parameters are provided in Figure A.5–A.8 for all the streams combined on similar scales for visual comparison.

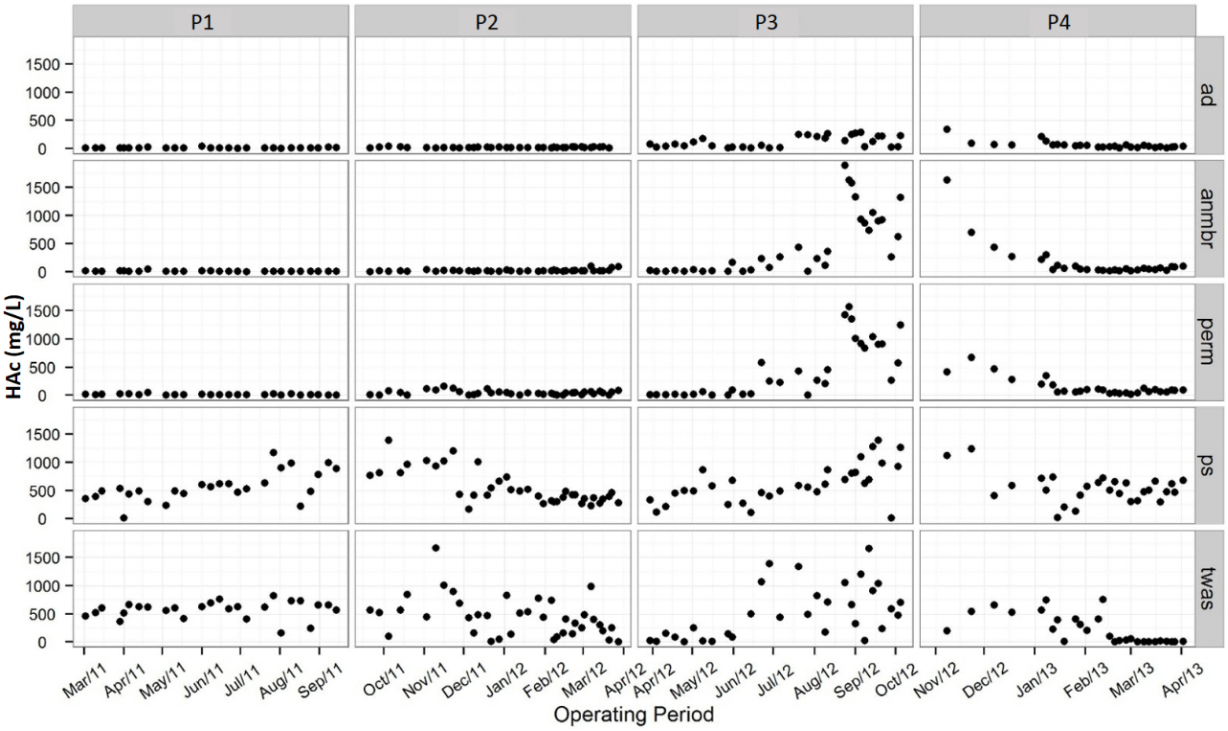

Figure A.5: The HAc for P1–P4 and five streams (AD, AnMBR, Permeate, PS and TWAS)

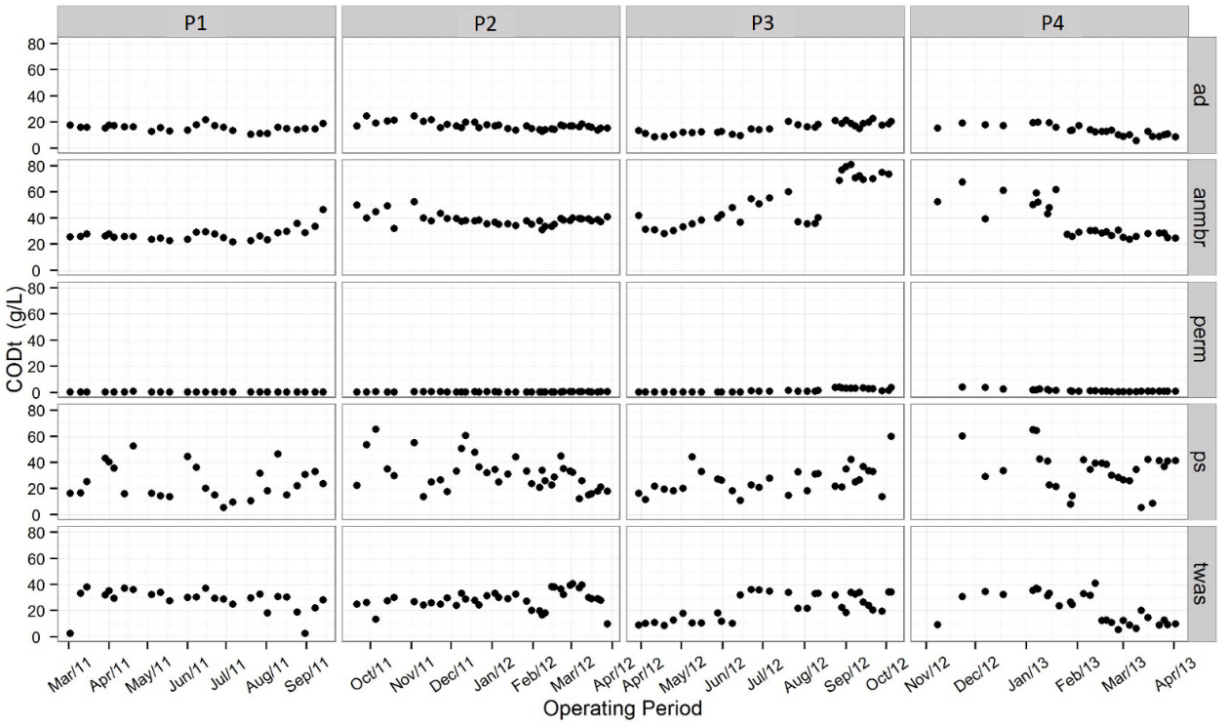

Figure A.6: The CODt for P1–P4 and five streams (AD, AnMBR, Permeate, PS and TWAS)

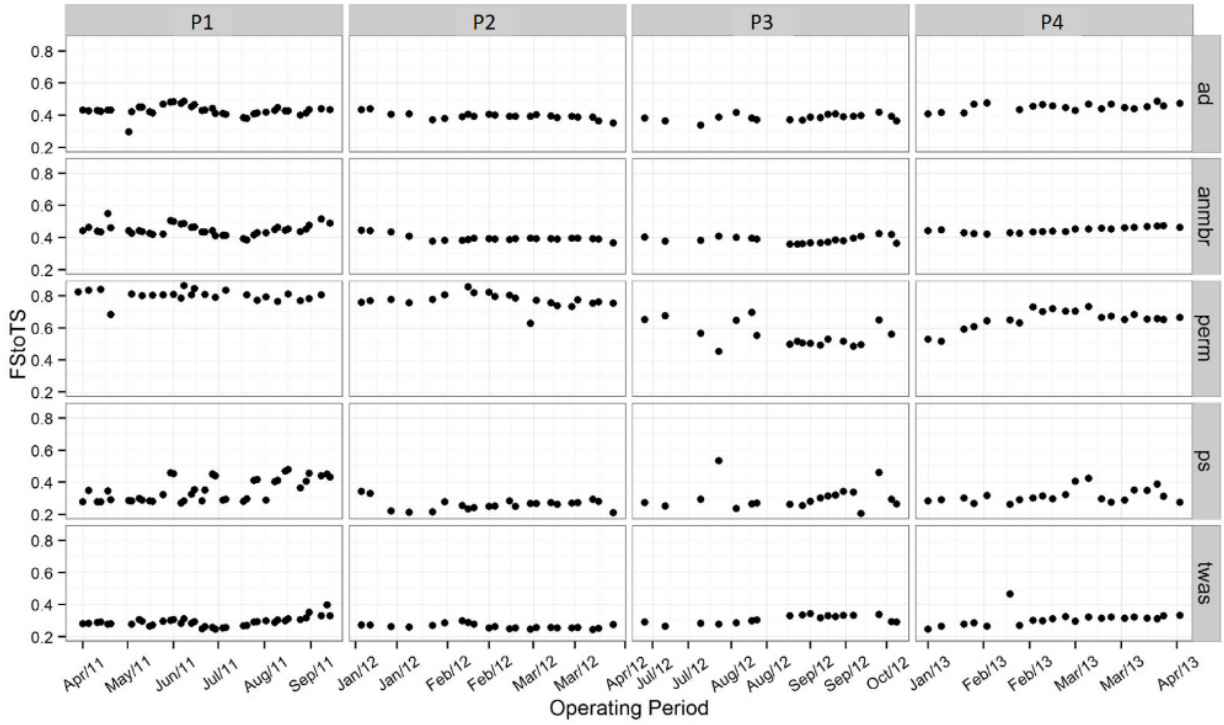

Figure A.7: The FS:TS for P1–P4 and five streams (AD, AnMBR, Permeate, PS and TWAS)

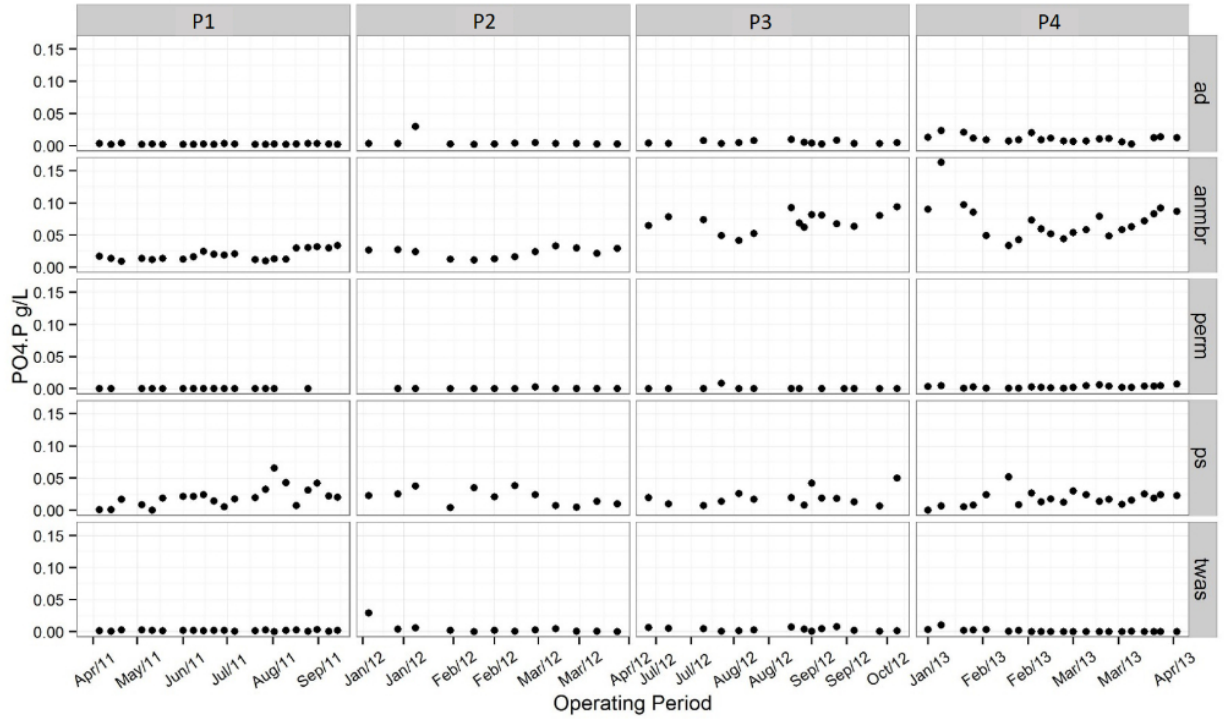

Figure A.8: The PO_4-P for P1–P4 and five streams (AD, AnMBR, Permeate, PS and TWAS)

Table A.2: Phase 1 PS, TWAS and Feed[a] solids concentrations (g/L) with descriptive statistics[b] during stable operating conditions

Day	PS (g/L)			TWAS (g/L)			Sludge Feed (g/L)		
	TS	TVS	TDS	TS	TVS	TDS	TS	TVS	TDS
90	48.9	26.7	3.0	30.4	21.1	3.4	39.6	23.9	3.2
95	28.1	20.5	2.4	38.5	27.6	3.3	33.3	24.1	2.8
97	26.5	19.0	2.7	31.1	21.4	4.2	28.8	20.2	3.4
102	17.8	12.0	2.1	43.3	31.1	4.0	30.5	21.6	3.1
104	17.0	11.0	2.3	34.4	24.3	4.1	25.7	17.6	3.2
109	13.7	9.8	2.0	28.8	21.6	2.5	21.2	15.7	2.2
111	13.9	9.0	2.1	28.9	21.3	3.3	21.4	15.2	2.7
116	5.1	2.8	1.8	32.5	24.1	3.1	18.8	13.4	2.4
118	5.5	3.1	1.7	28.8	21.7	3.2	17.1	12.4	2.4
123	8.1	5.8	1.8	21.3	15.9	2.2	14.7	10.8	2.0
125	7.9	5.6	1.8	22.6	16.8	2.4	15.3	11.2	2.1
137	8.9	6.4	1.7	28.7	21.0	2.6	18.8	13.7	2.1
139	8.3	5.8	2.0	28.3	20.7	3.4	18.3	13.3	2.7
144	33.0	19.4	3.6	31.7	22.5	2.8	32.4	20.9	3.2
146	31.9	18.6	3.4	31.0	21.9	2.8	31.4	20.2	3.1
152	15.0	10.7	2.5	17.1	12.0	1.2	16.1	11.3	1.8
158	50.8	30.3	3.3	30.5	21.7	2.3	40.6	26.0	2.8
160	50.5	29.8	3.6	29.4	20.5	3.5	40.0	25.1	3.6
165	18.0	9.6	1.9	30.9	21.7	2.9	24.4	15.6	2.4
167	17.6	9.2	2.0	29.5	20.3	3.2	23.6	14.7	2.6
175	22.0	14.0	1.8	18.2	12.6	1.6	20.1	13.3	1.7
179	22.6	13.4	2.2	24.5	16.7	2.0	23.6	15.1	2.1
181	25.3	13.8	2.4	22.3	14.5	2.7	23.8	14.2	2.6
189	33.2	18.6	2.9	21.3	14.3	2.1	27.2	16.5	2.5
193	18.9	10.4	1.5	21.9	13.2	2.4	20.4	11.8	1.9
195	22.7	12.9	2.6	27.8	18.6	2.9	25.2	15.8	2.8
n	26	26	26	26	26	26	26	26	26
Median	18.4	11.5	2.1	28.9	21.1	2.8	23.7	15.4	2.6
LCI	13.8	9.1	1.9	27.8	18.6	2.5	19.5	13.4	2.4
UCI	25.3	14.0	2.5	30.9	21.7	3.3	27.2	17.6	2.9
Mean	22.0	13.4	2.3	28.2	20.0	2.8	25.1	16.7	2.6
LCI	16.6	10.3	2.1	25.8	18.1	2.6	22.0	14.8	2.4
UCI	27.3	16.5	2.6	30.6	21.8	3.1	28.2	18.5	2.8
CV	1.7	1.8	3.8	4.8	4.4	3.9	3.3	3.6	5.1
nPV	0.71	0.52	0.61	0.49	0.35	0.99	0.83	0.24	0.98
lnPV	0.00	0.00	0.00	0.00	0.00	0.00	0.00	0.00	0.00

[a] Sludge feed characteristics were based on equal contribution of PS and TWAS by weight.
[b] n, is the number of samples; LCI and UCI, 95% lower and upper confidence intervals are based on nonparametric ordered statistics [172] for the median and Student's t-distribution for the mean; CV, coefficient of variation; nPV and lnPV, Normal and Log Normal p-value for the two-sided 1-sample Kolmogorov-Smirnov test.

Table A.3: Phase 1 PS, TWAS and Feed[a] CODt, CODf and TKN concentrations with descriptive statistics[b] during stable operating conditions

Day	PS (g/L)			TWAS (g/L)			Sludge Feed (g/L)		
	CODt	CODf	TKN	CODt	CODf	TKN	CODt	CODf	TKN
90	44.4	2.5	1.4	30.2	2.6	2.0	37.3	2.6	1.7
97	36.0	2.3	1.0	30.4	0.9	2.1	33.2	1.6	1.6
104	20.1	2.4	0.7	37.0	3.3	2.3	28.6	2.9	1.5
111	14.9	2.1	0.5	29.4	2.4	1.9	22.1	2.2	1.2
118	15.2	1.6	0.2	28.8	2.7	2.0	22.0	2.1	1.1
125	19.6	1.8	0.4	24.8	1.4	1.6	22.2	1.6	1.0
139	10.5	1.8	0.4	29.7	2.3	1.8	20.1	2.1	1.1
146	31.7	3.8	1.0	32.6	3.0	1.8	32.1	3.4	1.4
152	18.2	3.0	0.6	18.3	0.5	1.0	18.2	1.7	0.8
160	46.5	4.1	1.3	30.8	2.8	1.9	38.6	3.4	1.6
167	15.0	1.5	1.0	30.4	2.7	2.0	22.7	2.1	1.5
175	22.1	1.6	0.9	18.8	0.9	1.1	20.5	1.3	1.0
181	30.8	2.5	0.9	25.2	2.3	1.8	28.0	2.4	1.3
189	32.9	3.8	1.0	22.2	2.2	1.4	27.5	3.0	1.2
195	23.6	3.2	0.9	28.2	2.1	1.8	25.9	2.7	1.3
n	15	15	15	15	15	15	15	15	15
Median	22.1	2.4	0.9	29.4	2.3	1.8	25.9	2.2	1.3
LCI	12.9	1.6	0.6	25.0	1.8	1.7	20.1	1.9	1.1
UCI	32.3	3.1	1.2	33.7	3.0	2.2	30.4	3.1	1.6
Mean	25.4	2.5	0.8	27.8	2.1	1.8	26.6	2.3	1.3
LCI	19.3	2.1	0.6	25.0	1.7	1.6	23.1	2.0	1.1
UCI	31.6	3.0	1.0	30.6	2.6	2.0	30.1	2.7	1.4
CV	2.3	3.0	2.4	5.5	2.6	4.9	4.2	3.6	5.0
nPV	0.74	0.78	0.82	0.59	0.40	0.52	0.54	1.00	0.99
lnPV	0.00	0.00	0.00	0.00	0.00	0.00	0.00	0.00	0.00

[a] Sludge total COD (CODt), filtered COD (CODf) and total kjeldahl nitrogen (TKN) feed characteristics based an equal contribution of the PS and TWAS by weight.

[b] n, is the number of samples; LCI and UCI, 95% lower and upper confidence intervals are based on nonparametric ordered statistics [172] for the median and Student's t-distribution for the mean; CV, coefficient of variation; nPV and lnPV, Normal and Log Normal p-value for the two-sided 1-sample Kolmogorov-Smirnov test.

Table A.4: Phase 1 PS, TWAS and Feed[a] TAN, ALK and HAc concentrations with descriptive statistics[b] during stable operating conditions

Day	PS (mg/L)			TWAS (mg/L)			Sludge Feed (mg/L)		
	TAN	ALK	HAc	TAN	ALK	HAc	TAN	ALK	HAc
90	97	2730	601	258	2890	628	178	2810	614
95		1590			3160			2375	
97	91	1650	564	291	2940	691	191	2295	628
102		4470			3810			4140	
104	136	1670	614	302	4820	757	219	3245	686
109		1300			1660			1480	
111	96	1240	621	217	1970	587	157	1605	604
116		940			2880			1910	
118	87	930	471	252	2920	625	170	1925	548
123		930			1280			1105	
125	94	1040	528	159	1650	407	126	1345	468
137		960			2320			1640	
139	80	980	635	217	3070	615	149	2025	625
144		1680			2780			2230	
146	71	2020	1170	286	2680	817	179	2350	994
152	104	1340	904	86	1000	159	95	1170	532
158		2610			1780			2195	
160	139	2770	988	245	2270	733	192	2520	860
165		2790			2980			2885	
167	440	3010	221	252	3620	731	346	3315	476
175	71	1160	484	91	1580	245	81	1370	364
179		1420			2520			1970	
181	92	1390	785	228	2220	655	160	1805	720
189	98	1620	994	232	1930	654	165	1775	824
193		1500			2030			1765	
195	89	1530	884	210	3230	566	150	2380	725
n	15	26	15	15	26	15	15	26	15
Median	94	1515	621	232	2600	628	165	1998	625
LCI	79	1230	546	214	2030	576	115	1770	448
UCI	101	1675	1037	280	2960	774	185	2365	722
Mean	119	1741	698	222	2538	591	170	2140	644
LCI	69	1398	559	186	2194	489	137	1852	553
UCI	169	2084	836	258	2882	694	204	2427	735
CV	1.3	2.1	2.8	3.4	3.0	3.2	2.8	3.0	3.9
nPV	0.03	0.06	0.53	0.41	0.96	0.28	0.37	0.66	0.89
lnPV	0.00	0.00	0.00	0.00	0.00	0.00	0.00	0.00	0.00

[a] Sludge total ammonia nitrogen (TAN), total alkalinity as $CaCO_3$ and acetic acid (HAc) concentration levels based an equal contribution of the PS and TWAS by weight; the filtered COD (CODf) samples for Phase 4 were corrupted. [b] n, is the number of samples; LCI and UCI, 95% lower and upper confidence intervals are based on nonparametric ordered statistics [172] for the median and Student's t-distribution for the mean; CV, coefficient of variation; nPV and lnPV, Normal and Log Normal p-value for the two-sided 1-sample Kolmogorov-Smirnov test.

Table A.5: Phase 1 AnMBR treated sludge COD (g/L) fractions during stable operating conditions

Day	tCOD	fCOD	sCOD	cCOD	pCOD
90	23.6	1.56	0.24	1.3	22.0
97	29.0	2.18	0.24	1.9	26.8
104	29.2	2.77	0.25	2.5	26.4
111	27.6	2.25	0.25	2.0	25.4
118	24.8	2.30	0.22	2.1	22.5
125	21.8	1.81	0.19	1.6	20.0
139	22.6	1.54	0.21	1.3	21.1
146	26.0	1.45	0.26	1.2	24.6
152	23.3	1.31	0.19	1.1	22.0
160	28.6	1.51	0.24	1.3	27.1
167	29.8	2.60	0.22	2.4	27.2
175	35.8	2.66	0.21	2.5	33.1
181	28.8	2.76	0.20	2.6	26.0
189	33.6	3.07	0.22	2.9	30.5
195	46.3	3.90	0.24	3.7	42.4
n	15	15	15	15	15
Median	28.6	2.2	0.24	2.0	26.0
M.LCI	22.7	1.4	0.21	1.2	21.0
M.UCI	29.5	2.7	0.25	2.5	27.1
Mean	28.7	2.2	0.23	2.0	26.5
LCI	25.3	1.8	0.22	1.6	23.3
UCI	32.2	2.6	0.24	2.4	29.6
CV	4.6	3.1	10.0	2.8	4.7
nPV	0.34	0.79	0.47	0.78	0.26
lnPV	0.00	0.00	0.00	0.00	0.00

[a] tCOD, total COD; filtered COD (1.2 μm filter paper); sCOD, soluble COD equivalent to the cCOD of the permeate stream; cCOD, colloidal COD calculated as the difference between the fCOD and sCOD; pCOD, particulate COD calculated as the difference between the tCOD and fCOD. [b] n, is the number of samples; LCI and UCI, 95% lower and upper confidence intervals are based on nonparametric ordered statistics [172] for the median and Student's t-distribution for the mean; CV, coefficient of variation; nPV and lnPV, Normal and Log Normal p-value for the two-sided 1-sample Kolmogorov-Smirnov test.

Appendix B

Membrane Performance

This appendix provides further details of the membrane operating parameters.

B.1 Operating Conditions

A comparison of the membrane operating J, ΔP, K and V_x during a stable operating period in P1–P4 is given in Figure B.1.

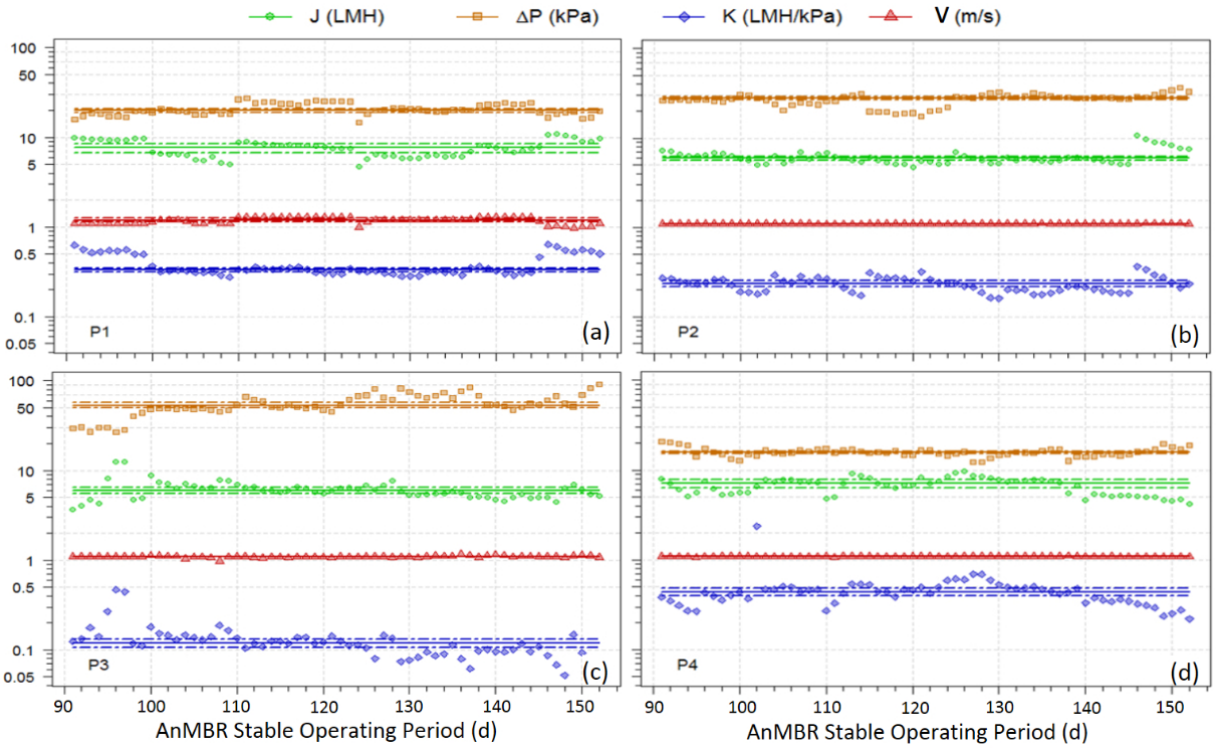

Figure B.1: Comparison of the membrane operating J, ΔP, K and V_x during a stable operating period in P1–P4.

summary statistics provided in Table B.1 including solids and COD fractions of the permeate and AnMBR digested sludge, along with calculated rheological parameters γ, η and τ.

Table B.1: The transmembrane pressure, flux and permeability in P1 - P4 corresponding to the permeate (p-) and AnMBR (m-) digested sludge COD and solids fractions[a]

Parameter	P1 Median (CI) n	P2 Median (CI) n	P3 Median (CI) n	P4 Median (CI) n
T (°C)	35.1 (0.0) 62	35.1 (0.1) 62	25.7 (0.8) 62	54.5 (0.6) 62
HRT (d)	14.5 (0.1) 62	7.3 (0.1) 62	7.7 (0.1) 62	6.9 (0.2) 62
SRT (d)	34.7 (0.5) 62	24.6 (0.3) 62	39.4 (0.8) 62	22 (1) 62
v (m/s)	1.20 (0.03) 62	1.10 (0.00) 62	1.10 (0.01) 62	1.10 (0.01) 62
ρ_s (kg/m^3)	1011 (3) 20	1020 (1) 23	1039 (5) 19	1005 (1) 24
Re	3300 (900) 20	4200 (400) 23	1650 (500) 19	2200 (300) 24
γ (s−1)	384 (10) 62	352 (1) 62	352 (1) 62	349 (16) 62
η (cP)	36 (8) 20	73 (6) 23	220 (60) 19	32 (2) 24
τ (Pa)	13 (3) 20	26 (2) 23	80 (20) 19	11 (1) 24
ΔP (kPa)	20 (1) 62	28 (1) 62	51 (1) 62	16 (1) 62
J_{20} (LMH)	7.1 (0.8) 62	6.1 (0.2) 62	6.0 (0.3) 62	6.7 (0.5) 62
K (LMH/kPa)	0.32 (0.01) 62	0.22 (0.02) 62	0.12 (0.01) 62	0.40 (0.02) 62
K_{20} (LMH/kPa)	0.23 (0.01) 62	0.16 (0.01) 62	0.10 (0.01) 62	0.20 (0.2) 62
p-COD_t (g/L)	0.25 (0.02) 11	0.35 (0.04) 22	3.0 (1.0) 19	0.85 (0.11) 22
p-TS (g/L)	1.6 (0.2) 10	1.5 (0.1) 21	2.4 (0.4) 22	1.6 (0.1) 18
m-COD_t (g/L)	26 (1) 11	38 (2) 22	71 (9) 19	28 (2) 22
m-COD_p (g/L)	23 (1) 11	35 (1) 22	57 (8) 19	26 (2) 22
m-COD_f (g/L)	2.1 (0.1) 11	2.7 (0.6) 22	14 (2) 19	1.7 (0.2) 22
m-COD_c (g/L)	1.8 (0.1) 11	2.4 (0.5) 22	10 (1) 19	0.8 (0.2) 22
m-TS (g/L)	29 (5) 20	43 (2) 23	66 (8) 19	32 (1) 24
m-TVS (g/L)	17 (2) 20	26 (1) 23	42 (3) 19	18 (1) 24
m-TFS (g/L)	12 (2) 20	17 (1) 23	24 (4) 19	14 (1) 24
m-TDS (g/L)	3.5 (0.4) 20	3.5 (0.4) 23	7 (3) 12	5 (1) 9
m-TSS (g/L)	25 (4) 20	39 (2) 23	52 (10) 12	25 (2) 9

[a] $m-COD_c$, AnMBR sludge colloidal COD was calculated as the difference of the filtered COD ($m-COD_f$) and soluble COD taken as the permeate total COD ($p-COD_t$); $m-TSS$, AnMBR sludge total suspended solids calculated as the difference of the total solids ($m-TS$) and ($m-TDS$).

B.2 Regression Example Results

Table B.2: Summary linear model of K_{20} versus TS and τ analysis results

Call: lm(formula = $K_{20} \sim$ TS + τ + $\tau\cdot$ TS)				
Residuals:				
Min	1Q	Median	3Q	Max
-0.11137	-0.02769	-0.00925	0.02073	0.19901
Coefficients	Estimate	Std. Error	t value	Pr(> $\|t\|$)
Intercept	0.4944	0.0417	11.85	$< 2 \cdot 10^{-16***}$
TS	-0.0066	0.0008	-8.10	$< 4.7 \cdot 10^{-12***}$
τ	-0.0306	0.0088	-3.48	0.00082^{***}
TS:τ	0.0005	0.0001	4.02	0.00013^{***}
Signif. codes: < 0.001 '***', 0.001 '**', 0.01 '*', 0.05 '.', 0.1, ' ' 0.1–1				
Residual standard error (RSE): 0.054 on 81 degrees of freedom Multiple R^2: 0.6, Adjusted R^2: 0.586 F-statistic: 40.6 on 3 and 81 DF, p-value: $4.14{\cdot}10^{-16}$				

K_{20} Versus eEPS Model

Figure B.2 provides a sample model analysis output from the *earth*-R package [10] which identifies the best fit model and priority parameters.

Table B.3: Summary linear model of K_{20} versus eEPS analysis results

Call: lm(formula = $K_{20} \sim$ $C_{b,pr} + C_{f,pr} + C_{b,pr}/C_{b,ch}$)				
Residuals:				
Min	1Q	Median	3Q	Max
-0.11953	-0.03421	-0.01373	0.00613	0.15490
Coefficients	Estimate	Std. Error	t value	Pr(> $\|t\|$)
Intercept	0.2416	0.0355	6.81	$< 9.1 \cdot 10^{-8***}$
$C_{b,pr}$	-4.76e-5	0.0000	-2.40	0.0220^{***}
$C_{f,pr}$	-1.56e-5	0.0000	-1.73	$0.0937^{\cdot}$
$C_{b,pr}/C_{b,ch}$	0.0105	0.0127	0.83	0.4118
Signif. codes: < 0.001 '***', 0.001 '**', 0.01 '*', 0.05 '.', 0.1, ' ' 0.1–1				
Residual standard error (RSE): 0.059 on 33 degrees of freedom Multiple R^2: 0.398, Adjusted R^2: 0.344 F-statistic: 7.28 on 3 and 33 DF, p-value: 0.000704				

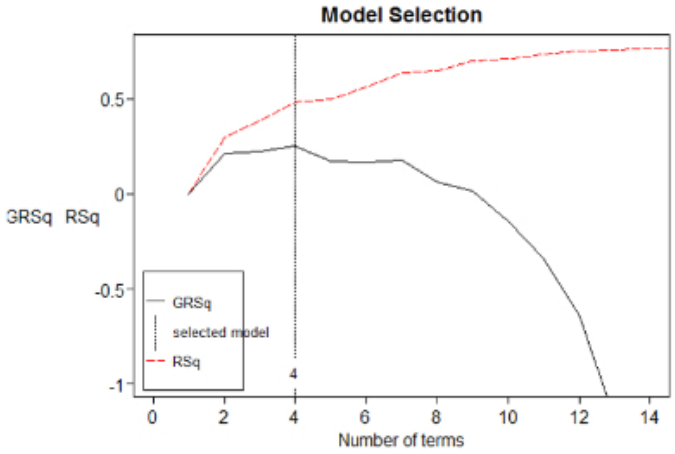


```
Call: earth(formula=K20~., data=k1, trace=4)

x[37,6]:                                                  y[37,1]:
    chEPSfp chEPSbp prEPSfp prEPSbp pcEPSfp pcEPSbp          K20
1       129     150     235     483     1.8     3.2   1    0.39
2       314     112    1469     342     4.7     3.1   2    0.39
28      166     131     455     263     2.7     2.0   3    0.20
...      84     184     322     381     3.8     2.1   ...  0.24
317     438     364    2004    1098     4.6     3.0   37   0.17

Forward pass: minspan 4 endspan 9    x[37,6] 1.73 kB    bx[37,21] 6.07 kB

         GRSq    RSq     DeltaRSq Pred     PredName         Cut  Terms   Par Deg
1      0.0000 0.0000                      (Intercept)
2      0.1615 0.3374       0.3374    4       prEPSbp         786  2   3         1
4      0.1660 0.4208      0.08336    4       prEPSbp        1032  4             1
6     -0.0092 0.4736      0.05278    5       pcEPSfp         3.3  5   6         1
8     -0.1194 0.5820       0.1084    1       chEPSfp         326  7   8         1
10    -0.5729 0.6068      0.02482    3       prEPSfp        1608  9   10        1
12    -0.8824 0.6282      0.02138    1       chEPSfp         457  11            1
14    -2.2211 0.6421      0.01393    2       chEPSbp         359  12  13        1
16    -2.6302 0.7199       0.0778    1       chEPSfp         310  14            1
18    -7.3007 0.7694      0.04953    6       pcEPSbp           3  15  16        1
20   -15.0276 0.8021       0.0327    5       pcEPSfp         2.7  17            1

Reached minimum GRSq -10 at 19 terms, 16 terms used (GRSq -15)
After forward pass GRSq -15.028 RSq 0.802
Forward pass complete: 19 terms, 16 terms used

Subset size        GRSq     RSq  DeltaGRSq nPreds  Terms (col nbr in bx)
          1      0.0000  0.0000     0.0000      0  1
          2      0.2117  0.2968     0.2117      1  1 2
          3      0.2223  0.3855     0.0106      2  1 6 7
chosen    4      0.2536  0.4817     0.0314      3  1 3 6 7
          5      0.1717  0.4989    -0.0819      3  1 3 6 7 11
          6      0.1650  0.5645    -0.0067      3  1 3 6 7 11 14
          7      0.1799  0.6355     0.0149      4  1 3 6 7 11 14 16
          8      0.0598  0.6489    -0.1201      5  1 3 6 7 10 11 14 16
          9      0.0181  0.6970    -0.0417      5  1 3 6 7 8 10 11 14 16
         10     -0.1455  0.7136    -0.1636      5  1 3 6 7 8 9 10 11 14 16
         11     -0.3397  0.7354    -0.1942      5  1 2 3 6 7 8 9 10 11 14 16
         12     -0.6442  0.7513    -0.3045      5  1 2 3 6 7 8 9 10 11 14 15 16
         13     -1.1881  0.7569    -0.5439      6  1 2 3 6 7 8 9 10 11 13 14 15 16
         14     -1.9996  0.7686    -0.8115      6  1 2 3 6 7 8 9 10 11 12 13 14 15 16
         15     -3.6756  0.7691    -1.6760      6  1 2 3 4 6 7 8 9 10 11 12 13 14 15 16
         16     -7.3007  0.7694    -3.6251      6  1 2 3 4 5 6 7 8 9 10 11 12 13 14 15 16

Prune method "backward" penalty 2 nprune null: selected 4 of 16 terms, and 3 of 6 preds
After pruning pass GRSq 0.254 RSq 0.482
```

Figure B.2: Sample model analysis output from the *earth*-R package [10] during the analysis of the assessment of the K_{20} dependency on eEPS fractions.

B.3 Membrane Resistance

A clean water flux test was conducted on a virgin membrane to determine the membrane intrinsic resistance (R_m). A best fit curve of R_m versus the filtered water volume (V, L) is shown in Figure B.3. Extrapolating the exponential curve fit to $V = 0$ gives the R_m value of $3.6 \cdot 10^{11}$ (m^{-1}). This value is consistent with the reported R_m value of the PVDF membrane of $1.0 \cdot 10^{11}$ (m^{-1}) measured in a membrane type comparative study by Fang et al (2005) [142] and our Rm value was used for subsequent calculations.

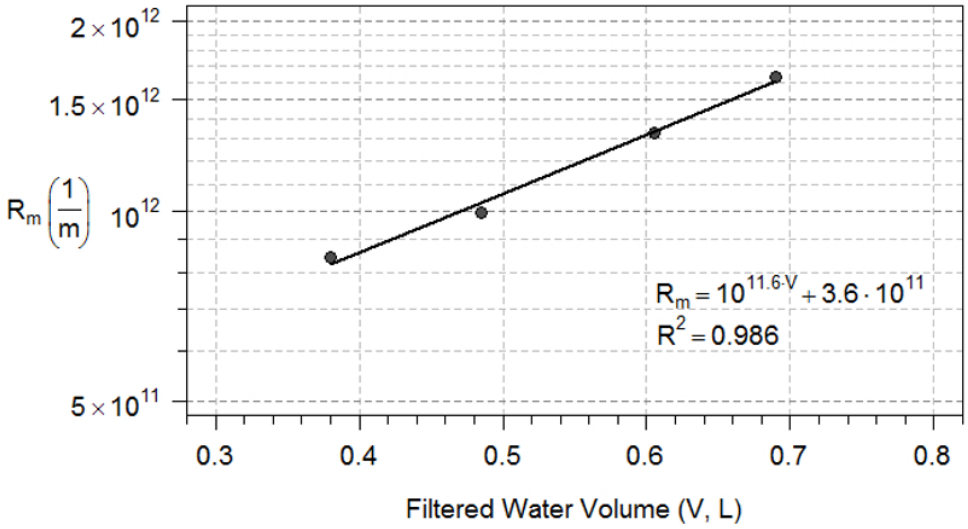

Figure B.3: Water flux test results on a clean membrane to determine the virgin membrane resistance (R_m, m^{-1}).

B.4 Flux Modeling

To determine the best fit blocking model the RSE values resulting from the flux model analysis, shown in Table B.4, were compared and the results shown in Figure B.4. Representative model fit curves for P1–P4 are provided in Figures B.5 to B.8.

Table B.4: Residual standard errors (RSE) comparison for best model fit determination[a]

Parameter	Cake Filtration (m=0) Median (CI) n	Intermediate Blocking (m=1) Median (CI) n	Standard Blocking (m=$\frac{3}{2}$) Median (CI) n	Complete Blocking (m = 2) Median (CI) n
RSE_1	0.26 (0.02) 114	0.31 (0.003) 114	1.2 (0.1) 114	0.38 (0.04) 114
RSE_2	1.17 (0.08) 224	1.19 (0.07) 224	1.56 (0.07) 224	1.20 (0.07) 224
RSE_3	1.50 (0.05) 131	1.55 (0.06) 131	1.89 (0.07) 131	1.54 (0.06) 131
RSE_4	1.56 (0.06) 193	1.59 (0.06) 193	2.25 (0.09) 193	1.61 (0.06) 193

[a] RSE_{1-4}, sum residual standard error for P1–P4.

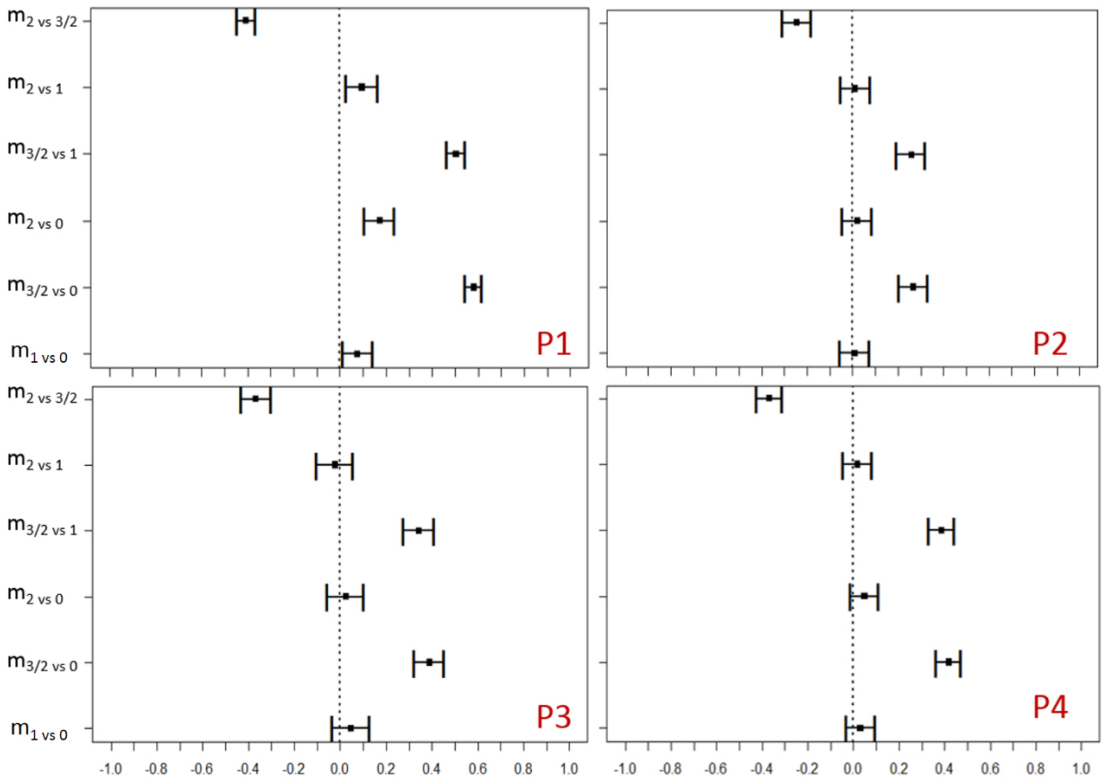

Figure B.4: Best fit model RSE comparisons of values in Table B.4 based on the 95% simultaneous confidence interval, Tukey contrast and Fisher method [11]

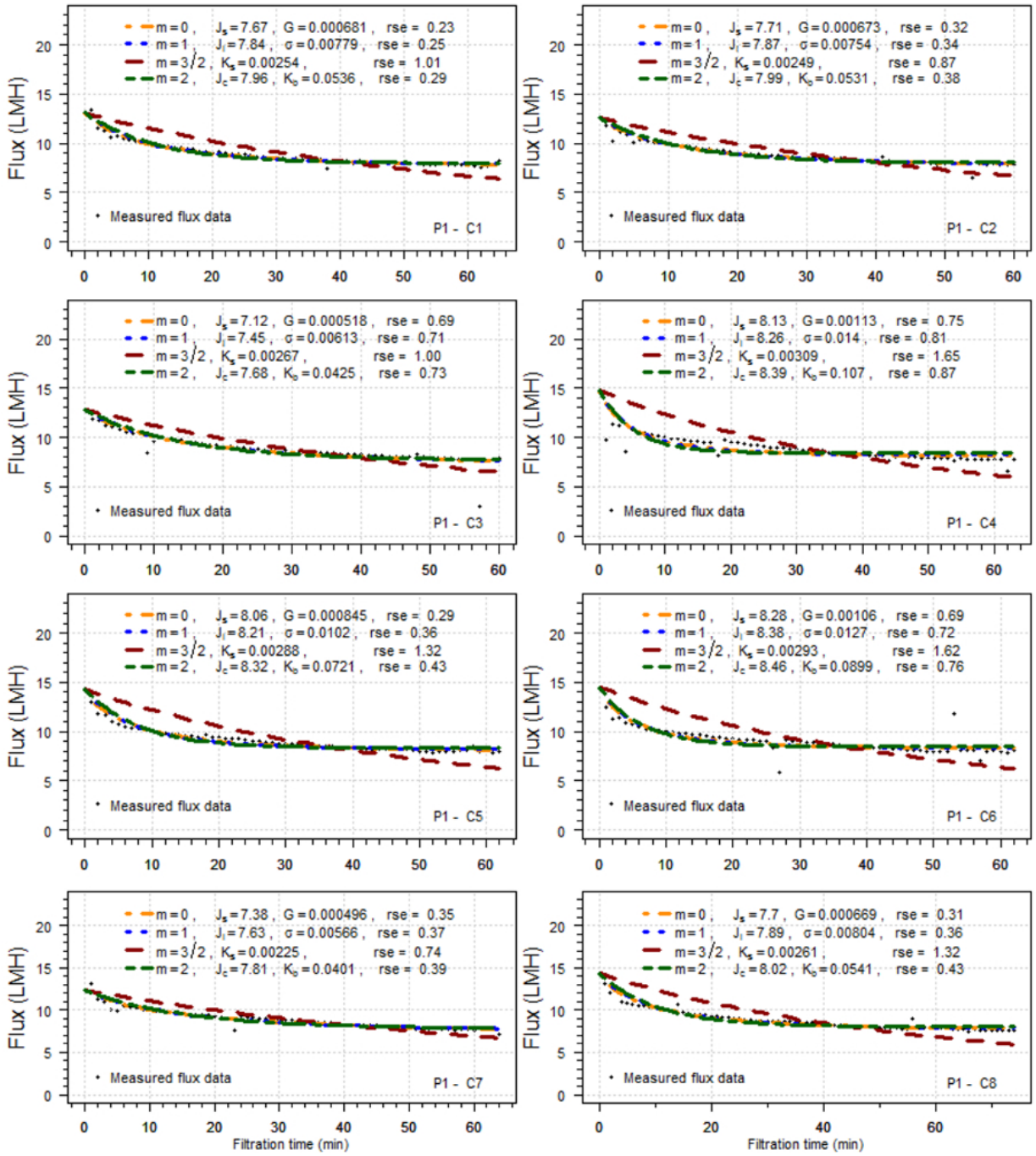

Figure B.5: Example P1 best model fit analysis curves.

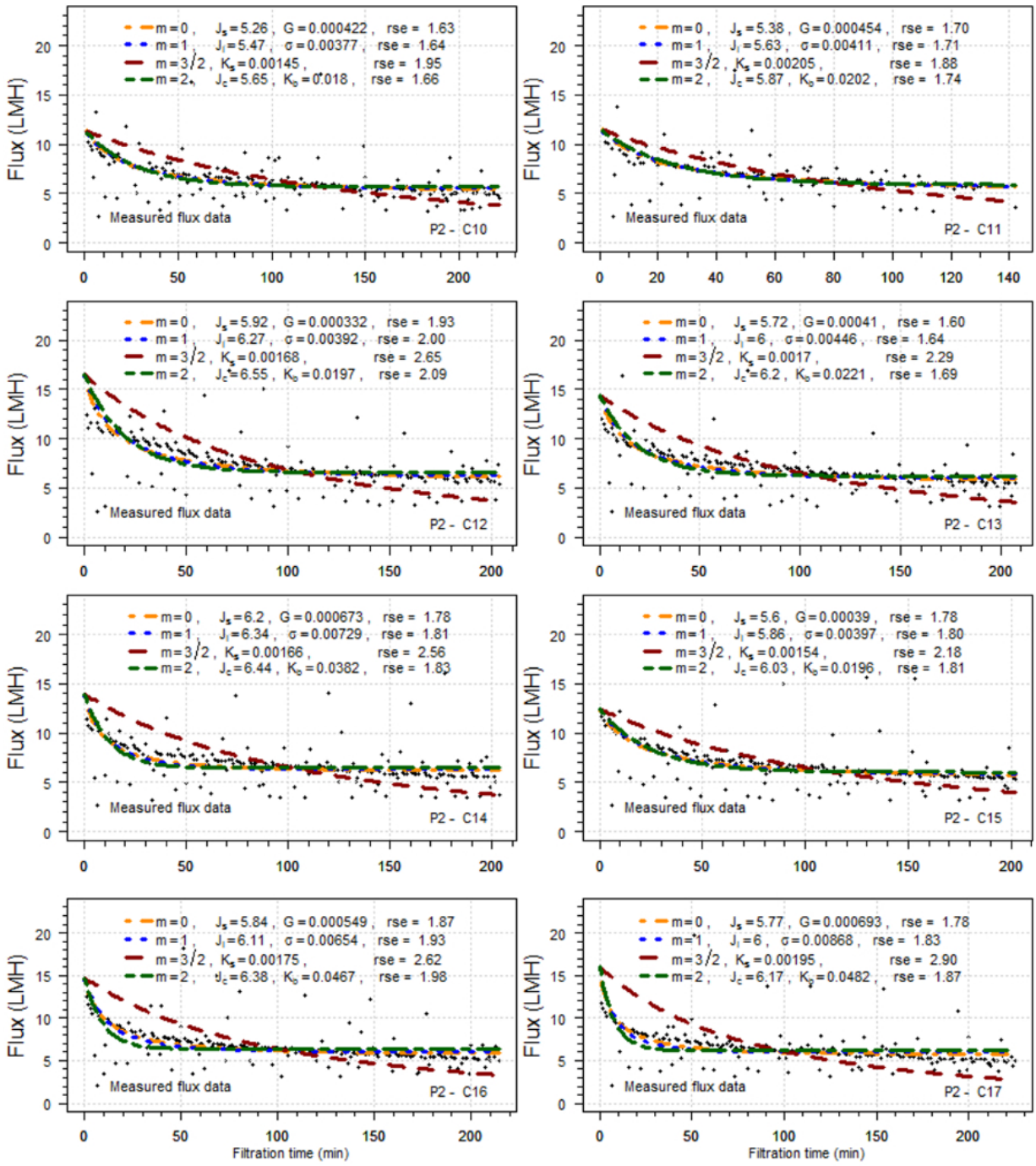

Figure B.6: Example P2 best model fit analysis curves.

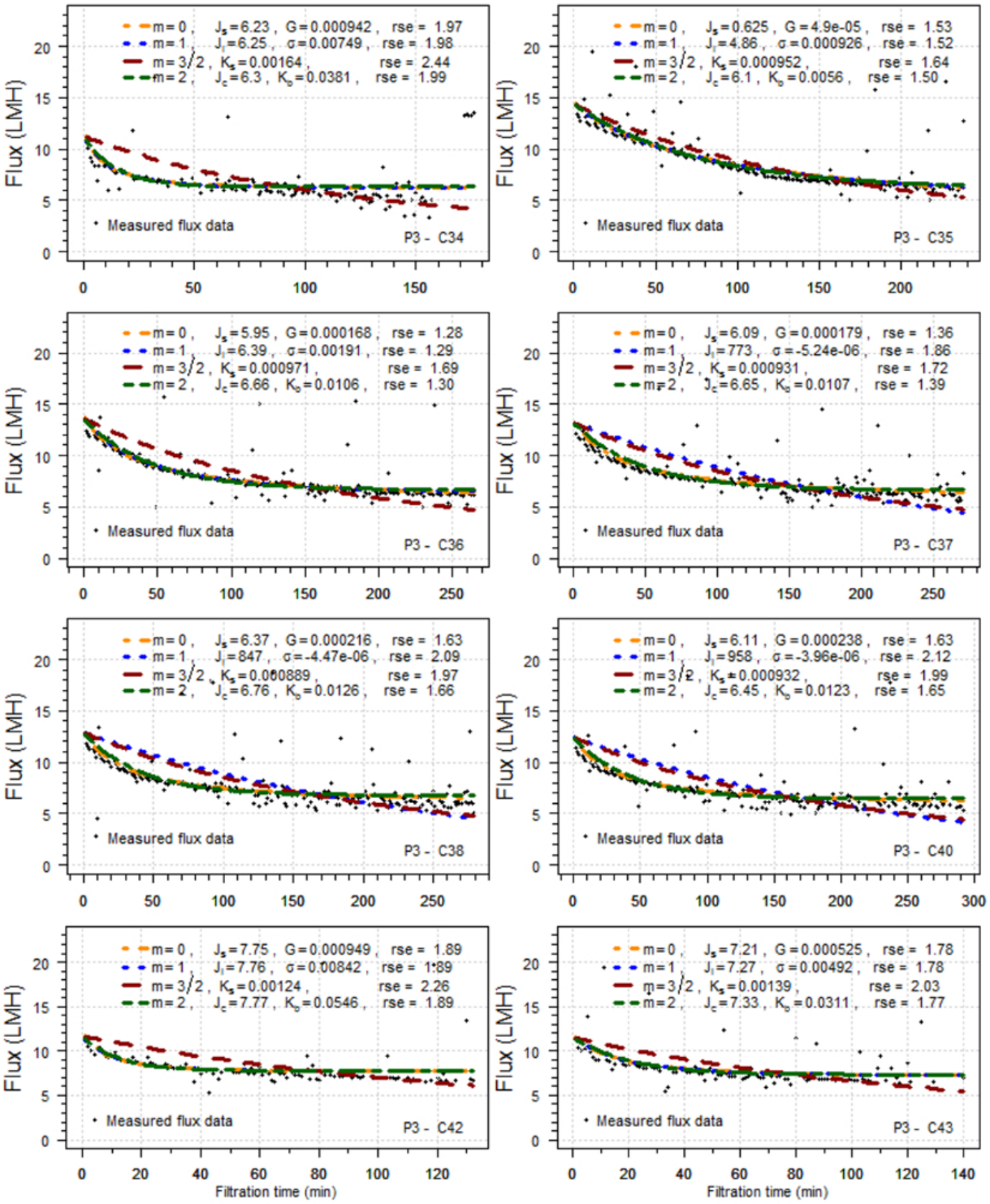

Figure B.7: Example P3 best model fit analysis curves.

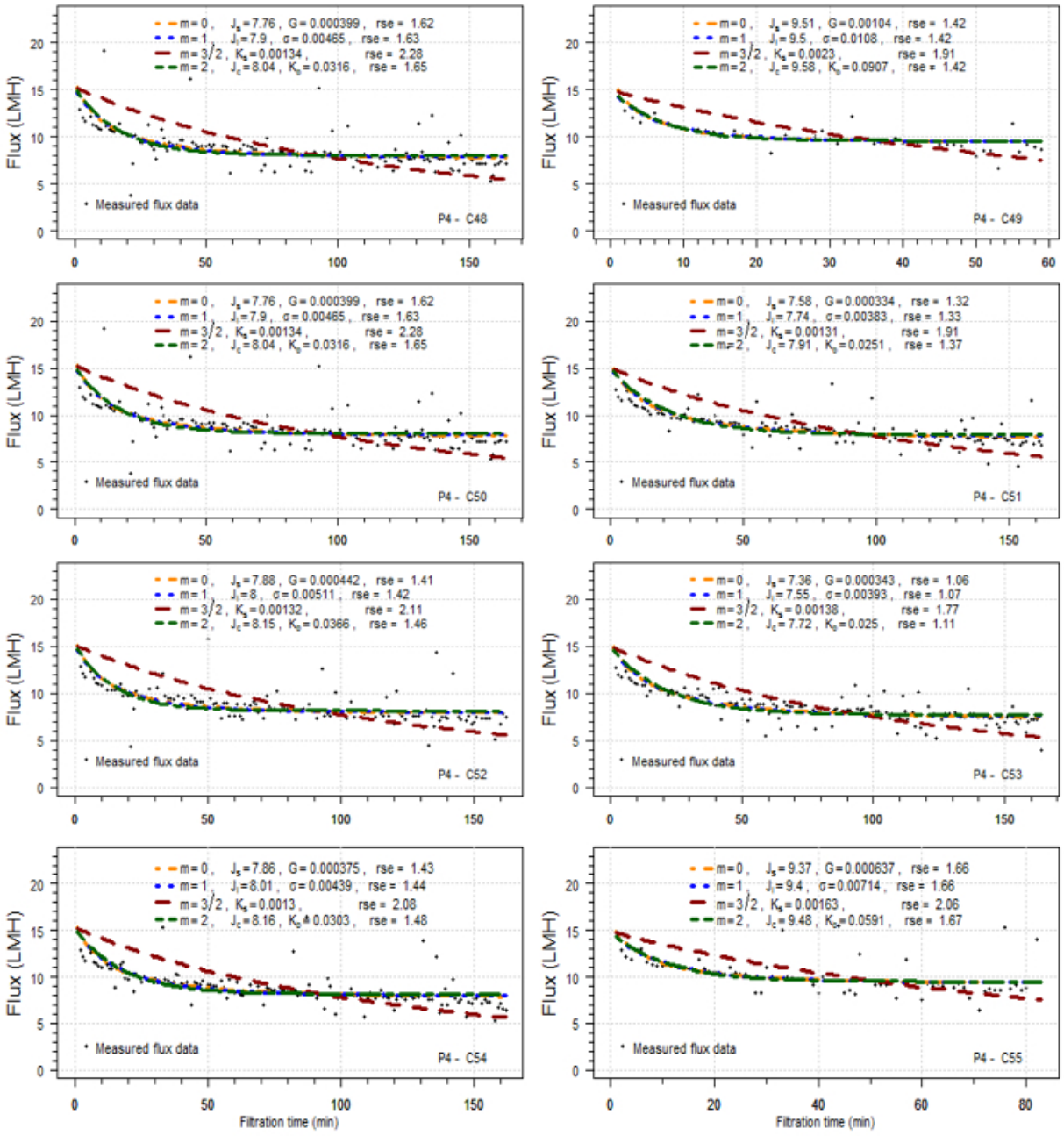

Figure B.8: Example P4 best model fit analysis curves.

B.5 Fouling Propensity Curves for Phase P1–P4

This section shows the complete individual fouling propensity figures as measured by the VFM curves representative of phase P1–P4 with each point on the curve representing a permeation cycle in a continuous sequence. Figure B.9, shows an example permeability sequence used to derive the first sequence P1 VFM curves shown in Figure B.10 P1–S1. Similar permeation sequences (not shown) were used to derive the VFM diagrams P1–S2 to P1–S4 for P1 and other VFM curves for P2–P4 shown in Figures B.11–B.13. These individual VFM curves within each phase were averaged to compute the median curves for each phase shown in Figure 4.3 for irreversible and reversible fouling.

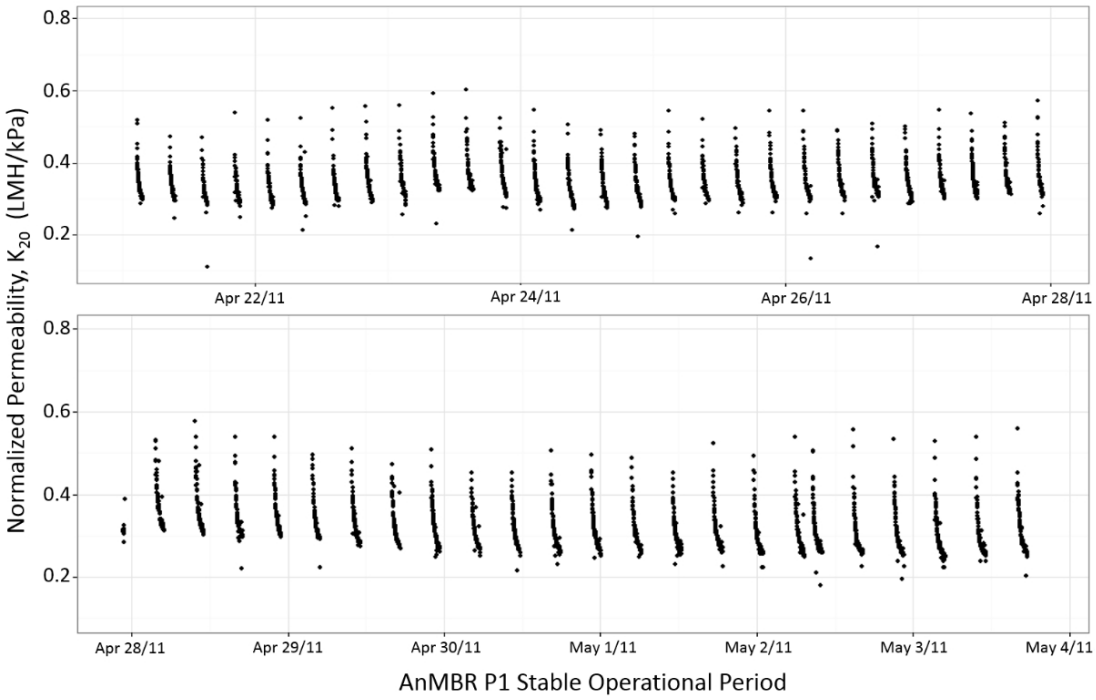

Figure B.9: Example normalized permeability sequence in P1 used to derive the VFM curve P1–S1 shown in Figure B.10

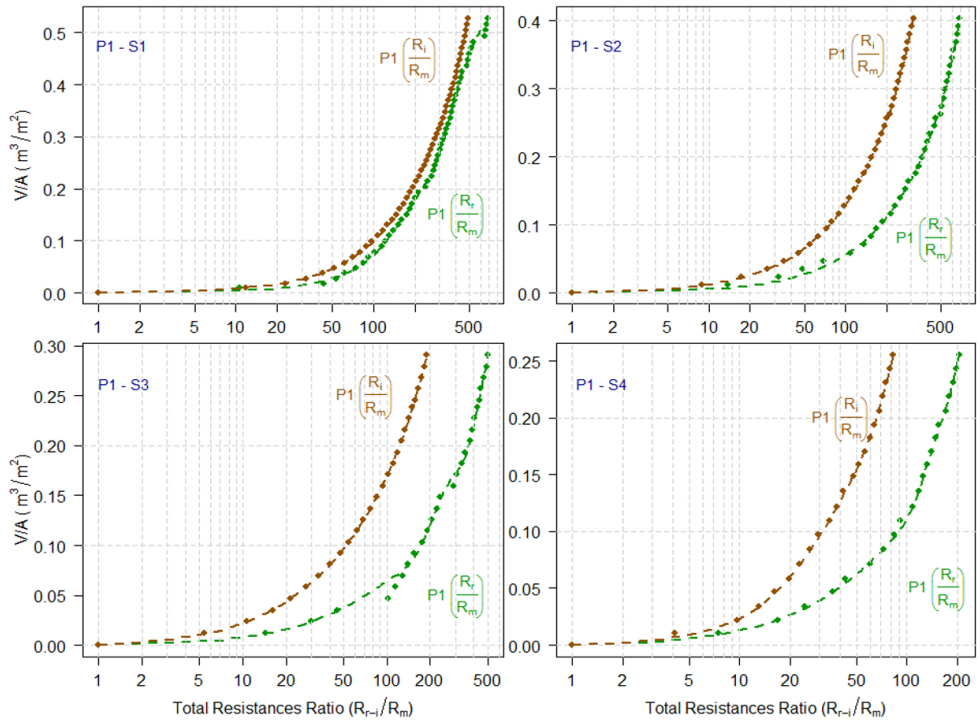

Figure B.10: Fouling propensity curves for P1 for four continuous permeation sequences including a total of 141 permeation cycles (m = 141).

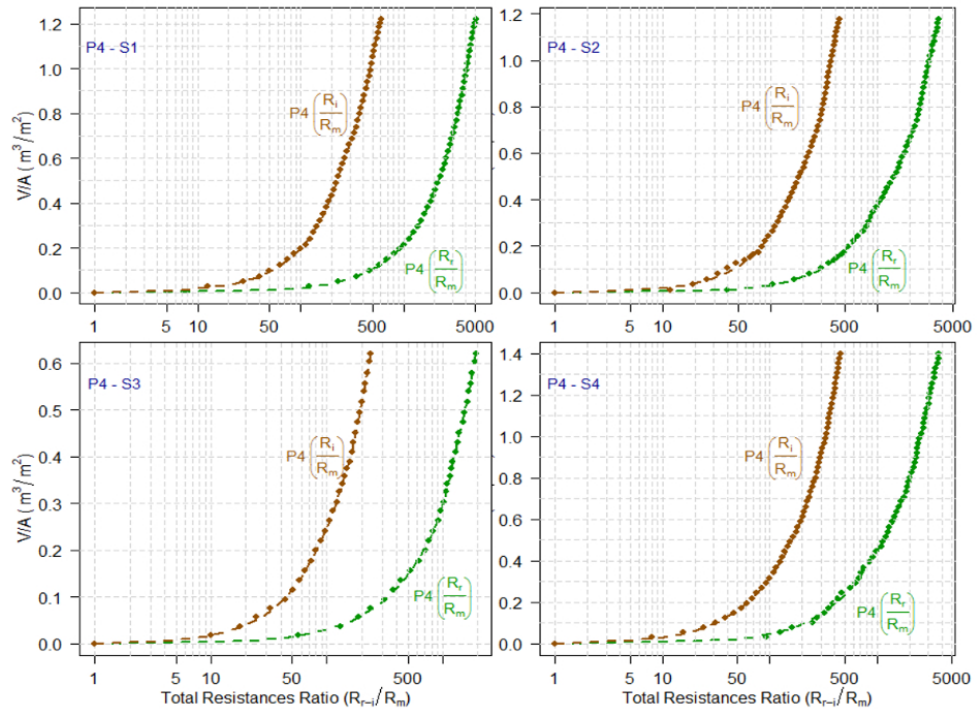

Figure B.11: Fouling propensity curves for P4 for four continuous permeation sequences including a total of 195 permeation cycles (m = 195).

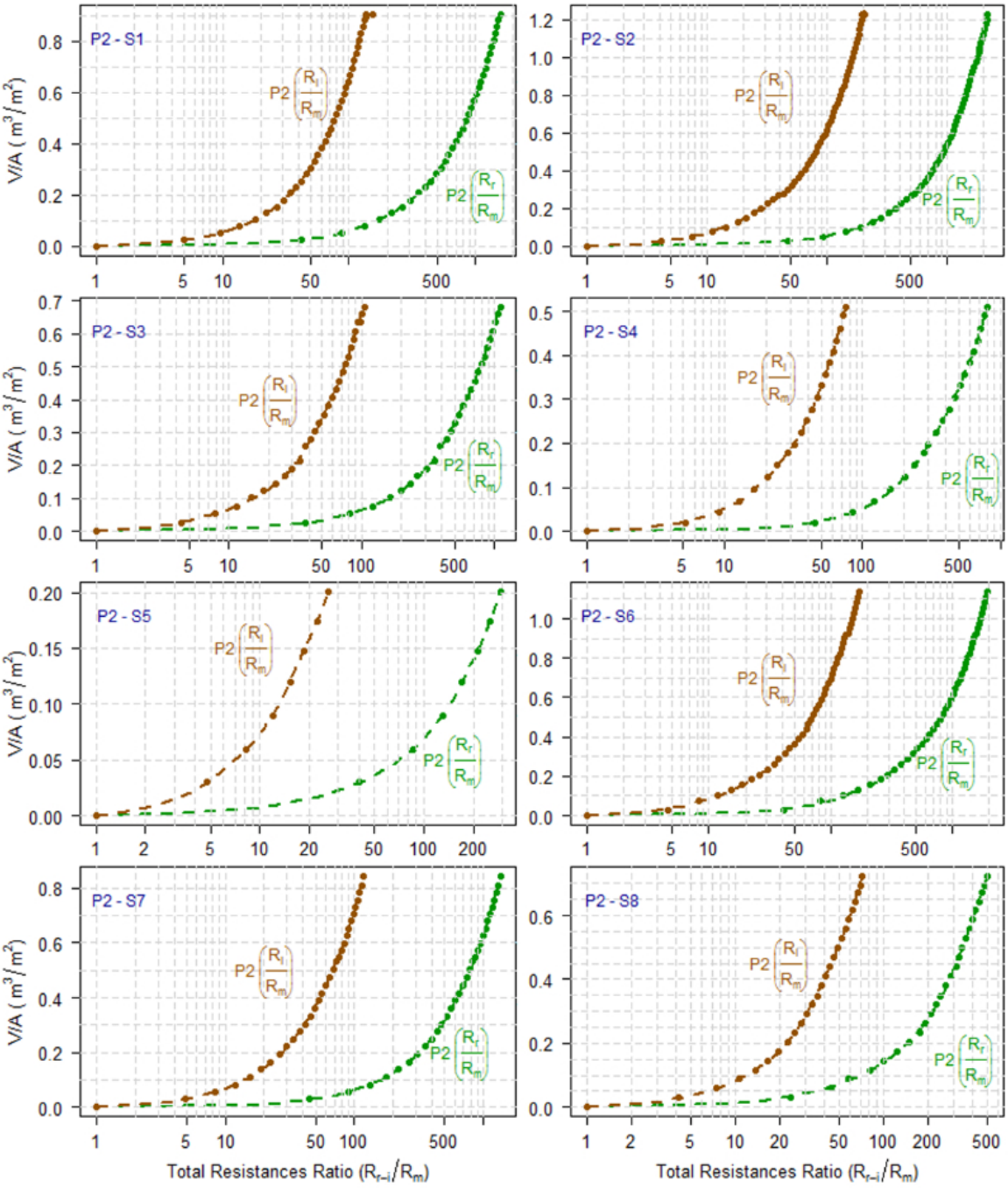

Figure B.12: Fouling propensity curves for P2 for eight continuous permeation sequences including a total of 242 permeation cycles (m = 242).

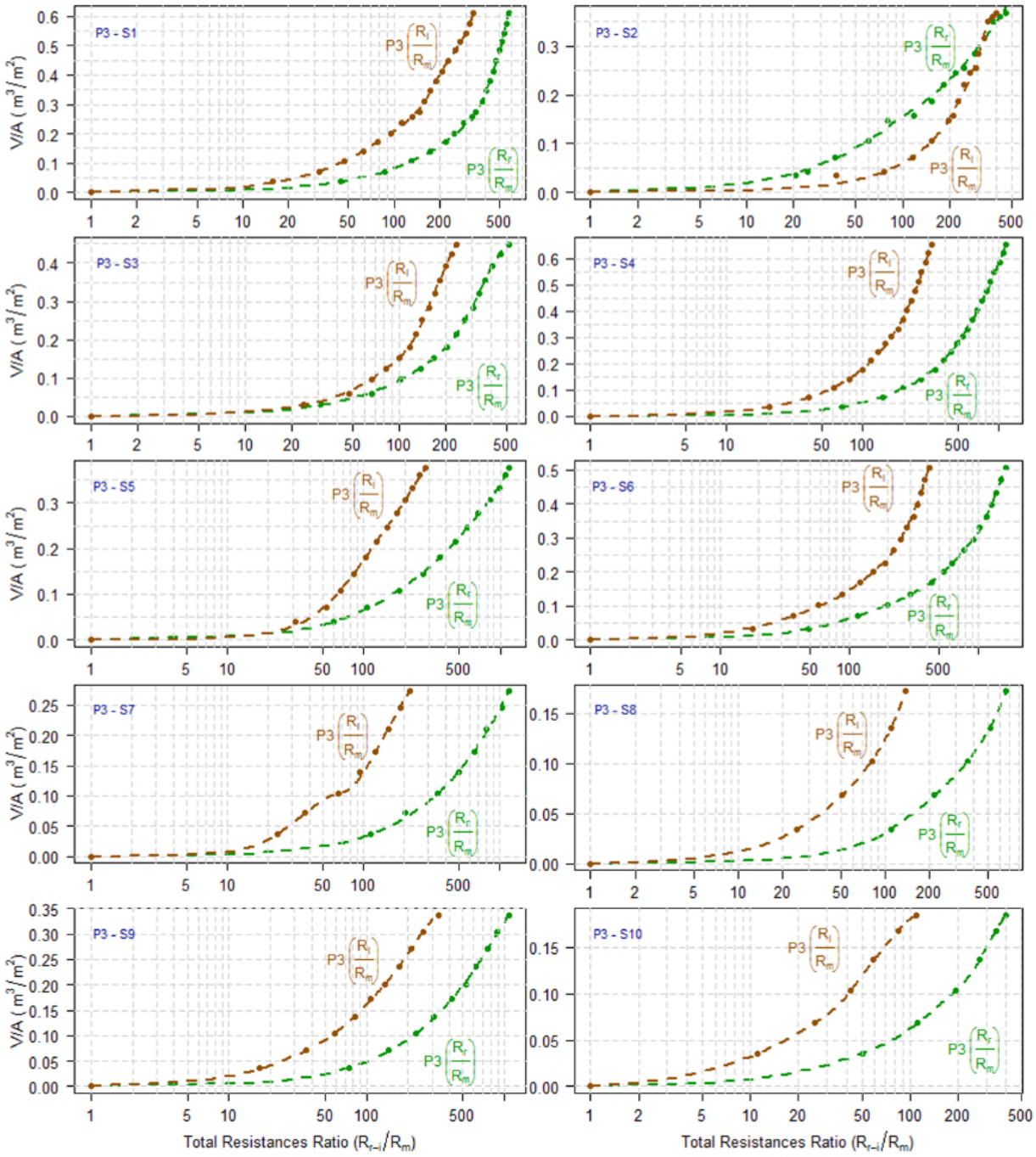

Figure B.13: Fouling propensity curves for P3 for ten continuous permeation sequences including a total of 122 permeation cycles (m = 122).

Appendix C

YES Bioassay Results

This appendix provides a detailed example of the YES analysis, tabulated summary results of the complete YES bioassay testing and example YES bioassay microtiter plates.

C.1 YES Titer Plate Analysis Process

The YES analyzes were conducted as described by Routledge and Sumpter (1996, [108]) and as modified by by Citulski (2012, [106]). Microtiter plates with 96-wells were used to grow a recombinant yeast strain exposed to E2-standard (positive control), ethanol (negative control) and various sample extracts, serially diluted, to determine the estrogenic responses based on absorbance measurements according to Eq. C.1:

$$A^c_{540} = A^s_{540} - (A^s_{620} - \bar{A}^b_{620}) \tag{C.1}$$

where A^c_{540} and A^s_{540} refer to the corrected and sample absorbance reading tuned to the red color absorbance of 540 nm wavelength, respectively. The A^s_{620} and $\bar{A}^b_{620}$ refer to the turbidity associated with the yeast cells of the sample replicates and average of the negative blank at 620 nm wavelength, respectively.

The corrected absorbance (A^c_{540}) measurement readings were used to generate dose-response curves and determine the EC50 for E2 standards and corresponding dilution factor for environmental samples. The calculations and graphical plots were conducted in R [117] by fitting a four-parameter log-logistic model [162] given by Eq C.2:

$$L(x) = c + \frac{d - c}{1 + exp(b \cdot log(x) - log(e))} \tag{C.2}$$

with the 4 parameters b, c, d and e. The parameter e is the 50 %-ile equivalent concentration producing a 50 % response (EC50), the dose or dilution (x) is the equivalent sample dilution producing a 50 % response located half-way between the lower limit c and upper limit d.

To obtain estrogenicity values for environmental samples, a correlation was made to E2 that would elicit an equivalent estrogenic response and referred to as "equivalent" to E2 according to the following equation [105, 106]:

$$EEQ\ \left(\frac{ng}{g}\right) = \left(\frac{EC_{50,E2}\ (\frac{ng}{ml})}{EC_{50,SE}}\right) \cdot \left(\frac{V_{AM}\ (\mu L)}{V_{SE}\ (\mu L)}\right) \cdot \left(\frac{V_{STE}\ (mL)}{M_S\ (g)}\right) \tag{C.3}$$

where EEQ, is the equivalent sample extract E2 concentration (ng/g); $EC_{50,E2}$, is the reference standard concentration (ng/mL) value that elicits 50 % of the maximal response

when calculated using YES bioassay in the 96-well microtiter plates; $EC_{50,SE}$, is the sample extract dilution-fraction that corresponds to the 50 % of the maximal response; V_{AM} (μL) volume of yeast enriched assay media volume added to each well of the 96-well microtiter plate; V_{SE} (μL), volume of sample extract added to the well; V_{STE}, volume (mL) of the stock extract reduced from the original sample volume and M_S, original sample mass(g. In the case of aqueous extracts V_S (L) would replace M_S (g) and the EEQ would be in ng/L. An application of Eq. C.3 for a 1 (g) sludge extract is given below.

An example YES 96-well microtiter plate with 2-samples analyzed (d1 and d2, September 16, 2013, replicates 1–3) in shown in Figure C.1 (a). Sample d2 is used as an example to describe the 2-step process of determining the sample EEQ_m (nq/g) value. The dose-response curve for the sample plate E2-standard associated with sample d2 is shown in Figure C.2 along with the input data, log-logistic 4-parameter curve fit and parameter determination for EC_{50} (parameter e corresponds to $EC_{50,E2}$ (M) (see Eq. C.1). The calculation of $EC_{50,E2}$ in ng/mL is then computed as follows:

$$\begin{aligned} EC_{50,E2} &= EC_{50,E2} \cdot MW_{E2} \cdot 10^9 \ \frac{ng}{g} \\ &= 1.93 \cdot 10^{-10} \ \frac{mol}{L} \cdot 272.38 \ \frac{g}{mol} \cdot 10^9 \ \frac{ng}{g} \\ EC_{50,E2} &= 52.6 \ \frac{ng}{L} = 0.053 \ \frac{ng}{mL} \end{aligned}$$

The sample dose-response dilution curve for sample d2 is shown in Figure C.3 with sample triplicate input data (n=3), log-logistic 4-parameter curve fit and parameter determination for $EC_{50,DF}$ value (parameter e corresponds to EC_{50} dilution (see Eq. C.2). The V_{AM} was 200 μL, the V_{SE} was 80 μL, final reduced extract volume (V_{STE}) was 2 mL and the original sludge sample mass (M_S) was 1 g with the resulting EEQ for sample d2 provided below:

$$\begin{aligned} EEQ(d2) &= \left(\frac{0.053 \ \frac{ng}{mL}}{5.2^{-1}} \right) \cdot \left(\frac{200 \ \mu L}{80 \ \mu L} \right) \cdot \left(\frac{2 \ mL}{1 \ g} \right) \\ &= 1.4 \ \frac{ng}{g} \end{aligned}$$

The EEQ values are reflective of the net estrogenic potency of the sample mixture and the higher the value the more oestrogenically potent the sample mixture. The EC_{50} values apply to individual compounds such as the YES standard β-estradiol (E2) and the lower the EC_{50} values the higher the net estrogenic potency of the specific compound.

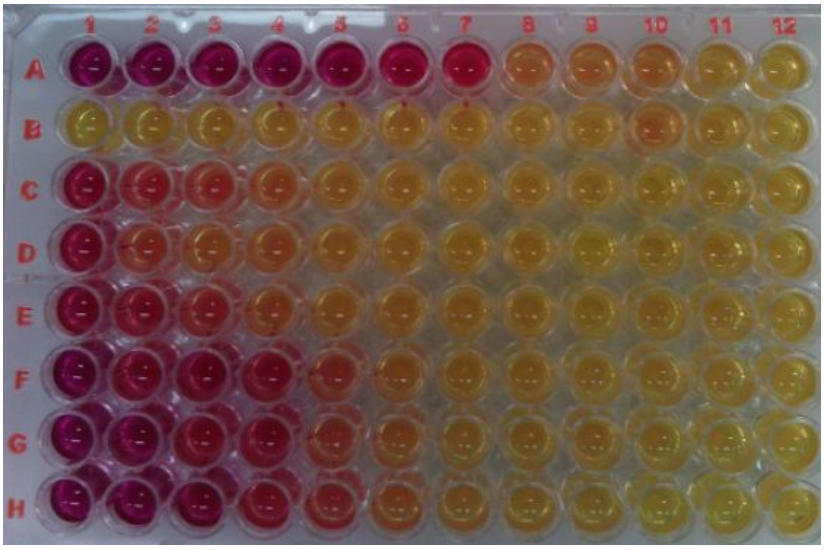

(a) Sample YES 96-well microtiter plate

<>	1	2	3	4	5	6	7	8	9	10	11	12	Reading Abs @ 540
A	3.72	3.91	3.79	3.54	3.37	3.00	2.62	1.64	1.63	1.62	1.56	1.54	E2 Positive Control
B	1.64	1.65	1.61	1.58	1.57	1.55	1.60	1.55	1.55	1.62	1.53	1.51	Negative Control
C	2.73	2.05	1.89	1.73	1.64	1.61	1.57	1.59	1.35	1.11	1.53	1.52	Sep16_d1_rep 1
D	2.79	1.75	1.18	1.65	1.65	1.60	1.56	1.55	0.92	1.07	1.50	1.49	Sep16_d1_rep 2
E	2.92	2.35	1.92	1.68	1.64	1.61	1.60	1.58	1.04	1.55	1.53	1.52	Sep16_d1_rep 3
F	3.75	2.61	2.89	2.43	1.82	1.63	1.57	1.59	1.55	1.54	1.54	1.51	Sep16_d2_rep_1
G	3.69	3.42	2.41	2.44	1.83	1.68	1.59	1.59	1.59	1.57	1.53	1.54	Sep16_d2_rep_2
H	3.66	3.75	3.32	2.35	1.96	1.74	1.66	1.62	1.61	1.49	1.54	1.55	Sep16_d2_rep_3

<>	1	2	3	4	5	6	7	8	9	10	11	12	Reading Abs @ 620
A	1.67	1.63	1.60	1.60	1.55	1.49	1.46	1.36	1.37	1.35	1.37	1.37	E2 Positive Control
B	1.47	1.47	1.42	1.40	1.39	1.36	1.40	1.37	1.37	1.34	1.33	1.34	Negative Control
C	1.41	1.43	1.43	1.41	1.42	1.41	1.39	1.39	1.16	0.92	1.35	1.34	Sep16_d1_rep 1
D	1.48	1.34	0.91	1.36	1.44	1.41	1.38	1.36	0.79	0.88	1.32	1.30	Sep16_d1_rep 2
E	1.51	1.48	1.41	1.40	1.45	1.40	1.41	1.40	0.86	1.36	1.34	1.35	Sep16_d1_rep 3
F	1.67	1.42	1.41	1.47	1.43	1.38	1.36	1.39	1.36	1.34	1.35	1.33	Sep16_d2_rep_1
G	1.60	1.62	1.42	1.50	1.45	1.42	1.39	1.39	1.38	1.38	1.36	1.36	Sep16_d2_rep_2
H	1.55	1.61	1.56	1.51	1.48	1.45	1.44	1.42	1.42	1.33	1.38	1.37	Sep16_d2_rep_3

<>	1	2	3	4	5	6	7	8	9	10	11	12	Calculation
A	3.44	3.67	3.57	3.32	3.20	2.90	2.55	1.66	1.65	1.66	1.58	1.56	E2 Positive Control
B	1.56	1.57	1.58	1.57	1.57	1.57	1.58	1.57	1.57	1.67	1.58	1.55	Negative Control
C	2.70	2.01	1.85	1.71	1.60	1.59	1.57	1.58	1.59	1.58	1.57	1.57	Sep16_d1_rep 1
D	2.70	1.79	1.65	1.68	1.59	1.58	1.58	1.58	1.52	1.57	1.58	1.57	Sep16_d1_rep 2
E	2.79	2.26	1.90	1.67	1.59	1.59	1.58	1.57	1.57	1.57	1.57	1.56	Sep16_d1_rep 3
F	3.47	2.58	2.87	2.35	1.78	1.64	1.60	1.59	1.57	1.59	1.57	1.57	Sep16_d2_rep_1
G	3.47	3.19	2.37	2.33	1.77	1.65	1.59	1.59	1.59	1.58	1.56	1.57	Sep16_d2_rep_2
H	3.50	3.53	3.15	2.23	1.87	1.68	1.61	1.59	1.58	1.55	1.55	1.57	Sep16_d2_rep_3

(b) Sample absorbance readings (top and middle) and calculation table (bottom)

Figure C.1: Sample YES calculation tables showing the readings of color absorbance at 540 nm (top), yeast turbidity at 620 nm (middle) and calculation of corrected absorbance (below) based on Eq. C.1.

Input Data to R - DRC

	Dose	Rep	Abs
1	1.00e-08	1	3.44
2	5.00e-09	1	3.67
3	2.50e-09	1	3.57
4	1.25e-09	1	3.32
5	6.25e-10	1	3.20
6	3.13e-10	1	2.90
7	1.56e-10	1	2.55
8	7.81e-11	1	1.66
9	3.91e-11	1	1.65
10	1.95e-11	1	1.66
11	9.77e-12	1	1.58
12	4.88e-12	1	1.56

Log-logistic 4-parameter fit

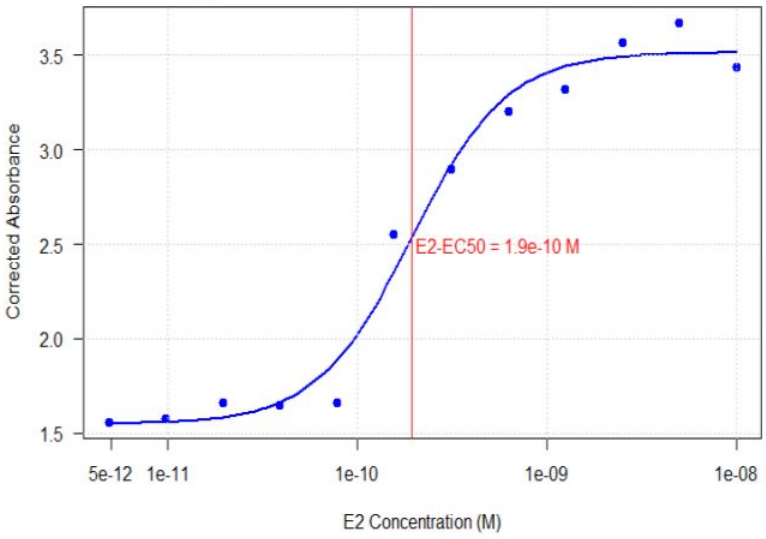

Output parameter values (b-e) for EC50 determination

```
Model fitted: Log-logistic (ED50 as parameter) (4 parms)

Parameter estimates:

                 Estimate  Std. Error     t-value p-value
b:(Intercept) -1.7302e+00  4.0976e-01 -4.2226e+00  0.0029
c:(Intercept)  1.5478e+00  8.1712e-02  1.8942e+01  0.0000
d:(Intercept)  3.5154e+00  8.6517e-02  4.0633e+01  0.0000
e:(Intercept)  1.9319e-10  2.8853e-11  6.6958e+00  0.0002

Residual standard error:

 0.1403741 (8 degrees of freedom)
```

Figure C.2: Sample E2 standard dose-response curve from input dose and absorbance data (input), log-logistic 4-parameter fit (figure) and parameter output for EC50 determination (e is the EC50 value).

Input Data to R - DRC

	Dose	Dil	Abs
1	1.00e-08	1	3.47
2	5.00e-09	2	2.58
3	2.50e-09	4	2.87
4	1.25e-09	8	2.35
5	6.25e-10	16	1.78
6	3.13e-10	32	1.64
7	1.56e-10	64	1.60
8	7.81e-11	128	1.59
9	3.91e-11	256	1.57
10	1.95e-11	512	1.59
11	9.77e-12	1024	1.57
12	4.88e-12	2048	1.57
13	1.00e-08	1	3.47
14	5.00e-09	2	3.19
15	2.50e-09	4	2.37
16	1.25e-09	8	2.33
17	6.25e-10	16	1.77
18	3.13e-10	32	1.65
19	1.56e-10	64	1.59
20	7.81e-11	128	1.59
21	3.91e-11	256	1.59
22	1.95e-11	512	1.58
23	9.77e-12	1024	1.56
24	4.88e-12	2048	1.57
25	1.00e-08	1	3.50
26	5.00e-09	2	3.53
27	2.50e-09	4	3.15
28	1.25e-09	8	2.23
29	6.25e-10	16	1.87
30	3.13e-10	32	1.68
31	1.56e-10	64	1.61
32	7.81e-11	128	1.59
33	3.91e-11	256	1.58
34	1.95e-11	512	1.55
35	9.77e-12	1024	1.55
36	4.88e-12	2048	1.57

Log-logistic 4-parameter fit (n=3)

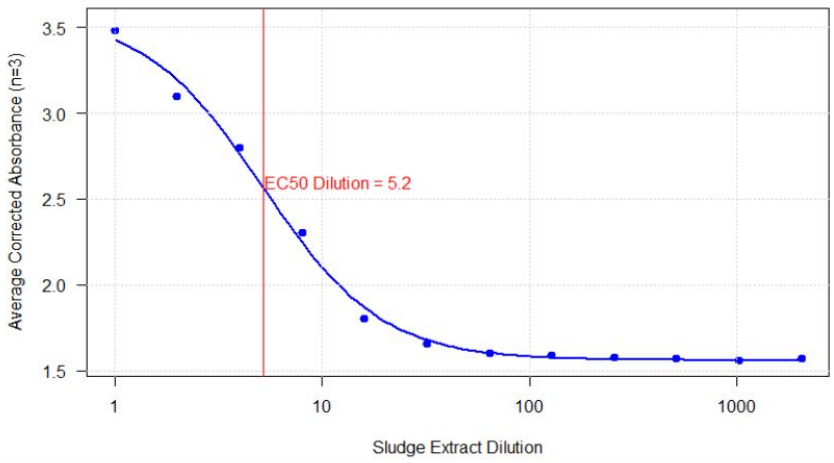

Output parameter values (b-e) for EC50 -Dilution determination

```
Model fitted: Log-logistic (ED50 as parameter) (4 parms)

Parameter estimates:

                Estimate Std. Error   t-value p-value
b:(Intercept)  1.519114   0.303938  4.998109       0
c:(Intercept)  1.561209   0.040773 38.290215       0
d:(Intercept)  3.580393   0.189979 18.846237       0
e:(Intercept)  5.169148   0.975464  5.299167       0

Residual standard error:

 0.1635062 (32 degrees of freedom)
```

Figure C.3: Sample dose-response dilution-curve from triplicate input dose and absorbance data (input, n=3), log-logistic 4-parameter fit (figure) and parameter output for EC50-dilution determination (e is the EC50 dilution value).

C.2 Phase 1–4 Sludge YES Results

The results of the YES analysis for P1 which included PS, TWAS, AD and AnMBR sludge extracts are given in Table C.1 with example microtiter plates shown in Figure C.4. The results of the YES analysis for P2 which included PS, TWAS, AD and AnMBR sludge extracts are given in Table C.2 with example microtiter plates shown in Figure C.5. The results of the YES analysis for P3 which included PS, TWAS, AD and AnMBR sludge extracts are given in Table C.3 with example microtiter plates shown in Figure C.6. The results of the YES analysis for P4 which included PS, TWAS, AD and AnMBR sludge extracts are given in Table C.4 with example microtiter plates shown in Figure C.7.

Table C.1: YES responses of P1 sludge samples

Stream	Sample ID	E2 EC_{50} (nM)	$EC_{50,E2}$ (ng/L)	Sample $EC_{50,DF}$	Sample EC_{50} EEQ_m (ng/g)
AD	a1-1	0.12	32	23	3.7
	a1-2	0.09	24	65	7.8
	a1-3	0.08	22	17	1.9
	a1-4	0.13	36	1	0.2
	a1-5	0.06	17	25	2.1
	a1-6	0.08	23	64	7.4
	a1-7	0.20	53	9	2.4
AnMBR	m1-1	0.12	32	28	4.5
	m1-2	0.09	24	35	4.2
	m1-3	0.08	22	13	1.4
	m1-4	0.13	36	2	0.4
	m1-5	0.06	17	17	1.5
	m1-6	0.08	23	15	1.7
	m1-7	0.20	53	2	0.5
PS	ps1-1	0.05	13	9	0.6
	ps1-2	0.16	43	45	10
	ps1-3	0.66	178	15	13
	ps1-4	0.07	20	2	0.2
	ps1-5	0.18	50	49	12
	pa1-7	0.12	32	8	1.3
TWAS	tw1-1	0.05	13	17	1.1
	tw1-2	0.16	43	50	11
	tw1-3	0.66	178	15	13
	tw1-4	0.07	20	72	7.2
	tw1-5	0.18	50	34	8.5
	tw1-7	0.12	32	111	18

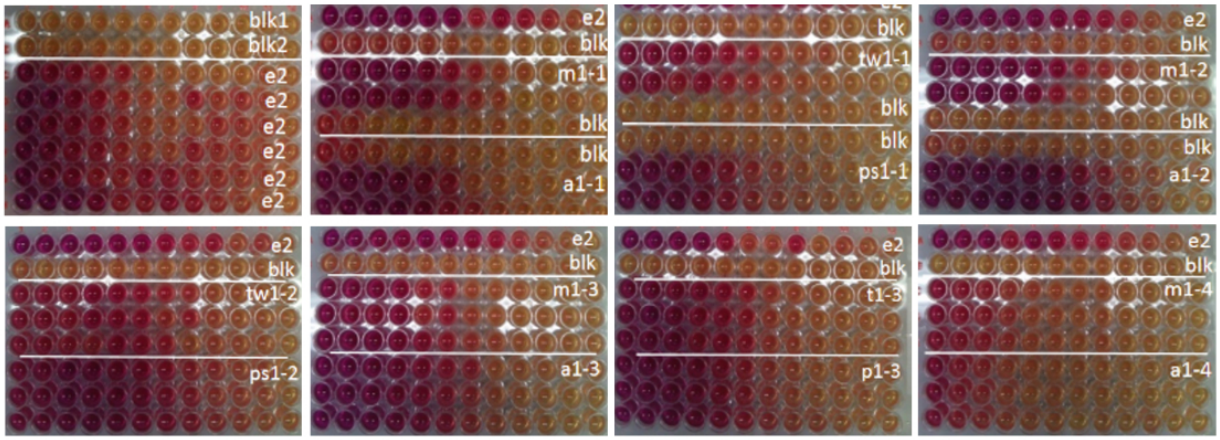

Figure C.4: Example P1 YES microtiter plates

Table C.2: YES responses of P2 sludge samples

Stream	Sample ID	E2 EC_{50} (nM)	$EC_{50,E2}$ (ng/L)	Sample $EC_{50,DF}$	Sample EC_{50} EEQ_m (ng/g)
AD	a2-1	0.16	42	33.7	7.1
	a2-2	0.08	22	5	0.6
	a2-3	0.08	22	34.8	3.8
	a2-4	0.10	27	21.7	2.9
	a2-5	0.13	35	12.2	2.1
	a2-6	0.24	66	2.4	0.8
	a2-7	0.35	95	0.9	0.4
	a2-8	0.06	17	97.5	8.3
AnMBR	m2-1	0.16	42	17.5	3.7
	m2-2	0.08	22	19.6	2.2
	m2-3	0.08	22	0.4	0.04
	m2-4	0.10	27	21.6	2.9
	m2-5	0.13	35	17.1	3.0
	m2-6	0.24	66	1.9	0.6
	m2-7	0.35	95	12.1	5.8
	m2-8	0.06	17	0.1	0.01
PS	ps2-2	0.14	37	96.8	18
	ps2-4	0.13	35	0.4	0.1
	ps2-5	0.17	46	49.4	11
	ps2-8	0.12	34	0.2	0.03
TWAS	tw2-2	0.14	37	58.5	11
	tw2-4	0.13	35	29.6	5.2
	tw2-5	0.17	46	33.7	7.8
	tw2-8	0.12	34	40.8	6.9

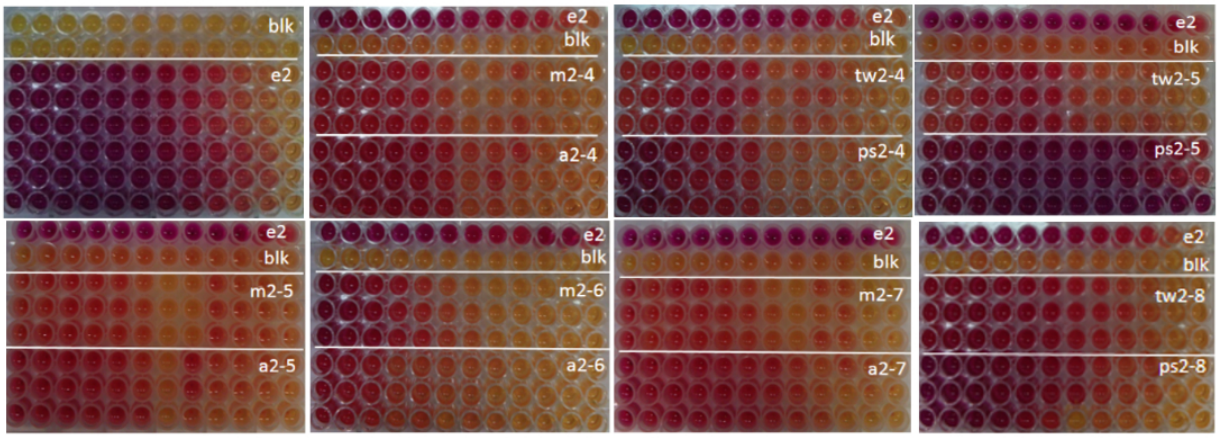

Figure C.5: Example P2 YES bioassay microtiter plates.

Table C.3: YES responses of P3 sludge samples

Stream	Sample ID	E2 EC_{50} (nM)	$EC_{50,E2}$ (ng/L)	Sample $EC_{50,DF}$	Sample EC_{50} EEQ_m (ng/g)
AD	a3-1	0.82	224	5	5.6
	a3-2	0.25	69	38	13
	a3-3	0.17	47	100	24
	a3-4	0.18	48	0.1	0.02
	a3-5	0.29	79	1.0	0.4
	a3-6	0.27	74	8	3.0
	a3-8	0.33	91	0.5	0.23
AnMBR	m3-1	0.29	79	24	9.5
	m3-2	0.25	69	38	13
	m3-3	0.18	48	36	8.6
	m3-4	0.80	219	0.1	0.1
	m3-5	0.27	74	0.9	0.3
	m3-6	0.17	47	14	3.3
	m3-8	0.33	91	0.5	0.2
PS	ps3-2	0.07	19	73	6.9
	ps3-4	0.31	84	0.2	0.1
	ps3-6	0.19	52	48	12
TWAS	tw3-2	0.07	19	79	7.5
	tw3-4	0.31	84	0.2	0.1
	tw3-6	0.19	52	113	29

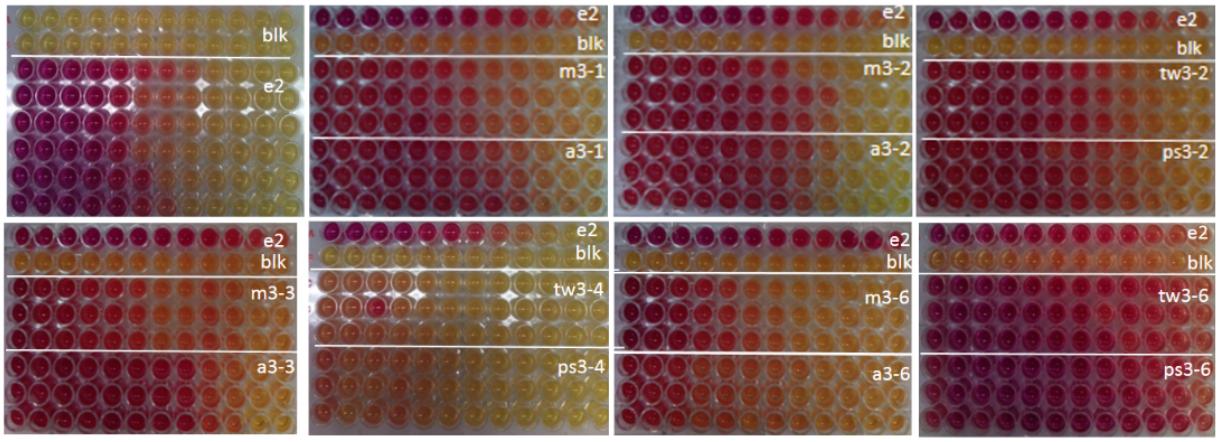

Figure C.6: Example P3 YES bioassay microtiter plates.

Table C.4: YES responses of P4 sludge samples

Stream	Sample ID	E2 EC_{50} (nM)	$EC_{50,E2}$ (ng/L)	Sample $EC_{50,DF}$	Sample EC_{50} EEQ_m (ng/g)
AD	a4-1	0.10	27	69	9.3
	a4-2	0.09	25	71	8.9
	a4-3	0.31	83	192	80
	a4-4	0.13	35	33	5.8
	a4-5	0.31	84	12	5.0
	a4-6	0.11	29	75	11
	a4-7	0.04	11	56	3.1
AnMBR	m4-1	0.10	27	45	6.1
	m4-2	0.09	25	53	6.6
	m4-3	0.31	83	73	30
	m4-4	0.13	35	202	35
	m4-5	0.31	84	132	55
	m4-6	0.11	29	193	28
	m4-7	0.04	11	677	37
PS	ps4-2	0.07	19	73	6.9
	ps4-4	0.02	6	310	9.3
	ps4-5	0.13	34	36	6.1
	ps4-8	0.08	22	237	26
TWAS	tw4-2	0.07	19	80	7.6
	tw4-4	0.02	6	152	4.6
	tw4-5	0.13	34	42	7.1
	tw4-8	0.08	22	42	4.6

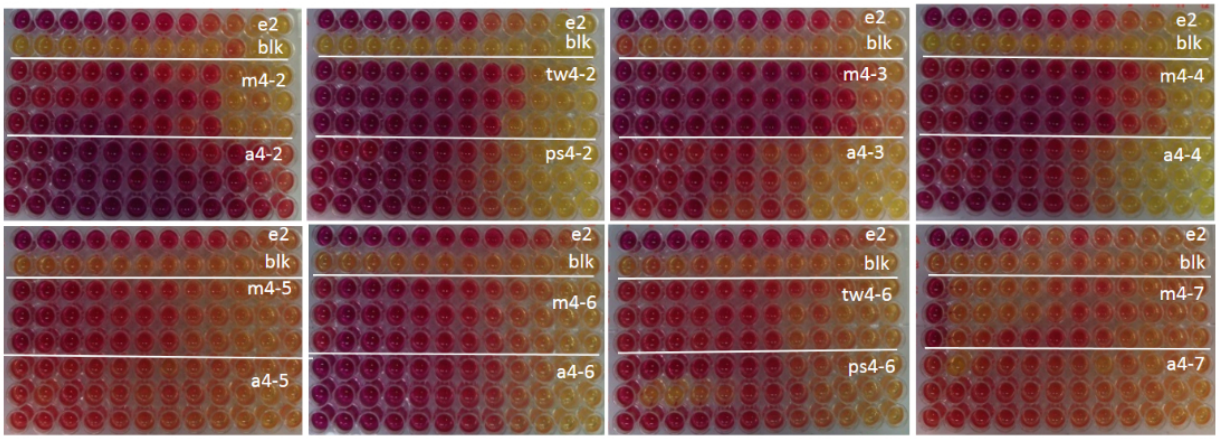

Figure C.7: Example P4 YES bioassay microtiter plates.

C.3 Permeate YES Results

The results of the YES bioassay permeate extracts analysis for P2–P4 are given in Table C.5 with example microtiter plates provided in Figure C.8.

Table C.5: AnMBR permeate YES bioassay net estrogenicity results

Stream	Sample ID	$EC_{50,E2}$ (nM)	$EC_{50,E2}$ (ng/L)	Sample $EC_{50,DF}$	Sample EEQ_v (ng/L)
2	p2-1	0.07	20	3.9	1.5
	p2-2	0.14	37	1.5	1.1
	p2-3	0.14	37	0.3	0.2
	p2-4	0.06	16	1.3	0.4
	p2-5	0.06	18	0.5	0.2
	p2-6	0.07	19	0.2	0.1
3	p3-1	0.12	32	0.2	0.1
	p3-2	0.10	26	4.2	2.2
	p3-3[a]	0.11	29	0.4	0.2
	p3-4	0.03	8	1.7	0.3
	p3-5[a]	0.05	13	1.3	0.3
	p3-6	0.07	18	1.9	0.7
	p3-7[b]	0.15	42	2.0	1.7
	p3-8	0.16	44	1.4	1.3
	p3-9	0.11	29	0.1	0.1
	p3-10	0.11	29	0.2	0.1
4	p4-1	0.07	20	1.3	0.5
	p4-2	0.07	20	1.5	0.6
	p4-3	0.05	13	2.1	0.5
	p4-4	0.05	13	0.1	0.02
	p4-5	0.04	11	1.3	0.3
	p4-6	0.04	11	0.1	0.03
	p4-7	0.04	12	3.2	0.7
	p4-8	0.07	20	0.2	0.1
	p4-9	0.07	20	2.5	1.0
	p4-10	0.09	26	1.0	0.5
	p4-11	0.09	23	1.2	0.6
	p4-12[a]	0.09	26	2.6	1.3
	p4-13	0.09	25	5.0	2.5
	p4-14[a]	0.06	18	8.5	3.0
	p4-15	0.03	9	0.1	0.01

[a] Average of duplicate permeate extracts. [b] Average of triplicate permeate extracts.

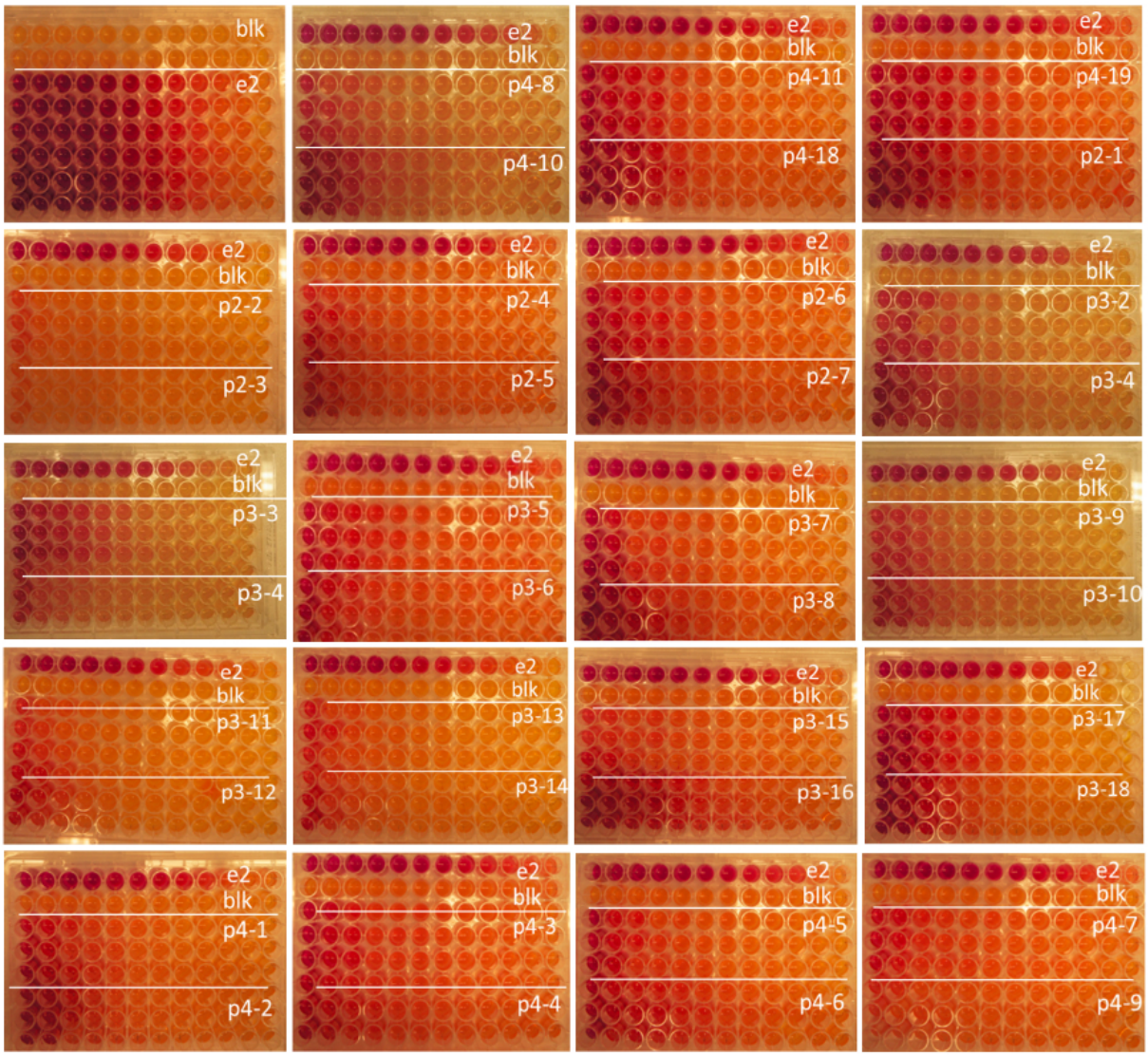

Figure C.8: Example AnMBR permeate YES microtiter plates P2-P4

C.4 AnMBR and AD Desorption Test

This section includes a tabulation of the YES bioassay results for the aqueous extracts of the AnMBR and AD treated sludge desorption testing. The process steps are shown in Figure C.9, summary results in Table C.6 and C.7 and example YES microtiter plates shown in Figure C.10 and C.11.

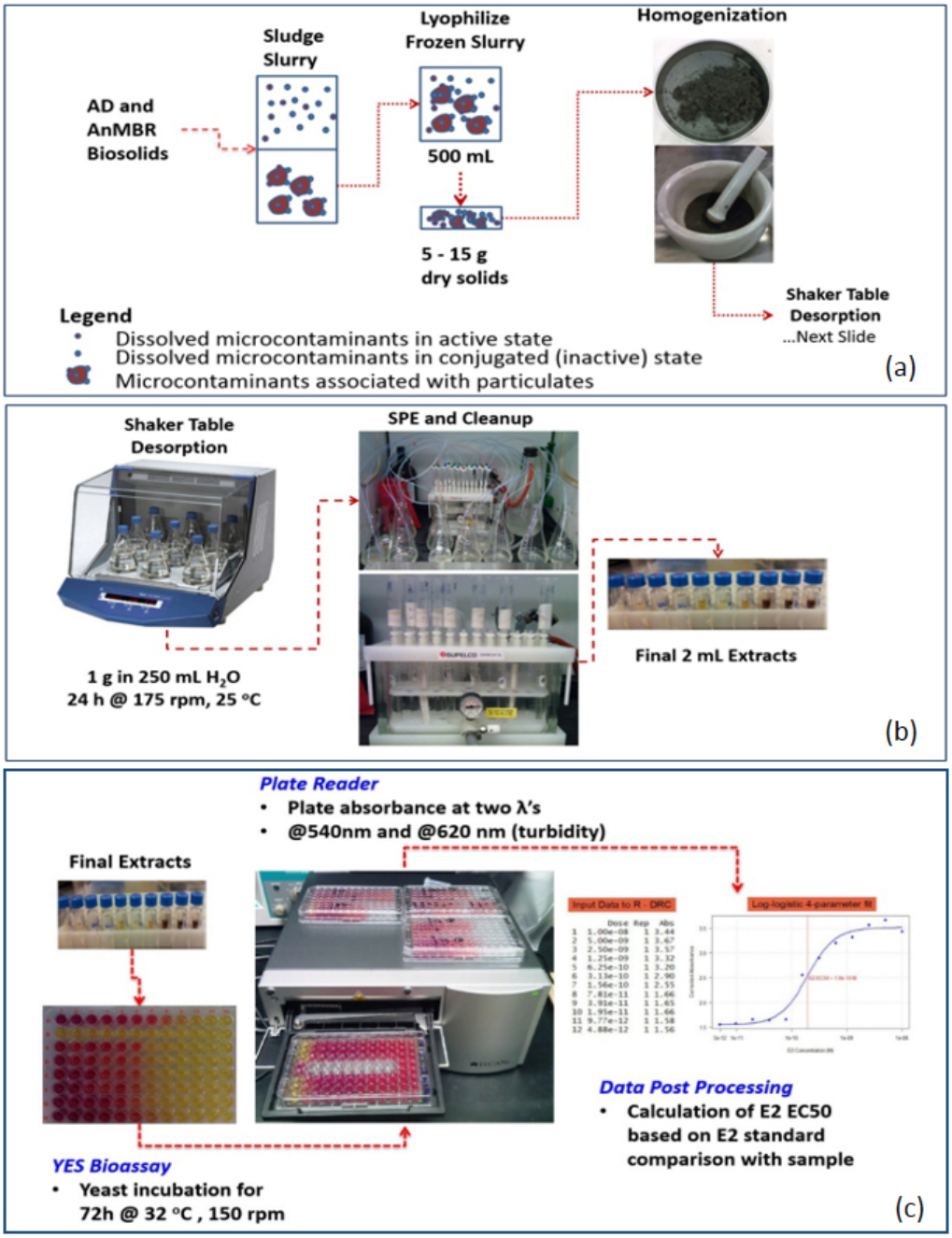

Figure C.9: Desorption test homogenization (a), desorption, extraction and cleanup steps (b) and YES microtiter plate analysis (c)

Table C.6: AnMBR sludge desorption aqueous extracts YES bioassay net estrogenicity results

Phase	Sample ID	$EC_{50,E2}$ (nM)	$EC_{50,E2}$ (ng/L)	Sample $EC_{50,DF}$	Sample EEQ_v (ng/L)
1	m1	0.19	53	0.2	0.2
	m2	0.19	53	5.2	5.5
	m3	0.09	25	4.4	2.2
	m4	0.09	25	1.9	1.0
	m5	0.17	47	2.0	1.9
2	m6	0.17	47	3.6	3.4
	m7	0.09	24	0.8	0.4
	m8	0.09	24	4.4	2.1
	m9	0.19	50	0.4	0.4
	m10	0.19	50	2.0	2.0
3	m11	0.12	32	6.5	4.2
	m12	0.12	32	8.2	5.2
	m13	0.08	23	9.2	4.2
	m14	0.08	23	6.1	2.8
	m15	0.07	19	20.9	7.9
4	m16	0.07	19	4.4	1.7
	m17	0.09	25	3.9	2.0
	m18	0.09	25	29.3	14.7
	m19	0.19	53	10.4	11.0
	m20	0.19	53	13.5	14.3

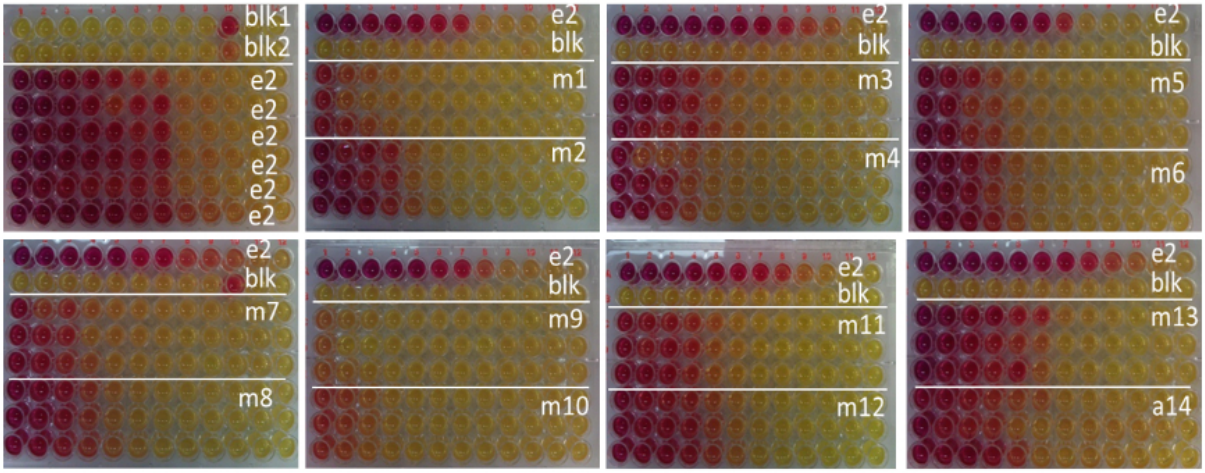

Figure C.10: Example AnMBR YES desorption microtiter plates P1-P4

Table C.7: AD sludge desorption aqueous extracts YES bioassay net estrogenicity results

Phase	Sample ID	$EC_{50,E2}$ (nM)	$EC_{50,E2}$ (ng/L)	Sample $EC_{50,DF}$	Sample EEQ_v (ng/L)
1	a1	0.29	80	2	3.2
	a2	0.29	80	6	9.6
	a3	0.09	23	7	3.2
	a4	0.09	23	8	3.7
	a5	0.05	14	11	3.1
2	a6	0.05	14	12	3.4
	a7	0.09	24	6	2.9
	a8	0.09	24	7	3.4
	a9	0.08	21	11	4.6
	a10	0.08	21	5	2.1
3	a11	0.11	31	12	7.4
	a12	0.11	31	4	2.5
	a13	0.09	24	8	3.8
	a14	0.09	24	10	4.8
	a15	0.05	13	10	2.6
4	a16	0.05	13	9	2.3
	a17	0.03	9	11	2.0
	a18	0.03	9	8	1.4
	a19	0.05	15	7	2.1
	a20	0.05	15	8	2.4

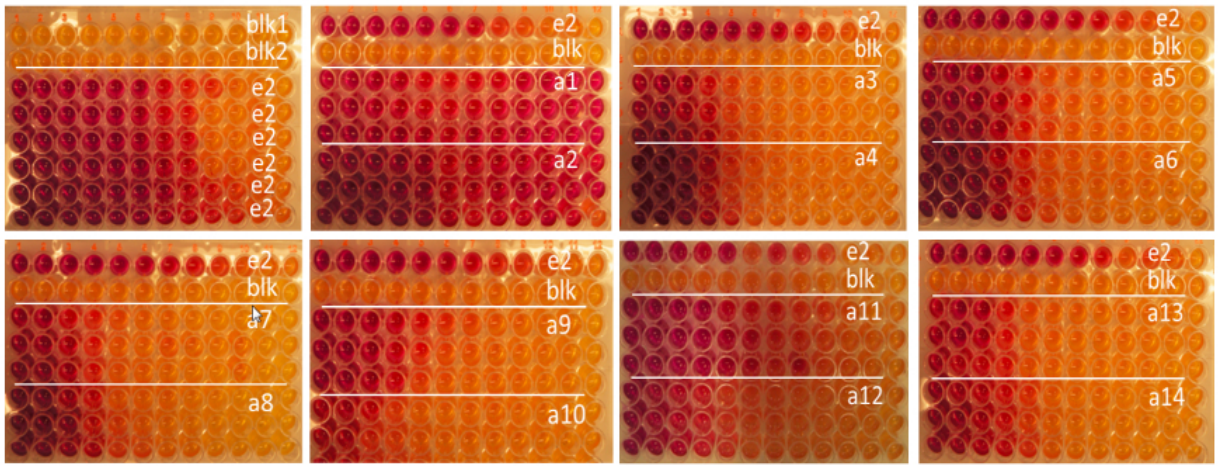

Figure C.11: Example AD YES desorption microtiter plates P1-P4

Appendix D

Trace Organic Contaminants (TrOCs) in Permeate

This appendix provides further details of the chemical analysis results of the TrOCs in the permeate during P1–P4.

D.1 Permeate Chemistry Analysis

The methodology in the extraction and analysis of the TrOCs suite of contaminants (Table D.1) is described Figure D.1).

Table D.1: Suite of TrOCs) CAS-RN, classification, isotope and MDLs[a] [6]

TrOCs	CAS-RN	Classification	Isotope	MDL (μg/L)
Acetaminophen	103-90-2	antipyretic	D_4-acetaminophen	0.1
Bisphenol A	80-05-7	estrogenic	D_{16}-bisphenol A	0.2
Carbamazepine	298-46-4	antiepileptic	D_{10}-carbamazepine	0.02
Ciprofloxacin	85721-33-1	antibiotic	$^{13}C_3{}^{15}N$-ciprofloxacin	0.1
Clofibric acid	882-09-7	lipid regulator	D_4-clofibric acid	0.05
Diclofenac	15307-86-5	analgesic	D_4-diclofenac	0.1
Equilin	474-86-2	estrogen	D_4-equilin	0.05
Estriol	50-27-1	estrogen	D_4-estriol	0.2
Estrone	53-16-7	estrogen	D_4-estrone	0.1
Ibuprofen	15687-27-1	analgesic	D_3-ibuprofen	0.1
Indomethacin	53-86-1	analgesic	D_4-indomethacin	0.1
Progesterone	57-83-0	estrogenic	D_9-progestrone	0.1
Sulfamethazine	57-68-1	antibiotic	$^{13}C_6$-sulfamethazine	0.02
Sulfamethoxazole	723-46-6	antibiotic	$^{13}C_6$-sulfamethoxazole	0.1

[a] MDL, method detection limit or the lower limit of quantitation using LC-MS-MS MOECC Method E3454 with isotopes to confirm quantification analysis [6].

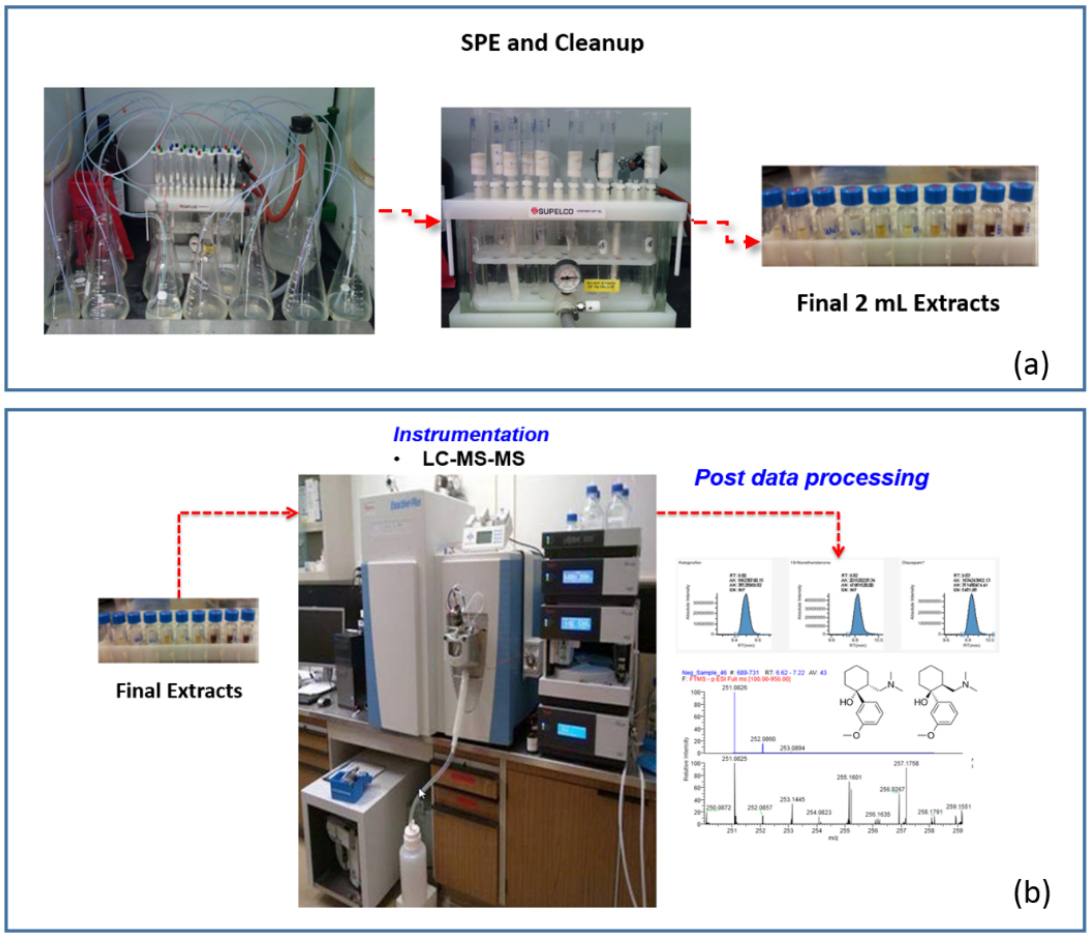

Figure D.1: Sequence of steps in the AnMBR permeate chemical analysis which included filtration of the permeate (0.4 μm) prior to SPE and cleanup (a) and followed by instrumentation analysis using LC-MS-MS at the MOE LaSB (b) [6].

D.2 Physical Chemical Properties

Table D.1 provides a list of physical-chemical properties of the suite of TrOCs investigated. The list of parameter values were determined by using the US EPA EPI Suite V.4.11 [7] which provides an extensive database which includes parameter values that were experimentally derived or based on model predictions. The chemical structures (Figure D.2) and physical chemical properties in increasing order (Figure D.3) were compared showing the full span of properties [7].

A screening level estimate of the biodegradability of the list of TrOCs (Table D.1 and Figure D.3), under anaerobic methanogenic conditions, was determined using Biowin7 Model (part of the US EPA EPI Suite V. 4.11) which was based on the "serum bottle" anaerobic biodegradation screening test and is assumed to be predictive of degradation in a typical anaerobic digester [7, 173].

The screening level estimate of the percent of the TrOCs adsorbed to sludge (Table D.1 and Figure D.3) was based on the STP Fugacity Model [174] which is based on a municipal activated sludge treatment system included in the US EPA EPI Suite V. 4.11 [7].

Table D.2: Physical chemical properties of the suite of trace organic contaminants (TrOCs) analyzed [7]

TrOCs	MW (g/mole)	S_w (g/L, 25 °C)	Log(K_{oc})	Log(K_{ow})	% Ads.[a]	Biowin 7[b]
Acetaminophen	151.17	14000	1.3	0.46	2	-0.11
Bisphenol A	228.29	173	3.1	3.32	9	-0.26
Carbamazepine	236.27	18	2.2	2.45	3	-0.07
Ciprofloxacin	333.15	30000	1.0	0.28	2	-2.30
Clofibric acid	214.65	583	1.6	2.57	3	-0.08
Diclofenac	296.15	2.37	2.6	4.51	56	-0.85
Equilin	268.36	1.41	3.1	3.4	10	-0.89
Estriol	288.39	441	1.6	2.45	3	-0.04
Estrone	270.37	147	3.0	3.13	7	-0.90
Ibuprofen	206.29	21	2.4	3.97	28	0.03
Indomethacin	357.8	0.94	2.3	4.27	43	-0.44
Progestrone	314.47	8.8	3.5	3.87	24	-1.73
Sulfamethazine	278.33	1500	1.5	0.19	2	-0.66
Sulfamethoxazole	253.28	610[c]	1.5	0.89	2	-0.29

[a] % Ads., refers to the screening level percent of the TrOCs adsorbed to sludge following activated sludge treatment [174] [b] Biowin 7, refers to a screening level anaerobic methanogenic biodegradation model prediction and a value of < 0.5 is indicative of a slow biodegradation potential [7, 173] [c] Sufamethoxazole S_w was measured at 37 °C.

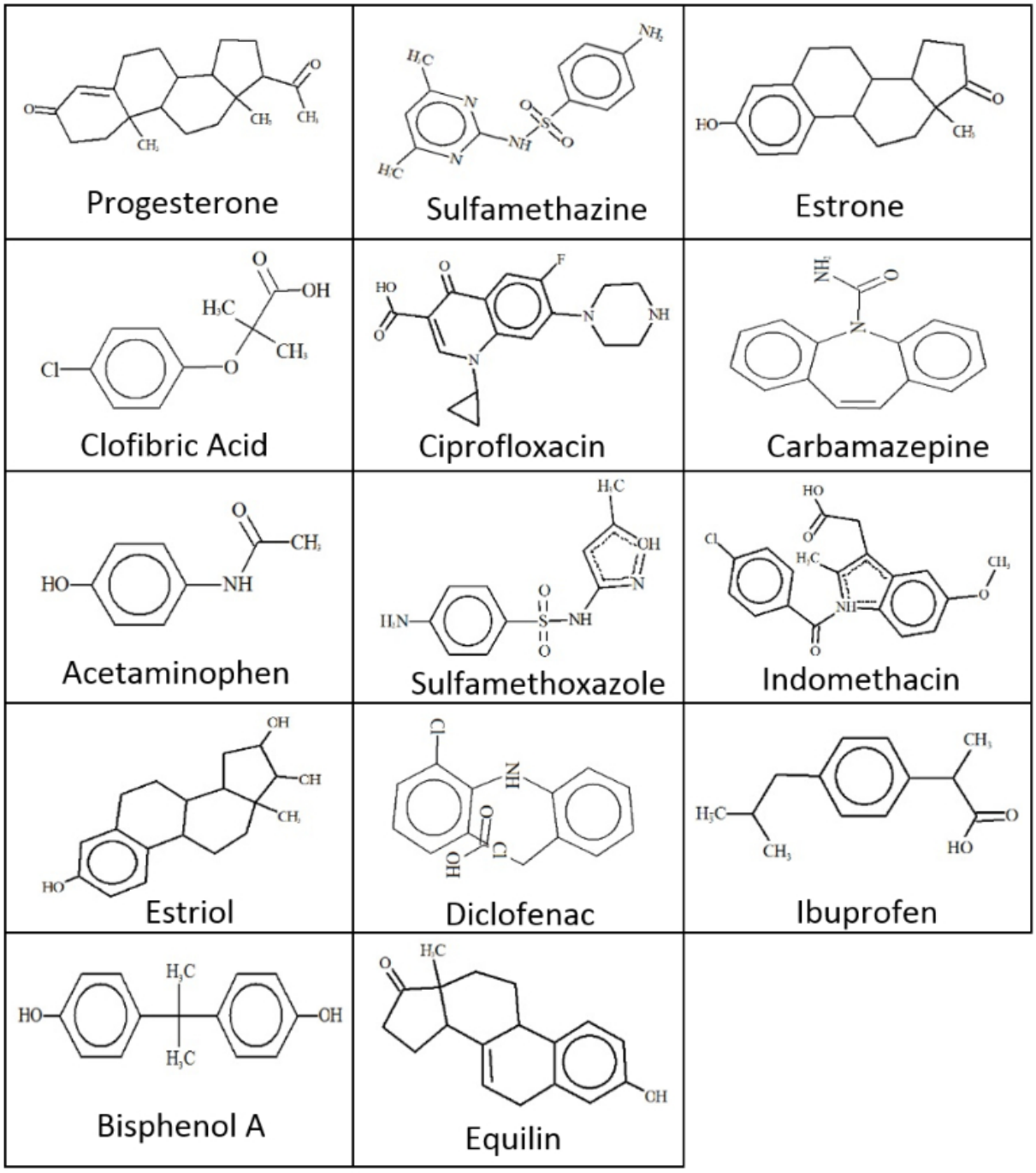

Figure D.2: Suite of trace organic contaminants (TrOCs) chemical structures analyzed for in the permeate [7].

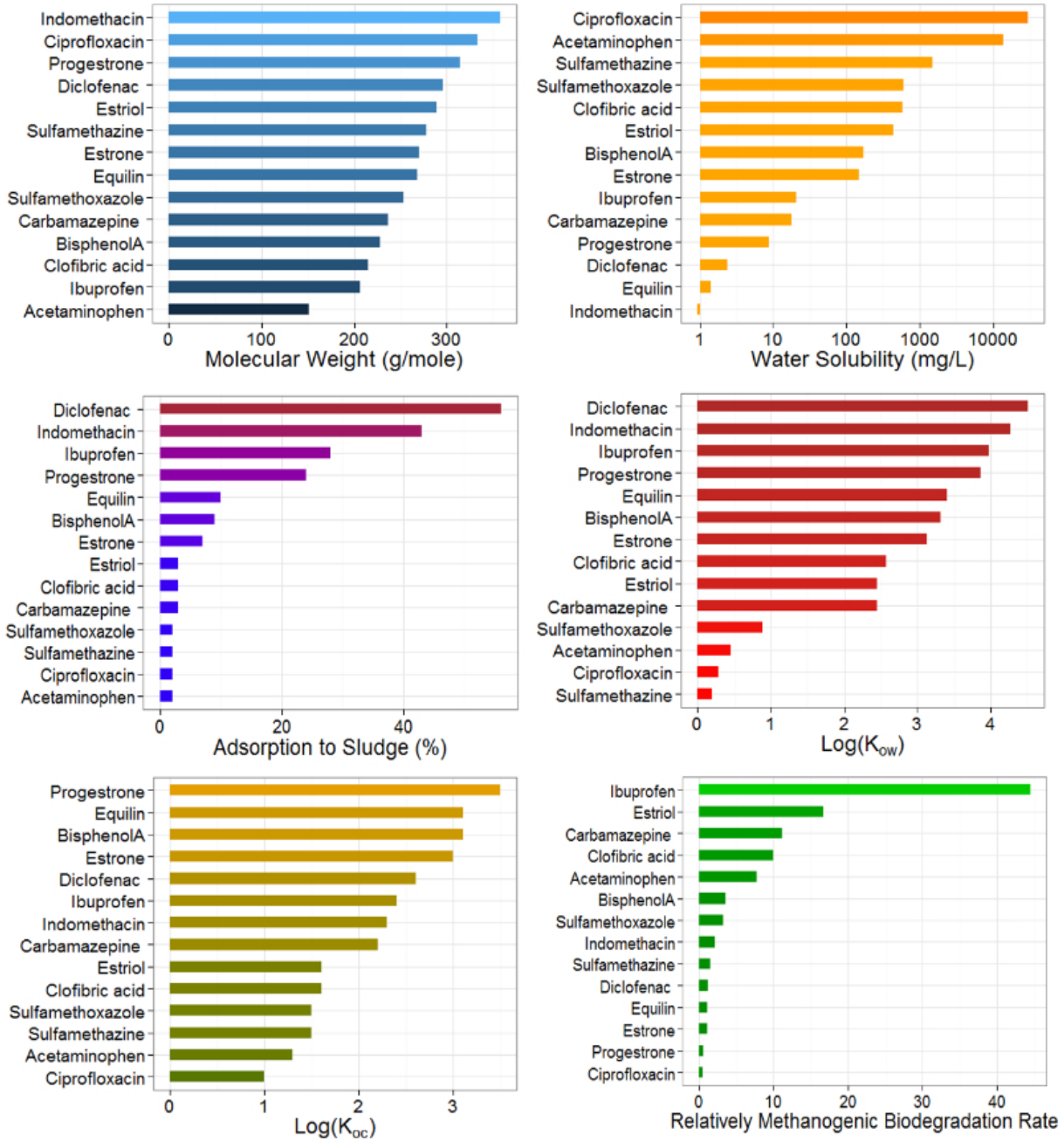

Figure D.3: Physical chemical properties between the TrOCs compared

D.3 Permeate Chemical Analysis Results

This section includes the complete permeate analysis of TrOCs results comparisons between P1–P4 in censored box plots (Figure D.4), censored cumulative probability distribution diagrams for each phase and combined P1–P4 (Figure D.5–D.7) and regression on-order logarithmic fit (Figure D.8) [12, 13, 117]. Note that values below the MDL, in all the box plots and ECDFs, are calculated values based on the best fit regression log-normal curve extended to include reported values < MDL (i.e., censored data) [12].

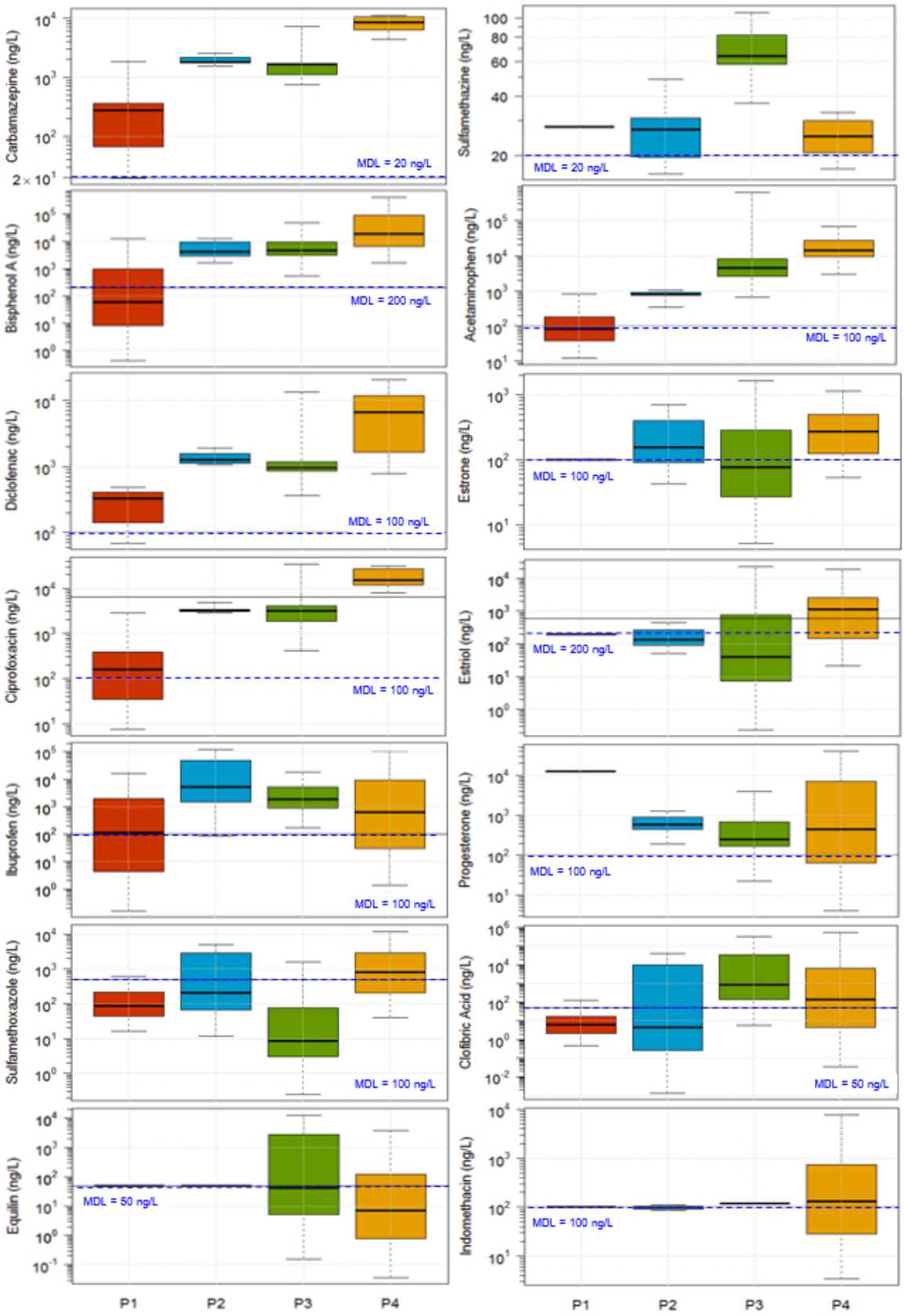

Figure D.4: Censored box plots comparisons of the TrOCs in the permeate extract in P1–P4

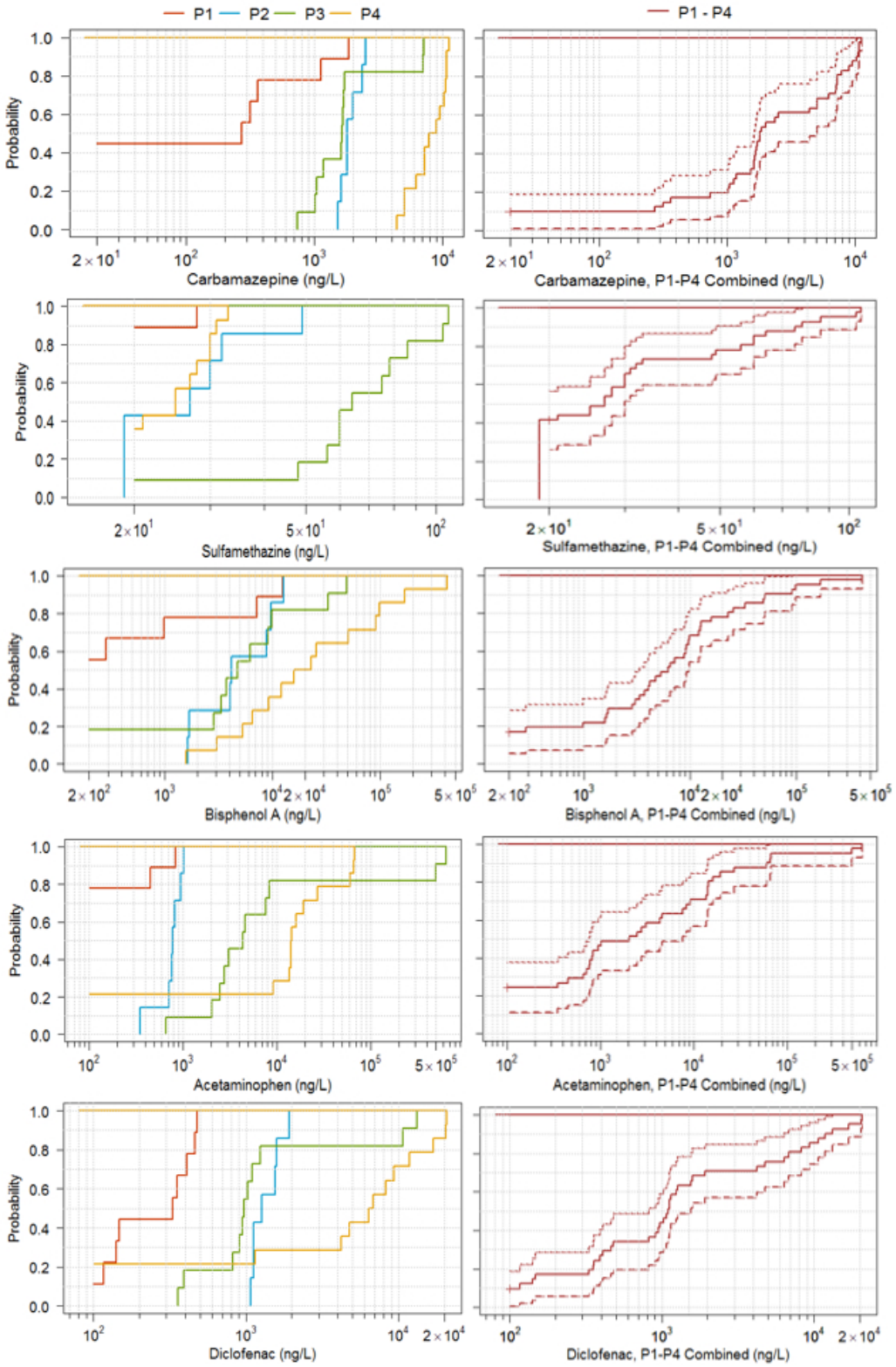

Figure D.5: Censored cumulative probability distribution diagrams of selected TrOCs by phase (P1–P4) (left) and all phases combined with 95% confidence band (right).

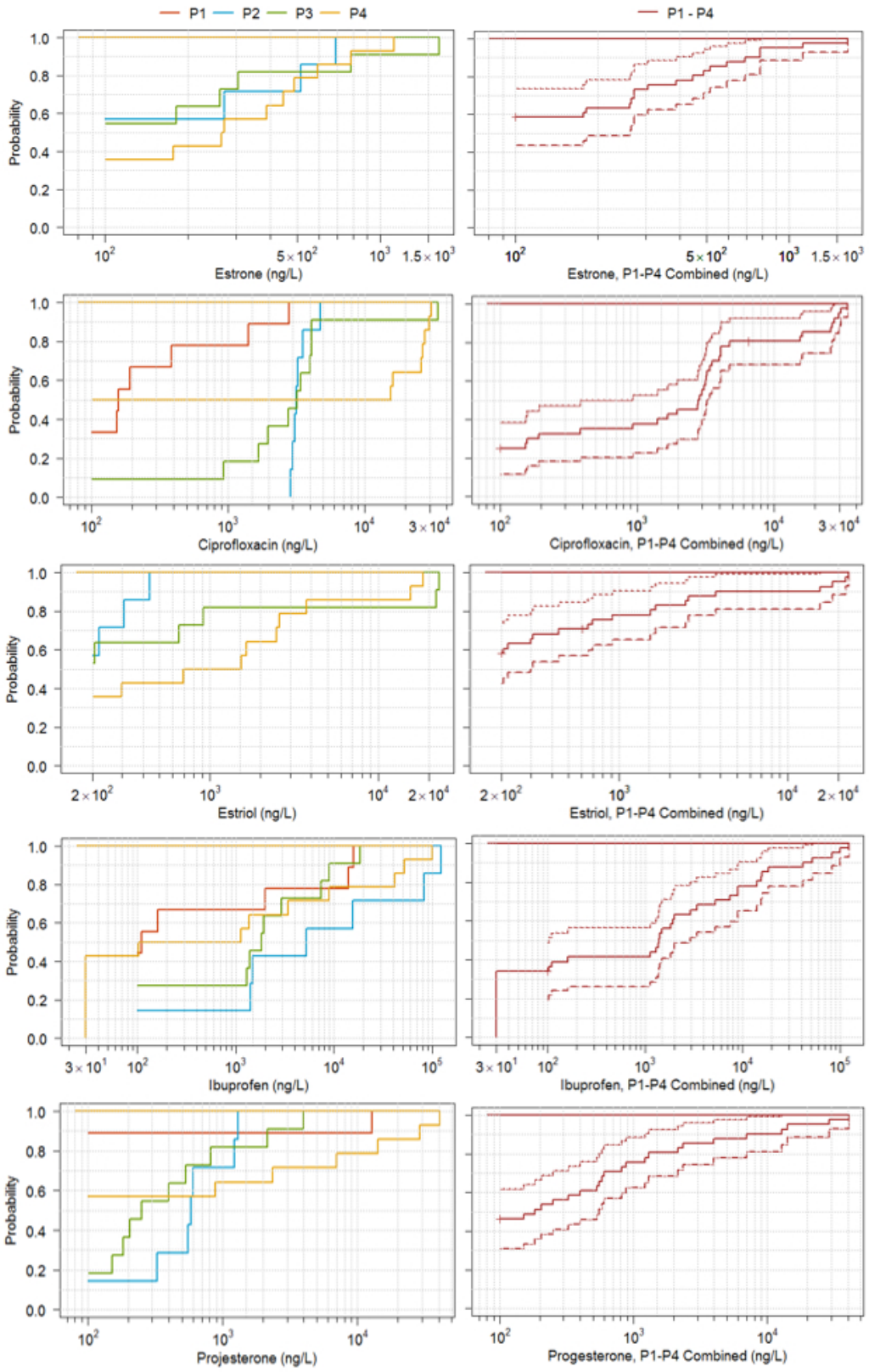

Figure D.6: Censored cumulative probability distribution diagrams of selected TrOCs by phase (P1–P4) (left) and all phases combined with 95% confidence band (right).

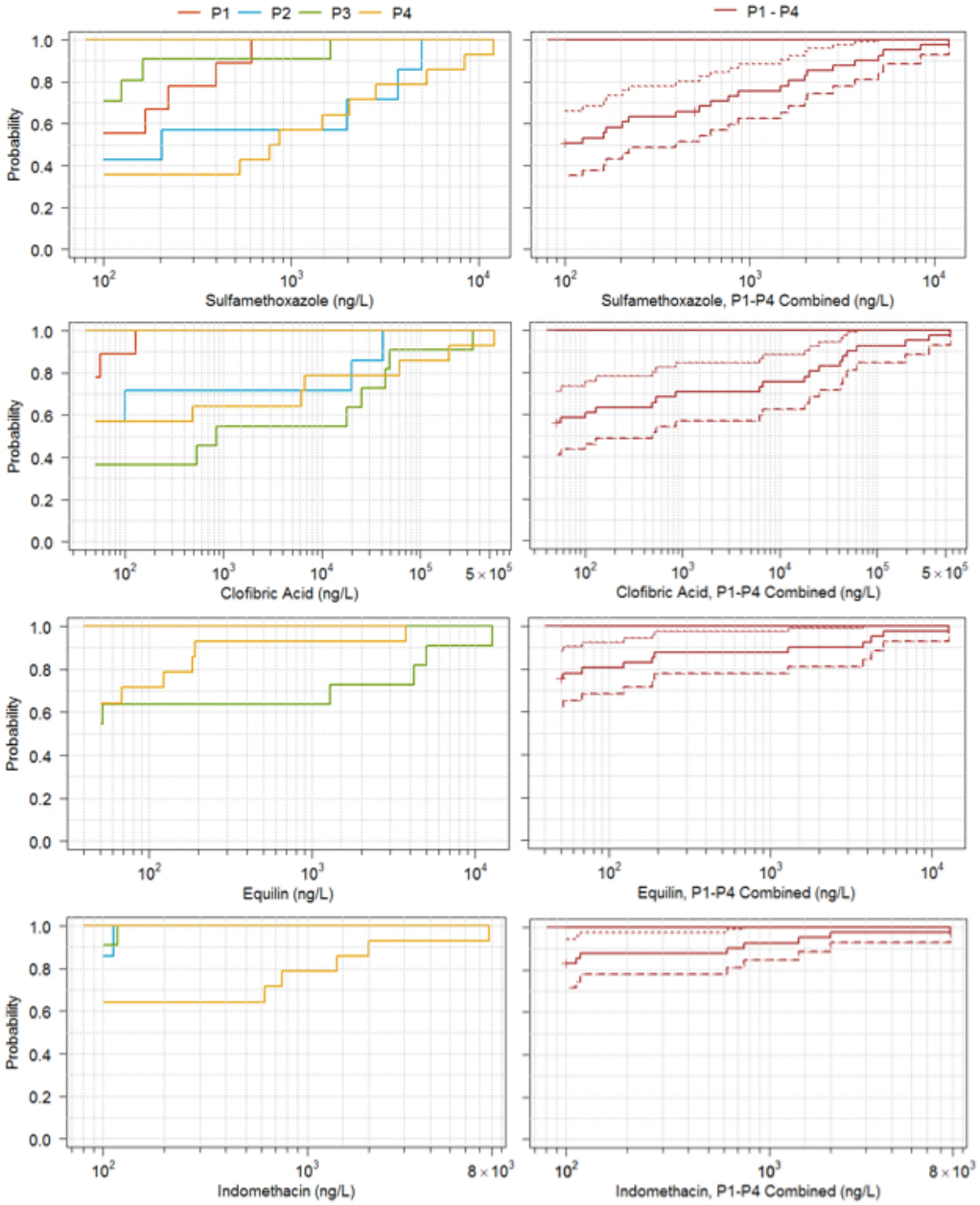

Figure D.7: Censored cumulative probability distribution diagrams of selected TrOCs by phase (P1–P4) (left) and all phases combined with 95% confidence band (right).

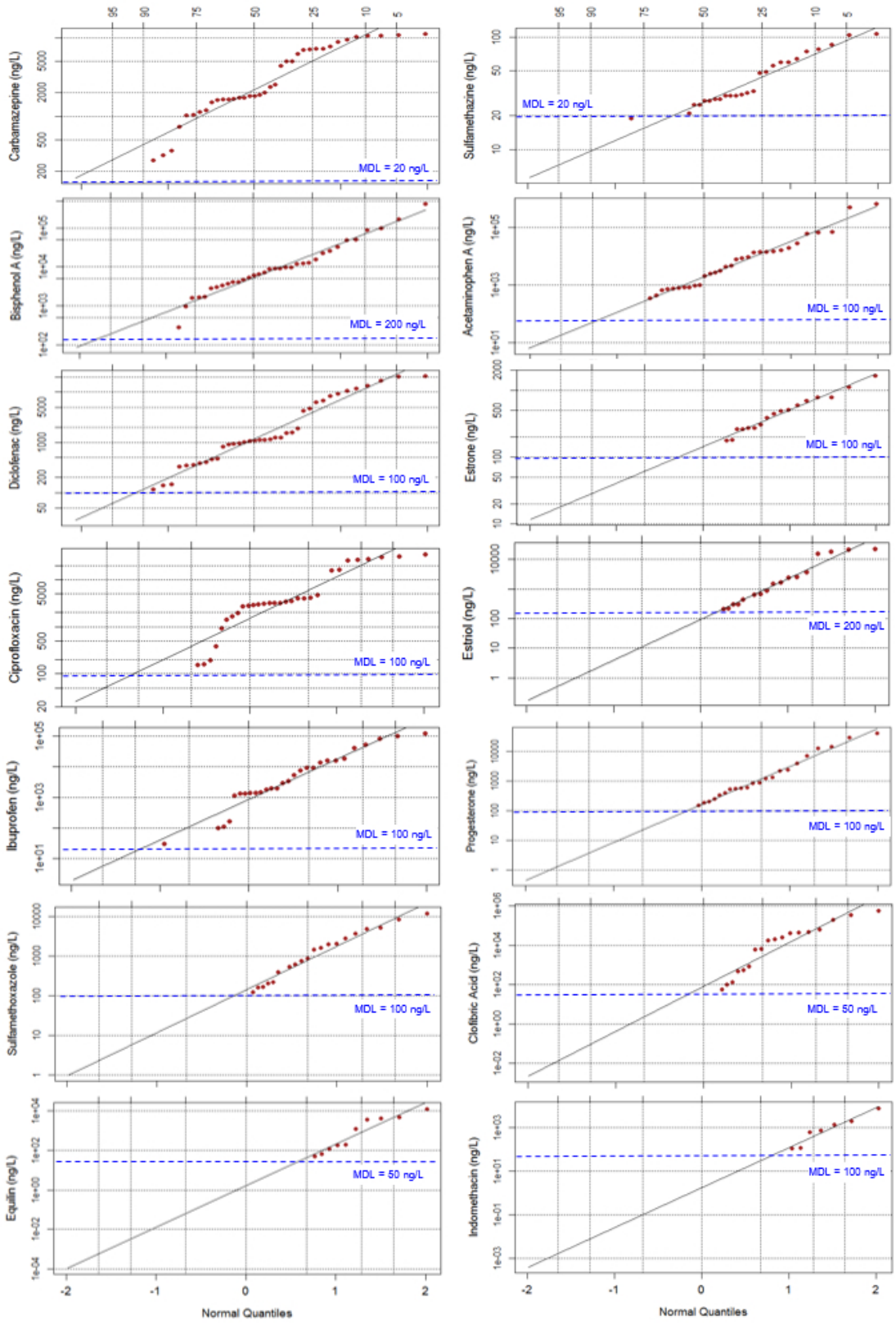

Figure D.8: Censored regression on order logarithmic data fit versus the normal scores (x-axis below) and percent exceedance (x-axis above) [12, 13]